Molecular insights into the zinc homeostasis of breast and prostate cancer cells

Shital Kumar Barman

Supervisory panel
Dr Ming J. Wu
A/Prof David A. Mahns
Dr Chandra S. Malladi

In fulfilment of the requirements
for the degree of Doctor of Philosophy

School of Science
Western Sydney University, Australia
February 2023

Dedication

To my parents Pabitra Rani Barman and Binay Chandra Barman

Statement of authenticity

This thesis is submitted in fulfilment of the requirements for the degree of Doctor of Philosophy at Western Sydney University, School of Science. The work presented in this thesis is, to the best of my knowledge and belief, original except as acknowledged in the text. I hereby declare that I have not submitted this material, either in full or in part, for any other degree at this or any other institution.

Shital Kumar Barman

February 2023

Declaration of COVID-19 impacts on research

COVID-19 pandemic disrupted severely my research progress in 2020 and 2021 due to lockdown and other restrictions. Following the rules of Australian goveronment during and after the lockdown, I have completed the experimental work for my PhD thesis.

[redacted]

Shital Kumar Barman

February 2023

Statement of support by the principal supervisor

[redacted]

Dr Ming J. Wu

February 2023

Acknowledgements

First of all, I am greatful to The Almighty.

The completion of my PhD would not be possible without the advice and immnese supports from my supervisory panel Dr Ming J. Wu, A/Prof. David A. Mahns and Dr Chandra S. Malladi. Heartily thank you to my supervisors for sharing their abundant knowledge in planning or doing experiements scientifically and writing scientific manuscript clearly throughout my PhD journey.

I would like to thank specially my primary supervisor Dr Ming Wu for his continuous advice and guidance throughout this research journey. Dr Ming, your humbleness and tireless work is truly inspirational. I am enriched with research knowledge as well as humane virtues because of you Ming. I have learnt so many things from you that I can't express in my words. I have learnt how to work hard with mental peace, be patient, learn from others, help to others, be kind to others, love to others, respect to others and finally lead happy life. I am really lucky getting you as primary and constant mentor.

I would like to bring forward this acknowledgement for the support from Dr Ming Wu's lab members particulary Dr. Mohammad S. Zaman. My stressful research journey would not be enjoyable without the presence of your smiling and joyful face.

I would like to express my gratitude to Sonja Starkovska, Dr Anu Shanu, Lisa Lam, Dr Sindy Kueh, Karena Gilroy, Dr Chun Ho, Lauren Hughes, Dr Malani Sutrisno and Dr Elise Wright for their heartfelt and unconditional technical supports. I am also greaful to Meena Mikhael for assisting me in liquid chromatography-tandem mass spectrometry analysis of the cellular protein samples.

I thank my wife Jharna Dash for her constant and uncoditional supports. I am greatful to my family in Bangladesh especially my elder brother Bikesh Chandra Barman.

The journey from Bangladesh to Australia was not smooth. I thank Dr Monokesh K. Sen specially for his enormous supports from my very first day in Australia.

My cordial gratitude goes to Western Sydney University for the provision of Postgraduate Research Scholarship which covers my tuition fees and living expenses in Australia.

Finally, thank School of Science, Western Sydney University and wonderful Australia for providing me the chance to persue PhD study.

Publications

Barman SK, Malladi CS, Mahns DA, Wu MJ. A confocal immunofluorescence study on the expression and localisation of zinc homeostasis-related proteins in breast and prostate cancer cells. Metallomics. (*Under review*)

Barman SK, Zaman MS, Veljanoski F, Malladi CS, Mahns DA, Wu MJ. Expression profiles of the genes associated with zinc homeostasis in normal and cancerous breast and prostate cells. Metallomics. 2022 14(8):mfac038. doi: 10.1093/mtomcs/mfac038. (IF 4.636)

Bekmukhametova A, Uddin MM, Houang J, Malladi C, George L, Wuhrer R, **Barman SK**, Wu MJ, Mawad D, Lauto A. Fabrication and characterization of chitosan nanoparticles using the coffee-ring effect for photodynamic therapy. Lasers in Surgery and Medicine. 2022 54(5):758-766. doi: 10.1002/lsm.23530. (IF 2.703)

Zaman MS, **Barman SK**, Corley SM, Wilkins MR, Malladi CS, Wu MJ. Transcriptomic insights into the zinc homeostasis of MCF-7 breast cancer cells via next-generation RNA sequencing. Metallomics. 2021 13(6):mfab026. doi: 10.1093/mtomcs/mfab026. (IF 4.636)

Conference presentations

Barman SK, Zaman MS, Veljanoski F, Malladi CS, Mahns DA, Wu MJ. Expression profiles of the genes associated with zinc homeostasis in normal and cancerous breast and prostate cells. Submission of Abstract for panel presentation in WSU Junior Researchers Conference 2022 (3rd Annual Junior Researchers Conference- 2022), 25th of May in Campbelltown.

Barman SK, Zaman MS, Malladi CS, Mahns DA, Wu MJ**.** Intricacy of Zinc Transporters and Protein Kinase CK2 in Breast and Prostate Cancer Cells. Presentation in 3MT School of Science Rounds 2021, 16th July 2021, Western Sydney University.

Barman SK, Zaman MS, Mahns DA, Wu MJ. The roles of zinc transporters and protein kinase CK2 in breast and prostate cancer cells. Submission of Abstract and presentation in School of Science on-line HDR conference, (SoSc) 3rd July 2020, Western Sydney University.

Barman SK, Zaman MS, Malladi CS, Mahns DA, Wu MJ. Molecular insights into Zn^{2+} homeostasis of breast and prostate cancer cells. Submission of Abstract and presentation in 'Western's Higher Degree Researchers Conference', 1st-4th December 2020. Research Continuity Student Council, Western Sydney University.

Zaman MS, **Barman SK,** Malladi CS, Wu MJ. Protein kinase CK2 regulates zinc homeostasis in breast and prostate cancer cells. Submission of Abstract and presentation in 'Western's Higher Degree Researchers Conference', 1st-4th December 2020. Research Continuity Student Council, Western Sydney University.

Table of contents

List of figures

List of tables

List of abbreviations

Abbreviation	Definition
T_0	0 min time point (control)
T_{120}	120 min time point
MTT	3-(4,5-Dimethylthiazol-2-yl)-2,5-Diphenyltetrazolium Bromide
CHAPS	3-[(3-cholamidopropyl)dimethylammonio]-1-propanesulfonate
T_{30}	30 min time point
DAPI	4',6-diamidino-2-phenylindole
Prism 8	A statistical analysis software
A600	Absorbance at 600 nm
ATP	Adenosine triphosphate
APS	Ammonium persulfate
ANOVA	Analysis of variance
X	Any amino acid
bp	Base pair
BPH	Benign prostate hyperplasia
β	Beta
BPE	Bovine pituitary extract
BSA	Bovine serum albumin
MCF-7	Breast cancer cell line
MDA-MB-231	Breast cancer cell line
CREB	cAMP response element-binding protein
cCBB	Colloidal coomassie brilliant blue
cDNA	Complementary deoxyribonucleic acid
CT	Cycle threshold
cAMP	Cyclic adenosine monophosphate
Δ	Delta
δ	Delta
dNTP	Deoxynucleotide triphosphates
DEPC	Diethyl pyrocarbonate treated water
DMSO	Dimethyl sulfoxide
DTT	Dithiothreitol

↓	Down-regulation of the genes or proteins
DMEM	Dulbecco's Modified Eagle Medium
ER	Endoplasmic reticulum
EMT	Epithelial-to-mesenchymal transition
EDTA	Ethylenediaminetetraacetic acid
e.g.,	Exempli gratia, for example
FBS	Foetal bovine serum
FC	Fold change
GAPDH	Glyceraldehyde 3-phosphate dehydrogenase
GSK3	Glycogen synthase kinase 3
GTP	Guanosine triphosphate
HER2	Human epidermal growth factor receptor 2
IRT	Iron regulated transporter
pI	Isoelectric point
L-15	Leibovitz's L-15 medium
LC-MS/MS	Liquid chromatography-tandem mass spectrometry
mTOR	Mammalian target of rapamycin
MFI	Mean fluorescence intensity
MRE	Metal-responsive element
MTF-1	Metal-responsive transcription factor 1
MT	Metallothioneins
MAPK	Mitogen-activated protein kinases
MCF10A	Normal breast epithelial cell line
RWPE-1	Normal prostate epithelial cell line
F12 Hams	Nutrient mixture for mammalian tissue culture
PBS	Phosphate buffer saline
PI3K	Phosphatidylinositol-3 kinase
GPS 5.0	Phosphorylation sites prediction software
PCR	Polymerase chain reaction
PR	Progesterone receptor
DU145	Prostate cancer cell line
PC3	Prostate cancer cell line
PSA	Prostate-specific antigen

Akt	Protein kinase B
CK2	Protein kinase CK2
PLGS	ProteinLynx Global Server
qRT-PCR	Quantitative polymerase chain reaction
RREB1	Ras-responsive element binding protein 1
ROS	Reactive oxygen species
STAT3	Signal transducer and activator of transcription 3
NaCl	Sodium chloride
SDS-PAGE	Sodium dodecyl sulphate-polyacrylamide gel electrophoresis
SD	Standard deviation
SEM	Standard error mean
SPSS	Statistical package for the social sciences
TEMED	Tetramethylethylenediamine
TRIS	Tris(hydroxymethyl)aminomethane
p53	Tumour suppressor protein
2-DE	Two-dimensional gel electrophoresis
T1DM	Type 1 diabetes mellitus
T2DM	Type 2 diabetes mellitus
↑	Up-regulation of the genes or proteins
ZRT	Zinc regulated transporter
$ZnSO_4$	Zinc sulphate
ZnT	Zinc exporter protein
ZO-1	Zonula occludens 1, tight junction protein
ZIP	ZRT IRT like Protein
CK2α	α catalytic subunit of mammalian CK2
CK2α'	α' catalytic subunit of mammalian CK2
CK2β	β catalytic subunit of mammalian CK2

Abstract

Zinc ion (Zn^{2+}) is essential to life as a structural or catalytic component of proteins. The cell has developed an elaborate molecular network over the extensive evolutionary timeline to maintain zinc homeostasis. Any disruption of such a network will lead to zinc dyshomeostasis, resulting in health problems such as cancers. Zinc dyshomeostasis is an intriguing phenomenon in breast and prostate cancers, with breast cancer cells exhibiting higher intracellular Zn^{2+} levels compared to their corresponding normal epithelial cells, in contrast to the low Zn^{2+} levels in prostate cancer cells compared to the normal prostate counterpart. Such contrasting zinc profiles of breast and prostate cancer cells provide an avenue for this PhD project to investigate the Zn^{2+} homeostasis of breast and prostate cancer cells by a systematic approach of gene profiling via quantitative reverse transcription polymerase chain reaction (qRT-PCR), immunofluorescence confocal microscopy and proteomic analysis with a panel of cell lines including two breast cancer cell lines (MCF-7, MDA-MB-231), two prostate cancer cell lines (PC3 and DU145), along with normal breast epithelial and prostate epithelial cell lines (MCF10A, RWPE-1).

In order to gain molecular insights into the zinc homeostasis of breast and prostate cancer cells, this study firstly profiled the expression of 28 genes, including 14 zinc importer genes (*SLC39A1-14*) which encode ZIP1-14 to transport Zn^{2+} into the cytoplasm, 10 zinc exporter genes (*SLC30A1-10*) which encode ZnT1-10 to transport Zn^{2+} out of the cytoplasm and 4 metallothionein genes (*MT1B*, *MT1F*, *MT1X*, *MT2A*) in breast (MCF10A, MCF-7, MDA-MB-231) and prostate (RWPE-1, PC3, DU145) cell lines in response to extracellular zinc exposures at a mild cytotoxic dosage and a benign dosage. The RNA samples were prepared at 0 min (T_0), 30 min (T_{30}) and 120 min (T_{120}) in a time course with or without zinc exposure, which were used for profiling the baseline and dynamic gene expression. The *SLC39A4, SLC39A6, SLC39A8* and *SLC39A11* were intrinsically up-regulated in breast and prostate cancer cells compared to their respective normal counterparts, suggesting their common roles in two distinctive cancers. The significant down-regulation of *SLC39A1* (ZIP1) along with the up-regulation of *SLC30A1* (ZnT1) gene provides explanation to the lower intracellular Zn^{2+} level in prostate cancer cells compared to the normal counterparts. In contrast, the down-regulation *SLC30A1*, *SLC30A4* and *SLC30A10* correlates with the elevated cytosolic Zn^{2+} in breast cancer cells. Significantly, the findings demonstrate that *SLC39A4* (encoding ZIP4) and *SLC3912*

(encoding ZIP12) play a role in zinc homeostasis of breast cancer cells, likely as an extracellular zinc sensor. The dynamically higher expression of *SLC39A12*, *SLC30A1* and 4 *MT* in basal breast cancer cells (MDA-MB-231) than luminal cancerous cells (MCF-7) in response to extracellular zinc exposure sheds light to their differential phenotypes such as the higher zinc tolerance and malignancy of the basal breast cancer cells (MDA-MB-231).

To follow up the findings in the gene profiling, immunofluorescence confocal microscopy was then carried out to determine the protein expression and the subcellular localisation of ZIP12, ZnT1, MT2A, which were differentially expressed at the gene level in breast and prostate cancer cells in response to extracellular zinc exposure. The catalytic subunits CK2α/α' and the regulatory subunit CK2β of protein kinase CK2 in breast and prostate cancer cells were also investigated, since CK2 is implicated in regulating Zn^{2+} homeostasis. Upon extracellular zinc exposure, ZIP12 was conspicuously localised in the plasma membrane of breast cancer cells but not in normal breast, neither in cancerous nor noncancerous prostate cells. Such localisation could enable ZIP12 for sensing extracellular Zn^{2+} as well as uptake for accumulating high intracellular Zn^{2+} in breast cancer cells. Intriguingly, protein kinase CK2 was demonstrated to be an ecto-kinase by the localisation of its subunits CK2α/α' and CK2β in close proximity to the plasma membrane of breast cancer cells. The localisation of both ZIP12 and CK2 in plasma membrane of the breast cancer cells demonstrates a likelihood that ZIP12 might be regulated by CK2 kinase via phosphorylation for extracellular Zn^{2+} sensing and uptake. ZnT1 was found to be localised in the plasma membrane of only breast cancer cells but not in the other cells such as prostate cancer cells. Such observation might explain Zn^{2+} efflux via ZnT1 in breast cancer cells. MT2A was distinctively localised in close proximity to the plasma membrane in breast cancer cells, indicating its necessity not only for Zn^{2+} sequestration but also for cancer invasion as well as progression.

To gain the holistic proteomic insights into Zn^{2+} homeostasis of breast and prostate cancer cells, top-down proteomics (i.e., two-dimensional gel electrophoresis followed by liquid chromatography-tandem mass spectrometry) was employed for profiling the proteins following extracellular zinc exposure. The proteomic profiles of MCF-7 breast cancer cells, MCF10A breast normal epithelial cells, PC3 prostate cancer cells and RWPE-1 prostate normal epithelial cells with or without exogenous zinc exposure have been generated following four comparisons (1) cancer cells versus (vs) respective normal epithelial cells without zinc treatment (T_0) including MCF-7 T_0 vs MCF10A T_0, PC3 T_0 vs RWPE-1 T_0, (2) cancer cells vs respective

normal epithelial cells under exogenous zinc exposure for 120 min (T_{120}) including MCF-7 T_{120} vs MCF10A T_{120}, PC3 T_{120} vs RWPE-1 T_{120}, (3) comparison in cancer cells between T_{120} and T_0 including MCF-7 T_{120} vs MCF-7 T_0, PC3 T_{120} vs PC3 T_0, and (4) comparison in normal epithelial cells between T_{120} and T_0 including MCF10A T_{120} vs MCF10A T_0, RWPE-1 T_{120} vs RWPE-1 T_0.

MCF-7 breast cancer cells exhibited 16% differentially expressed metal ion binding proteins whereas 13% in PC3 prostate cancer cells compared to their respective normal epithelial cells at T_0. Under exogenous zinc exposure breast cancer cells revealed 25 differentially expressed protein spots while 9 in prostate cancer cells at T_{120} compared to T_0. In contrast, normal prostate epithelial cells exhibited 24 differentially expressed protein spots but normal breast cell showed 9 spots following zinc exposure at T_{120} compared to T_0. These findings collectively show that more molecules are required in regulating higher intracellular Zn^{2+} and thus the findings reflect and explain the contrasting intracellular Zn^{2+} profiles in breast and prostate cancer cells compared to the respective normal cells.

The proteomic datasets demonstrate the differential expressions of different protein classes such as tumour proteins [tumour protein D53 (hD53), tumour protein D54 (hD54), α-smooth muscle actin (α-SMA), cathepsin D], antioxidants (peroxiredoxin 6, peroxiredoxin 2, superoxide dismutase Cu-Zn), metabolic enzymes (dihydrolipoamide S-succinyltransferase, glucose-6-phosphate 1-dehydrogenase, L-lactate dehydrogenase B chain), metal ion binding proteins (annexin A1, annexin A5), molecular chaperone or stress response proteins (heat shock protein 60 kDa and 70 kDa, heat shock protein β1), translational factors (elongation factor Tu, elongation factor 1γ, elongation factor δ) with or without zinc exposure. The proteomic analysis revealed the intrinsic down-regulation of tumour suppressor proteins (14-3-3 protein σ and θ) but up-regulation of antioxidant protein (peroxiredoxin 6) in breast and prostate cancer cells compared to their normal cells at T_0, which suggests the involvement of these proteins in breast and prostate cancers. The increased expression of antioxidants (peroxiredoxin 6 and 2) and stress response proteins (heat shock proteins 60 kDa and 70 kDa) indicates that they were needed for the survival of the cancer cells under zinc exposure. The overexpressed tumour proteins hD53 and hD54 following zinc exposure demonstrate that the elevated Zn^{2+} accumulation in breast cancer cells could trigger their proliferation. In contrast, zinc exposure reduced the expression of prohibitin (*PHB*), an anti-tumour protein, in prostate

cancer cells, which reflects low intracellular zinc level as a prerequisite for prostate cancer development.

The systematic experimental approach of this project returned the meaningful findings as just described, which enhances our knowledge and understanding of the zinc homeostasis in breast and prostate cancer cells. The molecular clues uncovered here should not only contribute to the elucidation of molecular network of zinc homeostasis but should also serve as potential molecular targets for anti-cancer drug development. As zinc dyshomeostasis is increasingly linked to the development and progression of cancers such as breast and prostate cancers, and zinc is emerging as an important signalling messenger in normal and cancerous cells, the findings of this project provide avenues for further studies on breast and prostate cancers.

Chapter 1 Introduction

1.1 Overview

This thesis investigated the molecular insights of zinc (Zn^{2+}) homeostasis in breast cancer cells, breast normal epithelial cells, prostate cancer cells and prostate normal epithelial cells, by the systematic experimental approach of quantitative reverse transcription polymerase chain reaction (qRT-PCR), top-down proteomics as well as immunofluorescence confocal microscopy.

Zn^{2+} is essential to life by functioning as a cofactor for over 300 enzymes and as a structural component for ~3000 human proteins (Andreini et al., 2006; Kambe et al., 2015; Padjasek et al., 2020). As a result, the cells have developed the tight and elaborate molecular network over the extensive evolutionary timeline to maintain zinc homeostasis (Jeong and Eide, 2013; Bin et al., 2018; Nishito and Kambe, 2019; Amos and Razzaque, 2022). Any disruption of such a network leads to zinc dyshomeostasis, resulting in health problems such as cancers (Bafaro et al., 2017; Li et al., 2020; Wang et al., 2020; Hu, 2021).

Zn^{2+} dyshomeostasis is a prominent phenomenon in breast and prostate cancers, with breast cancer cells showing elevated level of intracellular Zn^{2+} compared to their respective normal epithelial cells (Alam and Kelleher, 2012; Larner et al., 2015; Takatani-Nakase et al., 2016; Rusch et al., 2021), in contrast to the reduced intracellular Zn^{2+} level in prostatic cancer cells relative to their normal counterparts (Franklin et al., 2005; Johnson et al., 2010; Sauer et al., 2020).

In the past ten years, our lab has been focussing on zinc-related gene and protein profiling in breast and prostate malignant cells in order to understand the underlying molecular networks of Zn^{2+} homeostasis (Zaman et al., 2019; Zaman et al., 2021). Zaman et al. (2021) revealed the genes of Zn^{2+} homeostasis in MCF-7 breast cancer cells by RNA sequencing study which provided a basis for the gene profiling work of this thesis. I have further investigated the molecular network of Zn^{2+} homeostasis into breast and prostate cancer cells at protein level by the immunofluorescence confocal microscopy and top-down proteomic analysis.

The expression profiles of the 28 genes (*SLC39A1-14*, *SLC30A1-10*, *MT1B*, *MT1F*, *MT1X* and *MT2A*) associated with zinc homeostasis in normal and cancerous breast (MCF10A, MCF-7 and MDA-MB-231) and prostate (RWPE-1, PC3 and DU145) cells have been generated by qRT-PCR with or without zinc exposure. Differentially expressed genes were analysed at protein level by immunofluorescence confocal microscopy along with their cellular localisation in all six cell lines with and without exogenous zinc exposure. Similarly, the protein expressions and the localisations of the catalytic subunits CK2α/α' and regulatory subunit CK2β of protein kinase CK2 were also investigated by immunofluorescence in all cell lines, as the previous studies by our research team demonstrated that CK2 kinase is associated with Zn^{2+} homeostasis in the cells (Zaman et al., 2016; Johnson et al., 2017; Zaman et al., 2019).

Furthermore, the top-down proteomic analysis was employed here to identify the proteins associated with Zn^{2+} homeostasis in breast and prostate cancer cells with and without exogenous zinc exposure. The findings reported in this thesis should shed light on Zn^{2+} homeostasis in breast and prostate cancer cells, fill in some crucial knowledge gaps and reveal potential molecular targets for anticancer drug development.

1.2 Zinc

Zn^{2+} is an essential element of the cells. It is the second most abundant trace element after iron and crucial for the structures and functions of the numerous proteins, enzymes and transcription factors (Jen and Wang, 2016; Padjasek et al., 2020; Rakhra and Rakhra, 2021), as well as signalling pathways (Li et al., 2020). Therefore, the cells have an extensive molecular network for regulating intracellular Zn^{2+} (Kambe et al., 2021; Yin et al., 2022).

Chemically, Zn^{2+} is not able to participate into redox reactions due to lack of unpaired electrons and filled *d* shell, but it interacts with the ligands such as amino acid residues (Laity et al., 2001), thereby provides the functionality and/or structural stability of the proteins in both intracellular and extracellular environments. Regulated Zn^{2+} homeostasis reflects cellular health whereas disruption of cellular Zn^{2+} balance has become the indicator of various cancers and many other diseases (Wang et al., 2020). For example, reduced intracellular Zn^{2+} in prostate cancer cells (Franklin et al., 2005; Johnson et al., 2010; Sauer et al., 2020) but elevated Zn^{2+} in breast cancer cells (Alam and Kelleher, 2012; Larner et al., 2015; Takatani-Nakase et

al., 2016; Rusch et al., 2021) compared to their respective normal counterparts are the hallmarks of breast and prostate cancer cells.

1.3 Biological roles of zinc

The requirement of Zn^{2+} in human body was recognised in 1963, although the importance of zinc emerged in 1961 with 21-year-old Iranian male patient having dwarfism, anaemia due to iron deficiency, hypogonadism, rough and dried skin, hepatosplenomegaly, prolonged geophagia and mental lethargy (Prasad et al., 1961; Prasad, 2013). Raulin (1869) firstly addressed Zn^{2+} as an indispensable element of living organisms by discovering that Zn^{2+} is involved in proliferating of a filamentous fungus *Aspergillus niger*. The biological roles of Zn^{2+} have been unravelled since the discovery of its essentiality as a catalytic cofactor for erythrocyte carbonic anhydrase in 1940 (Keilin and Mann, 1940). Spectrographic analysis showed the presence of Zn^{2+} in pancreatic bovine carboxypeptidase which was recognised as the second Zn^{2+}-containing enzyme (Vallee and Neurath, 1954).

The proteins bind to one or more metallic ions are called metalloproteins and similarly the proteins bind to Zn^{2+} are known as Zn^{2+} proteome. The percentage of Zn^{2+} proteome over the whole cellular proteome is 9% in eukaryotes, higher than that of prokaryotes (5-6%) (Andreini et al., 2009), suggesting that the number of Zn^{2+}-binding proteins are linearly correlated with the numbers of genes in a genome of a particular organism. Therefore, 10% (~3000 proteins) of the human proteome is Zn^{2+}-binding proteins, and Zn^{2+} fingers with Cys_4 and Cys_2His_2 are the most common classes of Zn^{2+}-binding motifs in human (Andreini et al., 2006; Maret, 2013). No wonder, Zn^{2+} plays a wide range of biological functions through Zn^{2+}-binding proteins. About 2-3 grams Zn^{2+}, carried by an adult human body are distributed in skeletal muscle (~60%), bone (~30%), liver (~5%) and skin (~5%) and other tissues (~2-3%) (To et al., 2020). The cell contains 50% of Zn^{2+} in the cytoplasm whereas 40% and 10% are nuclear and membranous, respectively (Kambe et al., 2015). Zn^{2+} serves as structural component, catalytic factor and signalling mediator in the cellular environment (Li et al., 2020; Padjasek et al., 2020; Rakhra and Rakhra, 2021).

1.3.1 Zn^{2+} as a structural component of the proteins

Zn^{2+} has the important roles in stabilising the structures of proteins, enzymes and transcriptional factors (Nguyen et al., 2020; Padjasek et al., 2020). The zinc-binding proteins are structurally and functionally diverse, involving in wide ranges of biological functions such as DNA replication (Bochkareva et al., 2000), DNA transcription (Li et al., 2022) and translation (Benhalevy et al., 2017; Vilas et al., 2018; Rakhra and Rakhra, 2021), DNA repair (Vilas et al., 2018), metabolism (Li et al., 2022), cell signalling (Cassandri et al., 2017) and cell growth (Cassandri et al., 2017; Li et al., 2022). Based on the structural properties, there are eight recognised groups of zinc fingers, they are classic zinc finger (Cys_2His_2 like finger), zinc ribbon, gag knuckle, TAZ2 domain like, treble clef finger, short Zn^{2+}-binding loop and metallothioneins (MT) (Krishna et al., 2003). Classic zinc finger domains consist of a β-hairpin and an α-helix (Krishna et al., 2003). Nine repetitive sequences of Cys and His (Cys_2His_2 finger) of transcription factor IIIA (TFIIIA) of *Xenopus laevis* are associated with binding nine Zn^{2+} (Miller et al., 1985). The repeated domains are linear, independently folded and centred on a Zn^{2+} which binds the long control region of 5S RNA gene and remains bound during the passage of an RNA polymerase. Cys_2His_2 fingers have also been reported in many DNA binding proteins (e.g., 1zfd, 1sp2, 2drp etc.) and in inhibitors of apoptosis (e.g., 1e31, 1jd5, 1c9q etc.). Two zinc-knuckles form zinc binding ligands in zinc ribbon fold (Krishna et al., 2003). Basically, the core of the structure is composed of two β-hairpins forming two structurally similar zinc-binding sub-sites. This family of zinc fingers mostly includes domains from the proteins involved in the translation/transcription machinery, such as transcription factors, primases, polymerases, topoisomerases and ribosomal proteins. Classical zinc ribbons are characterised by a long secondary hairpin (ribbon). RNA transcription factor IIB (TFIIB) zinc ribbon was shown to be essential for appointing RNA polymerase II into the pre-initiation complex whereas Brf zinc ribbon showed a defect in open complex formation but RNA polymerase III (Pol III) recruitment was normal (Hahn and Roberts, 2000; Chen and Hahn, 2003). It suggests that the same zinc ribbon domain can serve distinct roles in the Pol II and Pol III transcription machinery. Two β subunits of CK2 kinase make homodimer in which the zinc ribbon motif of each β subunit establishes many hydrophobic interactions to stabilise the structural and functional integrity of CK2 (Filhol et al., 2005). In addition, the zinc ribbon domain was also shown in stabilising threonine synthase structurally and functionally, an enzyme catalysing the terminal step of threonine biosynthesis (Kaur and Subramanian, 2017).

1.3.2 Zn^{2+} as an enzymatic cofactor

Zinc serves as the cofactor for a broad-spectrum of enzymes in both prokaryotes and eukaryotes (Andreini et al., 2006; Andreini et al., 2006; Andreini and Bertini, 2012). It was estimated that over 300 enzymes in human require Zn^{2+} as a cofactor (Prasad, 2012). Furthermore, analysis on enzymatic mechanisms showed the associations of different metal ions in around 40% enzyme-catalysed reactions and Zn^{2+} is very common in enzymes (Andreini et al., 2008). The presence of Zn^{2+} was established in six main classes of enzymes including ligase, transferase, isomerase, oxidoreductase, lyase and hydrolase (Kambe et al., 2015).

1.3.3 Zn^{2+} as a signalling mediator

Zn^{2+} serves as both extracellular and intracellular signalling mediator. A putative receptor senses extracellular Zn^{2+} and it can be activated at physiological Zn^{2+} concentration (Hershfinkel et al., 2007). Extracellular Zn^{2+} was reported to activate p70 S6 kinase via PI3K signalling which in turn led to the activation of AKT kinase in fibroblast cells (Kim et al., 2000). Also, Zn^{2+} was demonstrated to trigger extracellular kinase 1/2 and Src kinase-mediated signalling (Hershfinkel et al., 2007). Zn^{2+} is involved in Ras signalling (Bruinsma et al., 2002). Ras kinases serve as binary switches between ON and OFF states during signal transductions and they are the main workhorses of many signalling pathways in human diseases such as cancers (McKenna et al., 2003; Simanshu et al., 2017; Khan et al., 2019). Besides, protein kinase CK2 phosphorylates amino acid residues Ser^{275} and Ser^{276} of ZIP7 localised at the endoplasmic reticulum's membrane, leading to the gated release of Zn^{2+} and the increase cytoplasmic Zn^{2+} concentration which in turn results in the activation of AKT/mTOR/MAPK/PI3K signalling networks (Taylor et al., 2012; Nimmanon et al., 2017). Our research team also found the elevation of intracellular Ca^{2+} concentration in neuronal cells following exogeneous zinc exposure, which was prevented by the inhibition of CK2 kinase (Zaman et al., 2016). Therefore, CK2 has been recognised as a regulatory kinase for Zn^{2+} transport and signalling, and Zn^{2+} importer, ZIP7 is involved in regulating cytoplasmic Zn^{2+} concentration in the cell (Hogstrand et al., 2009). Interestingly, high extracellular Zn^{2+} concentration (100 µM) was positively related to intracellular Ca^{2+} concentration in primary hepatocyte (McNulty and Taylor, 1999) and neuroblastoma cells (Zaman et al., 2016). Ca^{2+} has been well established in numerous signalling pathways such as MAPK, IP3, Ca^{2+} channel (L-, N- and T-type) based, calmodulin mediated, cAMP-PKA, Wnt, PKC, RAS, RAF signalling

pathways (Song et al., 2019; Trebak and Kinet, 2019; Irnaten et al., 2021). Thus, Zn^{2+} signalling could be intertwined with Ca^{2+}-mediated signalling in the cell.

1.4 Regulation of Zn^{2+} homeostasis in the cell

According to what has been said so far, the cell clearly needs to maintain Zn^{2+} homeostasis for cellular functions, because Zn^{2+} plays a wide range of biological roles by being a structural component of many proteins, being a cofactor of numerous enzymes and being a second messenger of signalling transduction. Disruption of Zn^{2+} homeostasis leads to many health problems in human and animals (Prasad et al., 1961; Bafaro et al., 2017; Golan et al., 2017; Sauer et al., 2020; Wang et al., 2020). Zrt/Irt-like protein (ZIP) (Zn^{2+} importer), Zn^{2+} exporter (ZnT) and metallothionein (MT) are at the forefront in controlling intracellular Zn^{2+} (Kagara et al., 2007; Taylor et al., 2012; Kambe et al., 2021; Yin et al., 2022). There are 14 ZIP proteins (ZIP1-14), encoded by *SLC39A1-14*, which transport Zn^{2+} into the cytoplasm from outside the cells and intracellular organelles/compartments whilst 10 ZnT (ZnT1-10), encoded by *SLC30A1-10*, transport Zn^{2+} in the opposite direction of ZIP to maintain Zn^{2+} homeostasis as shown in **Figure 1.1**. And MT buffers cellular Zn^{2+} for maintaining zinc homeostasis.

1.4.1 ZIP and ZnT

The first Zn^{2+} transporter protein was discovered in *Saccharomyces cerevisiae* and the protein was accountable for conferring resistance to high Zn^{2+} concentration (Kamizono et al., 1989). The gene encoding for Zn^{2+} transporter protein was named Zn^{2+} resistance conferring (Zrc1) gene, which is an orthologue of human Zn^{2+} transporter 10 (ZnT10) protein. Iron-regulated transporter 1 (Irt1), a member of Zn^{2+} transporter protein family was first characterized in *Arabidopsis thaliana* (Zhao and Eide, 1996). In the same year, Zhao and Eide (1996) identified Zn^{2+} regulated transporter 1 (Zrt1) and Zrt2 in *Saccharomyces cerevisiae* based on Irt1 data. Since then, 14 ZIP and 10 ZnT proteins have been discovered (Yin et al., 2022). Based on the sequence similarities, ZIP protein family is divided into four subclasses, subfamily I (ZIP1, ZIP2, ZIP3), subfamily II (ZIP9), gufA subfamily (ZIP11) and LIV-1 (ZIP4, ZIP5, ZIP6, ZIP7, ZIP8, ZIP10, ZIP12, ZIP13, ZIP14) (**Table 1.1**) (Gaither and Eide, 2001; Bafaro et al., 2017).

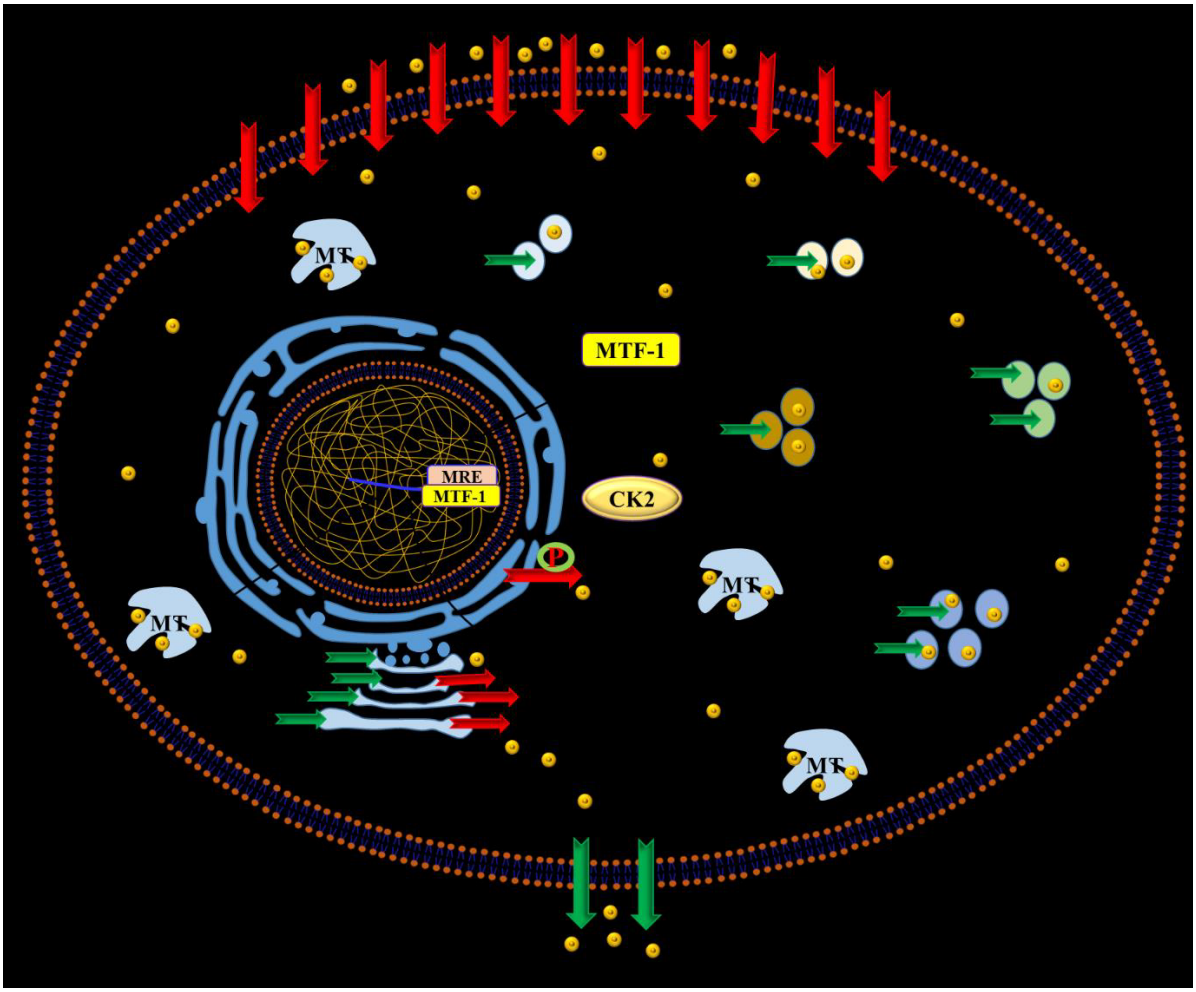

Figure 1.1 Maintenance of Zn^{2+} homeostasis by Zn^{2+} transporters ZIP/ZnT and metallothioneins in the cell. The function of ZIP and ZnT transporter families is to increase or to reduce the cytoplasmic Zn^{2+} concentration, respectively. The diagram also depicts the localisation of ZIP and ZnT. Metallothioneins (MT) are involved in Zn^{2+} sequestration. Metal-response element binding transcription factor 1 (MTF-1) is reported to regulate the expression of ZnT and MT.

Though 14 ZIPs belong to the same family, their encoding genes are in different chromosome as shown in **Table 1.1**. In addition, their expression profiles in tissues, subcellular localisations, molecular weights (MW) and lengths of protein sequences are also distinctive. **Table 1.1** describes the characteristics of ZIP such as their encoding genes, expression profiles in tissues and subcellular organelles, their roles in transporting Zn^{2+} (zinc ion), Co^{2+} (cobalt ion), Cd^{2+} (cadmium ion), Cu^{2+} (copper ion), Mn^{2+} (manganese ion) or $HSeO_3^-$ (selenite ion) (Gaither and Eide, 2001; Bin et al., 2018; Fujishiro and Kambe, 2022; Li et al., 2022; Yin et al., 2022).

The three-dimensional protein structure of ZIP or ZnT does not exist till the present. Zinc transport via the ZIP family is better understood by having the structural model of human ZIP4 on its extracellular and intracellular domains. The crystallographic structure of ZIP4 extracellular domain of *Pteropus alecto* (the fruit bat) exhibits a homodimer containing two subdomains (Zhang et al., 2016). The PAL sequence, conserved in LIV-1 subfamily, is located in the dimer core, consisting of the C-terminal subdomain and makes two helix-turn-helix folds (Zhang et al., 2016). The N-terminal residues make up the second subdomain which has a distinctive α-helical fold. It was determined that both C-terminal and N-terminal subdomains are necessary for the zinc transport activity. A disorganized linker region that connects the subdomains is essential for folding and transporting of the entire ZIP4 protein to plasma membrane and for Zn^{2+} transport (Zhang et al., 2016). The analysis conducted on N-terminal ectodomains of LIV-1 members concluded that dimerization of the subdomains is preserved except ZIP7 and ZIP13 (Zhang et al., 2016). Such ectodomains in ZIP7 and ZIP13 showed most divergence sequences compared to other ZIP members and it is unknown whether these ectodomains can oligomerize or not. Experimental evidence demonstrated that ZIP7 and ZIP13 proteins display homodimer formation in the membrane (Bin et al., 2011; Taylor et al., 2012). ZIP5 ectodomain was purified and its homodimeric status was established (Pocanschi et al., 2013). The ZIP4 dimerization hypothesis is backed by the evidence showing homodimers of other ZIP proteins, such as ZIP2, ZIP7 and ZIP13, as well as the heterodimer formation of ZIP6 and ZIP10 (Bin et al., 2011; Taylor et al., 2012; Franz et al., 2014; Taylor et al., 2016).

Table 1.1 ZIP zinc importers with their known subcellular localisations and functions in mammals

Gene name	Protein name	Subfamily	Gene ID	Chromosomal location	No. of exon	MIM No.	Length (Amino acid)	MW (kDa)	Gene expression	Subcellular localisation	Functions	References
SLC39A1	ZIP1	ZIPI	27173	1q21.3	7	604740	324	34.25	Prostate, small intestine, liver, kidney pancreatic α cells, lymphocytes	Plasma membrane, endoplasmic reticulum	Zn^{2+} uptake	(Lioumi et al., 1999; Gaither and Eide, 2001; Milon et al., 2001; Dufner-Beattie et al., 2003; Franklin et al., 2003; Gyulkhandanyan et al., 2008; Costello et al., 2011; Giacconi et al., 2012)
SLC39A2	ZIP2	ZIPI	29986	14q11.2	4	612166	309	32.74	Liver, ovary, prostate, uterine, skin, ectocervix, epithelial cells	Plasma membrane	Zn^{2+}, Co^{2+}, Cd^{2+}, Cu^{2+}, Mn^{2+} uptake	(Gaither and Eide, 2000; Cao et al., 2001; Gaither and Eide, 2001; Dufner-Beattie et al., 2003; Peters et al., 2007; Giacconi et al., 2012; Inoue et al., 2014)
SLC39A3	ZIP3	ZIPI	29985	19p13.3	3	612168	314	33.60	Testis, secretory mammary cells, pancreatic cells, lymphocytes	Plasma membrane	Zn^{2+} uptake	(Dufner-Beattie et al., 2003; Dufner-Beattie et al., 2005; Kelleher and Lonnerdal, 2005; Kelleher et al., 2009; Costello et al., 2012; Giacconi et al., 2012)
SLC39A4	ZIP4	LIV-1	55630	8q24.3	12	607059	647	68.41	Small intestine, stomach, colon, cecum, kidney, jejunal mucosa, pancreatic β-cells, enterocytes and endoderm cells	Plasma membrane	Zn^{2+} uptake	(Kury et al., 2002; Wang et al., 2002; Dufner-Beattie et al., 2003; Dufner-Beattie et al., 2003; Dufner-Beattie et al., 2004; Kim et al., 2004; Gyulkhandanyan et al., 2008)
SLC39A5	ZIP5	LIV-1	283375	12q13.3	13	615946	540	56.46	Liver, kidney, pancreas, spleen, colon, acinar cells enterocytes, visceral endoderm cells	Plasma membrane	Zn^{2+} uptake	(Dufner-Beattie et al., 2004; Wang et al., 2004)

SLC39A6	ZIP6	LIV-1	25800	18q12.2	11	608731	755	85.05	Testis, breast, prostate, placenta, kidney, pituitary and corpus callosum, endometrium, pancreatic β-cells	Plasma membrane	Zn^{2+} uptake	(Taylor et al., 2003; Bellomo et al., 2011; Croxford et al., 2011; Kong et al., 2014; Liu et al., 2015)
SLC39A7	ZIP7	LIV-1	7922	6p21.32	8	601416	469	50.12	Brain, liver, skeletal muscle, adenohypophysis, pancreatic β cells	Golgi apparatus, endoplasmic reticulum	Transported Zn^{2+} into cytosol, Zn^{2+} signalling	(Huang et al., 2005; Taylor et al., 2008; Hogstrand et al., 2009; Bellomo et al., 2011; Myers et al., 2013; Liu et al., 2015)
SLC39A8	ZIP8	LIV-1	64116	4q24	16	608732	460	49.63	Lung, liver, thymus, pancreas, placenta, spleen, testis, ovary, small intestine, colon, heart, leukocyte, lung epithelial cells, polarized cells	Plasma membrane, lysosome, endosome	Zn^{2+}, Cd^{2+}, Mn^{2+} $HSeO_3^-$ (selenite ion) uptake	(Begum et al., 2002; He et al., 2006; Girijashanker et al., 2008; Ryu et al., 2008; Croxford et al., 2011; Napolitano et al., 2012; Liu et al., 2013; Kim et al., 2014)
SLC39A9	ZIP9	ZIPII	55334	14q24.1	9	NA	307	32.25	Prostate, testis, breast etc. but highest in testis widely found in human tissues	Plasma membrane, Golgi apparatus	Regulate cytosolic Zn^{2+}	(Wang et al., 2008; Matsuura et al., 2009; Taniguchi et al., 2013; Thomas et al., 2014)
SLC39A10	ZIP10	LIV-1	57181	2q32.3	17	608733	831	94.13	Testis, kidney, breast, pancreas, dorsolateral prefrontal cortex, pancreatic α cells, red blood cells, hepatocytes, neuro 2A cells, B cells	Plasma membrane	Zn^{2+} uptake, transport Zn^{2+} into Sertoli cells and spermatocytes	(Kaler and Prasad, 2007; Pawan et al., 2007; Gyulkhandanyan et al., 2008; Ryu et al., 2008; Hogstrand et al., 2009; Croxford et al., 2011; Gumulec et al., 2011; Lichten et al., 2011; Kong et al., 2014; Miyai et al., 2014)
SLC39A11	ZIP11	gufA	201266	17q24.3-q25.1	21	616508	342	35.40	Mammary gland, testis, stomach, cecum, ileum, kidney, liver, jejunum, duodenum, pancreas, parietal cells of stomach	Nucleus, Golgi apparatus	Zn^{2+} uptake, maintaining mucosal integrity and function	(Kelleher et al., 2012; Martin et al., 2013; Yu et al., 2013)

SLC39A12	ZIP12	LIV-1	221074	10p12.33	13	608734	691	76.67	Brain, eye, lung, liver, skeletal muscle, small intestine, kidney, heart and pancreas, neurons, endothelial cells, smooth muscle and interstitial cells	Plasma membrane	Zn^{2+} uptake, neurulation and neuronal differentiation	(Nagase et al., 1999; Chowanadisai et al., 2013; Zhao et al., 2015; Bafaro et al., 2017)
SLC39A13	ZIP13	LIV-1	91252	11p11.2	13	608735	371	39.01	Kidney, skeletal and connective tissues, retinal pigment epithelial cell line, osteoblasts	Golgi body, endoplasmic reticulum	Transport Zn^{2+} into cytosol	(Fukada et al., 2008; Leung et al., 2008; Bin et al., 2011; Jeong et al., 2012)
SLC39A14	ZIP14	LIV-1	23516	8p21.3	16	608736	492	54.21	Duodenum, jejunum, liver, heart, kidney, white adipose tissue, skeletal muscle, spleen, pancreas, osteoblasts, pancreatic α cells, MDCK cells	Plasma membrane, mitochondria, endosome, lysosome	Zn^{2+}, Mn^{2+} and non-transferrin bound iron uptake	(Nomura et al., 1994; Taylor et al., 2003; Taylor et al., 2005; Liuzzi et al., 2006; Girijashanker et al., 2008; Gyulkhandanyan et al., 2008; Zhao et al., 2010; Hojyo et al., 2011; Hendrickx et al., 2018; Mukhopadhyay, 2018)

SLC stands for solute carrier, *SLC39A1-14* members of *SLC39A* family, MIM stands for online mendelian inheritance in man (OMIM), MW for molecular weight, kDa for Kilo Dalton, Zn^{2+} for zinc ion, Co^{2+} for cobalt ion, Cd^{2+} for cadmium ion, Cu^{2+} for copper ion, Mn^{2+} for manganese ion.

The structure of a bacterial ZnT homolog YiiP determined by cryoelectron and X-ray crystallography offers important mechanistic information about the ZnT family's action in zinc transport (Bin et al., 2018). YiiP is a homodimer that has six transmembrane (TM) helices with a helical bundle formed with TM1, TM2, TM4 and TM5 (Lu and Fu, 2007; Lu et al., 2009; Coudray et al., 2013). Three highly preserved aspartic acid residues (D) and one conserved histidine (H) in the helical bundle of TM2 and TM5 tetrahedrally co-ordinate a Zn^{2+} (Lu and Fu, 2007). This DD-HD zinc-binding site is crucial for transport activity and metal ion selectivity, as shown by mutagenesis experiments (Wei and Fu, 2005; Lu and Fu, 2007; Hoch et al., 2012; Lehvy et al., 2019). The zinc binding-induced re-orientation of TM5 drives conformational switching (Gupta et al., 2014). Thus, a paradigm for Zn^{2+} transportation via mammalian ZnT is provided by the bacterial YiiP structure. Mammalian ZnTs are believed to have six TM helices, a hallmark metal-binding site in TM2 and TM5, and to serve as Zn^{2+}/H^{+} exchangers, just as DD-HD sites in bacterial homolog proteins (Ohana et al., 2009; Shusterman et al., 2014). The bacterial DD-HD site permits the transport of Zn^{2+} and Cd^{2+}, whereas the ND-HD site in ZnT10 of humans confers Mn^{2+} specificity (Zogzas et al., 2016). Thus, the HD-HD motif is important for the Zn^{2+} specificity of ZnT. Human ZnT has a large cytoplasmic C-terminal domain which is associated with ZnT dimerization like bacterial ZnT dimerization (Salazar et al., 2009). ZnT1, ZnT2, ZnT3, ZnT4 and ZnT5 have YX(XX)(E/D) motif for the formation of homodimer (Fukunaka et al., 2009; Salazar et al., 2009; Golan et al., 2015). As the ZnT proteins which do not have YX(XX)(E/D) motif, they form heterodimer, for example ZnT6 forms heterodimer with ZnT5 by numerous C-terminal tyrosine residues (Golan et al., 2015).

All ZnT members (ZnT1-10) are believed to be structurally similar, but they are different in expression profiles in tissues, subcellular organelles, molecular functions, lengths of protein sequences as well as molecular masses (Bafaro et al., 2017; Bin et al., 2018), as shown in **Table 1.2**. Their encoding genes (*SLC30A1-10*) are also localised in different chromosomes. ZnTs show a wide range of biological functions including Zn^{2+}, Mn^{2+} or Cd^{2+} transportations and in causing different diseases (**Table 1.2**, **Table 1.3**) such as cancers (Lehvy et al., 2019) and diabetes (Murgia et al., 2009; Nicolson et al., 2009).

Table 1.2 ZnT zinc exporters with their known subcellular localisations and functions in mammals

Gene name	Protein name	Gene ID	Chromosomal location	No. of exon	MIM No.	Length (Amino acid)	MW (kDa)	Gene expressions	Subcellular localisation	Functions	References
SLC30A1	ZnT1	7779	1q32.3	2	609521	507	55.30	Brain, liver, intestine, breast, epithelial cells, enterocytes, pancreatic acinar cells, renal tubular cells	Plasma membrane, Golgi body, nuclear membrane, cytoplasm, intracellular vesicles	Removal Zn^{2+} from cytoplasm	(Palmiter and Findley, 1995; McMahon and Cousins, 1998; Sekler et al., 2002; Cousins et al., 2006; Lazarczyk et al., 2008; Dutta et al., 2011)
SLC30A2	ZnT2	7780	1p36.11	8	609617	372	40.56	Breast, prostate, intestine, kidney, testis, pancreas, retina	Plasma membrane, vesicles, lysosome, endosome, cytoplasm	Transported Zn^{2+} into milk-containing vesicles and lysosomes, Zn^{2+} secretory pathway in breast and prostate	(Palmiter et al., 1996; McMahon and Cousins, 1998; Ranaldi et al., 2002; Palmiter and Huang, 2004; Falcon-Perez and Dell'Angelica, 2007; Schroder et al., 2007; Kirschke and Huang, 2008; Leung et al., 2008; Lopez and Kelleher, 2009; Guo et al., 2010; Lee et al., 2015)
SLC30A3	ZnT3	7781	2p23.3	12	602878	388	41.95	Brain, pancreas, testis, breast, epithelial cells (breast), neurons	Vesicles, endosome, lysosome	Zn^{2+} transportation into synaptic vesicles	(Palmiter et al., 1996; Palmiter et al., 1996; Wenzel et al., 1997; McMahon and Cousins, 1998; Cole et al., 1999; Michalczyk et al., 2002; Falcon-Perez and Dell'Angelica, 2007; Gyulkhandanyan et al., 2008)
SLC30A4	ZnT4	7782	15q21.1	11	602095	429	47.48	Breast, brain, placenta, prostate, kidney, putamen	Plasma membrane, endosome, secretory vesicles, lysosome, trans-Golgi network (TGN), cytoplasm	Zn^{2+} transportation into mast cell and milk vesicles, Zn^{2+} secretion pathway in breast	(Huang and Gitschier, 1997; McMahon and Cousins, 1998; Michalczyk et al., 2002; Ranaldi et al., 2002; Asano et al., 2004; Seve et al., 2004; Falcon-Perez and Dell'Angelica, 2007; Kirschke and Huang, 2008; McCormick and Kelleher, 2012)

SLC30A5	ZnT5	64924	5q13.1-q13.2	16	607819	765	84.05	Heart, placenta, prostate, ovary, testis, thymus, bone, liver, kidney, brain, skin, T-cells, pancreatic beta cells	Plasma membrane, vesicles, nuclear membrane, Golgi apparatus, secretary granules	Zn^{2+} transportation into Golgi body and vesicles	(Inoue et al., 2002; Kambe et al., 2002; Asano et al., 2004; Seve et al., 2004; Jackson et al., 2007; Kirschke and Huang, 2008)
SLC30A6	ZnT6	55676	2p22.3	19	611148	461	51.12	Brain, lung, intestine, kidney, colon, eye, bone, cervix, ear, heart, muscle, pancreas, prostate, skin, stomach and testis, B-cells	Vesicles, Golgi apparatus	Zn^{2+} transportation into Golgi apparatus and vesicles	(Huang et al., 2002; Seve et al., 2004)
SLC30A7	ZnT7	148867	1p21.2	14	611149	376	41.63	Breast, heart, liver, spleen, small intestine, kidney, brain, lung, ovary, prostate, stomach, retina, muscle and testis	Plasma membrane, Golgi body, vesicles, cytoplasm	Zn^{2+} transportation into Golgi body	(Kirschke and Huang, 2003; Asano et al., 2004; Seve et al., 2004)
SLC30A8	ZnT8	169026	8q24.11	13	611145	369	40.76	Pancreas, adrenal gland, thyroid, testis, beta cells of islet of Langerhans	Secretory granules	Accumulates Zn^{2+} in intracellular vesicles and Golgi body	(Chimienti et al., 2004; Chimienti et al., 2005; Chimienti et al., 2006; Murgia et al., 2009)
SLC30A9	ZnT9	10463	4p13	18	617595	568	63.52	Brain, muscle, kidney, thymus, forebrain, foetus, skeletal muscle	Endoplasmic reticulum, cytoplasmic vesicles, nucleus, plasma membrane, cytoplasm	Unknown	(Sim and Chow, 1999; Perez et al., 2017)
SLC30A10	ZnT10	55532	1q41	6	611146	485	52.68	Small intestine, liver, testes, brain, ovary, colon, cervix, prostate, placenta, foetal brain and liver	Golgi body, endosomes, plasma membrane	Efflux Mn^{2+}	(Seve et al., 2004; Bosomworth et al., 2012; Zhao et al., 2016; Mercadante et al., 2019)

SLC stands for solute carrier, *SLC30A1-10* members of *SLC30A* family, MIM denotes online mendelian inheritance in man (OMIM), kDa for Kilo Dalton.

1.4.2 Metallothioneins

Mammalian metallothionein (MT) proteins are intracellular, metal-binding and low molecular weight (<7 kDa) proteins. They can bind 5-15% of cytosolic Zn^{2+} (Coyle et al., 2002; Kambe et al., 2015). MT protein consists of 61-68 amino acid residues in length with highly conserved 18-23 cysteine residues (about one-third). Each MT protein can coordinate seven Zn^{2+} ions (Coyle et al., 2002; Kambe et al., 2015). MT proteins are divided into four classes, MT1, MT2, MT3 and MT4. Among 17 *MT* genes, the cluster of at least 10 genes is observed on chromosome 16 that encode different isoforms of MT in human. MT1 (*MT1*) isoforms are encoded by eight genes (*MT1A*, *MT1B*, *MT1E*, *MT1F*, *MT1G*, *MT1H*, *MT1M* and *MT1X*), whereas other isoforms MT2A, MT3 and MT4 are encoded by a single particular gene *MT2A*, *MT3* and *MT4*, respectively, in human (Coyle et al., 2002; Kimura and Kambe, 2016). Importantly, numerous studies in a multitude of human cancers including breast and prostate cancers have shown the dysregulations of MT gene/protein expression (Garrett et al., 2000; Sens et al., 2001; Tai et al., 2003; Prueitt et al., 2008; Si and Lang, 2018; Barman et al., 2022; Li et al., 2022; Liu et al., 2022; Zhang and Liu, 2022), which indicates the remarkable participation of MT proteins in progression of cancers. As MT proteins are the part and parcel of zinc homeostasis network, dysregulation of MT expression also means the disruption of cellular Zn^{2+} homeostasis.

1.5 Dysregulation of Zn^{2+} homeostasis in cancers

Zn^{2+} dysregulation is well-documented in different human cancers (Sauer et al., 2020; Wang et al., 2020; Rusch et al., 2021). **Table 1.3** describes Zn^{2+} dysregulation and the ZIP/ZnT which are likely associated with the Zn^{2+} dyshomeostasis in various cancers. For example, high zinc accumulation in breast cancer cells is likely due to overexpressed ZIP6 and ZIP10 (Bafaro et al., 2017), while significant zinc reduction is observed in prostate cancer cells because of down-regulation or loss of ZIP1, ZIP2, ZIP3 (Franklin et al., 2005; Desouki et al., 2007). Thereby, cancer progression is connected to the intracellular Zn^{2+} level which is in turn linked to ZIP/ZnT expressions (Wang et al., 2020) or other regulators (Lehvy et al., 2019). Thus, ZIP and ZnT are critical for Zn^{2+} homeostasis and cancer development (Franklin and Costello, 2009; Franz et al., 2013; Bafaro et al., 2017).

Table 1.3 Disrupted zinc homeostasis in human cancers

Type of cancers	Levels of zinc in serum	Levels of zinc in tissues	Reported ZIP/ZnT related to the cancers
Breast cancer	Decreased (Sarita et al., 2012; Gumulec et al., 2014; Wang et al., 2020)	Increased (Gumulec et al., 2014; Wang et al., 2020)	ZIP6, ZIP7, ZIP9, ZIP10, ZnT2 (Jordan, 2003; Tozlu et al., 2006; Kagara et al., 2007; Taylor et al., 2008; Johnston, 2010; Lopez et al., 2011; Taylor et al., 2012; Thomas et al., 2014)
Prostate cancer	Decreased (Gumulec et al., 2014)	Decreased (Gumulec et al., 2014; Wang et al., 2020)	ZIP1, ZIP2, ZIP3, ZIP4, ZIP9, ZnT4 (Franklin et al., 2005; Johnson et al., 2010; Franz et al., 2013; Singh et al., 2016; Wang et al., 2020)
Lung cancer	Decreased (Diez et al., 1989; Gumulec et al., 2014; Wang et al., 2020)	Increased (Mulay et al., 1971)	ZIP4 (Wu et al., 2017)
Pancreas cancer	Not reported	Decreased (Costello et al., 2011; Wang et al., 2020)	ZIP3, ZIP4, ZIP6 (Li et al., 2007; Unno et al., 2009; Costello et al., 2011; Franklin et al., 2014; Xu et al., 2014)
Liver cancer	Insignificant change (Gumulec et al., 2014)	Decreased (Gumulec et al., 2014)	ZIP4, ZIP5, ZIP6, ZIP7, ZIP14, ZnT7, ZnT9 (Gaetke et al., 1997; Liuzzi et al., 2005; Aydemir et al., 2012; Aydemir et al., 2012; Franklin et al., 2012; Shen et al., 2013; Sun et al., 2014; Guthrie et al., 2015; Kim et al., 2017; Gartmann et al., 2018)
Esophagus cancer	Decreased (Gumulec et al., 2014)	Insignificant change (Gumulec et al., 2014)	ZIP5 (Li et al., 2016), ZIP6 (Wu et al., 2013)
Stomach cancer	Decreased (Gumulec et al., 2014)	Decreased (Margalioth et al., 1983; Reddy et al., 2003; Christudoss et al., 2010; Gumulec et al., 2014)	Not reported
Colon cancer	Insignificant change (Gumulec et al., 2014)	Insignificant change (Gumulec et al., 2014)	ZIP6, ZIP7, ZIP9, ZIP10, ZIP11, ZnT5, ZnT6, ZnT7, ZnT10 (Barresi et al., 2018)
Kidney cancer	Not reported	Decreased (Margalioth et al., 1983; Gumulec et al., 2014; Wang et al., 2020)	ZIP1, ZIP10 (Dong et al., 2014; Pal et al., 2014)
Bladder cancer	Decreased (Mao and Huang, 2013; Gumulec et al., 2014; Wang et al., 2020; Uddin and Wang, 2022)	Not reported	ZIP11 (Wu et al., 2015), ZnT1 (Liu et al., 2018)
Ovary cancer	Decreased (Kazi et al., 2007; Wang et al., 2020)	Decreased (Wang et al., 2020)	ZIP4 (Fan et al., 2017)
Cervix cancer	Decreased (Xie et al., 2018) (Wang et al., 2020)	Decreased (Wang et al., 2020)	ZIP6 (Zhao et al., 2007), ZIP7 (Wei et al., 2017)
Skin cancer	Decreased (Tasaki et al., 1993)	Not reported	ZIP13 (Lee et al., 2019)

1.5.1 Breast cancer and Zn^{2+}

The adult female breast consists of lobules, alveoli, ducts, fats, connective tissues as well as lymphatic vessels for draining excess fluid (**Figure 1.2**). Zn^{2+} plays critical roles in the development, functionality and remodelling during pre-lactation and post-lactation of the mammary glands (Kelleher et al., 2011). Hence, Zn^{2+} homeostasis is crucial for maintaining the health of the mammary cells, while disruption of Zn^{2+} homeostasis might lead to breast cancer (Taylor et al., 2012; Chandler et al., 2016) and other diseases such as transient neonatal zinc deficiency (Golan et al., 2017). Previous studies reported higher intracellular Zn^{2+} in malignant breast cells/tissues compared to the normal counterparts, and further investigations found the association of ZIP/ZnT with the elevated intracellular Zn^{2+} levels in breast cancer cells (**Table 1.3**) (Wang et al., 2020; Rusch et al., 2021). Also, the development of breast cancers depends on multiple factors including family history, age, hormonal level (e.g., estrogen), genetic alterations as well as unhealthy lifestyle. Based on the presence or absence of progesterone receptor (PR), estrogen receptor (ER) and epidermal growth factor receptor 2 (HER2), breast cancers are classified into four subtypes, luminal A ($ER^+/PR^+/HER2^-$), luminal B ($ER^+/PR^+/HER2^+$), basal ($ER^-/PR^-/HER2^-$) and HER2 enriched ($ER^-/PR^-/HER2^+$) (Chandler et al., 2016). These subtypes are different in incidence, severity, response to therapy and intracellular Zn^{2+} levels (Millikan et al., 2008; Parker et al., 2009; Prat and Perou, 2011; Chandler et al., 2016).

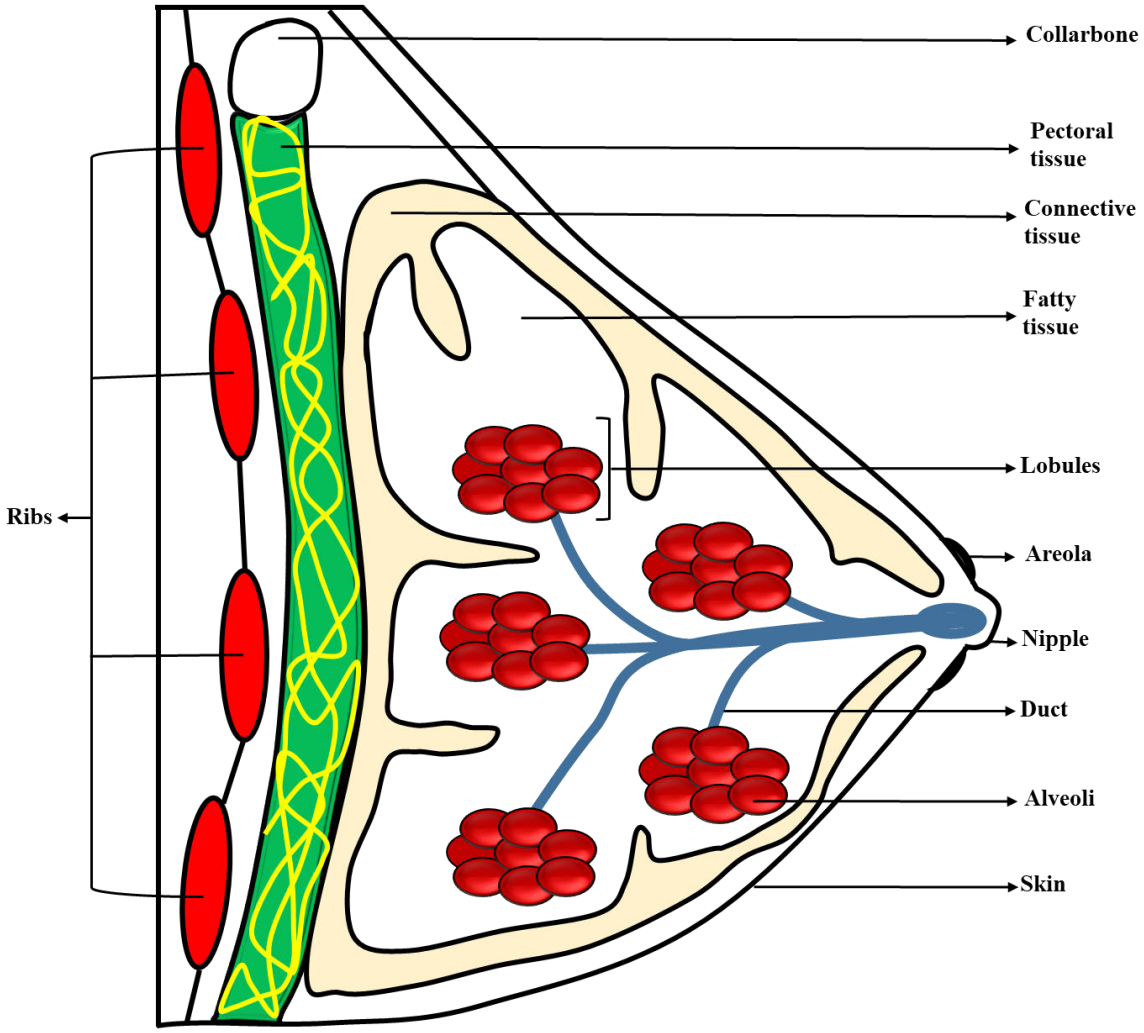

Figure 1.2 Female breast anatomy. The breast consists of lobules, ducts, fats, connective tissues, alveoli. Alveoli constitute a lobule and the lobules are linked to each other by the ductal networks.

ZIP importer proteins are the key players for zinc uptake in breast. For example, ZIP6, encoded by an estrogen-regulated *SLC39A6* gene, is localised in the plasma membrane for maintaining Zn^{2+} homeostasis via importing Zn^{2+} into mammary epithelial cells from blood plasma (MacDonald, 2000; Kelleher et al., 2009). The proliferation of breast cancer cells often depends on estrogen responsiveness. Since ~70% breast cancer patients was showed to have estrogen receptor α in their malignant mammary tissues, the expression level of estrogen receptor (ER) is considered for the therapeutic strategy of breast cancer (Selli et al., 2016). Experimental evidence demonstrated a positive correlation between ZIP6 up-regulation with oestrogen receptor α expression in breast carcinoma tissues (Schneider et al., 2006; Tozlu et al., 2006). Up-regulation of ZIP6 was observed in MCF-7 and ZR-75 breast cancer cells when they were treated with estrogen (Manning et al., 1988; El-Tanani and Green, 1997). Elevated ZIP6 showed positive relationship with metastasis in breast cancer (Alam and Kelleher, 2012).

Signal transducer and activator of transcription 3 (STAT3) is reported to regulate ZIP6 expression (Yamashita et al., 2004). Epidermal growth factor (EGF) has been reported to initiate epithelial-to-mesenchymal transition (EMT), a vital feature of malignancy, through STAT3 dependent up-regulation of ZIP6 (Hogstrand et al., 2013). However, the positive relationship between up-regulation of ZIP6 and breast cancer development and metastasis was questioned by the other findings. For example, ZIP6 attenuation resulted in lower intracellular Zn^{2+} pool in estrogen receptor positive ductal breast tumour cells (T47D) which consequently raised mitochondrial membrane potential along with decreasing apoptosis (Lopez and Kelleher, 2010). The same authors demonstrated that such reduced apoptosis significantly elevated breast cancer cell colony formation and that the decreased ZIP6 level was associated with lowering E-cadherin expression, hence promoting epithelial-to-mesenchymal transition (EMT) of ductal breast cancer cells (Shen et al., 2009; Lopez and Kelleher, 2010). These findings directly contradict the notion that overexpression of ZIP6 leads to the increase of intracellular zinc level and the development or metastasis of breast cancer.

A ZIP family member, ZIP7 and protein kinase CK2 were linked in a study of breast cancer cells (Taylor et al., 2008). Protein kinase CK2 phosphorylates Ser^{275} and Ser^{276} residues in ZIP7 to activate its gated release of Zn^{2+} from endoplasmic reticulum (ER) into cytoplasm in breast cancer cells (Taylor et al., 2012; Nimmanon et al., 2017). The resultant elevated cytoplasmic Zn^{2+} inactivates the phosphatase, which in turn accelerates tyrosine kinase Akt and extracellular regulated kinase 1/2 signalling pathways for cancer development and invasion (Taylor, 2008; Taylor et al., 2008; Taylor et al., 2012).

ZIP10 is another zinc importer involved in invasion and metastasis of breast cancer cells. Breast cancer tissues collected from the patients with lymph node metastasis showed higher ZIP10 mRNA level compared to non-metastatic tissues (Kagara et al., 2007). Furthermore, ZIP10 gene expression was significantly higher in metastatic breast cancer cell lines (MDA-MB-231 and MDA-MB-435S) than less metastatic breast cancer cell lines (MCF-7, T47D, ZR75-1 and ZR75-30) (Kagara et al., 2007). ZIP10 and ZIP6 can form a heterodimeric complex that provides novel histidine-rich cytoplasmic loops as a novel scaffold for binding glycogen synthase kinase-3 (GSK3) which in turn phosphorylates neuronal cell adhesion molecule 1 (NCAM1) to regulate epithelial-to-mesenchymal transition for cancer progression (Taylor et al., 2016; Brethour et al., 2017). Breast cancer cell migration induced by high glucose was inhibited by knockdown of ZIP10 and ZIP6 (Takatani-Nakase, 2013; Takatani-Nakase et al.,

2014). Zn^{2+} influx through ZIP6-ZIP10 heterodimer triggers mitosis for cell division (Nimmanon et al., 2021), thereby contributing to breast cancer progression.

X-ray analysis revealed Zn^{2+} hyper-accumulation of the periphery in luminal tumours while Zn^{2+} was disseminated identically in basal tumours (Chandler et al., 2016). Such distinctive intracellular Zn^{2+} distribution might be connected to the expression of Zn^{2+} transporter proteins. Overexpressed ZnT2 in luminal breast cancer cells is needed (Lopez et al., 2011), in contrast to basal breast cancer cells such as MDA-MB-231 cells which do not have functional ZnT2 due to proteasomal degradation (Chandler et al., 2016). Therefore, subtypes of breast cancer cells have specific mode of intracellular Zn^{2+} accumulation, which contributes to phenotypic differences in malignant breast cancer cells. In addition, ZnT2 acts as an auxiliary Zn^{2+} importer into mitochondria for regulating mitochondrial Zn^{2+}, and thereby, ZnT2 participates in bioenergetics and apoptosis of mammary epithelial cells (Seo et al., 2011). Also, ZnT2 is critically important for normal structural development and function of the mammary gland (Lee et al., 2015) and for enriching Zn^{2+} in breast milk (Chowanadisai et al., 2006). The mutation such as loss-of-function mutation in ZnT2 gene (*SLC30A2*) limits Zn^{2+} secretion into breast milk which in turn causes transient neonatal zinc deficiency in the babies (Golan et al., 2017). Hence, the accumulated evidence demonstrates the importance of zinc transport proteins ZIP and ZnT in breast cancer development and metastasis.

1.5.2 Prostate cancer and Zn^{2+}

The prostate gland consists of three zones, transition (5%), peripheral (70%) and central (25%) zones (**Figure 1.3**) (McNeal, 1988; Kumar and Majumder, 1995). Based on histological views, this largest exocrine gland shows central zone and peripheral zone, and the peripheral zone is mainly associated with secreting prostatic fluids (Kumar and Majumder, 1995). Exceptionally high intracellular Zn^{2+} and citrate accumulation is the special feature of the healthy prostatic epithelial cells (Costello et al., 2005; Costello and Franklin, 2016). Zn^{2+} concentrations in the most of mammalian cells are ~100-500 µM, whereas prostatic secretory epithelial cells contain ~800-1500 µM Zn^{2+} (Costello et al., 2011; Costello and Franklin, 2016). Most cells are prone to distributing ~40% of total intracellular Zn^{2+} in their mitochondria. The prostatic mitochondrial Zn^{2+} concentration is ~20 fold greater compared to the other cell's mitochondrial Zn^{2+} concentration, since prostate epithelial cells contain much higher intracellular Zn^{2+} (Liu et al., 1997). It is found that secretory prostate epithelial cells contain a distinctively expressed

Zn^{2+} importer ZIP1, which functions in accumulating elevated amount of Zn^{2+} to endow prostatic health (Costello et al., 1999). High intracellular Zn^{2+} inhibits mitochondrial aconitase (m-aconitase) and thereby the conversion of citrate into iso-citrate is reduced, and the TCA (tricarboxylic acid) cycle is in turn decreased and less energy is generated (**Figure 1.4**) (Feng et al., 2002; Costello and Franklin, 2016). The activity of terminal oxidation by TCA cycle and electron transport chain in prostate mitochondria is 50% lower than that of mitochondria in liver (Costello et al., 1976; Costello and Franklin, 2016). Thus, hyper-accumulation of citrates happens in prostate and the citrates are secreted into the prostatic fluids. Such citrate producing cells of the normal human prostate have been characterised as "high aerobic glycolysis, but low respiring" (Huggins, 1947; Costello and Franklin, 2016).

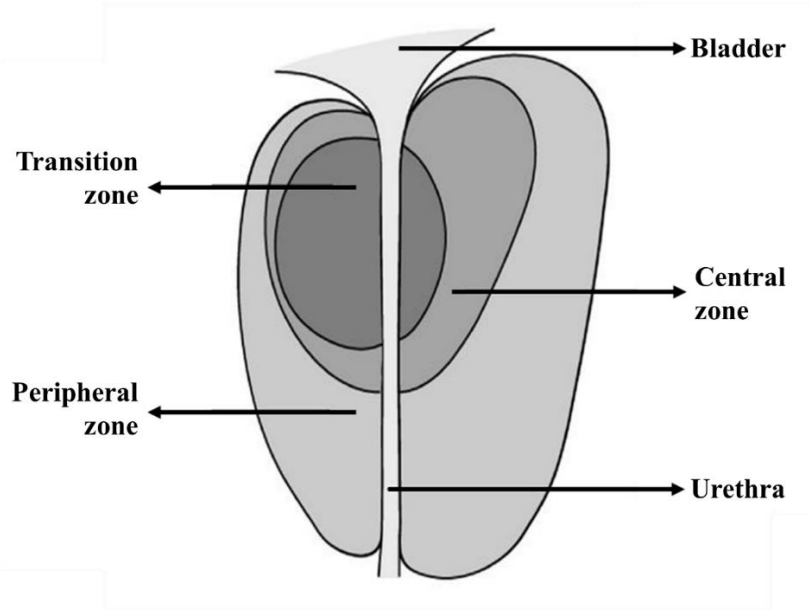

Figure 1.3 Prostate gland anatomy of male. The exocrine gland, prostate, has three zones, central, peripheral and transitional. The peripheral zone secretes prostatic fluids for maintaining the glandular health.

High intracellular Zn^{2+} concentration indicates healthy prostate whereas low intracellular Zn^{2+} concentration is the hallmark of prostate cancer. Interestingly, Zn^{2+} uptake was stimulated by prolactin and testosterone in prostate cancer cells (PC3, LNCaP) (Costello et al., 1999), suggesting Zn^{2+} transport activity can be modulated by hormonal treatment for Zn^{2+} accumulation (Franklin et al., 2003). ZnT1, a member of ZnT family, is the predominant Zn^{2+} exporter localised in plasma membrane of the cells (McMahon and Cousins, 1998; Lichten and Cousins, 2009). Marked up-regulation of ZnT1 gene was observed in prostate cancer tissues compared to the benign counterpart of European American populations, whereas there was no

difference between cancerous and normal prostate tissues in the context of gene expression of African American people (Singh et al., 2016). The expression level of ZnT1 was reported as significantly high in most prostate cancer tissue samples (Beck et al., 2004). Though overexpression of ZnT1 was observed in prostatic tumours, but strongly down-regulated in all the cultured prostate cancer cell lines tested in the study (Singh et al., 2016). Intriguingly, it is found that ZnT1 showed extremely high rates of loss-of-function mutations in prostate cancer as compared to healthy controls (Lehvy et al., 2019). Therefore, overexpression of mutated ZnT1 would not reduce intracellular zinc levels, and the low intracellular Zn^{2+} of prostate cancer cells is more related to the reduced expression of ZIP importers because, previous studies demonstrate that the lack of ZIP1 expression is the key reason for the markedly reduced intracellular Zn^{2+} concentration in prostatic malignant cells (Franklin et al., 2005).

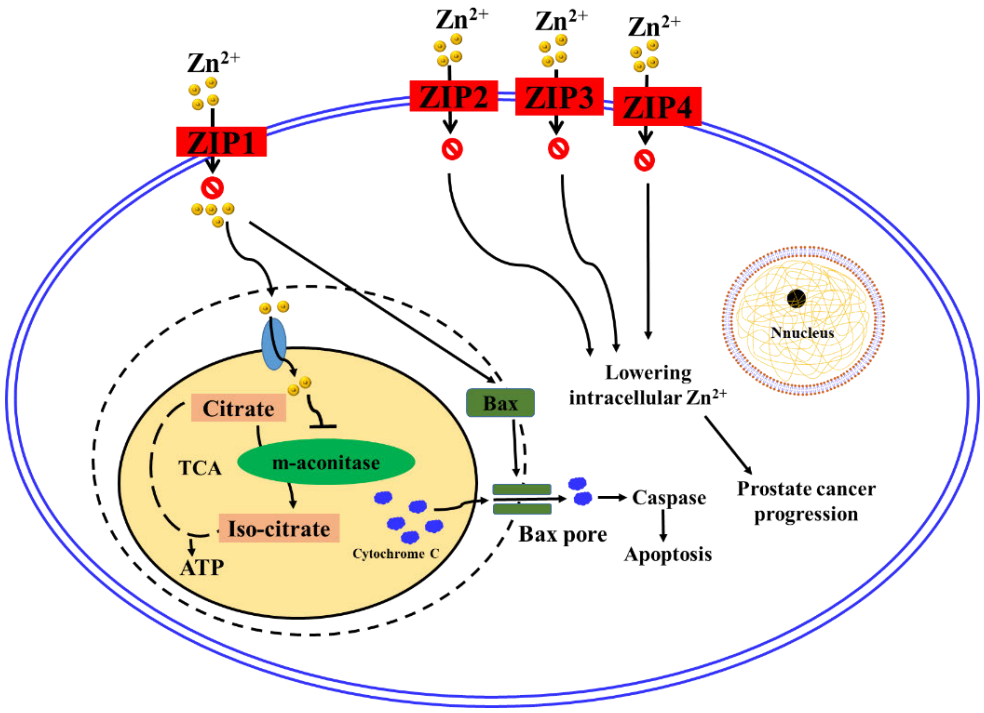

Figure 1.4 Roles of Zn^{2+} and its transporter proteins in healthy and cancerous prostate cells. ZIP1 is the principal importer Zn^{2+} into cells for maintaining cellular Zn^{2+}. In normal prostatic cells, cytoplasmic Zn^{2+} ions are transported into mitochondria where the high Zn^{2+} concentration inhibits mitochondrial aconitase (m-aconitase), an enzyme catalysing the conversion of citrate into iso-citrate, and thereby truncates Krebs cycle to limit energy generation. In addition, elevated Zn^{2+} induces Bax for forming Bax pore in outer mitochondrial membrane through which cytochrome C is released into cytosol in order to react with caspase for modulating apoptosis. Thus, citrate accumulation and limiting energy generation endow prostatic health. Contrastingly, in prostatic cancer cells, Zn^{2+} transport is disrupted due to lack of ZIP1 expression, and the intracellular Zn^{2+} concentration is reduced remarkably compared to the healthy prostatic epithelial cells. Therefore, the inhibition of m-aconitase is no longer present, Krebs cycle is not truncated anymore, leading to more energy generation and promoting cell proliferation.

ZIP1 is a key Zn^{2+} importer in the plasma membrane which is absent or down-regulated in prostate cancerous tissues compared to normal counterparts (Franklin et al., 2005; Johnson et al., 2010). Study on transgenic adenocarcinoma of mouse prostate (TRAMP) model showed loss of ZIP1 together with strikingly decreased Zn^{2+} and citrate levels in TRAMP tumour (Costello et al., 2011). Similarly, prostate cancer cell lines also exhibit low expression of ZIP1 (Huang et al., 2006). Thereby ZIP1 is most likely involved in prostate cancer development, but the regulation of ZIP1 expression is still unclear. Further investigations found that overexpression of Ras-responsive element binding protein 1 (RREB1), a Zn^{2+} finger transcription factor was involved in down-regulating ZIP1 at both gene and protein levels (Milon et al., 2010; Zou et al., 2011). RREB1 is up-regulated during prostate cancer progression and it also acts as a downstream effector in Ras signalling pathways.

ZIP2 and ZIP3 are expressed abundantly in the apical membrane of the epithelial cells in normal and benign hyperplastic prostate. They are associated with Zn^{2+} re-uptake from prostatic fluids whereas ZIP1 is in basolateral membrane, responsible for Zn^{2+} uptake from extracellular environment such as microvasculature (Desouki et al., 2007). ZIP2 and ZIP3 were undetected in cancerous prostatic tissues (Desouki et al., 2007). Therefore, down-regulation or loss of ZIP1, ZIP2 and ZIP3 are responsible for lowering intracellular Zn^{2+} in malignant prostatic cells.

The water and the diets are highly enriched in minerals such as Zn^{2+} in Africa continent. It is believed that the Africans somehow (either genetic inheritance or aging) maintain lower Zn^{2+} absorption capacity otherwise they would develop neurodegenerative disorders due to more Zn^{2+} absorption. Further investigations revealed very low expression levels of ZIP1 and ZIP2 in prostatic cancerous tissues of African American males compared to age and Gleanson score-matched Caucasian males (Rishi et al., 2003). In addition, African Americans have lower ZIP2 expression than age-matched Caucasian healthy individuals. Therefore, it is likely that the low absorption capacity of Zn^{2+} due to lower expression of ZIP1 and ZIP2 renders African descendants highly predisposed to prostate cancer (Rishi et al., 2003).

ZIP3 was identified in the lysosome of RWPE-1 non-tumorigenic prostate cells, but it was not found in the same compartment of RWPE-2 tumorigenic prostate cells (Huang et al., 2006). Thus, Zn^{2+} from the lysosome could not be transported into the cytoplasm in prostate cancer cells (Huang et al., 2006). However, ZIP4 overexpression restrains invasion and proliferation of the prostate cancer cells (Chen et al., 2012), probably by increasing Zn^{2+} uptake.

ZnT2, localised in the membrane of vesicles such as lysosomes and endosomes, involves in compartmentalising Zn^{2+} to decrease cytoplasmic Zn^{2+} concentration (Palmiter et al., 1996). The significant decrease of ZnT2 mRNA was observed in prostate cancer cell lines whereas ZnT2 mRNA was undetectable in most human prostate cancer tissue samples (Singh et al., 2016). It suggests that prostate cancer cells are reluctant to store vesicular Zn^{2+} via ZnT2. However, a study demonstrated that ZnT2 gene expression in prostate gland might rely on individual's age as 21-fold increase of ZnT2 expression was reported in the prostates of aged rats compared to the prostates of young rats (Iguchi et al., 2011).

1.5.3 Zn^{2+} homeostasis and other cancers

The reduced intracellular Zn^{2+} in ductal and acinar epithelium cells is one of the main features of pancreatic cancer and thereby ZIP and ZnT are involved (**Table 1.3**). Both ZIP3 and Ras-responsive element binding protein 1 (RREB1) were down-regulated at the early stage of pancreatic cancer progression (Costello et al., 2011; Franklin et al., 2014). RREB1 acts as a positive modulator of ZIP3 gene expression and the down-regulation of RREB1 contributes to the silencing of ZIP3, resulting in lowering intracellular Zn^{2+} level. The significant up-regulation of ZIP4 gene was observed in 94% of human pancreatic cancerous tissues compared to normal adjacent tissues (Li et al., 2007). Thus, ZIP4 can serve as biomarker for diagnosing human pancreatic cancer (Xu et al., 2014; Jin et al., 2018). ZIP4 is localised in the plasma membrane of β-pancreatic cells and its overexpression is linked to the increase of pancreatic cell proliferation (Li et al., 2007; Li et al., 2009). Similarly, overexpression of ZIP4 led to 13-fold tumour growth by volume and 7.2-fold increase in primary tumour weight in the nude mice model with xenograft compared to normal control (Li et al., 2007; Li et al., 2009). Since ZIP4 has been recognised as an important player in pancreatic cancer development, numerous studies investigated how ZIP4 is involved in this cancer pathogenesis. ZIP4 overexpression led to elevation of IL-6 (interleukin 6) transcription via zinc finger transcription factor, cAMP response element-binding protein (CREB) to activate signal transducer and activator of STAT3 which in turn resulted in increased expression of cyclin D1 to achieve enhanced cell proliferation and tumour progression (Zhang et al., 2010). Up-regulated ZIP4 also enhances cancer progression by suppressing ZO-1 (zonula occludens-1) and claudin-1 (Liu et al., 2018).

A study conducted on the expression profiles of 14 ZIP and 10 ZnT observed the up-regulating propensity of ZIP and the down-regulating tendency of ZnT in lung cancer cell lines and malignant tissues (Huang et al., 2016). ZIP4 was overexpressed among the ZIP members in six lung cancerous cell lines as well as 59% malignant lung specimens, which is similar to the findings from cancer datasets including TCGA (Huang et al., 2016). Also, ZIP4 overexpression was significantly correlated with the increased tumour size, metastasis to regional lymph nodes and shorter overall survival (Wu et al., 2017). Reduced cellular Zn^{2+}, up-regulation of E-cadherin, down-regulation of the mesenchymal markers FSP-1 and N-cadherin were observed as the result of silencing ZIP4. Moreover, knockdown of ZIP4 accelerated cisplatin induced death of lung cancer cells, suggesting that ZIP4 may be an effective diagnostic marker and therapeutic target (Wu et al., 2017).

ZIP4 is also highly expressed in malignant liver tissues compared to normal counterparts, and its overexpression is strongly associated with the tumour sizes, recurrences and tumour metastatic stages in liver cancer (Xu et al., 2014). ZIP4 promotes the cancer cell migration and invasiveness through increasing the expression of pro-metastatic genes (MMP-2, MMP-9) and inhibiting pro-apoptotic gene expression (caspase-3, caspase-9, Bax) (Xu et al., 2014). ZIP6 showed the elevated expression in 61% hepatocellular carcinoma cases and hepatocellular carcinoma cell lines compared to normal adjacent liver tissues and normal cell line, respectively (Shen et al., 2013). Knockdown of ZIP6 expression inhibited liver cell proliferation *in vitro* along with decreasing the tumour size *in vivo* (Shen et al., 2013). The expression of cell adhesion protein such as E-cadherin is negatively related to ZIP6 expression in hepatocarcinoma cells (Hep-G2) (Shen et al., 2013) and thus ZIP6 might be involved in the EMT of liver cancer cells. The clinical relationship between low Zn^{2+} level and down-regulation of ZIP14 was established in developing liver cancer (Wright and Dormandy, 1972; Costello and Franklin, 2014). Down-regulation of ZIP14 leads to the reduced intracellular Zn^{2+} level and such low Zn^{2+} contents likely protect the liver cancer cells from tumour suppressor effects of Zn^{2+} (Franklin et al., 2012).

Zn^{2+} is dysregulated in oesophageal cancer patients (**Table 1.3**), indicating the involvement of ZIP/ZnT. Overexpression of ZnT7 and ZIP5 in cancerous oesophageal tissues compared to normal counterparts has been reported (Kumar et al., 2007). Similarly, oesophageal squamous cell carcinoma (ESCC) exhibited up-regulation of ZnT7. Knockdown of ZIP5 expression resulted in decreased COX2, cyclin D1 and E-cadherin expression which in turn led to inhibiting ESCC progression (Jin et al., 2015). The study revealed ZIP6 overexpression in oesophageal cancer cells and knockdown of ZIP6 suppresses cancer cell growth and invasion (Wu et al., 2013). Also, estrogen-regulated ZIP6 was up-regulated in the human cervical cancer cell line (HeLa) and tissues compared to their respective normal counterparts (Zhao et al., 2007). The knockdown of ZIP6 expression leads to decrease cell proliferation (Zhao et al., 2007) and thereby ZIP6 shows its association with cervical cancer.

Glioma is the common tumour of the central nervous system. Identification of specific biomarkers in glioma can simplify diagnosis, prognosis and treatment of the cancer. Overexpression of ZIP3, ZIP4, ZIP8, ZIP14, ZnT5, ZnT6, ZnT7 but lower expression of ZnT10 in gliomas grade IV compared to grade II are reported (Lin et al., 2013). Among all 24 Zn^{2+} transport proteins, ZIP4 is most significantly up-regulated and associated with high grade of

gliomas tumour (Lin et al., 2013). Another study investigated the expression profile of ZIP4, ZIP9, ZIP11, ZnT9 and the correlation of these ZIP/ZnT with isocitrate dehydrogenase 1 (IDH1) mutation (Kang et al., 2015), which is the biomarker of glioma (Parsons et al., 2008).

1.6 Zn^{2+} homeostasis and other diseases

Apart from cancers, dysregulations of Zn^{2+} and ZIP/ZnT are involved in various other human diseases and health complications as listed in **Table 1.4**. Those diseases could also trigger the development of cancers, such as diabetes increases the risks of breast cancer, colon cancer and pancreatic cancer (**Figure 1.5**).

ZnT8 in pancreatic α- and β-cells has been extensively studied in diabetes (Lemaire et al., 2009; Nicolson et al., 2009; Énée et al., 2012; Pound et al., 2012; Huang et al., 2019). ZnT8 expression and cellular Zn^{2+} of the β-cells were reduced in diabetic mice, suggesting the involvemnts of ZnT8 in insulin biosynthesis or release, and direct or indirect impairment of the β-cell functions (Yi et al., 2016; Huang et al., 2019). In addition, non-synonymous single nucleotide polymorphism (SNP), rs13266634 (a C/T polymorphism), which encodes either arginine (R) by the C allele or tryptophan (W) by the T allele at aa325 of the secretory granular ZnT8 (Sladek et al., 2007), was found to be associated with type 2 diabetes (T2DM) (Nicolson et al., 2009; Huang et al., 2019). This ZnT8 variant lowers the zinc transport acitivity of ZnT8, which can also behave as an autoantigen targeted by the autoimmune response in 60-80% of new cases of type 1 diabetes mellitus (T1DM) onset (Wenzlau et al., 2007; Nicolson et al., 2009; Singh et al., 2016).

Table 1.4 Associations of ZIP and ZnT in numerous non-cancerous diseases and health complications

Diseases/complications	Associated ZIP/ZnT	References
Alzheimer disease (AD)	ZnT1, ZnT3, ZnT4, ZnT6, ZnT7, ZnT10, ZIP1	(Lovell et al., 2005; Beyer et al., 2009; Lyubartseva et al., 2010; Zhang et al., 2010; Beyer et al., 2012; Bosomworth et al., 2013)
Prion disease	ZIP5, ZIP6, ZIP10	(Ehsani et al., 2011; Ehsani et al., 2011)
Parkinson	ZnT10	(Quadri et al., 2012)
Major depressive disorder (MDD)	ZnT1, ZnT3, ZnT4, ZnT5, ZnT6	(Rafalo-Ulinska et al., 2016)
Pulmonary hypertension	ZIP12	(Zhao et al., 2015)
Atherosclerosis	ZnT7	(Hartiala et al., 2014)
Carotid artery disease	ZIP2	(Giacconi et al., 2008)
Diabetes	ZnT3, ZnT8, ZIP4, ZIP14	(Wenzlau et al., 2007; Lemaire et al., 2009; Nicolson et al., 2009; Petersen et al., 2011; Énée et al., 2012; Pound et al., 2012; Hardy et al., 2015; Aydemir et al., 2016; Singh et al., 2016; Huang et al., 2019; Maxel et al., 2019)
Allergy	ZnT5	(Nishida et al., 2009)
Obesity	ZnT4, ZnT5, ZnT9, ZIP1, ZIP4, ZIP6	(Noh et al., 2014).
Ehlers-Danlos syndrome	ZIP13	(Fukada et al., 2008; Munemasa et al., 2014)
Ischemia-reperfusion	ZnT1	(Beharier et al., 2012)
Skin development/diseases and Acrodermatitis Enteropathica (AE)	ZIP2, ZIP4, ZIP10, ZIP13	(Maverakis et al., 2007; Bin et al., 2011; Bin et al., 2014; Bin et al., 2014; Inoue et al., 2014; Kasana et al., 2015; Bin et al., 2017; Bin et al., 2017)
Intestinal health and diseases (e.g., Crohn's disease)	ZIP7, ZIP8, ZIP14, ZnT2, ZnT4	(Geiser et al., 2012; Li et al., 2016; Ohashi et al., 2016; Podany et al., 2016)
Schizophrenia	ZIP12	(Scarr et al., 2016)
Asthma	ZIP14	(Lang et al., 2007)
Osteopenia and male-specific sudden cardiac death	ZnT5	(Inoue et al., 2002)
Embryonic death	ZnT1	(Andrews et al., 2004)
Lung tissue damage/ cytoprotection of lung epithelial cells	ZIP8	(Besecker et al., 2008; Knoell et al., 2020)

The immature pale insulin progranules in the ZnT8 deficient β-cells are bigger than the mature ones, demostrating ZnT8 expression dependent insulin crystalisation (Lemaire et al., 2009). The absence of ZnT8 in mice resulted the loss of Zn^{2+} release in the exocytic granules but the insulin biosynthesis, contents and release rates of glucose were normal, indicating that ZnT8 expression was not required for maintaining glucose homeostatsis. But, Zn^{2+} is a prerequisite element for the formation and crystalisation of hexameric insulin (Nicolson et al., 2009). The

roles of ZnT8 depend on sex, age and dietary supplements (Lemaire et al., 2009; Nicolson et al., 2009; Pound et al., 2012; Huang et al., 2019). Intriguingly, knockdown of both ZnT3 and ZnT8 enhanced apoptosis of pancreatic β-cells (INS-1E) whereas knockdown of only ZnT3 significantly decreased insulin secretion but ZnT8 knockdown increased intracellular insulin contents along with lowering secretion (Petersen et al., 2011). As ZnT8 expression was reduced in T2DM, it is directly or indirectly related to causing breast cancer in females (Hardefeldt et al., 2012; Huang et al., 2019). The endocrine roles of ZIP14 have been recently elucidated in pancreatic β-cells (INS-1E). The study showed the overexpression of ZIP14 in pancreatic β-cells following high glucose stimulation but ZIP14 silencing led to reduced expressions of different metal-binding proteins, proliferating marker Mki67 and other proteins associated with secreating insulin and β-cell functions (Maxel et al., 2019). Since low level of ZIP14 was also observed in T2DM pancreas, ZIP14 might serve as the future pharmacological target for treating β-cell dysfunction, T2DM and other glucose-related disorder (Aydemir et al., 2016; Maxel et al., 2019). Also, consistent high expression of ZIP6 and ZIP7 in islets and β-cells of human and mice have been reported to play important roles in maintaining zinc homoestatsis and secreting glucose-stimulated insulin in pancreatic β-cells (Liu et al., 2015).

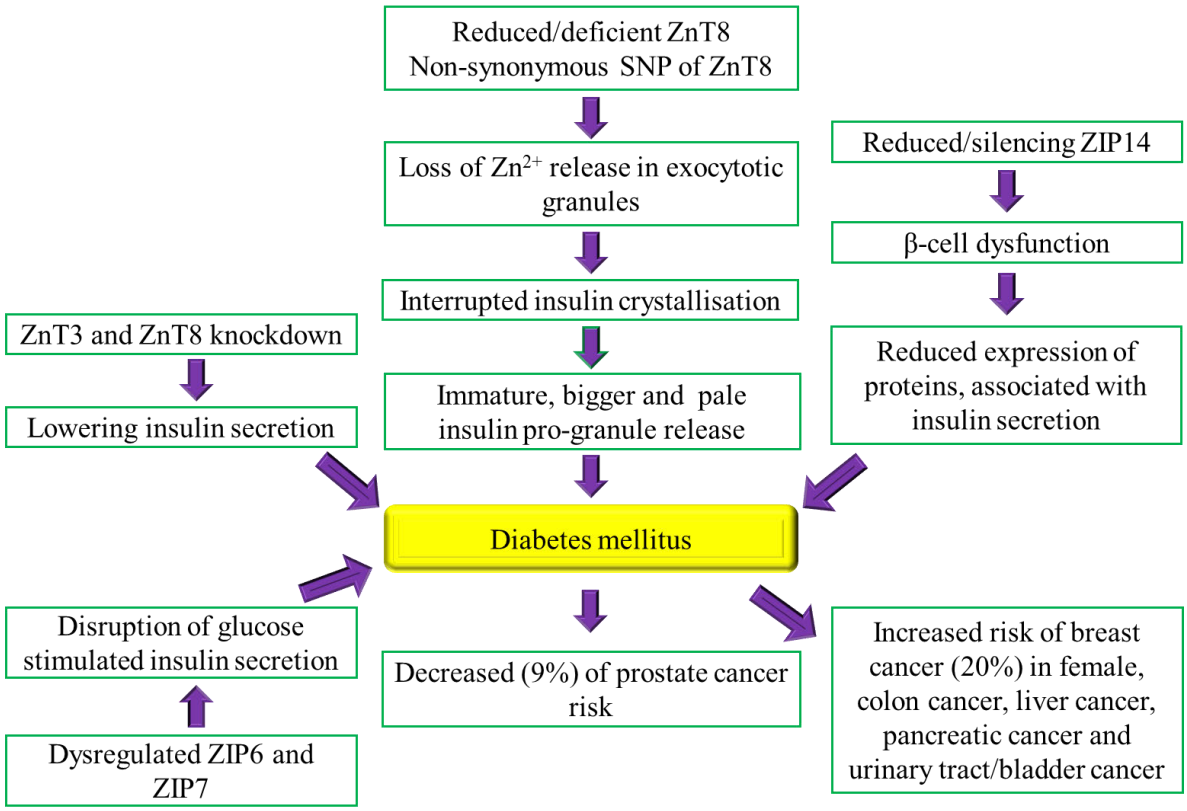

Figure 1.5 Diabetes is linked to human cancers. The abberant expression ZIP6, ZIP7, ZnT3 and ZnT8 leads to disruption of insulin secretion in causing diabetes. Silencing of ZIP14 leads to β-cell dysfunction through suppressing the proteins associated with β-cell functions. ZnT8 dysregulation or non-synonymous single nucleotide polymorphism (SNP) of ZnT8 distrub insulin crystallization contributing to cause diabetes. Diabetes increases or decreases cancer risks in human.

The abberant expression of ZIP6, ZIP7, ZIP14, ZnT3 and ZnT8 could result in diabetes (**Figure 1.5**). Diabetes was diagnosed in a siginificant number of patients with various malignancies, including colon, liver, pancreatic, urinary system or bladder, and breast cancers (Attner et al., 2012). Studies demonstrated 20% increased risk of breast cancer in the individuals having diabetes (Attner et al., 2012; Hardefeldt et al., 2012; Hsieh et al., 2012; Ronco et al., 2012). Investigations confirmed that particularly T2DM increased breast cancer risks in females (Michels et al., 2003). Interestingly, diabetes resulted in reduced prostate carcinoma risks in male individuals (Kasper et al., 2009; Attner et al., 2012). A study conducted on about 9000 prostate cancer patients demonstrated the 9% reduced risks of developing prostate carcinoma in those patients suffering from diabetes (Bonovas et al., 2004). So, there is a link between diabetes and prostate carcinoma (Gong et al., 2006; Calton et al., 2007; Velicer et al., 2007; Darbinian et al., 2008; Kasper et al., 2009).

1.7 Protein kinase CK2

Protein kinase CK2, a pleiotropic, serine/threonine and ubiquitous kinase, was first discovered in rat mitochondria in 1954 (Burnett and Kennedy, 1954). It phosphorylates more than 300 substrates, therefore regulates a myriad of cellular processes such as cell cycle and signal transduction (Allende and Allende, 1995; Meggio and Pinna, 2003). CK2 phosphorylates the hydroxyl group of serine or threonine residue in its substrates (**Figure 1.6**). The enzyme was previously named as casein kinase 2 as it phosphorylated caseins *in vitro* assay and the numerical designation 2 describes its elution fraction from diethylaminoethyl (DEAE) cellulose chromatographic column (Burnett and Kennedy, 1954; Johnson and Wu, 2016). Since casein is not a physiological substrate for the kinase, it was re-named in 1994 as CK2 kinase avoiding the confusion (Venerando et al., 2014; Johnson and Wu, 2016).

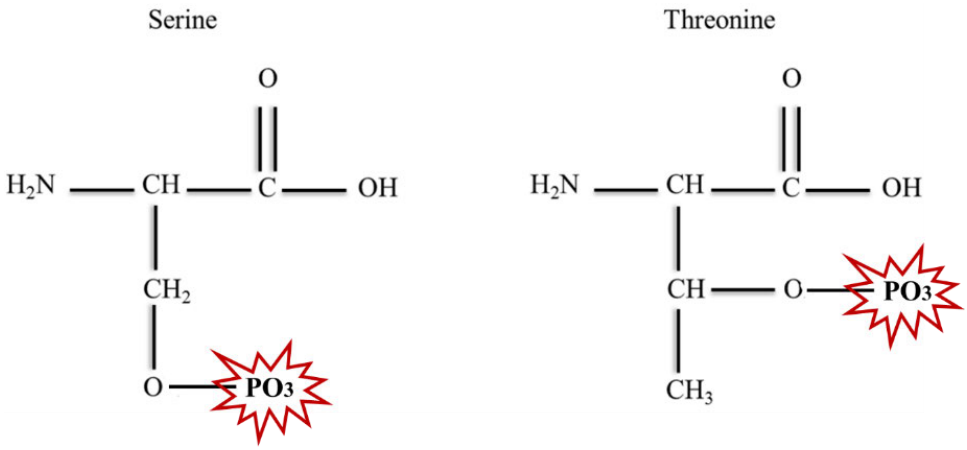

Figure 1.6 Phosphorylating hydroxyl group of serine and threonine by CK2.

1.7.1 Structure of CK2 kinase

CK2 consists of two catalytic subunits (α and α') and two regulatory β subunits (Hathaway and Traugh, 1979). Zinc is crucial to keep the two identical regulatory β subunits together. CK2 can have different tetrameric configurations, including αα'ββ, ααββ or α'α'ββ (Litchfield, 2003), as shown in **Figure 1.7**. Two catalytic subunits CK2α and CK2α' are encoded by two different genes *CSNK2A1* and *CSNK2A2*, respectively (Ackermann et al., 2005). CK2β subunits are encoded by the single *CSNK2B* gene in mammalian cells. The protein sequences of two catalytic subunits have more than 90% similarities in their N terminus but less homologous in C-terminus in mammalian cells. Third catalytic isoform CK2α'' has been discovered in human which is practically identical to CK2α excluding the last 32 amino acid residues in the C-

terminus (Kramerov and Ljubimov, 2012). The affinity of subunit CK2α′ for CK2β is 12 times lower than the affinity of CK2α for CK2β (Bischoff et al., 2011). In contrast, four subunits of CK2 in *Saccharomyces cerevisiae* are encoded by four different genes *CKA1* (CK2α), *CKA2* (CK2α'), *CKB1* (CK2β1) and *CKB2* (CK2β2). CK2 can exist in *Saccharomyces cerevisiae* in three ααβ1β2, αα'β1β2 and α'α'β1β2 different quaternary configurations like mammalian CK2 (Meggio and Pinna, 2003).

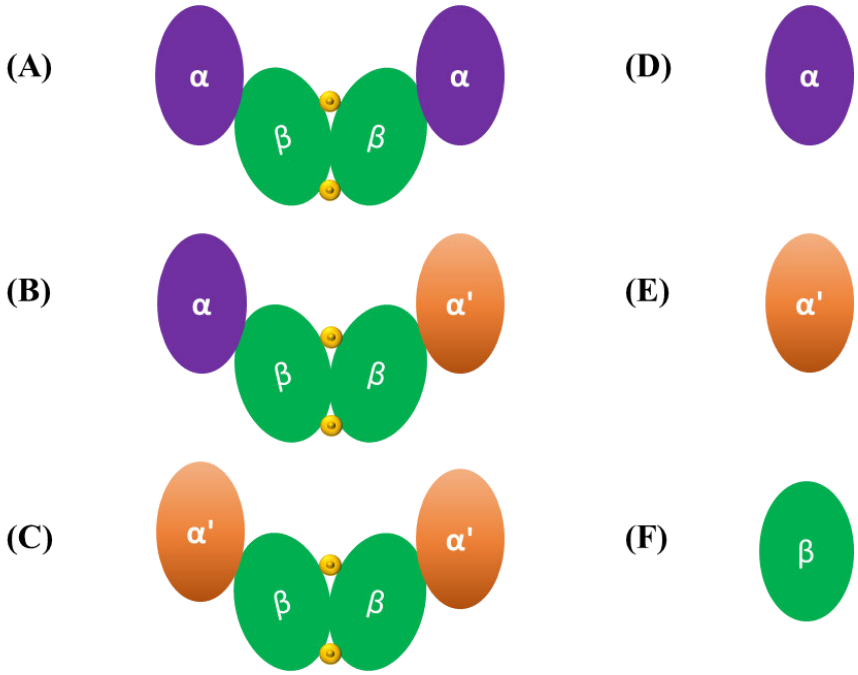

Figure 1.7 Mammalian tetrameric holoenzyme of CK2 kinase and its functional monomeric subunits. (A) The mammalian cells show three tetrameric functional forms ααββ (A), αα'ββ (B) and α'α'ββ (C) of CK2. Two β subunits form homodimer which is attached by catalytic subunits α or α' to form tetramers with three different combinations of the catalytic α and α' subunits (A, B, C). In mammals, CK2α, CK2α' and CK2β are encoded by three different genes *CSNK2A1*, *CSNK2A2* and *CSNK2B*, respectively. The yellow dots represent zinc ions.

The enzyme CK2 has two domains, a N-terminal domain with a β-sheet-based structure and a C-terminal domain with many α-helices as shown in **Figure 1.8**, according to its crystal structure (Pechkova et al., 2003; Bischoff et al., 2011). CK2's active site is situated in a cleft between the two domains (Bischoff et al., 2011). There are several three-dimensional arrangements as a result of the variations in the α and α' subunits (Bischoff et al., 2011). Four amino acid cysteine residues in a zinc finger-like motif are the feature of CK2β subunits (Allende and Allende, 1995). Zinc finger motif participates into the formation of CK2β homodimer that establishes the interactions between CK2 holoenzyme and its substrates

(Mackay and Crossley, 1998). The phosphorylation of protein substrates is a key mechanism for the regulation of a wide range of basic physiological activities (Litchfield, 2003; Meggio and Pinna, 2003). Each protein kinase is able to phosphorylate numerous protein substrates in the cell and similarly CK2 can also phosphorylate over 300 protein substrates (Meggio and Pinna, 2003). The shared signature sequence among the substrate proteins may be the reason for such a wide spectrum of substrates (Meggio and Pinna, 2003). Because of this, CK2 exhibits a wide range of functions including cell growth and apoptosis, as the number of possible protein targets of CK2 grows. Apart from ZIP7, which has already been shown to be phosphorylated by CK2 (Taylor et al., 2012), other ZIP and ZnT proteins may also be phosphorylated by CK2 (Johnson and Wu, 2016).

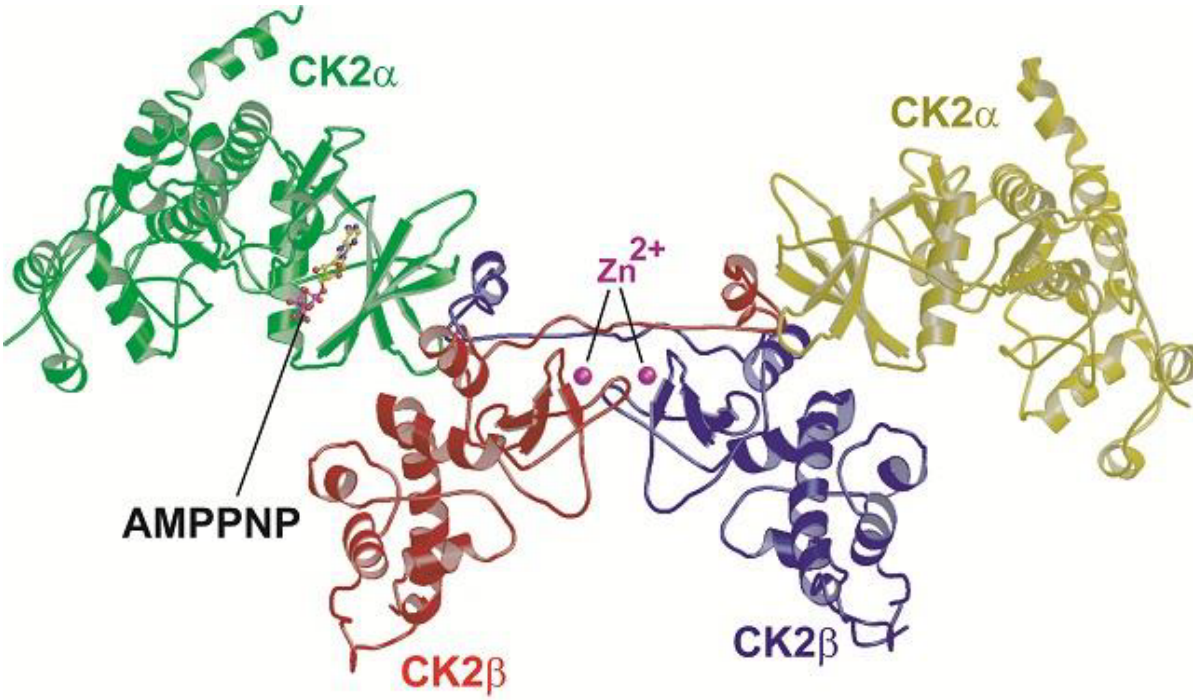

Figure 1.8 An illustration of the CK2 tetrameric (ααββ) configuration. Tetrameric CK2's crystal structure is depicted in a ribbon diagram (obtained from Protein Data Bank). The core homodimer of CK2β subunits is flanked by CK2α subunits. ATP binds to the active site of CK2 and is competitively inhibited by AMPPNP.

1.7.2 Protein kinase CK2 in cancers

CK2 is historically associated with different types of cancers in human as it regulates growth, proliferation and apoptosis of the cells (**Figure 1.9**) (Ruzzene and Pinna, 2010; Taylor et al., 2012; Ortega et al., 2014; Zaman et al., 2016; Johnson et al., 2017; Nimmanon et al., 2017; Zaman et al., 2019). G1/S and G/M transition need CK2 for cell proliferation (Litchfield, 2003; Zatta et al., 2009). It has been shown that CK2α and CK2β are phosphorylated in mitotic cells, which adds more proof that CK2 plays a regulatory role in cell cycle (Zatta et al., 2009; Schnitzler et al., 2014). CK2 phosphorylates DNA/RNA polymerase, DNA topoisomerase, tumour suppressor p53 and so on (Meggio and Pinna, 2003), thus contributes to cell proliferation (Allende and Allende, 1995). Increased CK2 activity was also observed in fast growing tissues (Guerra et al., 1999), though CK2 is recognised as an oncogene (Trembley et al., 2009). A transcription factor called TAL1 and overexpressed CK2 have been found for promoting leukemia (Kelliher et al., 1996). CK2 also participates in regulating various cell signalling networks, so CK2 is recognised as a 'druggable' kinase for drug development (Sandholt et al., 2009).

1.7.3 CK2 in breast and prostate cancers

Oncomine database analysis showed up-regulation of CK2α and CK2β but down-regulation of CK2α' at gene level in breast cancers (Ortega et al., 2014). Ductal but not lobular breast cancer exhibited higher CK2α gene expression, whereas both invasive and non-invasive breast cancers displayed CK2α' down-expression. CK2β gene is significantly over-expressed in invasive breast cancer cells (Ortega et al., 2014). A previous study presented that overexpression of CK2α potentiates Wnt/β-catenin signalling in mammary epithelial cells, which could cause breast cancer in human (Landesman-Bollag et al., 2001).

A study revealed similar expression levels of CK2 subunits in both LNCaP and PC3 prostate cancerous cells, but markedly higher enzymatic activity was observed in hormone refractory PC3 cells than hormone sensitive cells (Hessenauer et al., 2003). CK2α is overexpressed in prostate cancers (Ortega et al., 2014). Another study demonstrated that nuclear-localised CK2α subunit was strongly correlated to poor prognosis of human prostate cancer (Laramas et al., 2007).

1.7.4 CK2 regulates metal ion homeostasis

Our research team along with the others have demonstrated the roles of CK2 in aluminium toxicity (Adams et al., 2002; Becaria et al., 2002), arsenic toxicity (Johnson et al., 2016) and chromium homeostasis (Johnson, 2016). Subsequently, CK2 has also been demonstrated in regulating Zn^{2+} homeostasis in breast cancer and prostate cancer cells (Taylor et al., 2012; Taylor et al., 2012; Zaman et al., 2016; Nimmanon et al., 2017; Zaman et al., 2019). Therefore, immunofluorescence confocal microscopy was employed in this project to determine the protein expressions and cellular localisations of CK2α/α' and CK2β in breast cells (MCF10A, MCF-7, MDA-MB-231) and prostate cells (RWPE-1, PC3, DU145). Since CK2 expression and localisation are corelated to cancer development and migration (Laramas et al., 2007), the findings of this project should enhance our understanding CK2's roles in Zn^{2+} homeostasis.

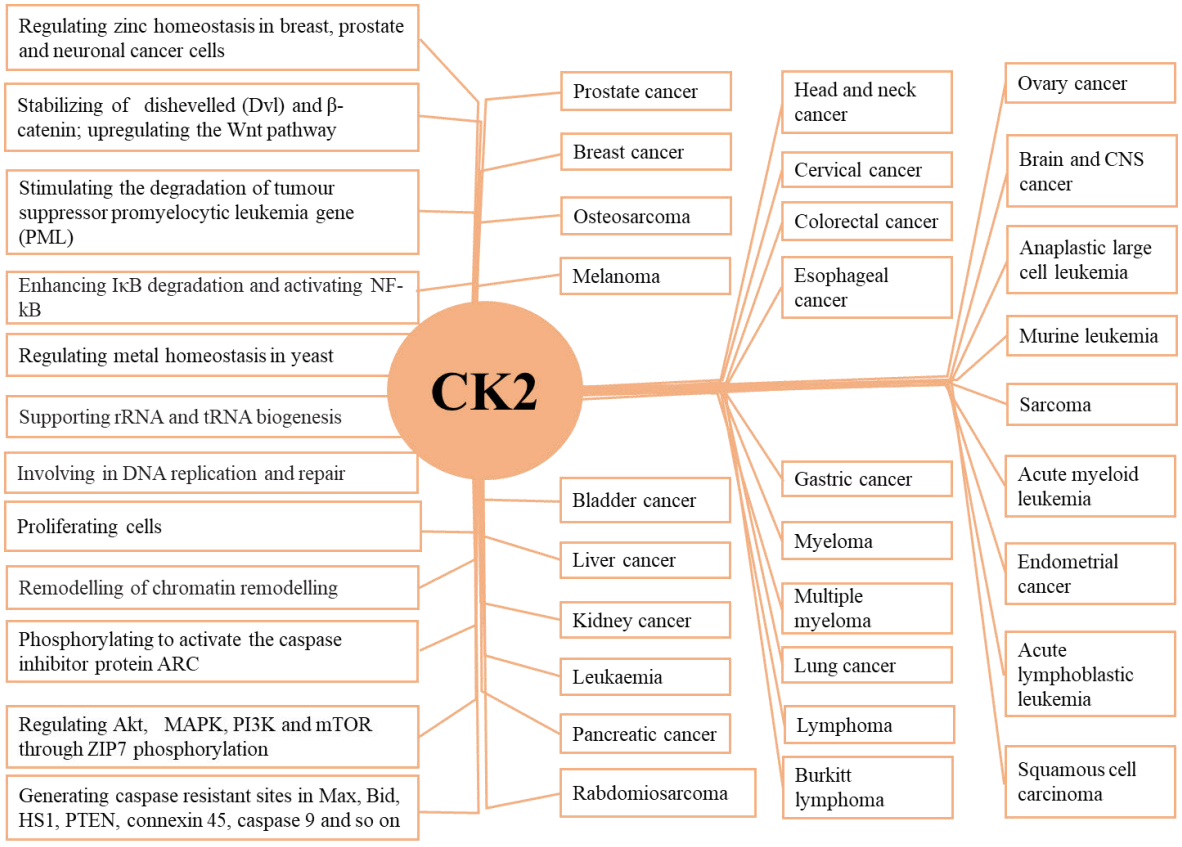

Figure 1.9 CK2 functions and its involvement in human cancers. CK2 displays a wide range of cellular functions including cell proliferation, apoptosis, nucleic acid (DNA, RNA) biogenesis and repairs, regulation of numerous signalling networks (e.g., MAPK, PI3K, Akt, mTOR) as well as cellular zinc homeostasis. Its involvement in such a wide range of cellular functions enables CK2 to be associated with numerous human cancers.

1.8 Experimental perspectives

1.8.1 Rationale of employing breast and prostate cancerous cell lines

Normal and cancerous human cell lines are extensively used in biological research (Sharma et al., 2010; Gillet et al., 2013). To investigate the roles of ZIP/ZnT and CK2 kinase in Zn^{2+} homeostasis, numerous studies have employed breast cancer cells (MCF-7, MDA-MB-231) (Taylor et al., 2012; Taylor et al., 2012; Chandler et al., 2016; Zaman et al., 2021) and prostate cancer cells (PC3, DU145) (Albrecht et al., 2008; Zaman et al., 2019). In addition, breast cancer cells MCF-7 (Barman et al., 2022; Dasgupta et al., 2022; Ejaz et al., 2022; Zhang et al., 2022) and MDA-MB-231 (Ejaz et al., 2022; Estirado et al., 2022; Sánchez-Quesada et al., 2022; Valashedi et al., 2022) are extensively used to investigate different aspects of breast cancer research. Similarly, prostate cancer cells PC3 (Bennett et al., 2023; Hernroth and Tassidis, 2023) and DU145 (Su et al., 2023; van Santen et al., 2023) are often employed in prostate cancer research. To validate the findings from the cancerous cells, normal breast epithelial MCF10A cells (Soule et al., 1990; Tait et al., 1990; Al-Humaidi et al., 2022; Chumsuwan et al., 2022; Vedoya et al., 2022) and normal prostate epithelial RWPE-1 cells (ErgÜN et al., 2022; Muñoz-Moreno et al., 2022; Soler-Agesta et al., 2022) are used by the numerous studies. So, this study employs normal breast epithelial cells (MCF10A), breast cancerous cells (MCF-7, MDA-MB-231), normal prostatic epithelial cells (RWPE-1) and prostate cancerous cells (PC3, DU145), and their salient features are enlisted in **Table 1.5**.

As is reviewed previously, breast and prostate cancer cells exhibit diametrically opposite intracellular Zn^{2+} profiles, i.e., the intracellular zinc level in breast cancer cells is markedly higher than the normal breast epithelial cells, whilst the intracellular zinc level in prostate cancer cells is much lower than the normal prostate epithelial cells (Sauer et al., 2020; Wang et al., 2020; Rusch et al., 2021). This study takes advantage of such a contrasting feature between breast and prostate cancer cells to carry out the investigation into the zinc homeostasis of breast and prostate cancer cells, by employing the panel of breast and prostate cells (**Table 1.5**).

Table 1.5 Characteristics of the mammary and prostatic cells

Cell line	Ethnic sources	Origin	Cell type	Year	Presenting model	P53 status	Karyotype
MCF10A	White, 36 years	Breast	Epithelial	1984	Normal breast epithelial cell	Wild type	Diploid
MCF-7	Caucasian female, 69 years	Breast (metastatic sites, pleural effusion)	Epithelial	1973	Luminal subtype breast cancer, poorly aggressive, non-invasive and low metastatic	Wild type	Hypertriploidy to hypotriploidy
MDA-MB-231	Caucasian female, 51 years	Breast (metastatic sites, pleural effusion)	Epithelial	1978	Basal subtype breast cancer, highly aggressive	Mutated	Close to triploid range
RWPE-1	Caucasian, male, 54 years	Prostate tissue	Epithelial	1979	Normal prostate epithelial cell	Wild type	Diploid
PC3	Caucasian, male, 62 years	Bone (metastatic sites)	Epithelial	1979	Highly metastatic	P53 null/-	Close to triploid
DU145	Caucasian male, 69-year-old	Brain (metastatic sites)	Epithelial	1975	Moderate metastatic	Mutated	Hypotriploid karyotype

1.8.2 qRT-PCR for quantification of gene expression

The qRT-PCR is a widely employed molecular method for the quantification of gene expression (Fleige and Pfaffl, 2006; Bustin and Nolan, 2017). This sensitive molecular technique detects the amplified PCR products by using fluorescent emission of the reporter dyes and this emission is proportional to the amplified PCR products at the exponential phase of amplification (**Figure 1.10**) (Bustin, 2002). Cycle threshold (CT) values are required for precise measurement of the fluorescent signal. The concentration of the PCR target virtually doubles with each cycle after the PCR enters the exponential amplification phase (**Figure 1.10**) (Freeman et al., 1999). Therefore, the expression profiles of *SLC39A1-14*, *SLC30A1-10* and *MT* (*MT1B*, *MT1X*, *MT1F*, *MT2A*) genes related to zinc homeostasis were generated in this study by qRT-PCR in breast (MCF10A, MCF-7, MDA-MB-213) and prostate cells (RWPE-1, PC3, DU145) with and without zinc exposure in order to identify differentially expressed genes.

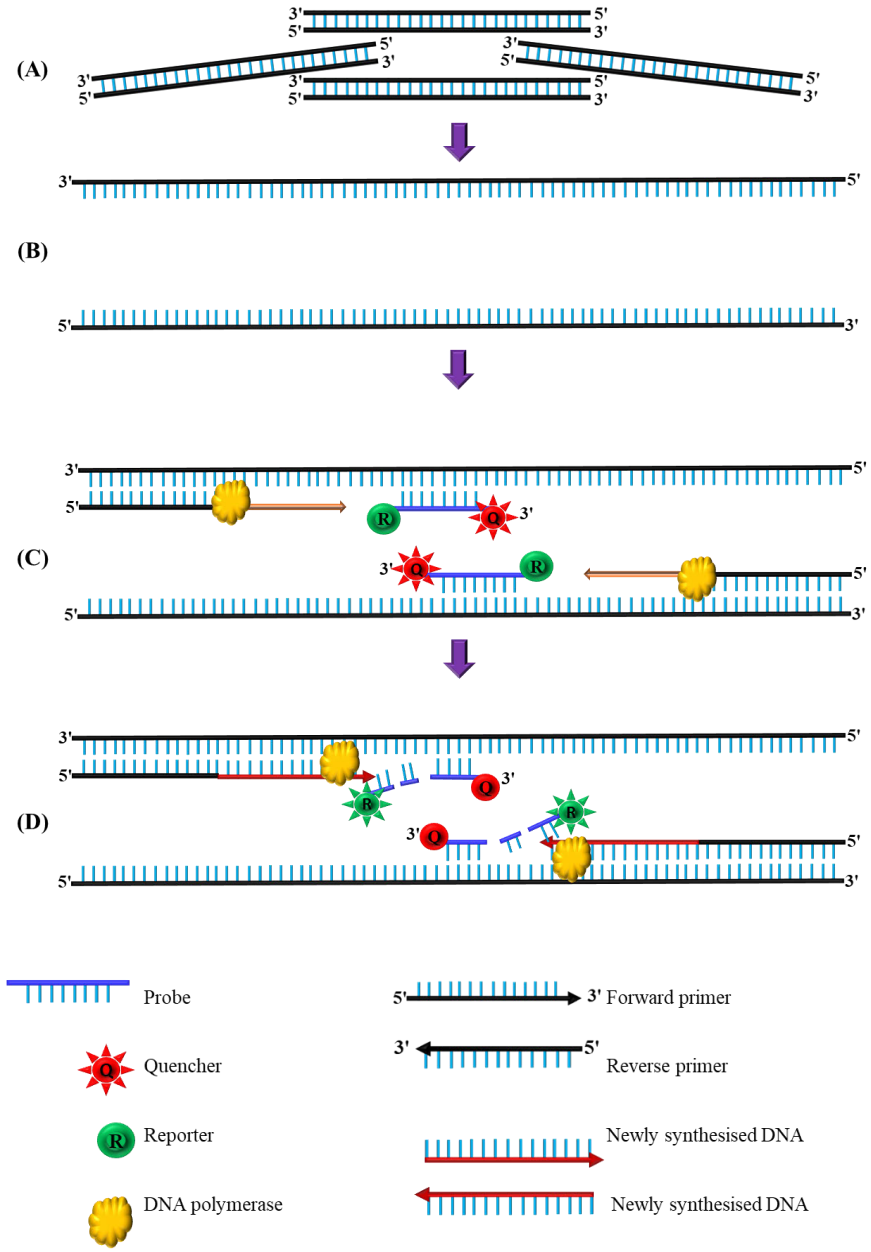

Figure 1.10 Principle of TaqMan technology for gene expression assay process. (A) Before doing qPCR it is compulsory to synthesise cDNA from the purified RNA samples using appropriate cDNA synthesis kits. These synthesised double stranded cDNA are subjected to qPCR for the measurement of gene expression. (B) In the first step of qPCR, the double stranded cDNAs are separated or denatured at high temperature (95° C). This denaturation step provides single stranded template for the next step. (C) The temperature is decreased at 55-66°C so the primers (forward and reverse) and TaqMan probes can bind to their complementary sequences of the separated cDNA template. The fluorescence of reporter (R) dye is quenched by the quencher dye when the locate close to each other. (D) The new DNA strand is started to synthesise from the primers by the enzyme DNA Taq polymerase, an enzyme isolated from a thermophilic bacterium named Thermus aquaticus. The extension is not started from the probe as the hydroxyl group of 3´ positioned carbon of ribose sugar is removed to limit the opportunity for making new phosphodiester bond with the next coming dNTP. Taq polymerase recruits dNTPs to extend the new DNA strand. When Taq polymerase reaches a TaqMan probe sitting on the template, it breaks the probe with its endogenous 5' nuclease activity to extend newly synthesised DNA strand. As a result, the reporter dye is separated and go away from the quencher dye to emit positive reaction signals which are captured by the qPCR machine to provide gene expression measuring data.

1.8.3 Immunofluorescence confocal microscopy for determining the expression and cellular localisation of the proteins

The differentially expressed genes (*SLC39A*, *SLC30A*, *MT*) involved in Zn^{2+} homeostasis with or without exogenous zinc exposure detected by qRT-PCR have been further validated at protein level by immunofluorescence confocal microscopy. This imaging technology also provides cellular localisation details of the target proteins. Immunofluorescence confocal microscopy is commonly used to quantify protein expressions along with their cellular localisations (Lee et al., 2015; Koepke et al., 2020; Abdo et al., 2021; Shihan et al., 2021). ZIP7 expression level and cellular localisation was determined by confocal microscopy in breast cancerous tissues (*in vivo*) and cells (*in vitro*) (Ziliotto et al., 2019). The expression and localisation of ZnT2 were also investigated by employing immunofluorescence microscopy in the breast tissues (Lee et al., 2015). Immunofluorescence confocal imaging revealed the expressions and localisations of ZIP1, ZIP2 and ZIP3 in prostate normal and cancerous tissues (Franklin et al., 2005; Desouki et al., 2007). Protein kinase CK2 is reported in regulating zinc homeostasis. So, the localisation of CK2 subunit such as CK2α was determined in prostate malignant tissues by immunofluorescence and nuclear localisation of CK2α is shown to be associated with poor prognosis in human prostate cancer (Laramas et al., 2007). The nuclear and nucleolar localisations of CK2α were reported in breast cancer and CK2α's intracellular localisation is also recognised as prognostic factor in breast cancer (Homma et al., 2021). Therefore, this study aims to determine the expressions and cellular localisations of ZIP12, ZnT1, MT2A, CK2α/α' and CK2β in breast cells (MCF10A, MCF-7, MDA-MB-231) and prostate cells (RWPE-1, PC3, DU145) with and without exogenous zinc exposure by immunofluorescence confocal microscopy in this study.

1.8.4 Top-down proteomics for the identification and quantification of proteins

With the advancement of molecular biology, the emphasis shifts from the genomics to the proteomics. As the proteins are ultimately accountable for the malignant phenotype of cancers, proteomics has its advantages (Ornstein and Tyson, 2006). Hence, we employed top-down proteomics, i.e., the combination of two-dimensional gel electrophoresis (2-DE) and liquid chromatography tandem-mass spectrometry (LC-MS/MS) to generate the proteomic profiles of breast cancer cells (MCF-7), breast normal epithelial cells (MCF10A), prostate cancer cells (PC3) and prostate normal epithelial cells (RWPE-1) with or without exogenous zinc treatment. The proteomic datasets with or without extracellular zinc exposure in both cancerous and

normal cells will uncover the proteins associated with Zn^{2+} homeostasis of breast cancer and prostate cancer cells. Top-down proteomic analyses typically involve two steps, that is, protein separation and protein identification (Garbis et al., 2005). Protein separation in the first dimension by isoelectric points is carried out by isoelectric focusing, often utilising precast immobilised pH gradient (IPG) strips (Bjellqvist et al., 1982; Görg et al., 2000). Proteins are further separated based on their molecular weights using linear gradient sodium dodecyl sulphate polyacrylamide gel electrophoresis (SDS-PAGE) in the second dimension (Almuslehi et al., 2022). Protein identification for the protein spots separated by high-resolution two-dimensional (2-D) gels is performed by LC-MS/MS analysis (Asgarov et al., 2021; Almuslehi et al., 2022). For the identification of differentially expressed proteins or biomarkers, the proteomic approach was widely used in numerous studies on breast and prostate cancers (Flores-Morales and Iglesias-Gato, 2017; Ziegler et al., 2018; Katsogiannou et al., 2019; Yoneten et al., 2019; Zhou et al., 2019). Similarly, the differentially expressed proteins in cancerous and normal cells of breast and prostate following exogenous zinc manipulation were identified in this study by the proteomic approach as described above for gaining more insights into the understanding of zinc homeostasis in breast and prostate cancer cells.

1.9 Hypotheses

- The dynamic expression profiles of *SLC39A* (ZIP), *SLC30A* (ZnT) and *MT* (MT) in response to extracellular zinc exposure can be uncovered by qRT-PCR gene profiling in cancerous and normal breast and prostate cells.
- Expression and cellular localisation of differentially expressed proteins such as ZIP, ZnT, MT and CK2 subunits in cancerous and normal cells of breast and prostate can be revealed by immunofluorescence confocal microscopy.
- Differential proteomic profiles in breast cells (MCF10A and MCF-7) and prostate cells (RWPE-1 and PC3) with or without exogenous zinc exposure can be obtained by the described top-down proteomic approach.

1.10 Aims

- To generate the expression profiles of 28 genes (14 *SLC39A*, 10 *SLC30A*, *MT1B*, *MT1F*, *MT1X* and *MT2A)* associated with zinc homeostasis in normal and cancerous breast and prostate cells by qRT-PCR.
- To investigate the expression and localisation of the proteins encoded by the differentially expressed genes uncovered in the first aim, by immunofluorescence confocal microscopy in normal and cancerous breast and prostate cells with or without zinc exposure.
- To identify differentially expressed proteins related to the zinc homeostasis of breast and prostate cancer cells by top-down proteomic analysis (2-DE/LC-MS/MS).

Chapter 2 Materials and methods

2.1 General materials and reagents

In this study, the common reagents and consumables were obtained from Sigma-Aldrich (Sydney, Australia), Thermo Fisher Life Technologies (Australia), Lonza (Switzerland), Applied Biosystems (Australia), CHOICE Analytical (Australia), Labcon (North America) and Greiner Bio-One (Germany). The required chemicals or solvents were purchased from commercial suppliers detailed in the methods. The water from the Milli-Q™ system (Merck™ Milli-Q™ Reference Ultrapure Water Purification System, Thermo Fisher Scientific) was used in the preparation of the needed buffers and stock solutions. The Milli-Q water was used for washing and rinsing the suitable equipment.

2.2 General operational practice

The general experimental operations were carried out in PC2 laboratory facility of Western Sydney University, Australia. The cell culture work such as initiation, passaging, seeding, treating and making the stocks of the cells were conducted aseptically in a class II biological safety cabinet (Gelaire AS-2252.2). The biosafety hood was sterilised through cleaning with 70% (v/v) ethanol and 45 minutes of UV exposure immediately. The cell culture reagents, instruments PBS, Milli-Q water and other required miscellaneous items were autoclaved at 121 °C (Tuttnauer 3150EL, Australia). The media for tissue culture and its constituent parts, such as FBS, penicillin/streptomycin, were bought in sterile form. The working lab benches were cleaned with 70% ethanol regularly for the experiments. The planning and execution of the experimental work was always systematic, and it was done so with great care to avoid any contamination.

2.3 Preparation of phosphate buffer saline (PBS)

For the preparation of one litre of 1x PBS, sodium chloride (NaCl), potassium chloride (KCl), disodium hydrogen phosphate (Na_2HPO_4) and monobasic potassium (KH_2PO_4) were weighed by balance following the calculation in the **Table 2.1**. 800 mL of Milli-Q water (Merck™ Milli-Q™ Reference Ultrapure Water Purification System, Thermo Fisher Scientific) was dispensed into a clean two litre glass bottle. 8 g of NaCl, 0.2 g of KCl, 1.4 g of Na_2HPO_4 and 0.272 g of KH_2PO_4 were added in the two-litre bottle one by one. It was made sure that the chemicals

were dissolved completely. Then pH was measured and adjusted, typically 7.4 if required. Finally, Milli-Q water was added until the solution volume was one litre.

Table 2.1 Required components for 1x PBS

Chemicals	1 Litre	2 Litres	Final concentration
NaCl (MW: 58.4 g/mol)	8 g	16 g	0.137 M
KCl (MW: 74.551 g/mol)	0.2 g	0.4 g	0.0027 M
Na_2HPO_4 (MW: 141.96 g/mol)	1.4 g	2.8 g	0.01 M
KH_2PO_4 (MW: 136.086 g/mol)	0.272 g	0.544 g	0.0018 M (~0.002 M)

2.4 Preparation of 4% (w/v) paraformaldehyde (PFA)

Eight grams of paraformaldehyde (PFA) (Sigma-Aldrich) powder were weighed and poured into a glass beaker containing ~150 mL of 1x PBS. The powder was not immediately dissolved. PFA suspension was heated at approximately 60 °C and stirred carefully to avoid boiling. pH of the solution was raised by adding 1N NaOH dropwise until the solution became transparent. Once PFA was dissolved, the solution was allowed to be cooled and then filtered. The pH was rechecked and adjusted by adding 6 mM HCl to 6.9. The volume was adjusted to 200 mL by adding required volume of 1x PBS. 4% (w/v) PFA solution was aliquoted into 15 mL falcon tubes (Greiner Bio-One, Germany) and stored at -30° C for further usage.

2.5 Cell culture and maintenance

2.5.1 Maintaining and passaging the cells

MCF-7 human breast cancer cells (ATCC® HTB-22™) were cultured in DMEM (Life Technologies, Australia) supplemented with 10% (v/v) foetal bovine serum (FBS) (Life Technologies, Australia), 1% (v/v) penicillin/streptomycin (Sigma-Aldrich, Australia) and L-glutamine (Life Technologies, Australia). MDA-MB-231 human breast cancer cells (ATCC® HTB-26™) were cultured in Leibovitz's L-15 medium (Life Technologies, Australia) supplemented with 10% (v/v) FBS, 1% (v/v) penicillin/streptomycin and L-glutamine. MCF10A normal human breast cells (ATCC® CRL-10317™) were cultured in DMEM/F12 medium (Invitrogen, Australia) supplemented with 5% (v/v) horse serum (ThermoFisher Scientific, Australia), 1% (v/v) penicillin/streptomycin, cholera toxin (100 ng/mL, Sigma-Aldrich, Australia) and MEGM™ mammary epithelial cell growth medium SingleQuots™ Kit (Lonza, CC-4136) [human epidermal growth factor (20 ng/mL), hydrocortisone (0.5 mg/mL)

and insulin (10 µg/mL)]. PC3 (ATCC® CRL-1435™) and DU145 human prostate cancer cells (ATCC® HTB-81™) were cultured in RPMI 1640 (Life Technologies, Australia) supplemented with 10% (v/v) FBS, 1% (v/v) penicillin/streptomycin and L-glutamine. RWPE-1 human normal prostate epithelial cells (ATCC® CRL-11609™) were cultured in keratinocyte serum free medium (K-SFM) which was supplemented with bovine pituitary extract (0.05 mg/mL) and human epidermal growth factor (5 ng/mL) (ThermoFisher Scientific, Australia). The cells were cultured at 37 °C, 5% CO_2 and observed daily. According to the formulations of the media used here and the available data for the zinc contents in foetal bovine serum (McClung and Bobilya, 1999) and horse serum (De et al., 1988; Murase et al., 2013), the base level of zinc for the complete DMEM, Leibovitz's L-15 and RPMI 1640 media is approximately 5 µM, for the complete DMEM/F12 approximately 2 µM and for the complete keratinocyte serum free medium 0.5 µM.

2.5.2 Cryopreservation of the cells

Every cell line was cultured in their standard media and conditions as described. The cells were grown until reaching ~80% confluency in 75 cm^2 flasks. The cells were washed with sterile 1x PBS once, trypsinised and deactivated the trypsin with their respective complete culture media. The cell suspension was then transferred into the sterile 50 mL falcon tube and centrifuged (Allegra X-15R) at 350 g for 3 min. The supernatant was decanted, the cells were resuspended in cell freezing media (3 mL per 75 cm^2 flask) and aliquoted into the cryovials (1 mL per cryovial) (Greiner Bio-One, Germany). Importantly, the freezing media were prepared following the instructions given by ATCC except MCF10A human normal breast epithelial cells. The freezing media of MCF10A cells contains 70% (v/v) complete growth media, 20% (v/v) horse serum and 10% (v/v) dimethyl sulfoxide (DMSO) (https://brugge.med.harvard.edu/protocols). The cryovials were placed in an insulated (Styrofoam) container in -80 ºC freezer (Thermo Scientific -80 °C ULT) overnight and finally transferred to the liquid nitrogen tank at -196 °C for long term storage.

2.5.3 Initiation of the cells from cryopreservation

The biosafety cabinet, cell culture media, cell culture 75 cm^2 flasks and other essential logistics for cell culture were prepared. The cryovials were taken from the liquid nitrogen storage and were immediately thawed in a 37 °C water bath (LAB-Tech, Australia). Once thawed, the cryovials were taken into the cleaned and sterilized biosafety cabinet and the cell suspension

was transferred immediately into a sterile 50 mL falcon tube with 12 mL of the complete medium and finally, centrifuged at 350 g for 3 min. The supernatant was decanted to get the cell pellet and the cells were resuspended in 12 mL complete medium. Then, the homogeneous cell suspension was transferred into a 75 cm^2 flask and incubated at 37 °C, 5% CO_2 to reach ~80% confluency.

2.6 Determination of $ZnSO_4$ dosages for all cell lines by MTT assay

The cells were counted by a hematocytometer and aliquoted 7000 cells into each well of 96-well plates (Greiner Bio-one) in a volume of 190 µL. After the incubation of 32 h at 37 °C, 5% CO_2, 10 µL of each $ZnSO_4$ (Sigma-Aldrich, Australia) concentration (20x stock) was added to each well except the control wells which had 10 µL sterile water instead. The titration range of $ZnSO_4$ concentrations 0, 20, 50, 100, 150, 200, 250, 300, 350, 400, and 500 µM was applied to each cell line. At the end of 6 h incubation, 50 µL per well of MTT [3-(4,5-dimethyliazol-2-yl)-2,5-diphenyl-2H-tetrazolium bromide (Sigma-Aldrich, Australia), 5 mg/mL in 1x phosphate buffered saline (PBS) was added and the plates were incubated for further 2 h at 37 °C, 5% CO_2. The medium was then removed carefully and 100 µL of dimethyl sulfoxide (DMSO) (Sigma-Aldrich, Australia) was added directly into each well to solubilise the purple-coloured formazan crystals. Prior to measuring the absorbance at 600 nm using a spectrophotometer (Multiskan GO, Thermo Fisher Scientific), the plates were shaken on an orbital shaker (MICROMIXER-MX4, FINEPCR) for 2 min. The mild cytotoxic dosage for $ZnSO_4$ was defined as the dosage which resulted in between 70% and 85% cell viability at the end of 2 h zinc sulfate treatment. A benign $ZnSO_4$ dosage was also determined for breast cell lines. The benign dosage was defined as the dosage that is not harmful to cell viability during the course of treatment. The rationale for selecting the mild cytotoxic dosages of $ZnSO_4$ is to obtain the datasets on differentially expressed genes and proteins prodded by the dosages without severely compromising the overall health of the cells in the culturing flasks of this study. The viability of cells between 70% and 85% is ideal for this study, which allows the findings to be relevant to the physiological state of the cells and provides maximum data possible. The mild cytotoxic zinc concentrations selected for this study cannot be possibly relate to the pathogenic conditions for breast and prostate cancer tissues, because there are no definite data available for the zinc concentrations in breast or prostate cancer cells within the respective cancer tissues. For example, Rusch et al. (2021) demonstrated that the zinc contents in breast cancer tissues were in the range of 12 ppm (184.62 µmole) to 68.1 ppm (1047.69

µmole) by assaying the cancer tissue sections, but it is not possible to convert these numbers into zinc concentrations in breast cancer tissues.

2.7 Determination of cell viability by MTT assay

The viability of each cell line was enumerated at 30 min (T_{30}) and 120 min (T_{120}) by MTT assay under mild cytotoxic zinc treatment. The viability of MCF10A, MCF-7 and MDA-MB-231 cells was determined following the benign zinc dosage exposure at T_{30} and T_{120}. The cell viability without zinc treatment (T_0) was also measured in the same way. Multiple 96-well plates were prepared by seeding 7000 cells per well with 190 µL of complete medium and incubated for 32 h. Each cell line was then treated with the respective mild cytotoxic and the benign $ZnSO_4$ dosage for 30, 60, 90 and 120 min. 10 µL of 20x concentrated of the mild cytotoxic and the benign $ZnSO_4$ dosage solutions was used for the treatment whereas 10 µL of sterile Milli-Q H_2O was added per well for the experimental controls. Following the completion of 2 h incubation, 50 µL per well of MTT [3-(4,5-dimethyliazol-2-yl)-2,5-diphenyl-2H-tetrazolium bromide (Sigma-Aldrich, Australia), 5 mg/mL in 1x phosphate buffered saline (PBS) was added and the plates were incubated for further 2 h at 37 °C, 5% CO_2. At the end of the incubation, MTT assay was conducted as described previously, to estimate the cell viability in percentage (%). Finally, the values were graphed in excel.

2.8 RNA extraction from $ZnSO_4$ treated and untreated cells

Cells were grown in 75 cm^2 flasks for 32 h at 80% confluency, the medium was then aspirated and replaced with 11.9 mL of fresh complete medium. $ZnSO_4$ at 120x stock concentration of each dosage for each cell line was prepared in sterile Milli-Q H_2O (Milli-Q® Advantage A10 Water Purification System, Merk). The cells were treated with 100 µL of their respective $ZnSO_4$ stocks. The control cells were treated with 100 µL of sterile Milli-Q water. The cells were maintained through the time course and the RNA extraction was performed at T_0, T_{30} and T_{120}. For RNA extraction, the cells were firstly washed with 10 mL of sterile 1x PBS, followed by adding 1 mL of TRIzol™ reagent (Thermo Fisher Scientific, Australia) directly into the flasks to ensure cell lysis. After gentle mixing, the lysates were pipetted up and down several times and then transferred into 2 mL microfuge tubes. The resultant lysates were incubated for 5 min at room temperature to allow complete dissociation of the nucleoproteins. Subsequently, 200 µL of absolute chloroform (Sigma-Aldrich, Australia) was added and mixed gently, followed by a further 3 min incubation at room temperature. The samples were then centrifuged

(Beckman Coulter Microfuge 22R) at 12 000 g, 4 °C for 15 min to allow complete separation of the lysates into three phases. The RNA containing upper phase was aspirated carefully and transferred into new pre-labelled microfuge tubes. The RNA was then precipitated by adding 0.5 mL of isopropanol (Sigma-Aldrich, Australia). After 10 min of incubation the RNA was pelleted by centrifugation for 10 min at 12 000 g, 4 °C. The supernatant was discarded and the RNA pellet was washed in 1 mL of 75% (v/v) ethanol (Sigma-Aldrich, Australia) by vortexing for 5 secs and then 5 min centrifugation at 7500 g, 4 °C. The resultant RNA pellet was allowed to air-dry for ~20 min, then dissolved in 30 µL of diethylpyrocarbonate (DEPC) treated water (Sigma-Aldrich, Australia) and quantified by NanoDrop™ 2000 (Thermo Fisher Scientific, Australia). Each treatment or control has three biological replicates, which means three RNA samples for each time point of a given treatment or control.

2.9 cDNA synthesis

A high-capacity cDNA reverse transcription kit (Thermo Fisher Scientific) was used to synthesise cDNA following the manufacturer's instruction. Firstly, in a sterile PCR tube 10 µL of master mix was prepared with 2 µL of 10x reverse transcription buffer, 0.8 µL of 25x dNTP mix, 2 µL of 10x reverse transcription random primers, 1 µL of Multiscribe™ reverse transcriptase and 4.2 µL of DEPC treated water. Subsequently, 10 µL of master mix was combined with 10 µL of 0.1 µg/µL RNA from a given treatment or control. The reaction cocktails in the tubes were mixed carefully and then run on a Veriti 96-well thermal cycler (Applied Biosystems) with the following setting: step 1 at 25 °C for 10 min, step 2 at 37 °C for 120 min, step 3 at 85 °C for 5 s. cDNA was thereby synthesised from eukaryotic RNA (**Figure 2.1**). Synthesised cDNA was quantified by measuring the UV absorbance (A_{260}, A_{280}, A_{260}/A_{280}) with NanoDrop™ 2000 (Thermo Fisher Scientific, Australia).

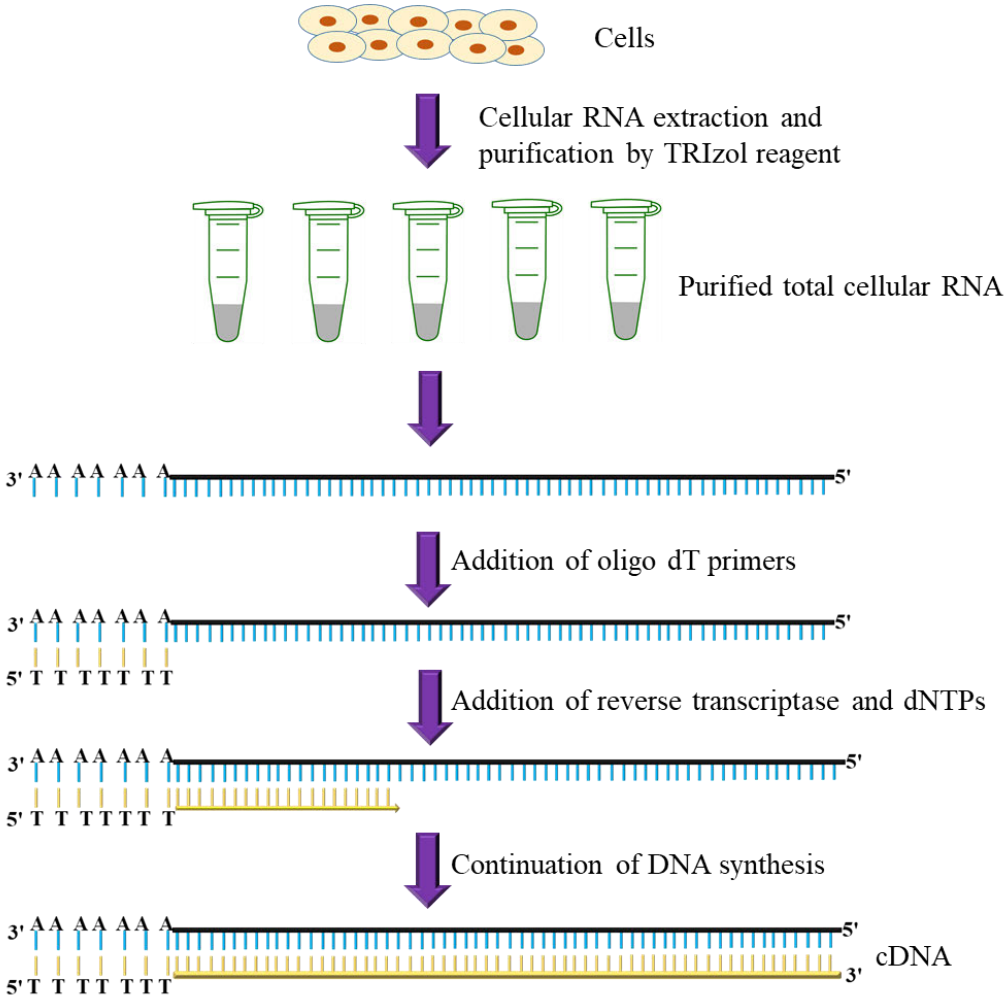

Figure 2.1 cDNA synthesis from eukaryotic RNA. This molecular technique synthesises DNA using RNA template by enzyme reverse transcriptase. Reverse transcriptase needs a short oligonucleotide, called primers. Three basic primers are available for cDNA synthesis using oligo (dT) primers, random primers, and gene-specific primers. The eukaryotic RNAs have 3´ poly (A) tail on which oligo (dT) primers anneal. Reverse transcriptase enzyme recruits dNTPs to synthesise DNA strand 5´ to 3´ direction using RNA as template. The synthesised DNAs in this way are cDNA.

2.10 Quantitative reverse transcription polymerase chain reaction (qRT-PCR)

qRT-PCR was performed with high quality TaqMan real-time PCR assays (Thermo Fisher, Life Technology) for each of the 28 genes including 14 *SLC39A* (ZIP), 10 *SLC30A* (ZnT) and 4 *MT* genes, as well as the housekeeping gene, *GAPDH* (encoding glycerolaldehyde-3-phosphate dehydrogenase) (**Table 2.2**). Each 20 µL reaction mix was prepared by adding 8 µL of DEPC treated water, 10 µL of TaqMan gene expression master mix (Thermo Fisher Scientific, Australia), 1 µL of 20x TaqMan assay and 1 µL of cDNA sample (500 ng/µL) or 1 µL of DEPC water to serve as the no-template control (negative control). The reaction mixture

was heated at 95 °C for 10 min, then followed by the cycle at 95 °C for 15 sec and 60 °C for 1 min, for a total of 40 cycles (**Table 2.3**). Thus, the cycle threshold (CT) values were acquired of each gene at control or experimental conditions (**Appendix A**).

Table 2.2 Primer and probe details of TaqMan Gene Expression Assay from Thermo Fisher, Life Technologies

Target genes	Assay ID	Amplicon Length	Target genes	Assay ID	Amplicon Length
SLC39A1	Hs00205358_m1	80	*SLC30A2*	Hs00936934_m1	82
SLC39A2	Hs00205860_m1	71	*SLC30A3*	Hs00185728_m1	93
SLC39A3	Hs00536788_m1	109	*SLC30A4*	Hs00203308_m1	73
SLC39A4	Hs00214912_m1	83	*SLC30A5*	Hs00224708_m1	122
SLC39A5	Hs00379938_m1	113	*SLC30A6*	Hs01071782_m1	101
SLC39A6	Hs00202392_m1	78	*SLC30A7*	Hs00981941_m1	66
SLC39A7	Hs00199596_m1	79	*SLC30A8*	Hs00545183_m1	73
SLC39A8	Hs00223357_m1	87	*SLC30A9*	Hs00197118_m1	78
SLC39A9	Hs04276955_m1	78	*SLC30A10*	Hs00218883_m1	59
SLC39A10	Hs00393794_m1	84	*MT1B*	Hs01875377_s1	121
SLC39A11	Hs00911336_m1	99	*MT1F*	Hs00744661_sH	86
SLC39A12	Hs00398303_m1	74	*MT1X*	Hs00745167_sH	131
SLC39A13	Hs00378317_m1	90	*MT2A*	Hs02379661_g1	82
SLC39A14	Hs00299262_m1	60	*GAPDH*	Hs99999905_m1	122
SLC30A1	Hs00253602_m1	97			

The qRT-PCR data were analysed by employing the $2^{-\Delta\Delta CT}$ method (Schmittgen and Livak, 2008). ΔCTc was calculated first where the cycle threshold for the gene of interest in control condition was subtracted by the cycle threshold of the housekeeping gene *GAPDH* in the control condition. ΔCTe was then calculated where the cycle threshold of the gene of interest under each treatment was subtracted by the cycle threshold of *GAPDH* under each experimental treatment. Finally, ΔΔCT was calculated by subtracting ΔCTc from ΔCTe. Subsequently $2^{-\Delta\Delta CT}$ represents the fold change of the gene expression relative to *GAPDH*. The relative fold change of each gene in each cell line was obtained from three biological replicates. The expression data were analysed by heatmap hierarchical cluster analysis using MeV (Multi Experiment Viewer) software (https://www.tm4.org/mev.html).

Table 2.3 Run parameters for the qRT-PCR thermal cycler

Stage	Temperature (°C)	Time (min:s)
Hold	50	2:00
Hold	95	10:00
Cycle (40 cycles)	95	0:15
	60	1:00

The expression of each gene in the cancer cells compared to normal cells was calculated according to Schmittgen and Livak (Schmittgen and Livak, 2008). The CT value of *GAPDH* was subtracted from the CT value of the gene of cancer and normal cells to obtain ΔCT of each gene. Then $2^{-\Delta CT}$ values of each gene were determined. The fold change for a gene expression in cancer cells compared to normal cells was calculated by dividing the mean of $2^{-\Delta CT}$ for the gene in cancer cells by the mean of $2^{-\Delta CT}$ of the same gene in normal cells.

2.11 Analysis of *SLC39A*, *SLC30A* and *MT* gene expression in breast and prostate cancerous tissues

In order to relate our data from the cell lines to clinical cancer tissues, we examined the expression levels of 14 *SLC39A*, 10 *SLC30A* and 4 *MT* genes in breast and prostate cancerous tissues against their normal counterparts, using the available databases UALCAN (http://ualcan.path.uab.edu), (Chandrashekar et al., 2017) gene expression profiling interactive analysis 2 (GEPIA2) (http://gepia2.cancer-pku.cn/#index) (Tang et al., 2019) and gene expression database for normal and tumour tissues (GENT2) (http://gent2.appex.kr) (Park et al., 2019).

2.12 Immunostaining and confocal imaging

The cells were seeded 12000 cells/mL into each well of 24-well culture plates in the appropriate growth medium. Each well had a sterile circular coverslip (Marienfeld circle coverslip, Adelab Scientific, South Australia). The cells were grown at 37 °C, 5% CO_2 for about 24 h on a coverslip. MCF10A, MCF-7, MDA-MB-231, RWPE-1, PC3 and DU145 cells were treated with the mild cytotoxic 195.5 µM, 320 µM, 350 µM, 186.88 µM, 110 µM and 150 µM $ZnSO_4$ dosages, respectively, and immunostaining was carried out at T_{30} and T_{120}. In addition, three breast (MCF10A, MCF-7 and MDA-MB-231) cell lines were also treated with a single benign

50 µM $ZnSO_4$ dosage, followed by immunostaining at T_{30} and T_{120}. For the control (T_0), the cells were treated with sterile Milli-Q water and immunostaining was conducted at the same time.

For immunostaining and confocal imaging, the cells were rinsed once with pre-warmed 1x PBS [NaCl (0.137 M), KCl (0.0027 M), Na_2HPO_4 (0.01 M), KH_2PO_4 (0.0018 M)] (pH 7.4) at 37 °C in water bath followed by fixation with 4% (w/v) paraformaldehyde in 1x PBS (pH 7.4) for 15 min at room temperature on a shaker. The cells were then rinsed three times with ice-cold 1x PBS and incubated in 0.1% (v/v) Triton X-100 in 1x PBS for 15 min, which should permeabilise the plasma membrane of the cell and facilitate the entry of antibodies or DAPI. To prevent non-specific binding of the primary antibodies, the cells were incubated in 300 µL of 1% (w/v) BSA (bovine serum albumin) (Sigma-Aldrich, Australia) in 1x PBS for 30 min on a shaker. The cells were then incubated in a humidified chamber for overnight at 4 °C with the primary antibodies including anti-ZIP12 (Sigma-Aldrich) at 1:200 dilution, anti-SLC30A1 (ZnT1) (Sigma-Aldrich) at 1:70 dilution, anti-MT2A (Sigma-Aldrich) at 1:50 dilution, anti-CK2α/α´ at 1:100 and anti-CK2β at 1:200 (CK2α/α' and CK2β antibodies were kindly provided by Prof. David W. Litchfield, University of Western Ontario, Canada). The anti-CK2α/α' antibody reacts with both catalytic subunits (CK2α and CK2α') of CK2 kinase. For negative control, 1% (w/v) BSA in 1x PBS was left in the wells of 24-well plates on a shaker without any primary antibody. At the end of the incubation step, the cells were washed thrice with 1x PBS, 5 min. Subsequently, the cells were incubated for 1 h at room temperature in the dark with the fluorescence-labelled goat anti-rabbit secondary antibody (Thermo Fisher Scientific) at 1:500 (4 µg/mL) in 1% (w/v) BSA, followed by three washes with 1x PBS, 5 min each in the dark. The cell nucleus was counter stained with DAPI (0.5 µg/mL) for 3 min, followed by a wash with 1x PBS. Finally, the coverslips were mounted with fluoroshield mounting medium (Sigma-Aldrich) and sealed with nail polish. The fluorescence images were acquired using the confocal laser scanning microscope LSM-800 (ZEISS, Germany). The same master gain and all other microscope settings for the microscope allow the unbiased quantification of the protein expression (Koepke et al., 2020; Abdo et al., 2021). For each analysis against ZIP12, ZnT1, MT2A, CK2α/α' and CK2β respectively, the images taken at 40X objective were used to measure the mean fluorescence intensity (MFI) which indicates the expression level of the protein using Image-J software (https://imagej.nih.gov/ij/download.html) (Koepke et al., 2020; Abdo et al., 2021). The images were also taken at 100X objectives for illustrating the cellular localisation details of the proteins of the cells.

2.13 Prediction of phosphorylation site by GPS5.0 software

GPS5.0 software (http://gps.biocuckoo.cn/download.php) (Wang et al., 2020) was used to predict the phosphorylation sites of protein kinase CK2 in ZIP12, ZnT1 and MT2A proteins. The FASTA sequences of all the isoforms of ZIP12, ZnT1 and MT2A proteins (*Homo sapiens*) available in the database (https://www.ncbi.nlm.nih.gov/protein/) were analysed for the possible phosphorylation sites. Default settings (threshold selected as medium) were employed for the analysis. The localisations of the potential amino acid residues to be phosphorylated by CK2 kinase were determined by using the Uniprot database (https://www.uniprot.org/).

2.14 Protein extraction from $ZnSO_4$-treated and untreated cells

The previously determined mild cytotoxic $ZnSO_4$ dosages of MCF-7 (320 µM), MCF10A (195.5 µM), PC3 (110 µM) and RWPE-1 (186.88 µM) cells were used for the zinc treatment in proteomic analysis. MCF-7, MCF10A, PC3 and RWPE-1 cells were grown in 75 cm^2 flasks until achieving ~80% confluency and then the spent medium was aspirated and replaced with 11.9 mL of fresh complete medium. $ZnSO_4$ at 120x stock concentration of each dosage for each cell line was prepared in sterile Milli-Q H_2O (Milli-Q® Advantage A10 Water Purification System, Merk). The cells were treated with 100 µL of their respective $ZnSO_4$ stocks. The control cells were treated with 100 µL of sterile Milli-Q water. The cells were incubated for 120 min (T_{120}) and then the protein extraction was performed. Each treatment or control has three biological replicates, which means three protein samples for each time point of a given treatment or control. Each protein sample was prepared with three 75 cm^2 flasks of ~80% confluence.

Following the completion of incubation period, the medium was discarded, the cells were then washed with 10 mL per flask of sterile 1x PBS once and discarded. The cells were trypsinised with 1 mL of 1x trypsin followed by deactivation with their respective complete culture media adding 10 mL per flask. The cell suspensions were collected into 50 mL falcon tubes and centrifuged at 350 g, 3 min at 4 °C. The supernatant was decanted and the cells were washed with 15 mL of ice cold 1x PBS twice. Finally, the cell pellet was resuspended into 1 mL of ice cold 1x PBS and transferred into prelabelled sterile 1.5 mL Eppendorf tubes. The cells were centrifuged at 6000 rpm at 4 °C for 5 min and the supernatant was discarded making sure no liquid in the tubes. The cells were snap frozen in liquid nitrogen and stored at -80 °C freezer for protein extraction.

The 150-200 µL of total protein extraction buffer containing 8 M urea (Amresco), 2 M thiourea (Amresco), 4% (w/v) CHAPS (Amresco) and 1x protease inhibitors, was added to the cell pellet in the 1.5 mL of Eppendorf tubes keeping on ice. The cells were homogenised by an ultrasonic probe homogenizer (Across International). The probe sonication was applied for 3-4 s for cellular disruption and kept the sample for ~20 s on ice by for avoiding protein degradation, repeated this cycle for at least 4 times in order to get complete cellular homogenisation. The samples were transferred into ultra-clear centrifuge tubes (5 x 41 mm) (Beckman Coulter), balanced through weighing and centrifuged at 32,000 rpm at 4°C (Beckman Coulter) for 1 h. The total proteins in the supernatant were collected into 0.65 mL fresh Eppendorf tubes for either protein estimation or storage at -80 °C freezer.

2.15 Estimation of protein concentration

The protein concentrations were estimated using the EZQ™ protein quantitation kit (Life Technologies, Eugene, OR, USA) according to the manufacturer's instructions. The bovine serum albumin (BSA) (Amresco) was used as the standards. The BSA was dissolved in 2% (w/v) sodium dodecyl sulphate (SDS) (Merk, Germany) to prepare 12 mg/mL standard stocks. A wide range (0.5 µg/mL to 0.025 µg/mL) of working concentrations was prepared from the BSA stock. On a clean Whatman paper (10 x 7 cm), 2 µL of each working standard and protein samples was spotted with triplicates. The paper was allowed to air-dry for ~10 min and then it was submerged in absolute (100%) methanol (Astral Scientific, Australia) in a container for 5 min on the orbital shaker (50 rpm). The filter paper was allowed to air-dry for ~10 min removing methanol carefully and again incubated in new EZQ fluorescent dye solution for 30 min on gentle shaking in the dark at room temperature. Following the completion of incubation period, the paper was washed thrice with the solution containing 7% (v/v) acetic acid and 10% (v/v) methanol for 20 s each time. Finally, the Whatman paper was scanned by FUJI LAS-4000 (GE Healthcare, USA). The intensity of each spot was measured employing Multi Gause software to prepare standard curve (Churchward et al., 2005) as well as estimating the protein sample concentrations.

2.16 Reduction and alkylation of the proteins

The proteins were reduced and alkylated before subjecting to isoelectric focussing. The 100 µg of each protein sample in the protein extraction buffer was put in the sterile 0.65 mL Eppendorf tubes. The equal volume of rehydration buffer [protein extraction buffer having 2% (v/v)

carrier ampholytes with pH ranging 3 to 10 (Bio-Rad)] was added to each protein sample. The sample was mixed with 2.42 µL of reduction buffer [0.3702 g (2 M) DTT salt dissolved in 600 µL of TBP (0.2 M) and by adding Milli-Q water to make the final volume to 1.2 mL] and incubate at 25 °C for 1 h on a heating block (Dry Block Heater, Thermoline Scientific, Australia). This reducing buffer enhances the reduction of disulphide bonds to linearise proteins after alkylation. Following completion of the incubation, 5.1 µL acrylamide (5.6 M) was added to each protein sample for alkylation, mixed by vortex and again incubate at 25 °C for further 1 h on a heating block. The samples were ready for the first dimensional run on the immobilised pH gradient strip (Bio-Rad) followed by rehydration.

2.17 Rehydration of immobilised pH gradient (IPG) strip with the protein sample

The non-linear 7 cm long IPG strips having pH 3-10 gradients were hydrated with 100 µg protein sample from 125 µL suspension. Firstly, 125 µL of each protein sample was dispensed into a well of the cleaned rehydration tray. The IPG strip was peeled off using the cleaned forceps and then the strip (gel side down) was placed over the protein sample in the well. It was ensured that there were no air bubbles underneath the strip. After completion the IPG strip loading into the tray, the tray was closed with its lid and covered with the cling wrap. At last, the trays were left on a levelled lab bench for 16 h at room temperature to allow loading of the protein samples.

2.18 Isoelectric focussing (IEF) on IPG strip

The proteins in the rehydrated IPG strip were separated based on the charges of the protein by conducting isoelectric focusing (IEF). The rehydrated IPG strips were transferred into the wells of isoelectric focusing (IEF) tray from the rehydration tray and overlaid with mineral oils (Amresco). The paper wicks prepared by cutting Whatman paper at size ~2.5 cm (length) x ~4 mm (width) was used to connect IPG strip with both positive and negative platinum electrodes. IEF tray was placed in Protean IEF cell system (Bio-Rad) and applied 250 V for 15 min, linearly increased to 4000 V at 50 µA/gel for 2 h. The wicks papers were changed during voltage ramping to improve desalting. IEF focusing was conducted as follows, desalting 15 min, linear gradient 2 h, Vh 37500 and holding at 17 °C and 500 V. Following completion of the focusing, the strips were used immediately for second dimensional protein separation.

2.19 Second dimensional gel electrophoresis

The proteins in the IPG strip of the first dimension were separated based on their molecular weight (MW) by sodium dodecyl sulphate polyacrylamide gel electrophoresis (SDS-PAGE) using 12.5% (w/v) acrylamide (Bio-Rad) gel (1 mm thick 8.4 x 7 cm). The resolving gels (12.5%, w/v) were casted accordingly to **Table 2.4** in gel casting apparatus (Mini-protean, Bio-Rad) the day before the run and stored overnight in 1x tris-glycine-SDS running buffer for homogenous polymerization at 4 °C. The focused IPG strips were incubated in 130 mM DTT in equilibration buffer for 10 min followed by 10 min alkylation with 350 mM acrylamide at room temperature on a gentle shaker. Both buffers ensure the reduction and alkylation of the cysteine residues. Additionally, it assists to minimise the vertical streaks and enhances protein separation. The SDS-PAGE gels were placed in the casting racks and the gels were overlaid with warm agarose solution (0.5%, w/v) with 0.003% (v/v) bromophenol blue dye (Bio-Rad). Instantly, the IPG strip was placed in warm agarose layer over the stacking gel (prepared as per **Table 2.5**) with extra care using the forceps. It was ensured that there were no air bubbles below the IPG strips. Once the agarose layer was solidified after ~2 min, the gels were placed in 1x tris-glycine-SDS running buffer in the electrophoretic tank (Bio-Rad). The electrophoresis run was carried out in the cold room at 4 °C for about 5 min at 120 V, then at 90 V for about 3 h until the tracking bromophenol dye reached the glass plate's bottom. At last, the gels were taken out of the glass plates and promptly dipped into the fixatives for gel fixation (Asgarov et al., 2021; Almuslehi et al., 2022).

Table 2.4 Recipe of the resolving gel (12.5%, w/v; pH 8.8)

Serial No.	Items	For 2 gels (mL)	For 6 gels (mL)
1	40% (w/v) Acrylamide stock (Bio-Rad)	4.69	14.07
2	1.5 M TRIS buffer (pH 8.8) (Amresco)	3.75	11.25
3	10% (w/v) SDS solution (Merck)	0.15	0.45
4	Milli-Q water	6.25	18.75
5	10% (w/v) APS solution (Bio-Rad)	0.15	0.45
6	100% TEMED (Amresco)	0.02	0.06
	Final volume (mL)	15	45

Prepared 10% (w/v) ammonium per sulphate (APS) lasts for one week at 4 °C.

Table 2.5 Recipe of the staking gel (5%, w/v; pH 6.8)

Serial No.	Items	For 2 gels (mL)	For 6 gels (mL)
1	40% (w/v) Acrylamide stock (Bio-Rad)	1.7	5.1
2	1.5 M TRIS buffer (pH 8.8) (Amresco)	2.5	7.5
3	10% (w/v) SDS solution (Merck)	0.1	0.3
4	Milli-Q water	5.7	17.1
5	10% (w/v) APS solution (Bio-Rad)	0.1	0.3
6	100% TEMED (Amresco)	0.01	0.03
	Final volume (mL)	10.11	30.33

2.20 Gel fixation and staining

The proteins separated in the gels two-dimensionally were fixed in fixative solution containing 10% (v/v) methanol and 7% (v/v) acetic acid applying gentle shaking (50 rpm) at room temperature for 1 h. The fixative solution was removed from the gels by rinsing them with Milli-Q water three times for 20 min each time. The gels were then stained with very sensitive 50 mL colloidal Coomassie Brilliant Blue (cCBB) (Amresco) (**Table 2.6**). The gels were incubated in cCBB solution for 20 h on a shaker at 50 rpm. The cCBB solution was removed and the gels were washed with 0.5 M NaCl thrice (15 min each time) on a shaker. The gels were imaged by FUJI LAS-4000 (GE Healthcare, USA). Finally, the gels were stored in Milli-Q water for short period of time or in 20% (w/v) ammonium sulphate (50 mL/gel) solution for long duration at 4 °C until further analysis (Gauci et al., 2013; Noaman and Coorssen, 2018).

Table 2.6 Recipe of colloidal CBB solution

Serial No.	Items	Needed (mL)
1	2% (w/v) CBB (Amresco)	5
2	30% (v/v) phosphoric acid (Sigma-Aldrich)	5
3	20% (w/v) ammonium sulphate (Sigma-Aldrich)	25
4	100% methanol (Sigma-Aldrich)	20
5	Milli-Q water	45
	Final volume (mL)	100

2.21 Protein spot detection and quantitative analysis

The protein spots were detected and quantitatively analysed in the gel images by employing Delta2D (version 4.0.8, DECODON Gmbh, Germany) as described previously (Almuslehi et al., 2022). The protein spots in the gel images were quantitatively analysed in cancer cells compared to normal cells with or without zinc treatment. Similarly, the protein spots were analysed in each cell line with or without zinc treatment. In each comparison, the gel images were warped and fused to make master gel using 'union fusion'. The spots were then transferred to each image in their group to ensure consistent spot matched (100% matching) in all biological replicates (n = 3) in each group. The molecular weight marker lane and the edges were excluded manually during spot estimation. The background subtracted spots volumes were reported as grey values, fold changes, *p* values (t-test) and relative standard deviation (RSD). Based on *p* value ($p < 0.05$) and ratio of grey value, the candidate spots were considered for further proteolytic digestion and liquid chromatography-tandem mass spectrometry (LC-MS/MS) to identify the proteins. Thereby, the differentially expressed proteins were identified in all comparisons.

2.22 Experimental molecular weight and *pI* calculation

Three calibration gels with isoelectric focusing (*pI*) standards (Bio-Rad) and molecular weight (MW) markers (Bio-Rad) were used to estimate the experimental MW and *pI* of the resolved proteoforms. The term "proteoform" means all the protein forms of a given protein due to all the possible modifications at DNA level (genetic variation including mutation, polymorphism), RNA level (RNA splicing) and protein level (post-translational modifications including glycosylation, phosphorylation, methylation, acetylation, alkylation, truncation, lipidation) (Smith and Kelleher, 2013; Forgrave et al., 2022). The gels were stained with cCBB and imaged by FUJI LAS-4000 (GE Healthcare, USA). The migration distances by each standard band (MW markers) against the dye front were measured by the ruler from the top of the resolving gel. Relative mobility (R_f, retention factor) was calculated dividing the migration distance of the protein by the migration distance of the dye front. The values of Log MW were plotted (y axis) against R_f values (x axis) to generate the standard curve along with equation (**Figure 2.2A)**. The above steps were repeated and calculated R_f for the spots of unknown proteoforms in the 2-D gels. The experimental MW was thereby calculated using the equation [$y = -0.475\ln(x) + 1.0013$] established from the standard curve. Similarly, the migration distances by each *pI* standard spot and by the dye front were measured by the ruler from the

left (pH 3) starting point of IPG strip gel to the right end (pH 10) of IPG gel observed in the resolving gel. The migration distance by the dye front was confirmed measuring the length of IPG strip gel at complete hydrated condition. The pH values were plotted (y axis) against the percentage (%) of total IPG strip length (x axis) to generate the *pI* standard curve and *pI* calculating equation (**Figure 2.2B**). Thus, *pI* of the spot of unknown proteins was estimated.

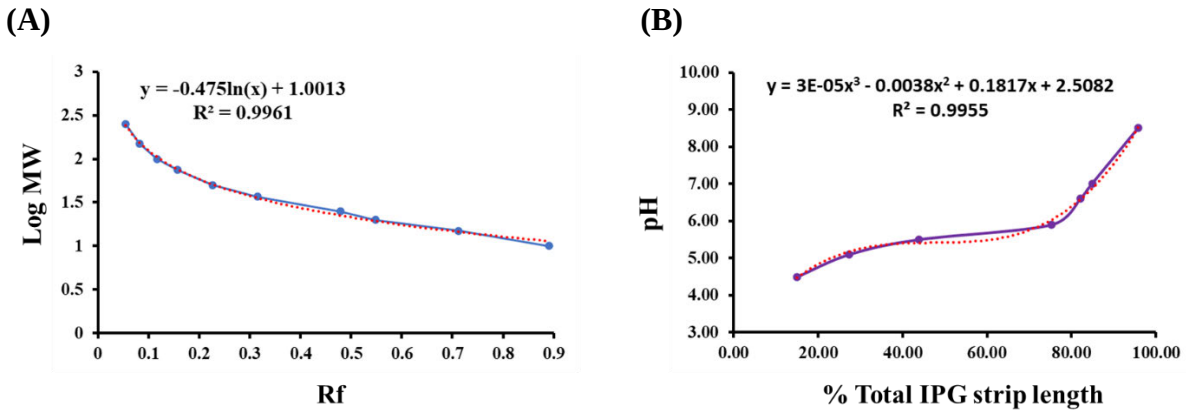

Figure 2.2 Determination of the MW (A) and pI (B) of an unknown protein. The MW and pI of an unknown are determined by the standard curves established by running protein standards in two-dimensional gel electrophoresis (2-DE).

2.23 In-gel protein spot digestion and peptide extraction for LC-MS/MS

The protein spots were excised with a micro tip (Sigma-Aldrich) from the gels and quickly transferred into pre-labelled 0.65 mL sterile Eppendorf tubes (Corning Incorporated). Then gel pieces were stored at -30 °C or they could be digested immediately by trypsin for peptide extraction. For peptide extraction, washed and cleaned lab coat, mask, gloves, special helmet were worn to avoid contamination from other proteins such as keratin. Biosafety hood and working area were properly cleaned with 70% (v/v) ethanol. The 0.65 mL tubes were taken out from -30 °C fridge. About 500 µL (enough to submerge the gel pieces) of 50 mM ammonium bicarbonate (NH_4HCO_3) (MS grade ammonium bicarbonate, Sigma-Aldrich) solution was added into each tube, vortexed for 10 s, quickly spun and incubated for 5-10 min to make sure the gel pieces were at correct pH. NH_4HCO_3 solution was removed and 200 µL of destain solution [50% (v/v) acetonitrile + 50% (v/v) NH_4HCO_3 of 50 mM solution] (MS grade acetonitrile, Sigma-Aldrich) was added, vortexed for 10 s, quickly spun and incubated for 5 to 15 min. Destaining step was repeated generally 2-3 times (until gel pieces turned into colourless). 200 µL of 100% acetonitrile was added, shortly vortexed and incubated for 10 min

at room temperature in the hood. Acetonitrile was aspirated off and kept the tubes open for 30 min in order to drying the gel pieces out completely. The gel pieces got shrunken and turned into white following incubation. These dried gel pieces could be stored at room temperature or subjected to trypsin digestion.

For trypsin digestion, 20 µL (0.0781 ng/µL) of trypsin (MS grade trypsin gold 100 µg, Promega) (enough to emerge gel pieces) was added into each tube for the rehydration of gel pieces at 4 °C for 30 min on ice. Low temperature (4 °C) was maintained to get sucked trypsin as much as possible and keep it functional. Then 20 µL (volume may be more to cover gel pieces) of 50 mM NH_4HCO_3 was added to cover the gel pieces. The protein spots were digested overnight (~12 h) at 4 °C in the fridge. The tubes containing gel pieces were subjected to sonication using Soniclean 160TD Ultrasonic Cleaner (Mektronics, Australia Pyt Ltd) at maximum power for 30 min. The tubes were quickly vortexed and spun. The supernatant was transferred into the fresh pre-labelled 0.65 mL tubes. Enough (usually 30 µL) volume of 50% (v/v) acetonitrile (i.e., destain solution) + 2% (v/v) formic acid (MS grade formic acid, Sigma-Aldrich) solution was dispensed into each tube to cover the gel pieces. The tubes were vortexed and spun shortly and again supernatant was collected to combine with the initial digested supernatant. The tubes were spun by Speed Vac RVC 2-25 CD plus (CHRIST) to reduce the volume 10-12 µL and finally the peptide solutions were transferred into the pre-labelled auto glass screw neck vials (12 x 32 mm) (Waters) for loading the sample onto the LC-MS/MS or storing at -30 °C.

2.24 Liquid chromatography-tandem mass spectrometry (LC-MS/MS)

The digested protein samples were analysed by LC-MS/MS in the mass spectrometry facility of Western Sydney University, using a Waters nanoAcquity LC-MS/MS sample manager fitted with a binary solvent manager. Mass spectrometric detection was conducted using a Waters Synapt G2-Si. The Separation of the digested peptides from each protein spot of the 2-DE gels consisted of two mobile phases. Mobile phase A [0.1% (v/v) formic acid in Milli-Q water] and mobile phase B [0.1% (v/v) formic acid in acetonitrile, ACN]. The trapping column was a Waters nanoEase M/Z Symmetry C18 trap column (180 µm x 20 mm) and the analytical column was a Waters nanoAcquity LC-TMS 1.7 µm BEH130 C18 column (75 µm x 100 mm) thermostatted to 40 °C. Elution was achieved at a flow rate of 0.3 µL/min with each sample

run for 50 min. The gradient was 0 min 1% (v/v) B, 2 min 10% (v/v) B, 40 min 40% (v/v) B, 42 min 85% (v/v) B and 50 min 85% (v/v) B. Data was obtained in technical triplicates.

Mass spectrometry was conducted in positive ion mode with a capillary voltage of 3 kV and a sampling cone voltage of 30 V as well as a source offset of 30 V for electrospray ionizations. The source temperature was set at 80 °C. A desolvation source of nitrogen gas at 20 L/h and a desolvation temperature of 350 °C was used. Lock spray ion acquisition was conducted every 300 s with Glu1-fibrinopeptide B as the reference compound. Data acquisition was conducted over the mass to charge range of 50-2000. The data independent acquisition used an HDMSe experiment employing both low and high energy collision-induced dissociation of parent ions. Low energy collision was done at 6 V in the trap collision cell and at 4 V in the transfer collision cell. High energy collision used a collision energy ramp from 17 V to 60 V in the transfer collision cell. Scan time was 0.5 s and after each scan the system would switch from high to low energy collision.

2.25 Analysis for identifying the proteins

The protein identification was conducted employing ProteinLynx Global Server (PLGS) programme (version 3.0 Waters Corporation, USA) and the UniProt (*Homo sapiens*, human) database with the following settings

(a) The allowed maximum missed cleavages was set to 1.
(b) The allowed false discovery rate was set to 4% and the maximum protein size was set to 280 kDa.
(c) The peptide modifications were carbamidomethyl C (fixed) and oxidation M (variable).
(d) The minimum fragments per peptide was 3.
(e) The minimum peptide per protein was 1.
(f) The minimum fragments per protein was 7.

Finally, the identified proteins from each spot by LC-MS/MS had to meet the selection thresholds such as PLGS or protein score ≥ 200, sequence coverage $\geq 6\%$ and matched peptides ≥ 3.

2.26 Literature mining

The identified proteins from both breast and prostate cells were searched in PubMed (www.ncbi.nlm.nih.gov/pubmed/) to know their expression status, cellular localisation, molecular function and role in human cancers.

2.27 UniProt database application

The gene ID, cellular localisation as well as molecular function of the identified proteins were obtained from UniProt (www.uniprot.org) database.

2.28 PANTHER database application

PANTHER (www.pantherdb.org) database was used to classify the identified proteins into different protein classes (Almuslehi et al., 2022).

2.29 Data and statistical analysis

The data was analysed in Excel. The fold change for a given gene expression in cancer cells was compared to the fold change of the same gene expression in normal cells by the independent-sample t-test of SPSS statistical software. The fold change of a given gene expression in the time course was analysed by the one-sample t-test of SPSS statistical software.

The mean fluorescence intensities (MFI) of a particular protein under zinc treatment (T_{30}, T_{120}) were compared to the MFI of the same protein at the control condition (T_0) by one-way ANOVA of GraphPad Prism 8. The conditions (T_0, T_{30}, T_{120}) were compared by one-way ANOVA of GraphPad Prism 8 with Dunnett's multiple comparisons test, where statistical significance is represented by $p < 0.001$.

Chapter 3 Expression profiles of the genes associated with zinc homeostasis in normal and cancerous breast and prostate cells

3.1 Introduction

Zinc (Zn^{2+}) is the second most abundant trace element after iron, essential for cellular structures and functions in humans (Hennigar and Kelleher, 2012). Since 1939 when Zn^{2+} was first demonstrated as a component of the enzyme carbonic anhydrase of erythrocytes (Keilin and Mann, 1939), its biological roles have been delineated in the cell as a cofactor for well over 300 enzymes, as a structural component for approximately 10% of the human proteome (~3000 proteins) such as transcription factors with zinc finger motifs and as a second messenger in signalling pathways (Rink and Gabriel, 2000; Andreini et al., 2006; Kambe et al., 2015; Fong et al., 2018). Consequently, the cell has developed a tight molecular network for Zn^{2+} homeostasis, including Zrt/Irt-like proteins (ZIP), Zn^{2+} transporters (ZnT) and metallothioneins (MT), which are at the forefront of cellular Zn^{2+} uptake, export and sequestration for regulating the biological and functional behaviours of the cells (Kagara et al., 2007; Taylor et al., 2012).

There are 14 members of ZIP (ZIP1-14), encoded by *SLC39A1-14* genes, that function to increase cytoplasmic Zn^{2+} by importing Zn^{2+} into the cytosol from extracellular space or subcellular organelles such as the endoplasmic reticulum and 10 ZnT members (ZnT1-10) encoded by *SLC30A1-10* which function to decrease cytoplasmic Zn^{2+} by exporting Zn^{2+} out of the cell or sequestering cytoplasmic Zn^{2+} into subcellular organelles. The association of *SLC39A* and *SLC30A* with human cancers has been widely reported, such as in breast cancer (Taylor et al., 2012), prostate cancer (Franz et al., 2013; Singh et al., 2016), oesophageal cancer (Wu et al., 2013), pancreatic cancer (Unno et al., 2009; Xu et al., 2014; Liu et al., 2018), liver cancer (Franklin et al., 2012; Shen et al., 2013), brain cancer (Lin et al., 2013; Kang et al., 2015), ovarian cancer (Ma et al., 2015; Cheng et al., 2021), skin cancer (Lee et al., 2019), cervical cancer (Zhao et al., 2007), kidney and bladder cancers (Wu et al., 2015). Curiously, a single Zn^{2+} transport protein ZIP4 has been reported to be associated with multiple cancers such as liver cancer (Xu et al., 2014), prostate cancer (Chen et al., 2012), lung cancer (Wu et al., 2017), pancreatic cancer (Li et al., 2007; Xu et al., 2014), brain and spinal cord cancer (glioma) (Lin et al., 2013).

Previous studies reported higher Zn^{2+} accumulations in breast cancer cells compared to their normal epithelial cells (Alam and Kelleher, 2012; Larner et al., 2015; Takatani-Nakase et al., 2016). High intracellular Zn^{2+} is associated with malignancy and metastasis in breast cancer (Takatani-Nakase et al., 2014; Xu et al., 2014) and such Zn^{2+} accumulation is directly connected to the dysregulations of Zn^{2+} transporters such as ZIP6, ZIP7, ZIP10, ZnT1 and ZnT2 (Kagara et al., 2007; Taylor et al., 2008; Lopez et al., 2011; Taylor et al., 2012; Bafaro et al., 2017; Wang et al., 2020; Schilling et al., 2022). The normal prostate epithelial cells have an abundant expression of *SLC39A1* (ZIP1), which leads to high cytoplasmic Zn^{2+} to endow prostatic health (Costello et al., 1999). In contrast, low intracellular Zn^{2+} is the key feature of prostatic cancer cells as a result of the significant low expressions of *SLC39A1* (ZIP1), *SLC39A2* (ZIP2) and *SLC39A3* (ZIP3) (Costello et al., 1999; Franklin et al., 2003; Franklin et al., 2005; Johnson et al., 2010; Kolenko et al., 2013; Pan et al., 2017; Sauer et al., 2020). Therefore, this study takes advantage of the opposite intracellular zinc profiles of breast and prostate cancer cells to explore the expression landscape of *SLC39A* (ZIP) and *SLC30A* (ZnT) genes in order to gain insights into the zinc homeostasis of these two kinds of cancer cells.

Cytosolic metallothioneins (MT), a class of small cysteine-rich and metal-binding proteins, are also involved in maintaining Zn^{2+} homeostasis by sequestration of excess zinc (Maret, 2003; Kambe et al., 2015; Krężel and Maret, 2017; Abdo et al., 2021; Singh et al., 2021; Zaman et al., 2021). There are eight functional isoforms of MT identified in humans such as MT1A, MT1B, MT1E, MT1F, MT1G, MT1H, MT1X and MT2A (Werynska et al., 2013), and dysregulation of MT was reported in many human cancers (Jin et al., 2000; Tai et al., 2003; Tao et al., 2007; Li et al., 2017; Si and Lang, 2018; Masiulionytė et al., 2019; Dai et al., 2021). In addition, our previous study uncovered the marked elevation of *MT1B*, *MT1F*, *MT1X* and *MT2A* in MCF-7 breast cancer cells in response to extracellular zinc exposure (Zaman et al., 2021).

This study examined the expression profiles of 14 *SLC39A*, 10 *SLC30A* and 4 *MT* genes in breast cancer cells (MCF-7 and MDA-MB-231) and prostate cancer cells (PC3 and DU145) along with their normal counterparts (normal breast epithelial cell line MCF10A and normal prostate epithelial cell line RWPE-1). The profiling was carried out with quantitative reverse transcription polymerase chain reaction (qRT-PCR) under two varying dosages of $ZnSO_4$ and in three time points of a time course. The findings are valuable to our understanding of the molecular details for Zn^{2+} homeostasis in breast and prostate cancer cells.

3.2 Results

3.2.1 Cell viability under $ZnSO_4$ treatment

The mild cytotoxic $ZnSO_4$ dosages for the time course of zinc treatment of MCF10A, MCF-7, MDA-MB-231, RWPE-1, PC3 and DU145 cells were firstly determined at 195.5 µM, 320 µM, 350 µM, 186.88 µM, 110 µM and 150 µM $ZnSO_4$, respectively. Mild cytotoxic zinc dosage for normal breast epithelial cell (MCF10A) is 195.5 µM, much lower than mild cytotoxic zinc dosages of breast cancer cells (320 µM for MCF-7, 350 µM for MDA-MB-231), which demonstrates higher tolerance to zinc for the breast cancer cells compared to the normal breast epithelial cells. In contrast, the mild cytotoxic dosage for normal prostatic epithelial cells (RWPE-1) is 186.88 µM, much higher than PC3 (110 µM) and DU145 (150 µM), demonstrating lower tolerance to zinc for the prostate cancer cells compared to the normal prostate epithelial cells. These findings clearly show the divergent behaviours of breast and prostate cancer cells.

The viability of breast and prostate cells at T_0, T_{30}, T_{60}, T_{90} and T_{120} time points under the dosages was shown in **Figure 3.1**. The cell viability of MCF10A, MCF-7 and MDA-MB-231 under mild cytotoxic zinc exposures were 87%, 98%, 100%, respectively at T_{30} and 71%, 77%, 80%, respectively at T_{120} (**Figure 3.1A**). The benign $ZnSO_4$ dosage of three breast cell lines was determined at 50 µM, which led to the increase of cell viability to 106%, 111% and 107%, respectively, for MCF10A, MCF-7 and MDA-MB-231 cells at T_{120} (**Figure 3.1B**). RWPE-1 normal prostate epithelial cells were more tolerant to $ZnSO_4$ exposure in comparison to PC3 and DU145 prostate cancer cells, with the viability of RWPE-1 under 186.88 µM $ZnSO_4$ shown as 98% (at T_{30}), 85% (at T_{120}), whilst the viability of PC3 under 110 µM $ZnSO_4$ was 89% (at T_{30}) and 79% (at T_{120}) and the viability of DU145 under 150 µM $ZnSO_4$ was 94% (at T_{30}) and 83% (at T_{120}) (**Figure 3.1C**).

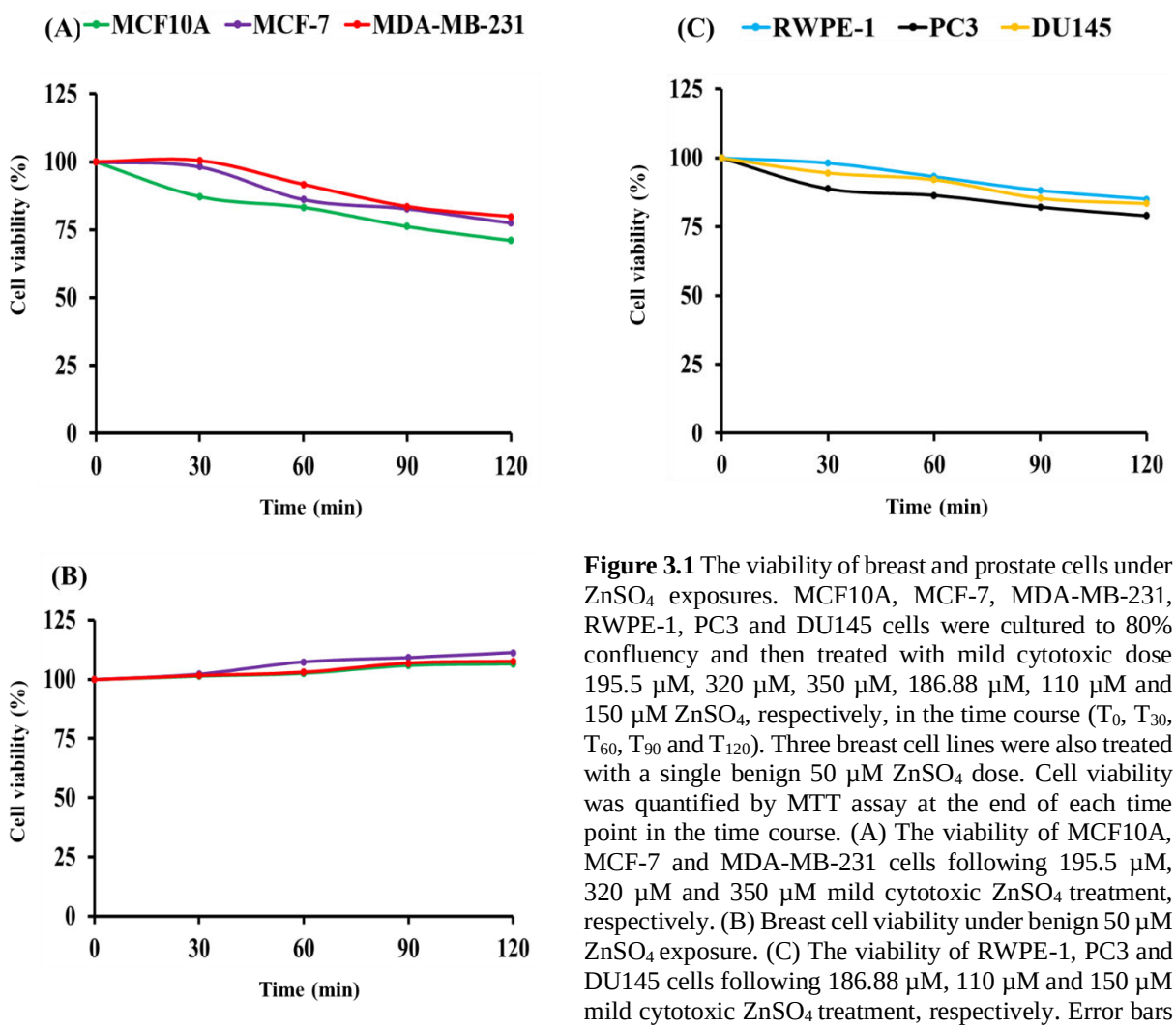

Figure 3.1 The viability of breast and prostate cells under $ZnSO_4$ exposures. MCF10A, MCF-7, MDA-MB-231, RWPE-1, PC3 and DU145 cells were cultured to 80% confluency and then treated with mild cytotoxic dose 195.5 µM, 320 µM, 350 µM, 186.88 µM, 110 µM and 150 µM $ZnSO_4$, respectively, in the time course (T_0, T_{30}, T_{60}, T_{90} and T_{120}). Three breast cell lines were also treated with a single benign 50 µM $ZnSO_4$ dose. Cell viability was quantified by MTT assay at the end of each time point in the time course. (A) The viability of MCF10A, MCF-7 and MDA-MB-231 cells following 195.5 µM, 320 µM and 350 µM mild cytotoxic $ZnSO_4$ treatment, respectively. (B) Breast cell viability under benign 50 µM $ZnSO_4$ exposure. (C) The viability of RWPE-1, PC3 and DU145 cells following 186.88 µM, 110 µM and 150 µM mild cytotoxic $ZnSO_4$ treatment, respectively. Error bars are too small to be seen, representing the standard deviation of at least 24 replicates.

The expression of *SLC39A*, *SLC30A* and *MT (MT1B*, *MT1F*, *MT1X*, *MT2A)* was determined following both mild cytotoxic and benign zinc treatment at T_0, T_{30} and T_{120}. Firstly, the suitability of *GAPDH* gene as a reference for this study was validated by the finding that there was no significant variation of *GAPDH* expression across the cell lines at T_{30} and T_{120} compared to T_0 (**Figure 3.2**).

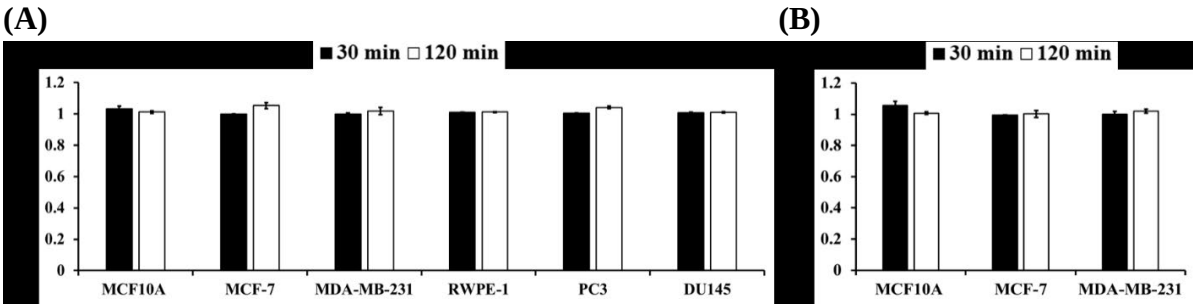

Figure 3.2 Expression of *GAPDH* under zinc treatment at T_{30} and T_{120} compared to T_0. (A) *GAPDH* expression under mild cytotoxic dosage of $ZnSO_4$ in normal and cancer cells of breast and prostate. Cells were grown to approximately 80% confluency. MCF10A normal breast epithelial cells and both MCF-7 and MDA-MB-231 breast cancer cells were treated with 195.5 µM, 320 µM and 350 µM $ZnSO_4$, respectively. RWPE-1 normal prostate epithelial cells and both PC3 and DU145 prostate cancer cells were exposed to 186.88 µM, 110 µM and 150 µM $ZnSO_4$, respectively. The cells for the control were treated with sterile Milli-Q H_2O. Total RNA was then prepared for each sample, cDNA was synthesised and finally qRT-PCR was conducted. Relative expression of *GAPDH* at T_{30} and T_{120} was quantified compared to T_0. (B) *GAPDH* expression under growth-promoting dosage of $ZnSO_4$ in normal and cancerous breast epithelial cells**.** The cells were treated with 50 µM $ZnSO_4$ for 30 and 120 min, and then processed in the same way as described previously. Error bar represents SEM of three biological replicates.

3.2.2 *SLC39A*, *SLC30A* and *MT* gene expression in breast and prostate cancer cells compared to normal cells without zinc treatment

The expression profiles of the 28 genes were examined in breast and prostate cancer cells compared to their normal counterparts without zinc treatment. The expression data was analysed by heatmap hierarchical cluster analysis (**Figure 3.3**). The fold changes of the gene expression are tabulated in **Table 3.1**. Cluster (a) revealed a shared pattern of gene expression for the cells of both breast and prostate cancers, that is, the marked elevation of *SLC39A4* ($p < 0.05$), *SLC39A6* ($p < 0.01$), *SLC39A8* ($p < 0.05$) and *SLC39A11* ($p < 0.01$) and the down-regulation of *SLC30A4* ($p < 0.001$). This finding is in agreement with the clinical setting, as the databases UALCAN (http://ualcan.path.uab.edu) (Chandrashekar et al., 2017), GEPIA2 (http://gepia2.cancer-pku.cn/#index) (Tang et al., 2019) and GENT2 (http://gent2.appex.kr) (Park et al., 2019) showed higher expression of *SLC39A4*, *SLC39A6*, *SLC39A11* in breast and prostate cancerous tissues than their normal counterparts (**Table 3.1**). The expression pattern of *SLC39A3*, *SLC39A7*, *SLC39A9*, *SLC30A1*, *SLC30A3* is divergent between the two different kinds of cancer cells, such as *SLC30A1* (ZnT1) which was up-regulated in prostate cancer cells but was either down-regulated or unchanged in breast cancer cells.

Cluster (b) shows *SLC30A2* and *SLC30A9* up-regulation across the breast and prostate cancer cell lines in **Figure 3.3**. The marked overexpression of *SLC30A2* (ZnT2) in MCF-7 ($p < 0.001$), PC3 ($p < 0.001$) and DU145 ($p < 0.01$) might indicate that ZnT2 is involved in Zn^{2+} efflux or compartmentalisation of zinc in those cells since it is localised in the plasma membrane and in the membrane of endosomes, lysosomes, or secretory vesicles. *SLC39A13*, *SLC39A14* and *SLC30A6* were up-regulated in prostate cancer cells compared to the breast cancer cells. Cluster (c) demonstrates strong up-regulation of *MT1B* ($p < 0.05$), *MT1F* ($p < 0.05$), *MT1X* ($p < 0.01$), *MT2A* ($p < 0.05$), *SLC30A5* ($p < 0.05$) but down-regulation of *SLC30A10* ($p < 0.05$) in all four cancer cell lines in **Figure 3.3**. Similarly, the elevation of *MT1B*, *MT1F* and *SLC30A5* expression was observed in prostatic cancer tissues (**Table 3.1**).

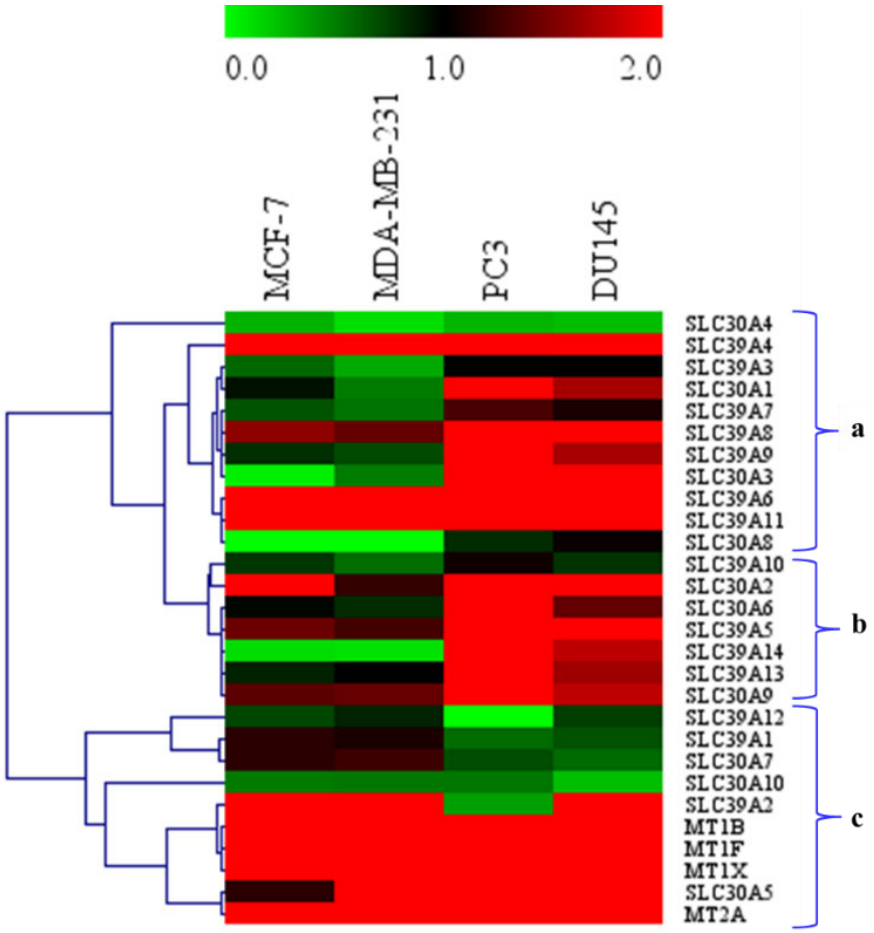

Figure 3.3 Expression profile of 14 *SLC39A*, 10 *SLC30A* and 4 *MT* genes in breast and prostate cancer cells compared to their corresponding normal cells. The colour scale (0.0-2.0) represents the expression levels of 28 genes (green colour denotes down-regulation whilst red denotes up-regulation). The hierarchical clustering of the genes is shown in the dendrogram at the left.

Table 3.1 Expression analysis of *SLC39A*, *SLC30A* and *MT* genes (fold changes) in breast and prostate cancer cells by qRT-PCR and in tissues based on databases (UALCAN, GEPIA2 and GENT2)

Name		Breast cancer vs normal cells		Breast cancer vs normal tissues			MCF-7 vs MDA-MB-231	Prostate cancer vs normal cells		Prostate cancer vs normal tissues			PC3 vs DU145
Proteins	Genes	MCF-7	MDA-MB-231	UALCAN	GEPIA2	GENT2		PC3	DU145	UALCAN	GEPIA2	GENT2	
ZIP1	*SLC39A1*	1 16	0.97	↑	↑	↑	1.20	0.57	0.67	–	↑	↓	1.55
ZIP2	*SLC39A2*	3 28	265.93	–	↑	↓	0.01	0.37	69.49	↓	↓	↓	0.01
ZIP3	*SLC39A3*	0 59	0.33	↑	↑	↑	1.76	0.98	0.99	↑	↑	↓	1.00
ZIP4	*SLC39A4*	1 98	240.27	↑	↑	↑	0.01	438.40	398.82	↑	↑	–	1.10
ZIP5	*SLC39A5*	1.42	0.38	↑	↓	↓	3.69	5.80	3.67	↑	↓	↓	1.58
ZIP6	*SLC39A6*	4.78	3.90	↑	↑	↑	1.23	44.46	55.86	↑	↑	↑	0.80
ZIP7	*SLC39A7*	0.66	0.54	↑	↑	↑	1.23	1.29	1.11	↑	↑	↑	1.16
ZIP8	*SLC39A8*	1 56	1.39	↓	↑	–	1.12	5.48	4.33	↑	↑	↑	1.27
ZIP9	*SLC39A9*	0.81	0.70	↑	↑	↑	1.16	2.10	1.66	↑	↑	↑	1.26
ZIP10	*SLC39A10*	0.78	0.56	↑	↑	–	1.38	1.06	0.79	–	↑	↑	1.34
ZIP11	*SLC39A11*	2.70	2.65	↑	↑	↑	1.02	7.61	8.92	↑	↑	↑	0.85
ZIP12	*SLC39A12*	0.72	0.86	–	↓	↓	0.84	0.003	0.75	–	↓	–	0.004
ZIP13	*SLC39A13*	0.86	0.99	↑	↓	↑	0.87	2.27	1.62	–	↓	↓	1.39
ZIP14	*SLC39A14*	0 13	0.11	↓	↓	–	1.15	2.91	1.74	↓	↓	↓	1.67
ZnT1	*SLC30A1*	0 93	0.51	↑	↑	↑	1.83	2.17	1.65	↓	↑	↑	1.31
ZnT2	*SLC30A2*	139.38	1.20	↓	↑	↓	115.43	14779.16	189.64	–	↓	↓	77.93
ZnT3	*SLC30A3*	0.06	0.51	↑	–	↓	0.12	19.27	16.69	–	↓	–	1.15
ZnT4	*SLC30A4*	0 29	0.12	↓	↓	↓	2.38	0.28	0.25	–	↑	↑	1.14
ZnT5	*SLC30A5*	1 50	2.74	↑	↑	↑	0.55	2.17	2.22	↑	↑	↑	0.98
ZnT6	*SLC30A6*	0 96	0.82	–	↑	–	1.17	2.22	1.39	↓	↑	↑	1.60
ZnT7	*SLC30A7*	1 17	1.24	↑	↑	↑	0.95	0.69	0.57	↑	↑	↑	1.20
ZnT8	*SLC30A8*	6.6E-5	6.8E-5	↑	↑	↓	0.97	0.82	1.04	–	↓	↓	0.80
ZnT9	*SLC30A9*	1 35	1.40	↑	↑	–	0.97	2.17	1.75	–	↑	↑	1.24
ZnT10	*SLC30A10*	0 52	0.53	–	↓	↓	0.97	0.52	0.25	–	–	–	2.08
MT1B	*MT1B*	26 27	65.29	–	–	–	0.40	26.91	22.76	–	↑	–	1.18
MT1F	*MT1F*	21.48	49.11	–	↓	↓	0.44	22.61	18.74	–	↑	↑	1.21
MT1X	*MT1X*	22 19	44.74	↓	↓	↓	0.50	13.80	14.97	↓	↓	↓	0.92
MT2A	*MT2A*	41 13	126.44	–	↓	↓	0.33	101.76	78.62	–	↓	–	1.29

The fold change values demonstrate the gene expression levels in breast cancer cells (MCF-7, MDA-MB-231) and prostate cancer cells (PC3, DU145) compared to their respective normal cells MCF10A and RWPE-1 without exogenous zinc exposure (T_0). The gene expression between cancer cells i.e., MCF-7 vs MDA-MB-231 and PC3 vs DU145 were also compared at T_0. The symbol ↑ denotes the up-regulation of the genes in cancerous tissues compared to normal tissues; symbol ↓ denotes the down-regulation of the genes in cancerous tissues compared to normal tissues; and blank cells denote the non-significant gene expression in cancer tissues vs normal tissues or the data not available or not well differentiated.

Additionally, the gene expression was also compared between the cancer cells (i.e., MCF-7 vs MDA-MB-231 and PC3 vs DU145) as shown in **Table 3.1**. *SLC39A5* ($p < 0.001$) and *SLC30A2* ($p < 0.001$) exhibited significant up-regulation in luminal breast cancer cells MCF-7 compared to basal breast cancer cells MDA-MB-231, while *SLC39A2* ($p < 0.001$), *SLC39A4* ($p < 0.001$), *MT1B* ($p < 0.01$), *MT1F* ($p < 0.01$), *MT1X* ($p < 0.01$) and *MT2A* ($p < 0.01$) were down-regulated without exogenous zinc exposure. *SLC30A2* ($p < 0.001$) demonstrated up-regulation in PC3 prostate cancer cells compared to DU145 prostate cancer cells whereas *SLC39A2* ($p < 0.001$) and *SLC39A12* ($p < 0.001$) were down-regulated.

3.2.3 Effects of extracellular zinc exposure on the expression of *SLC39A*, *SLC30A* and *MT* genes in breast and prostate cells

The expression levels of *SLC39A*, *SLC30A* and *MT* genes at T_{30} and T_{120} following mild cytotoxic $ZnSO_4$ treatment in breast and prostate normal and cancer cell lines were shown in **Figure 3.4** and **Table 3.2**. Cluster (a) shows the reduced expression of *SLC39A6* ($p < 0.05$) across all breast and prostate cells under mildly toxic $ZnSO_4$ treatment. *SLC39A13* ($p < 0.001$) is also down-regulated in breast cell lines. *SLC39A14* exhibited higher expression in prostatic cells compared to breast cells.

Cluster (b) in **Figure 3.4** exhibits the overexpression of *SLC39A2* ($p < 0.01$), *SLC39A4*, *SLC30A3* ($p < 0.05$), *SLC30A4* ($p < 0.01$), *SLC30A5*, *SLC30A6* ($p < 0.01$), *SLC30A7*, *SLC30A8* ($p < 0.05$), *SLC30A9* ($p < 0.05$) and *SLC30A10* under mild cytotoxic zinc exposure in both breast cancer cells whereas normal breast epithelial cells show decreased expression of *SLC39A2-3* ($p < 0.01$), *SLC30A4-7* ($p < 0.01$), *SLC30A9* ($p < 0.01$) and *SLC39A10* ($p < 0.05$). Interestingly *SLC39A1*, *SLC39A5*, *SLC39A10* and *SLC39A11* demonstrated higher expression in basal breast cancer cells (MDA-MB-231) compared to luminal breast cancer cells (MCF-7) under zinc exposure. *SLC39A2* ($p < 0.001$), *SLC39A4* ($p < 0.01$) and *SLC30A10* ($p < 0.05$) were increased in all three prostatic cell lines following zinc treatment, but less aggressive prostatic cancer DU145 cells showed greater expression of *SLC39A2*, *SLC39A4* and *SLC30A10* compared to normal RWPE-1 and cancerous PC3 cells. Also, DU145 cells exhibited greater expression of *SLC30A3-9* and *SLC39A3* compared to RWPE-1 and PC3 cells. Zinc treatment decreased *SLC39A1* and *SLC39A3* expression in RWPE-1 and PC3 cells. Surprisingly, *SLC30A6* ($p < 0.001$) and *SLC39A10* ($p < 0.001$) were significantly reduced in highly aggressive prostate PC3 cells.

Cluster (c) of **Figure 3.4** represents the overexpression of *SLC39A12* ($p < 0.05$), *SLC30A1* ($p < 0.05$), *SLC30A2* ($p < 0.05$), *MT1B* ($p < 0.05$), *MT1F* ($p < 0.05$), *MT1X* ($p < 0.05$) and *MT2A* ($p < 0.05$) in all six cell lines under mild cytotoxic $ZnSO_4$ exposure (**Table 3.2**). In normal prostate epithelial cells RWPE-1, the expression of *SLC39A12* gene was higher at T_{120} compared to T_{30} whereas the opposite was observed in PC3 and DU145 cancer cells. Similarly, breast epithelial normal MCF10A and cancer MDA-MB-231 cells showed greater expression at T_{120} compared to T_{30}. *SLC30A1* (except DU145) and *SLC30A2* (except MDA-MB-23 and DU145) showed greater expression at T_{120} than T_{30} in all cells (**Figure 3.4**, **Table 3.2**). The expression of *SLC39A12* in MCF-7, *SLC30A1* in DU145 and *SLC30A2* in DU145 and MDA-MB-231 was lower at T_{120} compared to T_{30}. The findings indicate that *SLC39A12* (ZIP12) is a key zinc importer gene in response to extracellular zinc fluctuation, whilst *SLC30A1* (ZnT1) and *SLC30A2* (ZnT2) are the key zinc exporter genes in dealing with excess of zinc in the cytoplasm. Breast cancer cells show higher *MT1B*, *MT1F*, *MT1X* and *MT2A* expression than the prostate cancer cells.

The gene expression of breast cancer cells and the normal breast epithelial cells under benign 50 µM $ZnSO_4$ is shown in **Figure 3.5** and **Table 3.3**. Sixteen genes were profiled, including 10 *SLC39A*, 2 *SLC30A* and 4 *MT* genes, because these ZIP and ZnT genes encode the plasma membrane-bound zinc transporters (Kelleher et al., 2009; McCormick et al., 2014; Bafaro et al., 2017) which are relevant to this benign $ZnSO_4$ dosage. The four *MT* genes (*MT1B*, *MT1F*, *MT1X*, *MT2A*) were also profiled here because of their significant up-regulation under mild cytotoxic zinc exposures (as shown in **Figure 3.4** and **Table 3.2**).

Cluster (a) in **Figure 3.5** exhibits *SLC39A6* down-regulation ($p < 0.01$) in breast cells following the benign zinc exposure which is consistent with its expression pattern under mild cytotoxic zinc treatment (**Figure 3.4**). *SLC39A2* was overexpressed in all three breast cell lines except at T_{120} for MDA-MB-231 cells. Cluster (b) shows the overexpression of *SLC39A12* ($p < 0.01$), *SLC30A1* ($p < 0.01$), *MT1F* ($p < 0.01$), *MT1X* ($p < 0.05$), *MT2A* ($p < 0.001$) and suppression of *SLC39A8* in breast cells under the benign $ZnSO_4$ treatment in **Figure 3.5**, which is consistent with their expression pattern in **Figure 3.4** under mild cytotoxic $ZnSO_4$ exposure. Furthermore, the expression of *SLC39A12*, *SLC30A1*, *MT1F*, *MT1X* and *MT2A* was greater at T_{120} than T_{30}. *SLC30A2* showed higher expression at T_{120} in normal breast cells compared to the cancerous cells. Interestingly, basal breast cancer cells (MDA-MB-231) demonstrated decreased

SLC30A2 expression at T_{120}, but its expression in luminal MCF-7 breast cancer cells remains constant. Surprisingly, *MT1B* was reduced at T_{120} compared to T_{30} in MCF-7 cells.

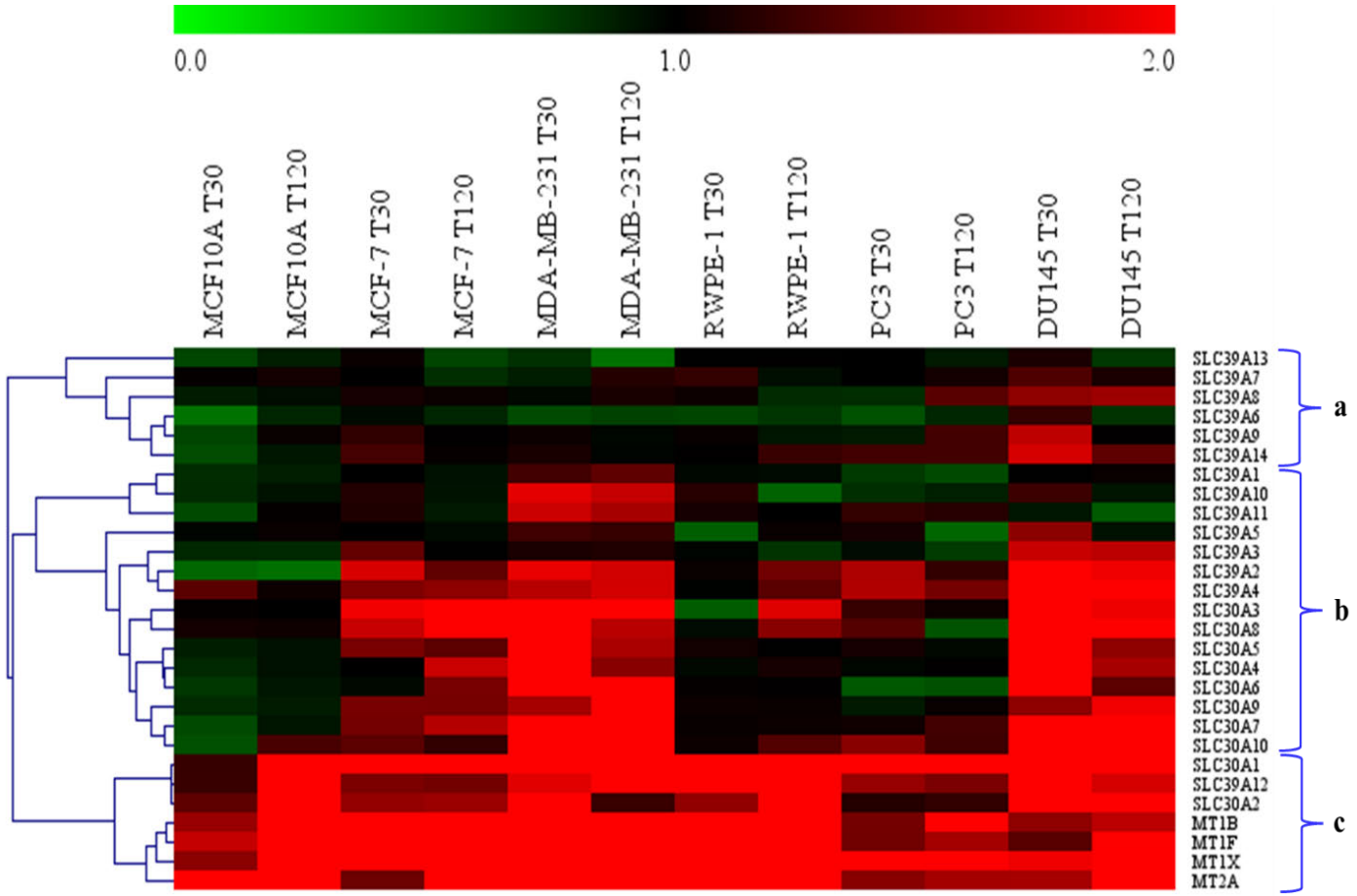

Figure 3.4 Expression profile of 14 *SLC39A*, 10 *SLC30A* and 4 *MT* genes in breast and prostate cells under mild cytotoxic $ZnSO_4$ exposures at T_{30} and T_{120} compared to T_0. The colour scale (0.0-2.0) represents the expression levels of 28 genes (green colour denotes down-regulation whilst red denotes up-regulation). The hierarchical clustering of the genes is shown in the dendrogram at the left.

Table 3.2 Effects of mild cytotoxic $ZnSO_4$ treatment at T_{30} and T_{120} on the expressions of *SLC39A*, *SLC30A* and *MT* genes in breast and prostate cell lines relative to T_0

	MCF10A		MCF-7		MDA-MB-231		RWPE-1		PC3		DU145	
Genes	T_{30}	T_{120}	T_{30}	T_{120}	T_{30}	T_{120}	T_{30}	T_{120}	T_{30}	T_{120}	T_{30}	T_{120}
SLC39A1	0.82	0.88	1.00	0.93	1.26	1.37	0.97	0.95	0.77	0.70	1.00	1.03
SLC39A2	0.59	0.55	1.85	1.38	1.91	1.82	1.03	1.44	1.68	1.20	2.38	1.94
SLC39A3	0.84	0.83	1.39	0.99	1.11	1.12	0.98	0.79	0.95	0.76	1.79	1.74
SLC39A4	1.35	1.05	1.50	1.55	1.72	1.83	0.98	1.35	1.69	1.45	2.34	2.10
SLC39A5	0.97	1.03	0.99	0.95	1.25	1.21	0.62	1.03	1.00	0.59	1.55	0.93
SLC39A6	0.54	0.85	0.96	0.85	0.70	0.74	0.72	0.79	0.68	0.84	1.21	0.80
SLC39A7	1.02	1.07	0.99	0.81	0.88	1.15	1.20	0.94	1.00	1.08	1.31	1.10
SLC39A8	0.88	0.94	1.08	1.04	0.96	1.10	1.05	0.83	0.82	1.34	1.55	1.61
SLC39A9	0.73	1.03	1.18	1.00	1.05	0.97	1.03	0.91	0.89	1.26	1.75	1.01
SLC39A10	0.83	0.92	1.13	0.92	1.90	1.77	1.16	0.61	0.81	0.87	1.23	0.91
SLC39A11	0.71	1.02	1.12	0.89	1.79	1.65	1.09	1.00	1.20	1.15	0.91	0.64
SLC39A12	1.22	4.88	1.49	1.45	1.88	2.00	3.40	27.89	1.59	1.48	2.33	1.84
SLC39A13	0.72	0.88	1.04	0.73	0.81	0.55	1.00	1.00	1.00	0.89	1.11	0.77
SLC39A14	0.69	0.91	1.27	1.02	1.09	0.98	1.00	1.22	1.26	1.26	1.84	1.37
SLC30A1	1.21	5.15	2.73	3.58	3.44	4.51	3.51	33.28	2.60	3.13	3.82	2.82
SLC30A2	1.37	16.89	1.58	1.61	2.11	1.23	1.57	185.36	1.14	1.20	3.14	3.03
SLC30A3	1.02	1.00	1.94	2.43	2.29	1.99	0.63	1.87	1.22	1.06	2.24	1.94
SLC30A4	0.84	0.93	0.99	1.79	2.43	1.54	0.96	1.09	0.97	1.01	2.23	1.66
SLC30A5	0.88	0.93	1.48	1.36	2.20	1.67	1.07	1.00	1.08	0.96	2.53	1.56
SLC30A6	0.78	0.90	0.96	1.47	2.57	2.27	1.02	1.01	0.65	0.68	2.42	1.36
SLC30A7	0.70	0.92	1.46	1.71	2.87	2.13	1.03	1.05	1.06	1.26	2.44	2.75
SLC30A8	1.08	1.06	1.78	2.01	2.35	1.73	0.95	1.54	1.33	0.67	2.06	3.04
SLC30A9	0.83	0.89	1.47	1.46	1.65	2.17	1.05	1.04	0.90	1.04	1.55	1.95
SLC30A10	0.68	1.28	1.36	1.20	2.17	2.08	1.05	1.32	1.54	1.24	2.11	2.31
MT1B	1.60	2.14	2.25	3.47	2.56	3.48	2.81	3.63	1.45	2.34	1.56	1.73
MT1F	1.77	2.47	2.35	3.40	2.34	3.49	2.27	3.91	1.44	1.65	1.34	1.99
MT1X	1.54	2.25	2.32	3.16	2.43	3.37	3.26	4.44	2.26	2.38	1.94	2.54
MT2A	2.23	2.49	1.43	3.12	2.25	3.24	2.98	4.08	1.53	1.65	1.66	2.85

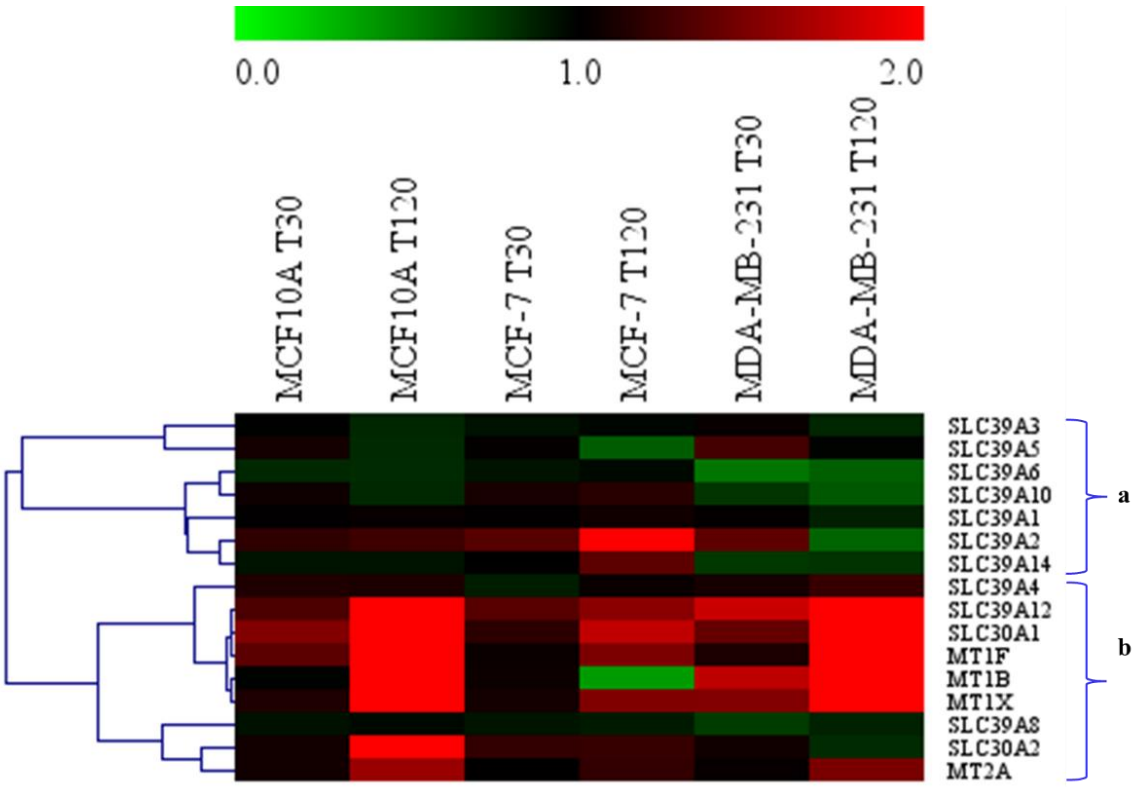

Figure 3.5 Expression profile of 10 *SLC39A*, 2 *SLC30A* and 4 *MT* genes in breast cells following benign 50 µM $ZnSO_4$ exposures at T_{30} and T_{120} compared to T_0. The colour scale (0.0-2.0) represents the expression levels of 16 genes (green colour denotes down-regulation whilst red denotes up-regulation). The hierarchical clustering of the genes is shown in the dendrogram at the left.

Table 3.3 Effects of benign 50 μM $ZnSO_4$ treatment at T_{30} and T_{120} on the expressions of *SLC39A*, *SLC30A* and *MT* genes in breast cell lines relative to T_0

		MCF10A		MCF-7		MDA-MB-231	
Proteins	**Genes**	**T_{30}**	**T_{120}**	**T_{30}**	**T_{120}**	**T_{30}**	**T_{120}**
ZIP1	*SLC39A1*	1.01	1.03	1.01	1.06	1.01	0.87
ZIP2	*SLC39A2*	1.18	1.24	1.34	2.28	1.37	0.60
ZIP3	*SLC33A3*	0.98	0.84	0.92	0.97	1.03	0.84
ZIP4	*SLC39A4*	1.12	1.11	0.88	1.04	1.09	1.22
ZIP5	*SLC39A5*	1.08	0.83	1.02	0.63	1.26	0.98
ZIP6	*SLC39A6*	0.84	0.83	0.92	0.96	0.53	0.62
ZIP8	*SLC39A8*	0.93	0.96	0.91	0.89	0.76	0.86
ZIP10	*SLC39A10*	1.05	0.84	1.10	1.15	0.79	0.64
ZIP12	*SLC39A12*	1.30	12.06	1.34	1.54	1.79	26.66
ZIP14	*SLC39A14*	0.92	0.92	1.00	1.36	0.77	0.79
ZnT1	*SLC30A1*	1.51	9.98	1.17	1.75	1.39	19.31
ZnT2	*SLC30A2*	1.07	12.81	1.19	1.21	1.06	0.83
MT1B	*MT1B*	0.98	2.76	1.05	0.38	1.74	18.72
MT1F	*MT1F*	1.36	5.46	1.04	1.49	1.11	13.27
MT1X	*MT1X*	1.12	2.15	1.08	1.50	1.51	7.48
MT2A	*MT2A*	1.07	1.61	1.00	1.20	1.03	1.48

3.3 Discussion

This study provides a landscape of gene expression for 14 *SLC39A* (ZIP), 10 *SLC30A* (ZnT) and 4 metallothioneins (MT) in breast cancer cells (MCF-7, MDA-MB-231), prostate cancer cells (PC3 and DU145), normal breast epithelial cells (MCF10A) and normal prostate epithelial cells (RWPE-1), in a time course under the mildly cytotoxic dosage and the benign dosage of zinc sulphate.

The gene expression details shed light on the divergence of intracellular Zn^{2+} levels for breast and prostate cancer cells. The *SLC39A1* (ZIP1) gene expression in breast cancer cells did not change compared to normal cells or in the time course under $ZnSO_4$ treatment. This suggests that the ZIP1 gene is essential for housekeeping in terms of zinc uptake of breast epithelial cells, regardless of whether they are normal or cancerous. This finding is supported by the previous study that demonstrated no significant difference in *SLC39A1* expression in mammary

tumours of mice with zinc supplemented diet (Sun et al., 2007). Contrastingly, *SLC39A2* (ZIP2) is up-regulated in breast cancer cells and divergently expressed as well in the time course of zinc treatment (**Figures 3.4** and **3.5**, **Tables 3.2** and **3.3**), with MCF-7 and MDA-MB-231 cells showing 3.28-fold and 265.94-fold overexpression, respectively, compared to MCF10A cells, in agreement with GEPIA2 server analysis which revealed up-regulation of *SLC39A2* in tumour breast tissue compared to normal counterpart. Furthermore, the overexpression of *SLC39A2* in MCF-7 and MDA-MB-231 breast cancer cells was also elicited by the benign $ZnSO_4$ dosage (**Figure 3.5**, **Table 3.3**). These findings suggest that *SLC39A2* (ZIP2) is intrinsically over-expressed in breast cancer cells and dynamically responsive as well to extracellular zinc level. The expression of *SLC30A2* (ZnT2) was increased in MCF-7 breast cancer cells but not varied in MDA-MB-231 cells against the normal breast epithelial cells (**Figure 3.3**, **Table 3.1**), which could be explained by the previous finding that ZnT2 protein is not functional in MDA-MB-231 cells due to proteasomal degradation (Chandler et al., 2016). This notion becomes conspicuous when MCF-7 cells were directly compared to MDA-MB-231 cells (**Table 3.1**). Therefore, *SLA30A2* gene expression is more relevant to MCF-7 breast cancer cells. Similarly, the up-regulation of *SLC30A2* ($p < 0.001$) in highly metastatic prostate cancer cells (PC3) was observed in comparison with the moderately metastatic prostate cancer cells (DU145) (**Table 3.1**). However, the relevance of this finding to clinical breast cancers needs to be investigated. In contrast to the breast cancer cells, *SLC39A1* (ZIP1) was significantly down-regulated in prostate cancer cells (**Figure 3.3**, **Table 3.1**) and clinical tissues (**Table 3.1**), which is consistent with the previous studies (Huang et al., 2006; Desouki et al., 2007; Franz et al., 2013; Fong et al., 2018). The marked reduction of *SLC39A2* (ZIP2) expression in PC3 prostate cancer cells (**Figure 3.3**, **Table 3.1**) is in agreement with the clinical finding (**Table 3.1**) and a previous study that demonstrated *SLC39A2* undetectable in prostate cancer cell lines (Albrecht et al., 2008).

The up-regulation of *SLC39A4, SLC39A6, SLC39A8* and *SLC39A11* in breast and prostate cancer cells (**Figure 3.3**, **Table 3.1**) suggests their significance in zinc transport of the cancer cells. All these ZIP genes, except *SLC39A11*, belong to LIV-1 family zinc importers which are responsive to estrogen (Taylor et al., 2007). ZIP4 and ZIP6, both located in plasma membrane, are the most studied LIV-1 ZIP members. The current knowledge in the structure and function of ZIP4 (encoded by *SLC39A4*) galvanises the significance of the above notion. The crystal structure of ZIP4 together with the functional studies demonstrated that its long extracellular N-terminal domain as well as its intracellular domains are involved in zinc sensing or

regulation of zinc uptake (Zhang et al., 2017; Chun et al., 2019; Hu, 2021). The involvement of these LIV-1 ZIP transporters in breast cancer cells is well-documented (Shen et al., 2009; Lopez and Kelleher, 2010; Takatani-Nakase et al., 2014; Chandler et al., 2016; Nimmanon et al., 2021), their roles in prostate cancer cells are, however, scarcely investigated. The down-regulation of *SLC39A12*, *SLC30A4* and *SLC30A10* in both breast and prostate cancer cells (**Figure 3.3**, **Table 3.1**) is supported by the down-regulation of *SLC39A12* and *SLC30A10* in clinical settings for both cancers (**Table 3.1**). The down-regulation of *SLC30A4* (ZnT4) and *SLC30A10* (ZnT10) may contribute to the elevated intracellular Zn^{2+} level in breast cancer cells, whilst their down-regulation in prostate cells suggesting that they are not needed because of the intrinsic low intracellular Zn^{2+} level in this kind of cancer cells. It also makes sense that *SLC30A1* (ZnT1) was down-regulated in breast cancer cells, but it was up-regulated in prostate cancer cells (**Figure 3.3**). Since ZnT1 is the only zinc exporter predominantly located in plasma membrane (Nishito and Kambe, 2019) and is prominently involved in zinc efflux (Fong et al., 2018; Lehvy et al., 2019; Zaman et al., 2021), its up-regulation may play a significant role in the low level of cytoplasmic zinc in prostate cancers compared to the normal prostate tissue. Further, according to the findings here, we think it is possible that the leaking of zinc via ZnT such as ZnT1, by a regulatory mechanism yet to be unravelled, is the driving force for the reduction of cytoplasmic zinc level in prostate cancers. Therefore, *SLC30A1* (ZnT1) could be a therapeutic target for prostate cancers.

Mildly cytotoxic zinc exposure elicited the dynamic changes in expression of *SLC39A*, *SLC30A* and *MT* genes in all cell lines under investigation (**Figure 3.4**, **Table 3.2**). The overexpression of *SLC39A2* (ZIP2) and *SLC39A4* (ZIP4) is conspicuous in both breast and prostate cancer cells, which again highlights the significance of ZIP4 as discussed previously. A study conducted on rat revealed up-regulation of *SLC39A2* mRNA, which might be responsible for higher Zn^{2+} in the lateral prostate compared to ventral and dorsal prostate (Iguchi et al., 2006). Interestingly, *SLC39A12*, *SLC30A1* and *SLC30A2* were overexpressed significantly, but *SLC39A6* was decreased in normal and cancerous breast and prostate cell lines following mildly cytotoxic zinc treatment (**Figure 3.4**, **Table 3.2**). This indicates that *SLC39A12, SLC30A1, SLC30A2* and *SLC39A6* are responsive to extracellular zinc level indiscriminately between normal and cancerous cells. It is understandable that mild cytotoxic zinc treatment leads to overexpression of *SLC30A1* (ZnT1) and *SLC30A2* (ZnT2) in all breast and prostate cells because they are the key zinc exporters to efflux excess of zinc out of the cell (Palmiter et al., 1996; Lopez and Kelleher, 2009; Guo et al., 2010; Bafaro et al., 2017). Up-regulation of

SLC30A1 is consistent with the other previous study in prostate cancer cells in response to $ZnSO_4$ treatment (Hasumi et al., 2003). Furthermore, according to **Figure 3.4**, the tendency of up-regulation of *SLC30A* genes in DU145, compared to PC3 prostate cancer cells, might explain their higher tolerance to extracellular zinc (150 µM $ZnSO_4$) against 110 µM $ZnSO_4$ for PC3 cells (**Figure 3.1C**), since higher expression of *SLC30A* (ZnT) genes could lead to more efficient efflux of cytoplasmic zinc.

In **Figure 3.4**, the expression of *SLC30A3* gene in RWPE-1 cells is in the opposite directions at T_{30} and T_{120} during the time course of $ZnSO_4$ treatment, with a marked decrease at T_{30}, then a big increase at T_{120}. This finding should be considered together with the increased expression of *SLC30A1* and *SLC30A2* during the entire time course. All these genes encode ZnT transporters responsible for exporting excess intracellular zinc out of the cell or into the intracellular compartments. The increase of gene expression at T_{120} for *SLC30A3* (encoding ZnT3) indicates that ZnT3 was needed for maintaining the balance of intracellular zinc although not required early at T_{30}. In contrast, *SLC30A8* was needed early at T_{30} but not at T_{120}. A notion must be made here that ZnT1 is the key zinc transporter for exporting excess zinc out of the cytoplasm, because *SLC30A1* expression was markedly elevated across the breast and prostate cells during the time course.

In **Table 3.1**, the genes such as *SLC39A2* (ZIP2), *SLC39A4* (ZIP4), *SLC30A2* (ZnT2) and *SLC30A8* (ZnT8) exhibited very big fold changes, which demonstrates that those genes in breast and prostate cells are responsive to the extracellular zinc level, therefore they play an important role in zinc homeostasis. The underlying reason for their marked increase or decrease in expression is likely due to their very low base level in normal breast and prostate cells according to the available literature. The urothelial cells, a specialised epithelial cells in the urinary system, showed very low expression of ZIP2 and ZnT2 (Satarug et al., 2021). ZnT2 was not detected in most of the organs (Yang et al., 2013). ZnT8 was expressed mainly in the pancreas, but at low to undetectable levels elsewhere (Yang et al., 2013). ZIP2 was found to be expressed in selective tissues such as the liver, skin and ovary (Hara et al., 2022) and at a very low level in many other human tissues (Gaither and Eide, 2000). Similarly to ZIP2 expression, ZIP4 is only expressed selectively in normal tissues such as the small intestine, whilst it is broadly expressed in a variety of cancers (Hu, 2021). This makes ZIP4 an attractive anti-cancer target.

The up-regulation of *SLC39A2*, *SLC39A4* and *SLC39A12* together with the up-regulation of ZnT genes such as *SLC30A1-10* in breast cancer cells following mild cytotoxic $ZnSO_4$ treatment (**Figure 3.4**, **Table 3.2**) clearly demonstrate the dynamic nature of these two groups of zinc transport genes which have opposite functions in terms of maintaining intracellular zinc level. Such dynamic changes for *SLC39A* and *SLC30A* genes were also demonstrated by Cousins et al. (2003) in human leukemia monocytic THP-1 cells and by Satarug et al. (2021) in human urothelial cells. These findings of the current study provoke the thought about two routes of zinc sensing and regulation in the cell, namely ZIP4 encoded by *SLC39A4* and MTF-1 (metal-response element binding transcription factor 1 encoded by *MTF1* gene). The up-regulated ZIP4, acting as an extracellular zinc sensor for zinc uptake (Zhang et al., 2017; Chun et al., 2019; Hu, 2021), is likely responsible for the up-regulation of ZIP genes such as *SLC39A2* and *SLC39A12*, while MTF-1, acting as an intracellular zinc sensor, is responsible for the up-regulation of ZnT genes such as *SLC30A1-10*. It is well documented that MTF-1 regulated ZnT genes (e.g., *SLC30A1*) (Langmade et al., 2000; Giedroc et al., 2001). We did not include MTF-1 gene in the current gene-profiling study, because our previous work by RNA-seq (Zaman et al., 2021) found that the expression of MTF-1 did not change in MCF-7 breast cancer cells upon mild cytotoxic zinc exposure. We have to stress the notion that the status quo of *MTF-1* expression in our previous study belies its significance in regulating the zinc homeostasis of breast cancer cells. And this study adds another level of details in terms of the likely role of ZIP4 in regulating ZIP gene expression.

Remarkably, the benign $ZnSO_4$ dosage exposure also elicited elevation of *SLC39A12* (ZIP12) in normal and cancerous breast cells (**Figure 3.5**, **Table 3.3**). ZIP12, a close homologue of ZIP4, probably also has a regulatory role in zinc homeostasis (Chun et al., 2019). The unchanged expression of *SLC39A1* (ZIP1) against the benign dosage again highlights its housekeeping role in zinc homeostasis.

Finally, *MT1B*, *MT1F*, *MT1X* and *MT2A* ($p < 0.05$) displayed elevated expression all the way through the cell lines of this study (**Figures 3.3**, **3.4** and **3.5**, **Tables 3.1**, **3.2** and **3.3**). The high expression of *MT* genes without zinc treatment, as shown in **Figure 3.3**, suggests an important role of metallothioneins in breast and prostate cancers. The significant down-regulation of *MT1F*, *MT1X* and *MT2A* ($p < 0.01$) in MCF-7 cells compared to MDA-MB-231 cells (**Table 3.1**) might reflect the weaker cancer aggressiveness of luminal breast cancer than the basal breast cancer, and this notion is in agreement with the previous studies (Tai et al., 2003; Si and

Lang, 2018). The finding supports the notion that metallothionein is regarded as a diagnosis and prognostic biomarker in breast cancers (Bay et al., 2006; Si and Lang, 2018; Wang et al., 2018). A higher *MT* gene expression in breast cancers is predictive of cancer development or worse patient outcomes after cancer treatment. Consequently, metallothionein isoforms are also considered as therapeutic targets (Si and Lang, 2018). With zinc treatment, *MT* genes were further up-regulated compared to T_0 in the time course (**Figures 3.4** and **3.5**), indicating that metallothioneins are critical in mediating intracellular zinc homeostasis of breast and prostate cancer cells. Considering the up-regulation of *SLC39A4* (ZIP4), *SLC39A6* (ZIP6), *SLC39A11* (ZIP11) in parallel with the up-regulation of *MT* genes (**Figure 3.3**), we reason that these two classes of genes could be linked. Indeed, a previous study demonstrated a link between *SLC39A6* (ZIP6) and *MT* gene expression (Dai et al., 2021).

3.4 Conclusion

This study explored the baseline expression profile of *SLC39A*, *SLC30A* and *MT* genes in breast and prostate cancer cells in the absence of extracellular zinc exposure and the dynamic gene expression in response to extracellular zinc treatment. With the varying dosages and time course, the findings revealed significant behaviours of individual target genes such as *SLA39A4*, *SLA39A12*, *SLC30A1*, *SLC30A2* and the *MT* genes. Altogether, the findings of this study enhance our understanding of zinc homeostasis in breast and prostate cancer cells. As *SLC30A8* (ZnT8) is unequivocally associated with diabetes (Daniels et al., 2020; Schumann et al., 2020) and *SLC39A4* (ZIP4) is linked to pancreatic cancer (Liu et al., 2018), this study should contribute to the hunt of target genes in *SLC39A* and *SLC30A* for drug development of breast and prostate cancers.

Chapter 4 A confocal immunofluorescence study on the expression and localisation of zinc homeostasis-related proteins in breast and prostate cancer cells

4.1 Introduction

Zinc ion (Zn^{2+}) is essential to life. It functions in the cell as a cofactor for over 300 enzymes and as a structural component for approximately 10% of the human proteome (Maret, 2017; Barman et al., 2022). Consequently, the cell has developed an elaborate molecular network over the extensive evolutionary timeline to maintain zinc homeostasis (Kambe et al., 2021). Any disruption of such a network leads to zinc dyshomeostasis, resulting in diseases such as cancers. This study seeks to gain more insights into the zinc homeostasis network of breast and prostate cancer cells.

The key components of zinc homeostasis network are 14 zinc importers (ZIP1-14 encoded by *SLC39A1-14*), 10 zinc exporters (ZnT1-10 encoded by *SLC30A1-10*) and metallothioneins (MT) for cytoplasmic zinc sequestration. ZIP1-14 increase cytoplasmic Zn^{2+} concentration by importing Zn^{2+} from outside of the cell or from the intracellular organelles, while ZnT1-10 decrease cytosolic Zn^{2+} concentration by exporting Zn^{2+} out of the cytoplasm or compartmentalising Zn^{2+} into the intracellular organelles such as endoplasmic reticulum and Golgi apparatus (Taylor et al., 2012; Nimmanon et al., 2017; Bin et al., 2018; Hara et al., 2022). MT is a group of small metal-binding proteins due to their rich content of cysteine residues which are involved in Zn^{2+} coordination. Eight functional MT isoforms including MT2A have been identified in humans (Werynska et al., 2013).

The pleotropic serine/threonine protein kinase CK2 was first discovered in rat mitochondria by Burnett and Kennedy in 1954 (Burnett and Kennedy, 1954). The mammalian CK2 protein kinase consists of two catalytic (CK2α and CK2α') and two identical regulatory (CK2β) subunits (Hathaway and Traugh, 1979). It can have different tetrameric configurations, including αα'ββ, ααββ or α'α'ββ (Litchfield, 2003). Two catalytic subunits CK2α and CK2α' are bound to the central regulatory homodimer of CK2β subunits (Ackermann et al., 2005). CK2 was shown to play an important role in the regulation of Zn^{2+} homeostasis of breast and prostate cancer cells (Taylor et al., 2012; Zaman et al., 2016).

Zinc dyshomeostasis is an intriguing phenomenon in breast and prostate cancers, with breast cancer cells exhibiting higher intracellular Zn^{2+} levels compared to their corresponding normal epithelial cells (Chandler et al., 2016; Rusch et al., 2021), in contrast to the lower Zn^{2+} levels in prostate cancer cells compared to the normal counterpart (Dowarha et al., 2020; Sauer et al., 2020). Consequently, we have been investigating the molecular network of zinc homeostasis by taking advantage of the diametrically opposite intracellular zinc profiles of breast and prostate cancer cells (Zaman et al., 2019; Zaman et al., 2021; Barman et al., 2022). Using the normal and cancerous breast cells (MCF10A, MCF-7, MDA-MB-231) and prostate cells (RWPE-1, PC3, DU145) with or without exogenous zinc exposure, we revealed dynamic changes in the expression of ZIP, ZnT and MT genes (Zaman et al., 2021; Barman et al., 2022). Here in this study, we attempted to investigate further the protein expression and localisation of ZIP12, ZnT1, MT2A and protein kinase CK2 subunits (α/α' and β) by immunofluorescence confocal microscopy.

4.2 Results

4.2.1 Cell viability under zinc exposure

The viability of MCF10A, MCF-7 and MDA-MB-231 cells under the mild cytotoxic zinc exposure were 87%, 98% and 100% at T_{30}, respectively; and were 71%, 77% and 80% at T_{120}, respectively (**Figure 4.1A**). The viability of these three breast cell lines at the benign $ZnSO_4$ dosage (50 µM) were 106%, 111% and 107% at T_{120}, respectively (**Figure 4.1B**). RWPE-1 normal prostate epithelial cells were more tolerant to $ZnSO_4$ exposure in comparison to PC3 and DU145 prostate cancer cells, with the viability of RWPE-1 under 186.88 µM $ZnSO_4$ shown as 98% at T_{30}, 85% at T_{120}, whilst the viability of PC3 under 110 µM $ZnSO_4$ was 89% at T_{30} and 79% at T_{120} and the viability of DU145 under 150 µM $ZnSO_4$ was 94% at T_{30} and 83% at T_{120} (**Figure 4.1C**).

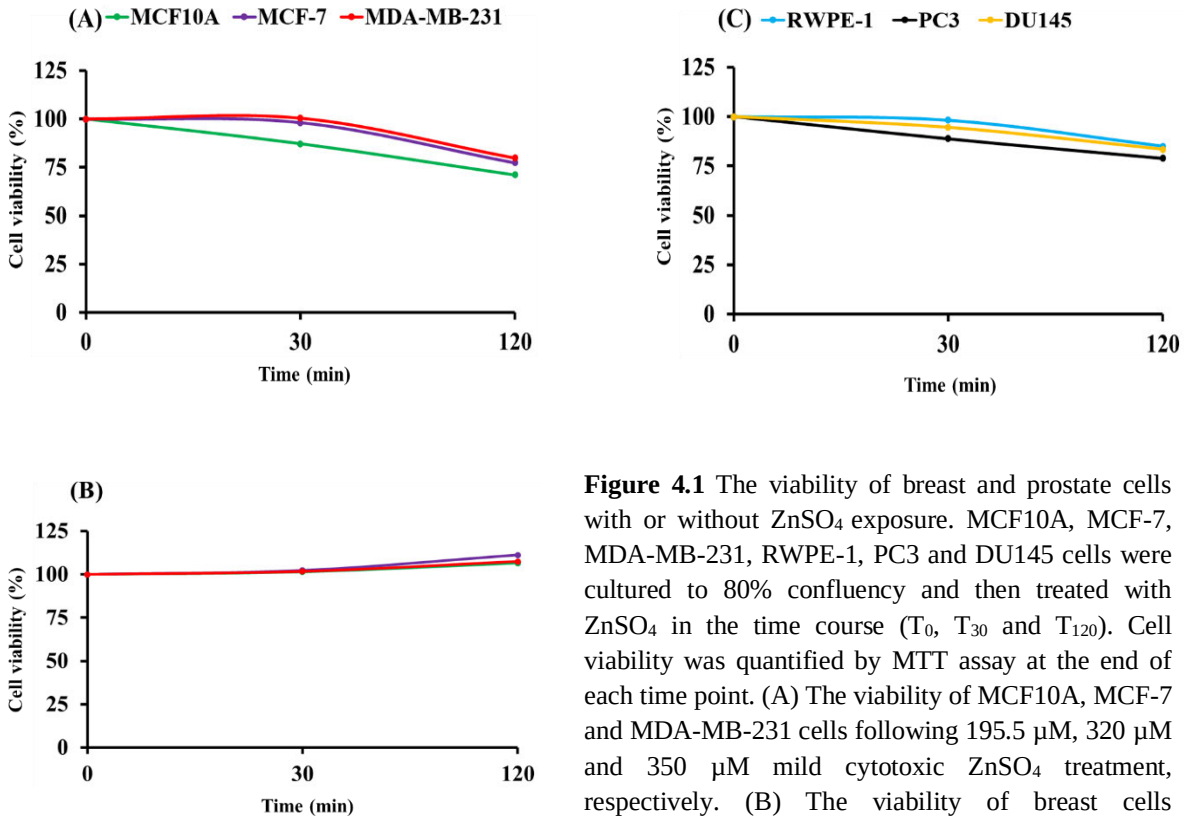

Figure 4.1 The viability of breast and prostate cells with or without $ZnSO_4$ exposure. MCF10A, MCF-7, MDA-MB-231, RWPE-1, PC3 and DU145 cells were cultured to 80% confluency and then treated with $ZnSO_4$ in the time course (T_0, T_{30} and T_{120}). Cell viability was quantified by MTT assay at the end of each time point. (A) The viability of MCF10A, MCF-7 and MDA-MB-231 cells following 195.5 µM, 320 µM and 350 µM mild cytotoxic $ZnSO_4$ treatment, respectively. (B) The viability of breast cells (MCF10A, MCF-7, MDA-MB-231) under benign 50 µM $ZnSO_4$ exposure. (C) The viability of RWPE-1, PC3 and DU145 cells following 186.88 µM, 110 µM and 150 µM mild cytotoxic $ZnSO_4$ treatment, respectively. Error bars are too small to be seen, representing the standard deviation of at least 24 replicates.

4.2.2 ZIP12 expression and localisation

ZIP12 was found to be overexpressed significantly in breast normal epithelial cells (MCF10A) compared to the cancerous cells (MCF-7 and MDA-MB-231) without zinc exposure (T_0) (**Table 4.1**). In contrast, prostate cancer cells (PC3 and DU145) showed higher ZIP12 expression than their normal RWPE-1 cells at T_0, particularly in DU145 cells (**Table 4.1**). Such a pattern continues to hold under both benign and mild cytotoxic zinc exposure since ZIP12 was significantly decreased in breast cancer MCF-7 and MDA-MB-231 cells at T_{30} and T_{120} compared to T_0 (**Figure 4.2A**). PC3 cells exhibited an increase of ZIP12 expression following mild cytotoxic zinc exposure while DU145 cells showed a decrease of ZIP12 expression (**Figure 4.2B**).

Table 4.1 Comparison of ZIP12, ZnT1, MT2A, CK2α/α' and CK2β expressions at control condition (T_0) in breast and prostate cells

	MFI values at T_0	**Comparisons**	***p* value**
ZIP12			
MCF10A	104.84	MCF-7 vs MCF10A	< 0.0001
MCF-7	80.39	MDA-MB-231 vs MCF10A	< 0.0001
MDA-MB-231	83.04		
RWPE-1	61.82	PC3 vs RWPE-1	< 0.0001
PC3	66.82	DU145 vs PC3	< 0.0001
DU145	101.36		
ZnT1			
MCF10A	18.49	MCF-7 vs MCF10A	< 0.001
MCF-7	21.06	MDA-MB-231 vs MCF10A	< 0.0001
MDA-MB-231	22.45		
RWPE-1	16.05	PC3 vs RWPE-1	< 0.0001
PC3	23.26	DU145 vs RWPE-1	< 0.0001
DU145	21.47		
MT2A			
MCF10A	70.85	MCF-7 vs MCF10A	< 0.0001
MCF-7	83.25	MCF-7 vs MDA-MB-231	< 0.0001
MDA-MB-231	71.13		
RWPE-1	91.93	PC3 vs RWPE-1	< 0.0001
PC3	110.28	DU145 vs RWPE-1	< 0.0001
DU145	73.06	PC3 vs DU145	< 0.0001
CK2α/α'			
MCF10A	45.94	MCF-7 vs MCF10A	< 0.016
MCF-7	51.07		
MDA-MB-231	47.60		
RWPE-1	38.42	PC3 vs RWPE-1	< 0.0001
PC3	74.73	DU145 vs RWPE-1	< 0.0001
DU145	81.76	DU145 vs PC3	< 0.0001
CK2β			
MCF10A	54.21	MCF-7 vs MCF10A	< 0.0001
MCF-7	33.84	MDA-MB-231 vs MCF10A	< 0.0001
MDA-MB-231	36.62		
RWPE-1	43.50	PC3 vs RWPE-1	< 0.0001
PC3	60.69	DU145 vs RWPE-1	< 0.0001
DU145	60.53		

MFI denotes mean fluorescence intensity, vs for versus.

Figure 4.3 showed ZIP12 localisation details of breast and prostate cells at T_0, T_{30} and T_{120}. ZIP12 was found to be localised in the cytoplasm and plasma membrane of breast cancer cells MCF-7 and MDA-MB-231 with and without exogenous zinc treatment (**Figure 4.3A**). In contrast, prostate cancer cells showed no localisation in the plasma membrane (**Figure 4.3B**). Both normal breast cells MCF10A (**Figure 4.3A**) and normal prostate cells RWPE-1 (**Figure 4.3B**) exhibited ZIP12 expression in the cytoplasm, not in the plasma membrane either with or without exogenous zinc exposure.

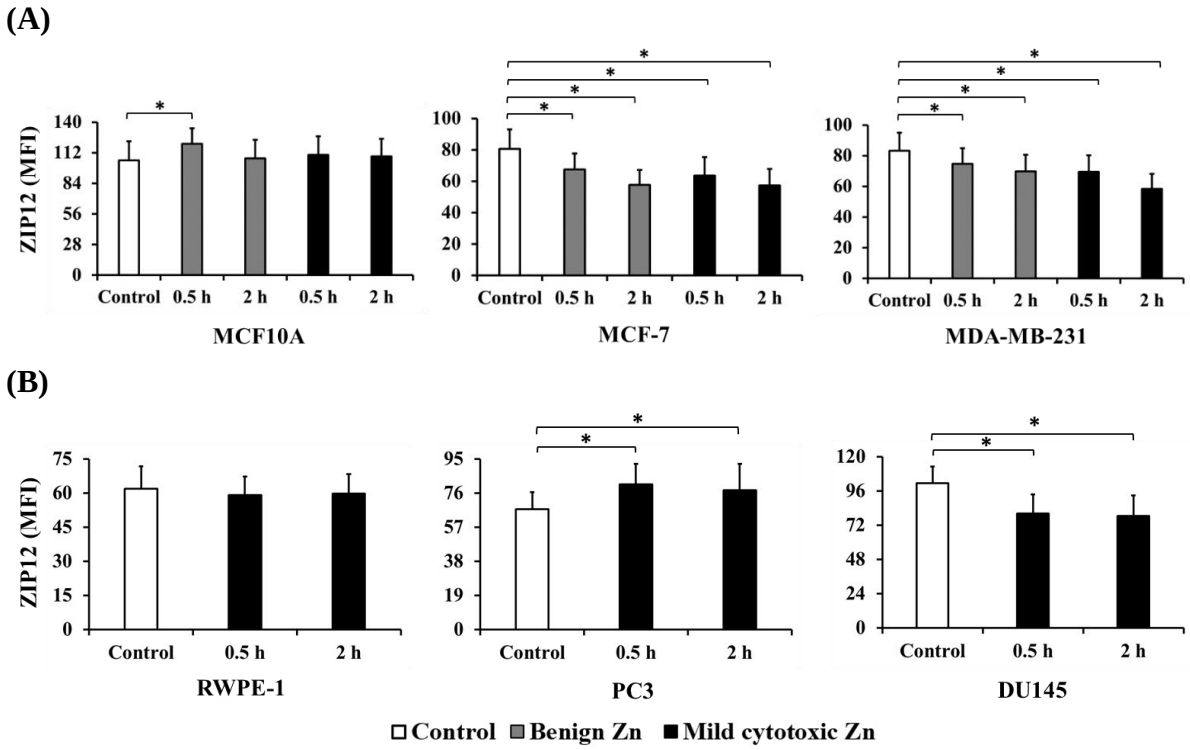

Figure 4.2 Quantification of ZIP12 protein expression in breast and prostate cells by immunofluorescence confocal microscopy. (A) Mean fluorescence intensity (MFI) of ZIP12 in MCF10A (left), MCF-7 (middle) and MDA-MB-231 cells (right) without zinc exposure (Control) and with the exposure of benign and mild cytotoxic zinc for 30 min (T_{30}) and 120 min (T_{120}). (B) Mean fluorescence intensity (MFI) of ZIP12 in RWPE-1 (left), PC3 (middle) and DU145 cells (right) without zinc exposure (Control) and with the exposure of mild cytotoxic zinc for 30 min (T_{30}) and 120 min (T_{120}). Each MFI value presented in the graphs is the average from the minimum 70 cells of three biological replicates. All the images were taken at 40X objective for quantifying MFI. The MFI values of ZIP12 at T_0, T_{30} and T_{120} were compared by one-way ANOVA with Dunnett's multiple comparisons test. * denotes $p < 0.001$.

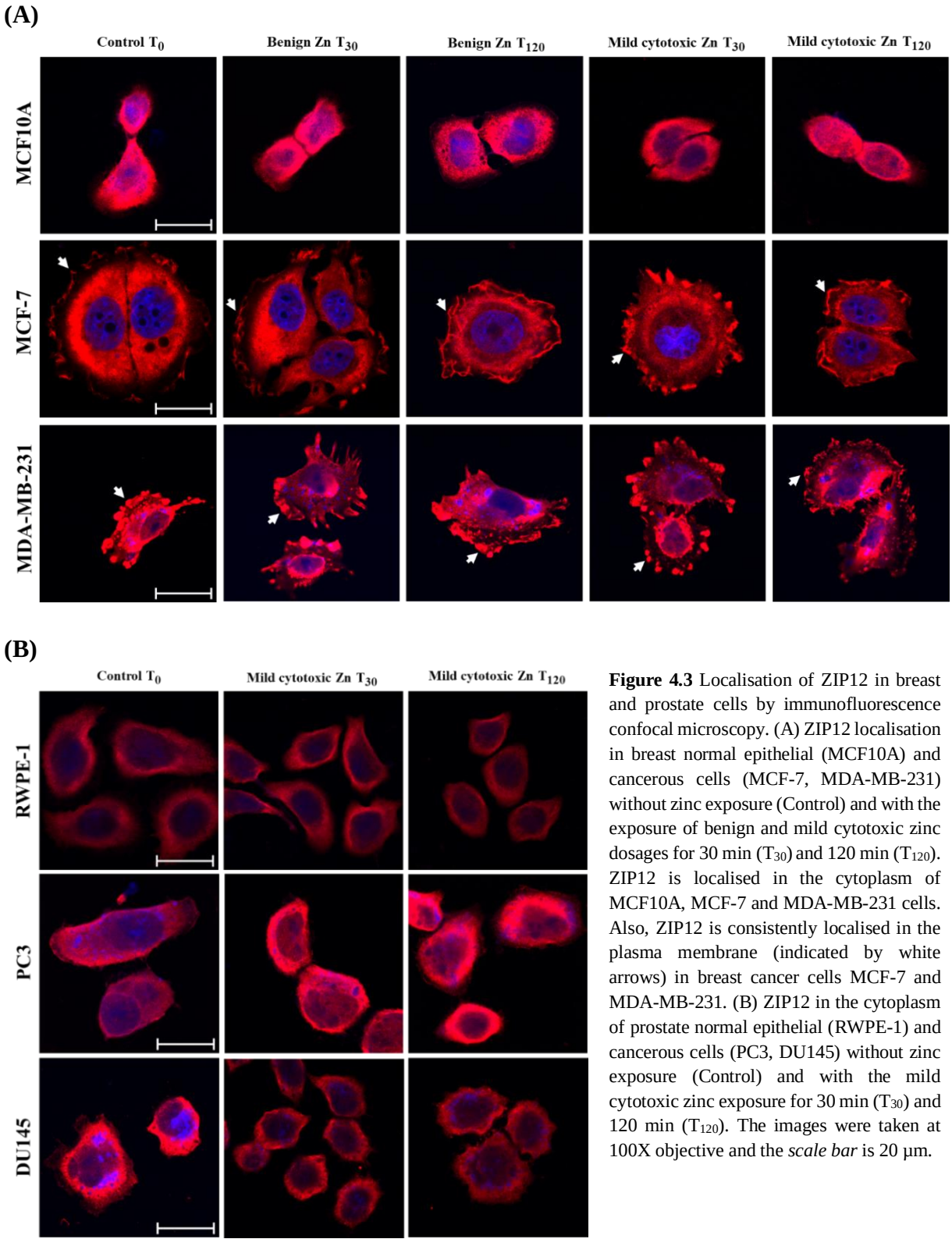

Figure 4.3 Localisation of ZIP12 in breast and prostate cells by immunofluorescence confocal microscopy. (A) ZIP12 localisation in breast normal epithelial (MCF10A) and cancerous cells (MCF-7, MDA-MB-231) without zinc exposure (Control) and with the exposure of benign and mild cytotoxic zinc dosages for 30 min (T_{30}) and 120 min (T_{120}). ZIP12 is localised in the cytoplasm of MCF10A, MCF-7 and MDA-MB-231 cells. Also, ZIP12 is consistently localised in the plasma membrane (indicated by white arrows) in breast cancer cells MCF-7 and MDA-MB-231. (B) ZIP12 in the cytoplasm of prostate normal epithelial (RWPE-1) and cancerous cells (PC3, DU145) without zinc exposure (Control) and with the mild cytotoxic zinc exposure for 30 min (T_{30}) and 120 min (T_{120}). The images were taken at 100X objective and the *scale bar* is 20 µm.

4.2.3 ZnT1 expression and localisation

ZnT1 protein expression at T_0 was higher in both breast cancer cells (MCF-7, MDA-MB-231) and prostate cancer cells (PC3, DU145) than their normal counterpart MCF10A and RWPE-1 cells (**Table 4.1**)**.** Both breast cancer cells MCF-7 and MDA-MB-231 exhibited significant down-regulation of ZnT1 following benign or mild cytotoxic zinc treatment at T_{30} and T_{120} compared to T_0 (**Figure 4.4A**). ZnT1 demonstrated overexpression at T_{120} compared to T_0 in normal prostate RWPE-1 cells (**Figure 4.4B**) while ZnT1 expression did not show a significant change in prostate cancer cells (PC3, DU145) following zinc treatment. ZnT1 was localised in the cytoplasm and plasma membrane of both breast cancer cells (MCF-7, MDA-MB-231) (**Figure 4.5A**) at T_0, T_{30} and T_{120}. ZnT1 was more prominently in the membrane of luminal type breast cancer cells (MCF-7) than basal type breast cancer cells (MDA-MB-231) (**Figure 4.5A**), while no localisation was observed in the plasma membranes of normal or cancerous prostate cells (**Figure 4.5B**).

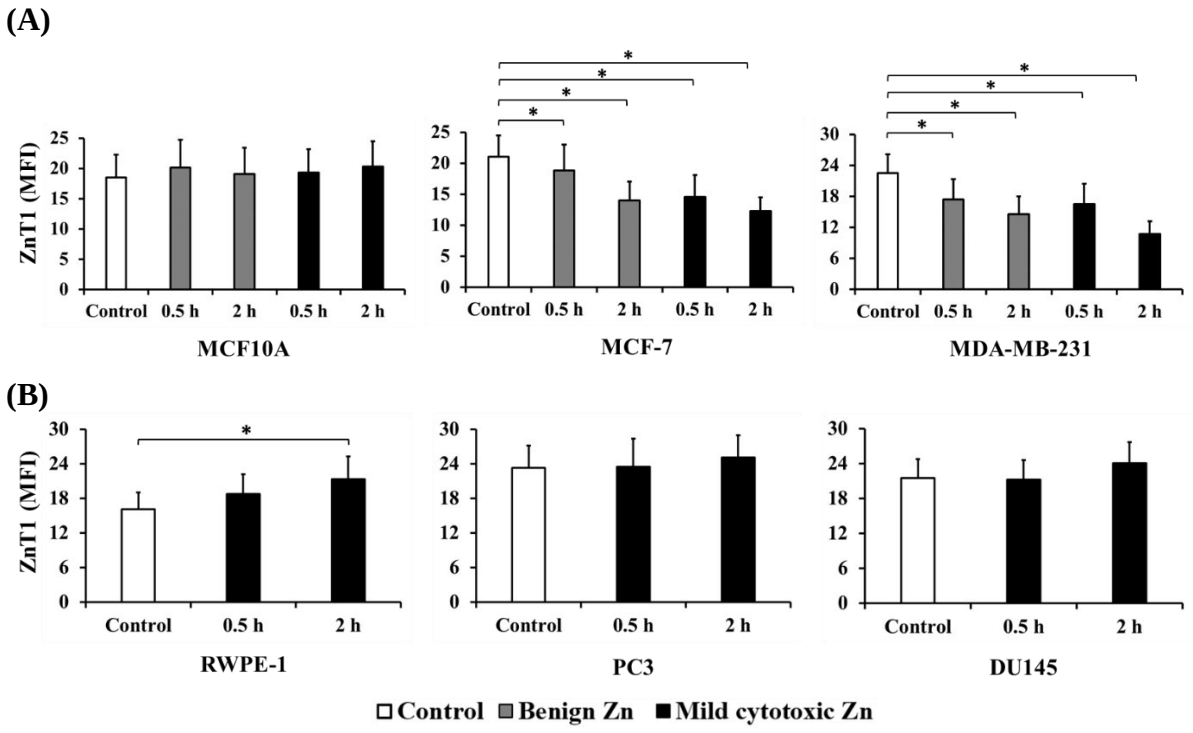

Figure 4.4 Quantification of ZnT1 protein expression in breast and prostate cells by immunofluorescence confocal microscopy. (A) Mean fluorescence intensity (MFI) of ZnT1 in MCF10A (left), MCF-7 (middle) and MDA-MB-231 cells (right) without zinc exposure (Control) and with the exposure of benign and mild cytotoxic zinc for 30 min (T_{30}) and 120 min (T_{120}). (B) Mean fluorescence intensity (MFI) of ZnT1 in RWPE-1 (left), PC3 (middle) and DU145 cells (right) without zinc exposure (Control) and with the exposure of mild cytotoxic zinc for 30 min (T_{30}) and 120 min (T_{120}). Each MFI value presented in the graphs is the average from the minimum 70 cells of three biological replicates. All the images were taken at 40X objective for quantifying MFI. The MFI values of ZnT1 at T_0, T_{30} and T_{120} were compared by one-way ANOVA with Dunnett's multiple comparisons test. * denotes $p < 0.001$.

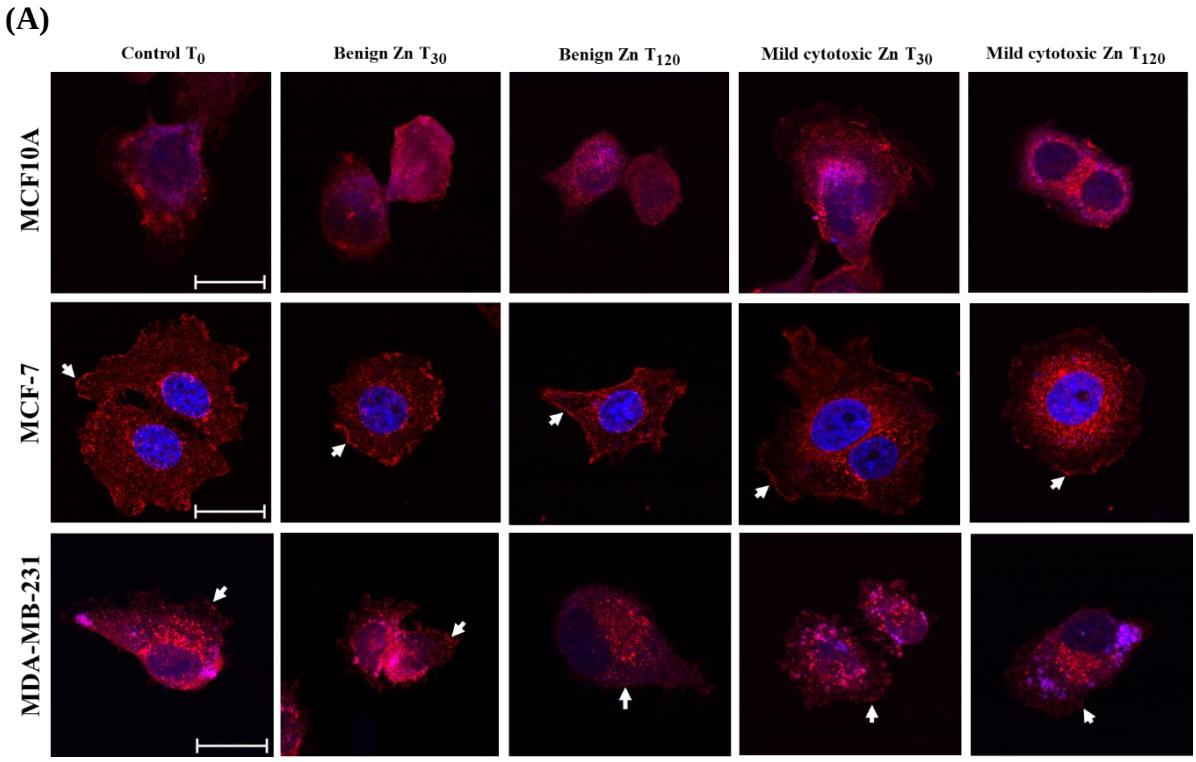

Figure 4.5 Localisation of ZnT1 in breast and prostate cells by immunofluorescence confocal microscopy. (A) ZnT1 localisation in breast normal (MCF10A) and cancer cells (MCF-7, MDA-MB-231) without zinc exposure (Control) and with the exposure of benign and mild cytotoxic zinc dosages for 30 min (T_{30}) and 120 min (T_{120}). ZnT1 is localised in the cytoplasm of MCF10A, MCF-7 and MDA-MB-231 cells. Also, ZnT1 is consistently localised in the plasma membrane (indicated by white arrows) in breast cancer cells MCF-7 and MDA-MB-231. (B) ZnT1 in the cytoplasm of prostate normal (RWPE-1) and cancer cells (PC3, DU145) without zinc exposure (Control) and with the mild cytotoxic zinc exposure for 30 min (T_{30}) and 120 min (T_{120}). The images were taken at 100X objective and the *scale bar* is 20 µm.

4.2.4 MT2A expression and localisation

As shown in **Table 4.1**, MT2A protein showed greater expression in breast cancer cells (MCF-7) and prostate cancer cells (PC3) relative to their normal counterparts MCF10A and RWPE-1 cells, respectively, at control condition (T_0). Prostate cancer cells DU145 exhibited lower expression of MT2A compared to RWPE-1 cells at T_0. MT2A demonstrated overexpression under benign zinc dosage but did not change in response to mild cytotoxic zinc dosage in MCF10A cells (**Figure 4.6A**). MT2A showed significant reduction at T_{30} and T_{120} compared to T_0 in MCF-7 cells following benign and mild cytotoxic zinc exposure. RWPE-1 and PC3 cells exhibited higher expression of MT2A following mild cytotoxic zinc treatment at T_{30} and T_{120} compared to T_0 (**Figure 4.6B**). MT2A was localised in the cytoplasm of the breast cells (MCF10A, MCF-7, MDA-MB-231) (**Figure 4.7A**) and prostate cells (RWPE-1, PC3, DU145) cells (**Figure 4.7B**). Surprisingly, MT2A was localised in proximity to the plasma membrane in breast cancer cells MCF-7 and MDA-MB-231 at T_0, T_{30} and T_{120} (**Figure 4.7A**).

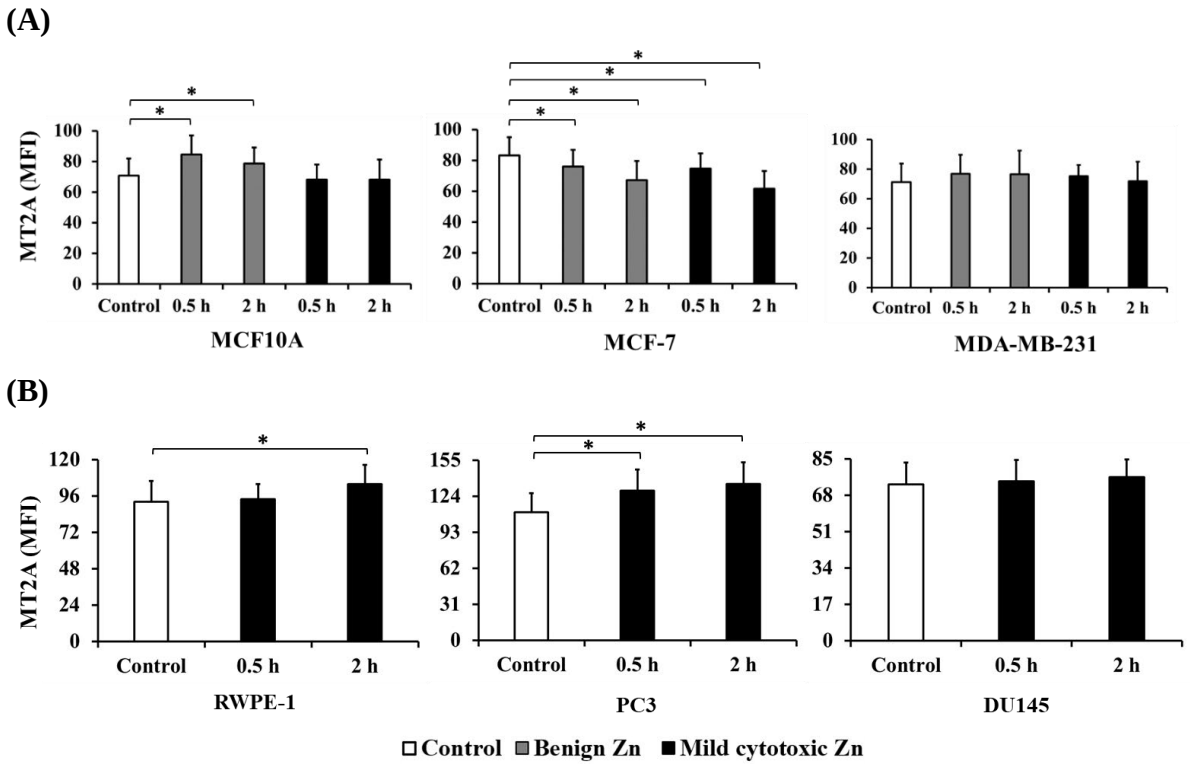

Figure 4.6 Quantification of MT2A protein expression in breast and prostate cells by immunofluorescence confocal microscopy. (A) Mean fluorescence intensity (MFI) of MT2A in MCF10A (left), MCF-7 (middle) and MDA-MB-231 cells (right) without zinc exposure (Control) and with the exposure of benign and mild cytotoxic zinc for 30 min (T_{30}) and 120 min (T_{120}). (B) Mean fluorescence intensity (MFI) of MT2A in RWPE-1 (left), PC3 (middle) and DU145 cells (right) without zinc exposure (Control) and with the exposure of mild cytotoxic zinc for 30 min (T_{30}) and 120 min (T_{120}). Each MFI value presented in the graphs is the average from the minimum 70 cells of three biological replicates. All the images were taken at 40X objective for quantifying MFI. The MFI values of MT2A at T_0, T_{30} and T_{120} were compared by one-way ANOVA with Dunnett's multiple comparisons test. * denotes $p < 0.001$.

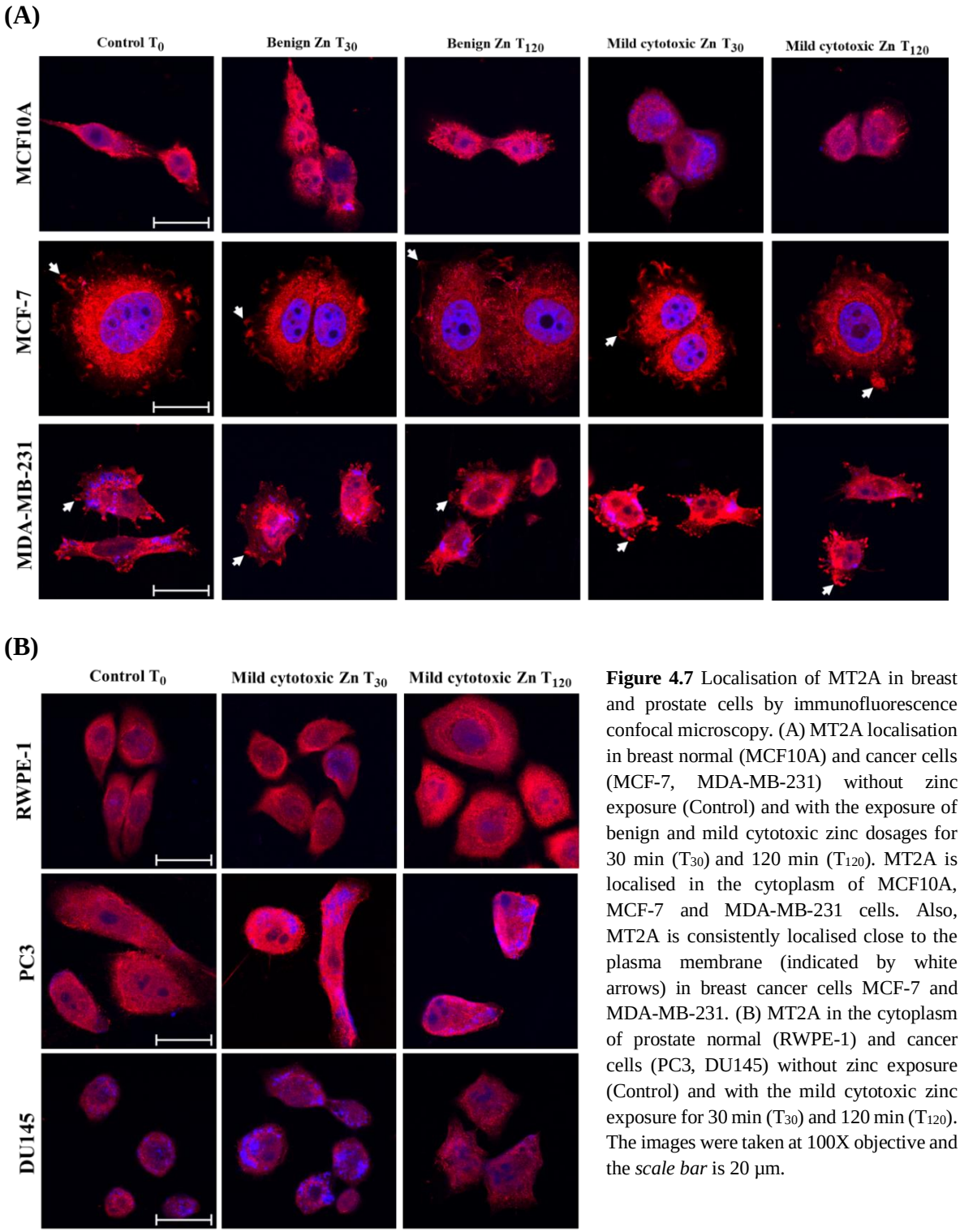

Figure 4.7 Localisation of MT2A in breast and prostate cells by immunofluorescence confocal microscopy. (A) MT2A localisation in breast normal (MCF10A) and cancer cells (MCF-7, MDA-MB-231) without zinc exposure (Control) and with the exposure of benign and mild cytotoxic zinc dosages for 30 min (T_{30}) and 120 min (T_{120}). MT2A is localised in the cytoplasm of MCF10A, MCF-7 and MDA-MB-231 cells. Also, MT2A is consistently localised close to the plasma membrane (indicated by white arrows) in breast cancer cells MCF-7 and MDA-MB-231. (B) MT2A in the cytoplasm of prostate normal (RWPE-1) and cancer cells (PC3, DU145) without zinc exposure (Control) and with the mild cytotoxic zinc exposure for 30 min (T_{30}) and 120 min (T_{120}). The images were taken at 100X objective and the *scale bar* is 20 µm.

4.2.5 CK2α/α' expression and localisation

CK2α/α' was up-regulated in breast cancer cells (MCF-7, MDA-MB-231) and prostate cancer cells (PC3, DU145) compared to their respective normal epithelial cells MCF10A and RWPE-1 without zinc treatment (T_0) (**Table 4.1**). CK2α/α' was also overexpressed in response to both benign and mild cytotoxic zinc dosages in MCF10A cells (**Figure 4.8A**). Opposite expression profiles of CK2α/α' in the breast cancer cells were exhibited at T_{120} where mild cytotoxic zinc exposure reduced CK2α/α' in luminal type breast cancer cells (MCF-7) but increased in basal type breast cancer cells (MDA-MB-231) (**Figure 4.8A**). Also, CK2α/α' was increased in highly metastatic prostate cancer cells (PC3) while decreased in moderate metastatic prostate cancer cells (DU145) in response to the mild cytotoxic zinc dosages (**Figure 4.8B**). CK2α/α' was localised throughout the cytoplasm and close to the cell membrane of both breast cancer cells MCF-7 and MDA-MB-231 (**Figure 4.9A**). In contrast, CK2α/α' localisation in proximity to the plasma membrane was not observed in normal breast epithelial cells MCF10A as well as all prostate cells (RWPE-1, PC3, DU145) cells (**Figure 4.9**).

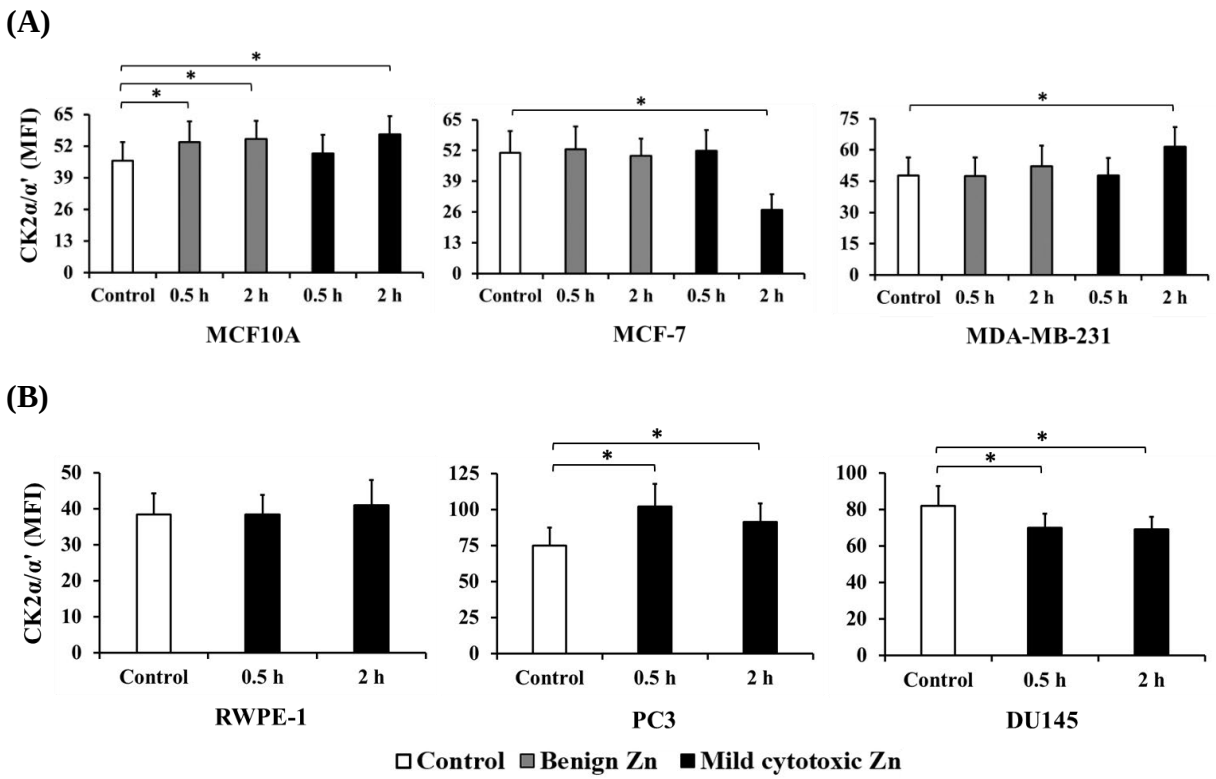

Figure 4.8 Quantification of CK2α/α' protein expression in breast and prostate cells by immunofluorescence confocal microscopy. (A) Mean fluorescence intensity (MFI) of CK2α/α' in MCF10A (left), MCF-7 (middle) and MDA-MB-231 cells (right) without zinc exposure (Control) and with the exposure of benign and mild cytotoxic zinc for 30 min (T_{30}) and 120 min (T_{120}). (B) Mean fluorescence intensity (MFI) of CK2α/α' in RWPE-1 (left), PC3 (middle) and DU145 cells (right) without zinc exposure (Control) and with the exposure of mild cytotoxic zinc for 30 min (T_{30}) and 120 min (T_{120}). Each MFI value presented in the graphs is the average from the minimum 70 cells of three biological replicates. All the images were taken at 40X objective for quantifying MFI. The MFI values of CK2α/α' at T_0, T_{30} and T_{120} were compared by one-way ANOVA with Dunnett's multiple comparisons test. * denotes $p < 0.001$.

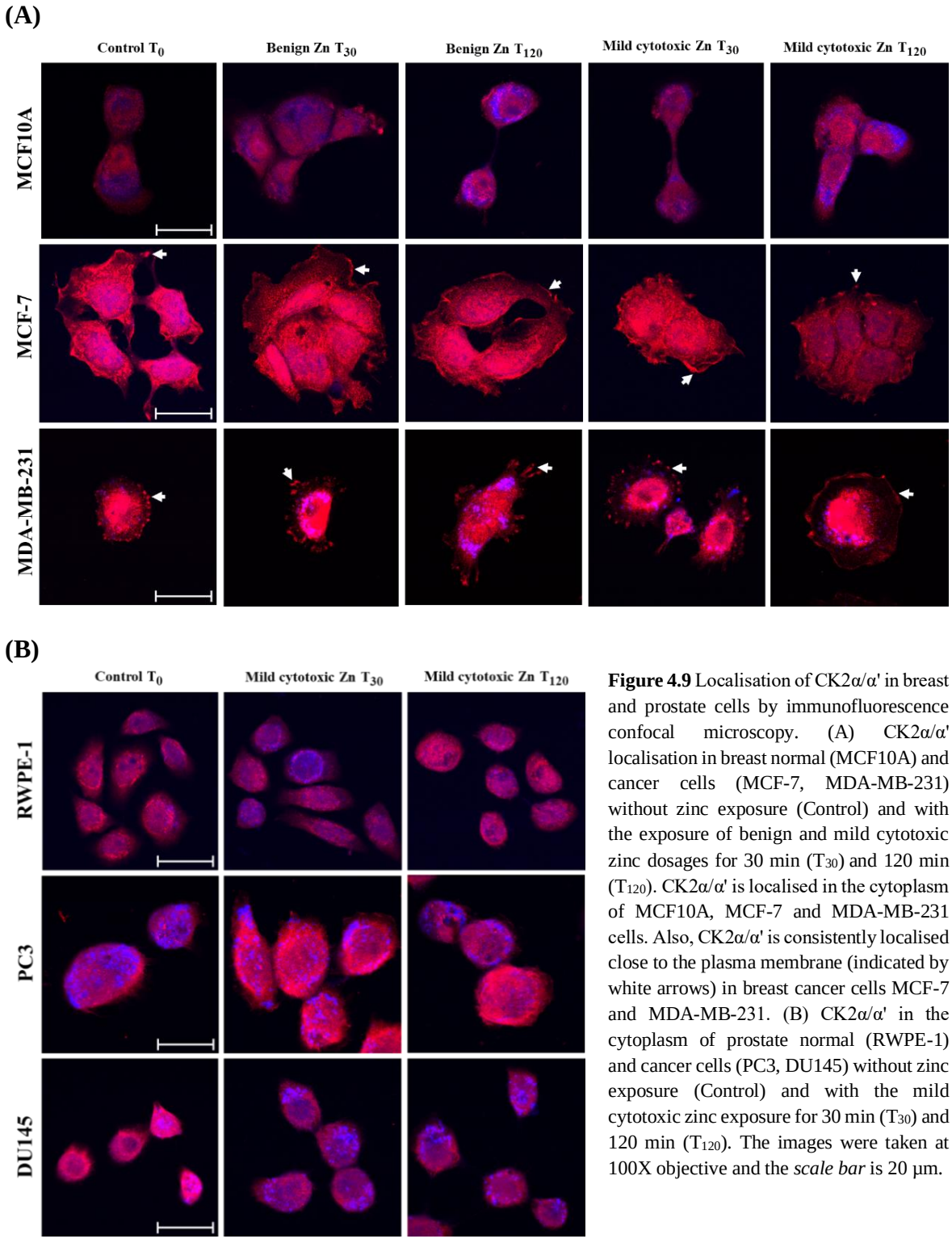

Figure 4.9 Localisation of CK2α/α' in breast and prostate cells by immunofluorescence confocal microscopy. (A) CK2α/α' localisation in breast normal (MCF10A) and cancer cells (MCF-7, MDA-MB-231) without zinc exposure (Control) and with the exposure of benign and mild cytotoxic zinc dosages for 30 min (T_{30}) and 120 min (T_{120}). CK2α/α' is localised in the cytoplasm of MCF10A, MCF-7 and MDA-MB-231 cells. Also, CK2α/α' is consistently localised close to the plasma membrane (indicated by white arrows) in breast cancer cells MCF-7 and MDA-MB-231. (B) CK2α/α' in the cytoplasm of prostate normal (RWPE-1) and cancer cells (PC3, DU145) without zinc exposure (Control) and with the mild cytotoxic zinc exposure for 30 min (T_{30}) and 120 min (T_{120}). The images were taken at 100X objective and the *scale bar* is 20 µm.

4.2.6 CK2β expression and localisation

CK2β was up-regulated in normal breast cells MCF10A compared to both cancerous cells MCF-7 and MDA-MB-231 at T_0 (**Table 4.1**). An opposite pattern was observed in prostate cells where prostate normal RWPE-1 cells exhibited down-regulation of CK2β relative to its cancerous counterparts PC3 and DU145 cells at T_0 (**Table 4.1**). CK2β was reduced significantly under benign and mild cytotoxic zinc dosages at T_{30} and T_{120} compared to T_0 in MCF10A cells (**Figure 4.10A**). MCF-7 cells exhibited overexpression of CK2β following benign zinc dosages compared to control (T_0) (**Figure 4.10A**). CK2β expression did not change in response to either benign or mild cytotoxic zinc exposure in MDA-MB-231 cells (**Figure 4.10A**). In contrast, mild cytotoxic zinc dosage reduced CK2β expression in prostate cells (RWPE-1, PC3, DU145) (**Figure 4.10B**). Like CK2α/α', CK2β was found to be localised in the cytoplasm and close to the plasma membrane of two breast cancer cells (MCF-7 and MDA-MB-231) (**Figure 4.11A**), however, such an expression in proximity to the plasma membrane was not observed in normal breast epithelial cells (MCF10A) or prostate cells (RWPE-1, PC3, DU145) (**Figure 4.11**).

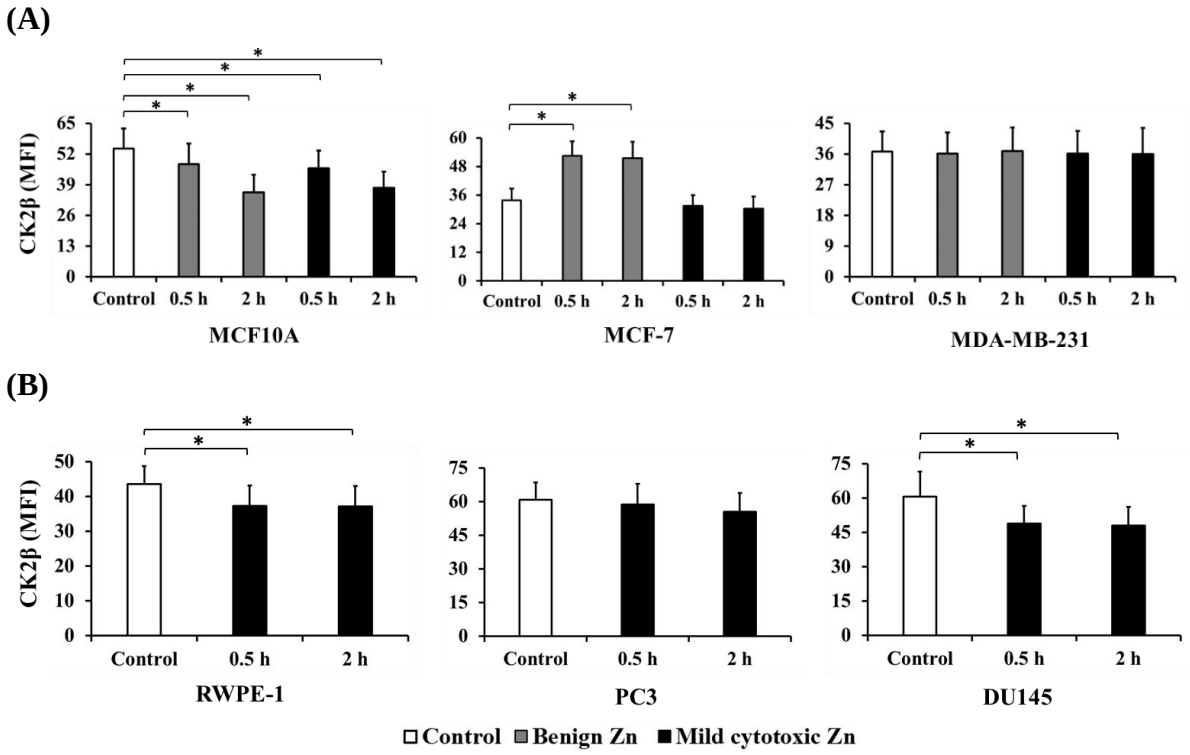

Figure 4.10 Quantification of CK2β protein expression in breast and prostate cells by immunofluorescence confocal microscopy. (A) Mean fluorescence intensity (MFI) of CK2β in MCF10A (left), MCF-7 (middle) and MDA-MB-231 cells (right) without zinc exposure (Control) and with the exposure of benign and mild cytotoxic zinc for 30 min (T_{30}) and 120 min (T_{120}). (B) Mean fluorescence intensity (MFI) of CK2β in RWPE-1 (left), PC3 (middle) and DU145 cells (right) without zinc exposure (Control) and with the exposure of mild cytotoxic zinc for 30 min (T_{30}) and 120 min (T_{120}). Each MFI value presented in the graphs is the average from the minimum 70 cells of three biological replicates. All the images were taken at 40X objective for quantifying MFI. The MFI values of CK2β at T_0, T_{30} and T_{120} were compared by one-way ANOVA with Dunnett's multiple comparisons test. * denotes $p < 0.001$.

(A)

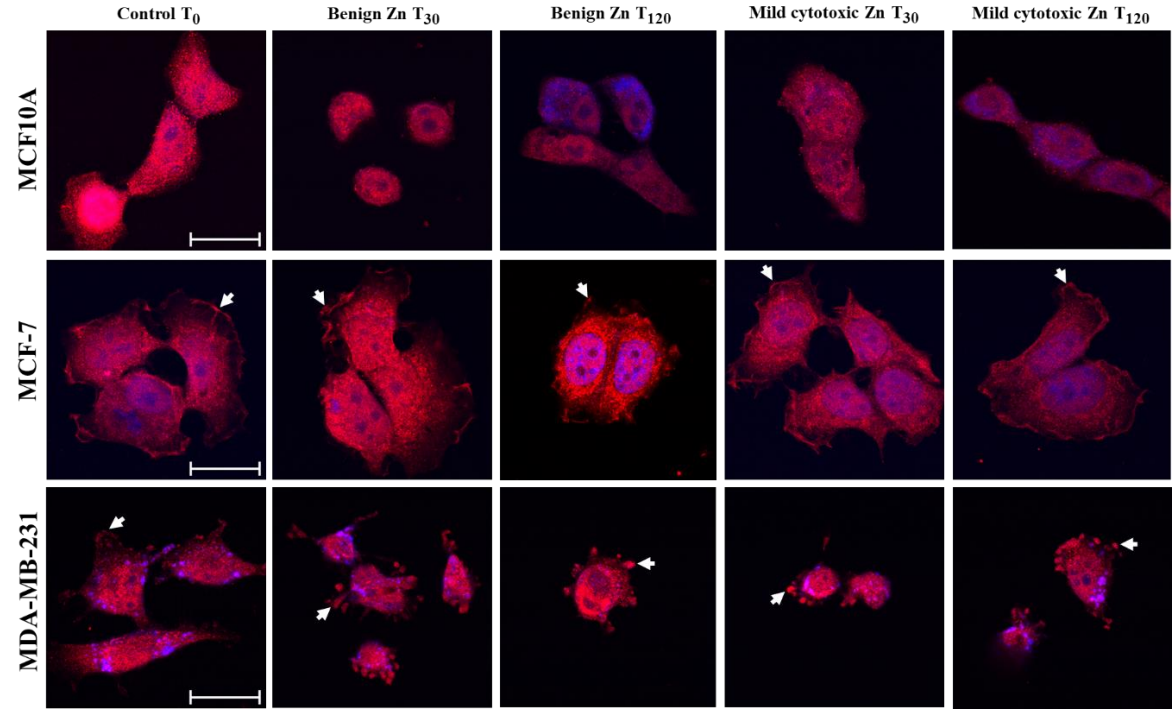

(B)

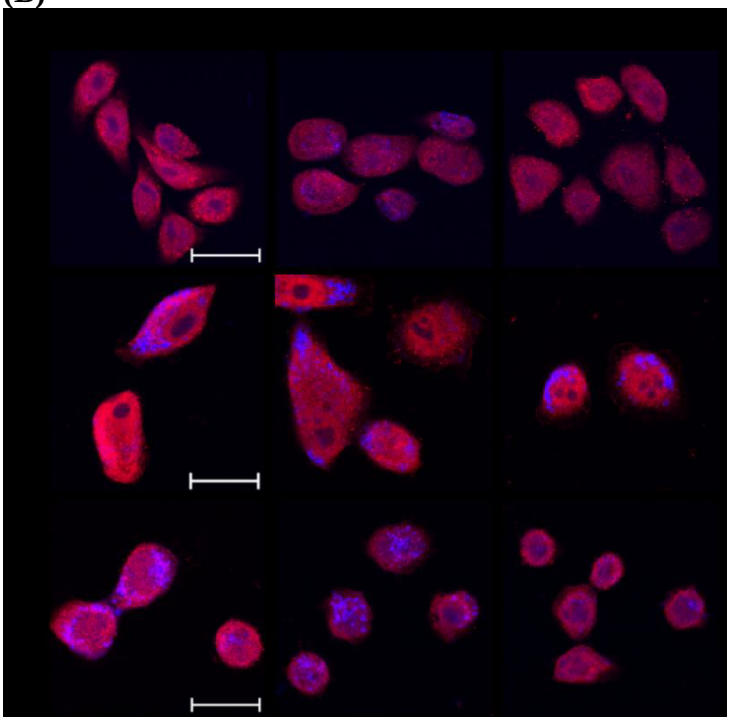

Figure 4.11 Localisation of CK2β in breast and prostate cells by immunofluorescence confocal microscopy. (A) CK2β localisation in breast normal (MCF10A) and cancer cells (MCF-7, MDA-MB-231) without zinc exposure (Control) and with the exposure of benign and mild cytotoxic zinc dosages for 30 min (T_{30}) and 120 min (T_{120}). CK2β is localised in the cytoplasm of MCF10A, MCF-7 and MDA-MB-231 cells. Also, CK2β is consistently localised close to the plasma membrane (indicated by white arrows) in breast cancer cells MCF-7 and MDA-MB-231. (B) CK2β in the cytoplasm of prostate normal (RWPE-1) and cancer cells (PC3, DU145) without zinc exposure (Control) and with the mild cytotoxic zinc exposure for 30 min (T_{30}) and 120 min (T_{120}). The images were taken at 100X objective and the *scale bar* is 20 µm.

4.2.7 Predicted phosphorylation sites in ZIP12, ZnT1 and MT2A

The predicted phosphorylation sites of protein kinase CK2 were not found in ZnT1 and MT2A proteins. However, ZIP12 showed numerous potential phosphorylation sites for CK2 kinase (**Table 4.2**, **Appendix B**).

Table 4.2 Predicted phosphorylation sites of protein kinase CK2 in ZIP12

Position	Amino acid residue	Amino acid sequence	Score	Localisation
26	S	DEDSSFLSQNETEDI	2.45	Extracellular
39	S	QDSRSRGSSGQPADL	3.57	Extracellular
51	S	ADLLQVLSAGDHPPH	3.95	Extracellular
63	S	KKSGIVSSEGANEST	4.26	Extracellular
116	S	RTNTLRLSELDQLLN	5.18	Extracellular
165	S	SSSMEKESEDGPVSW	4.52	Extracellular
197	S	KKSGIVSSEGANEST	4.26	Extracellular
250	S	RTNTLRLSELDQLLN	5.18	Cytoplasmic
258	S	TALVLFHSCEENYRL	3.17	Cytoplasmic
299	S	SSSMEKESEDGPVSW	4.51	Cytoplasmic
363	S	LALNSELSDQAGRGK	4.25	Cytoplasmic
392	S	TALVLFHSCEENYRL	3.17	Extracellular
431	S	AIGAAFSSSSESGVT	3.92	Cytoplasmic
433	S	GAAFSSSSESGVTTT	2.30	Cytoplasmic
476	S	VSPNDKKSPEDSQAA	3.38	Extracellular
480	S	DKKSPEDSQAAEMPI	4.56	Extracellular
496	S	LALNSELSDQAGRGK	3.94	Extracellular
497	S	LALNSELSDQAGRGK	4.25	Extracellular
511	S	AGMFLYLSLVEMLPE	3.65	Extracellular
528	S	AIGAAFSSSSESGVT	3.92	Extracellular
530	S	GAAFSSSSESGVTTT	2.30	Extracellular
564	S	AIGAAFSSSSESGVT	3.92	Cytoplasmic
565	S	AIGAAFSSSSESGVT	3.92	Cytoplasmic
566	S	GAAFSSSSESGVTTT	2.30	Cytoplasmic
567	S	GAAFSSSSESGVTTT	2.30	Cytoplasmic

The phosphorylation sites of protein kinase CK2 in ZIP12 were identified by GPS5.0 software. Default settings (threshold selected as a medium) were employed to analyse FASTA amino acid sequence of ZIP12. The predicted amino acid residues (underlined) along with the positions, amino acid sequence and the scores (higher score indicates more likely to be phosphorylated) were shown in the table.

4.3 Discussion

This study follows our previous work on expression profiles of genes associated with zinc homeostasis in breast and prostate cancer cells (Barman et al., 2022), by investigating the protein expression and localisation of ZIP12, ZnT1, MT2A, the catalytic CK2α/α' and regulatory CK2β subunits of protein kinase CK2 in the breast (MCF10A, MCF-7, MDA-MB-231) and prostate (RWPE-1, PC3, DU145) cells. The protein expression data from this study add another layer of details to our previous gene expression results (Barman et al., 2022) and the existing findings in the literature (Chandler et al., 2016), while the protein localisation data here are novel and significant as discussed below.

ZIP12 protein, encoded by *SLC39A12* gene located in the chromosome 10p12.33, is a plasma membrane-bound zinc importer and has high specificity for zinc (Chowanadisai et al., 2013). Its expression in human is primarily in the brain (http://biogps.org/#goto=welcome). Recently, ZIP12 was found as a major regulator of hypoxia-induced pulmonary vascular remodelling (Zhao et al., 2015), and as a regulator for monocrotaline-induced proliferation and migration of pulmonary arterial smooth muscle cells (Ye et al., 2022). The localisation of ZIP12 in the plasma membrane of breast cancer cells (MCF-7, MDA-MB-231) with or without zinc exposure (**Figure 4.3A**) is a clear contrast to the normal breast epithelial cells (MCF10A), signifying the role of ZIP12 in breast cancer cells. This novel finding demonstrates a role of ZIP12 in breast cancers. ZIP12 should be a worthwhile target for future therapeutic drug development. This also highlights the usefulness of immunofluorescence for protein localisation against gene profiling and immunoblotting, as both gene profiling by qRT-PCR or microarray and immunoblotting (Chandler et al., 2016; Barman et al., 2022) showed only expression levels without details where they were expressed.

In contrast to the breast cancer cells, ZIP12 is not localised in the plasma membrane of normal prostate epithelial cells (RWPE-1) and the prostate cancer cells (PC3, DU145) (**Figure 4.3B**), although ZIP12 protein is in cytoplasm. Since ZIP12 functions in the cell plasma membrane, it is unclear why ZIP12 protein is present in the cytoplasm of prostate cells, (RWPE-1, PC3, DU145). Differential expression of ZIP12 under exogenous zinc exposure confirms ZIP12 involvement in zinc homeostasis (Zhu et al., 2022). ZIP12 is a very close homologue of ZIP4 (Chun et al., 2019) which is implicated in zinc sensing or regulation of zinc uptake from the extracellular space (Zhang et al., 2017; Chun et al., 2019; Hu, 2021). The opposite localisation

profiles of ZIP12 in the plasma membranes of breast and prostate cancer cells might in part, reflect the opposite intracellular zinc levels, that is, the elevated zinc in breast cancer cells (Mulay et al., 1971; Margalioth et al., 1983; Raju et al., 2006; Majewska et al., 2007) against the normal breast epithelial cells, and the reduced cytoplasmic zinc level in prostate cancer cells compared to their counterpart in normal prostate cells (Costello and Franklin, 2006; Gumulec et al., 2014) ZIP12 has been scarcely investigated in breast and prostate cancer cells, our findings here revealed the prominence of ZIP12 in the zinc homeostasis of breast cancer cells.

ZnT1, encoded by *SLC30A1* in human, is a plasma membrane-bound zinc exporter. ZnT1 is localised in the plasma membrane of both breast cancer cells, MCF-7 cells in particular, but absence in the cell membrane of breast normal epithelial cells (**Figure 4.5A**), indicating that ZnT1 is required for Zn^{2+} efflux from cytoplasm of breast cancer cells. The absence of ZnT1 in the plasma membrane of prostate cancer cells (PC3 and DU145) (**Figure 4.5B**) reflects that ZnT1 is not needed for Zn^{2+} efflux because of the low intracellular Zn^{2+} level.

Metallothioneins are a group of small cysteine-rich proteins in the cytoplasm, which are mainly associated with metal homeostasis and anti-oxidative stress response. In our previous study, MT2A was found to be overexpressed at the gene level in MCF-7 and PC-3 cells compared to their respective normal MCF10A and RWPE-1 cells (Barman et al., 2022). The data in **Table 4.1** here further confirmed the overexpression of MT2A in breast and prostate cancer cells. The implication of this finding about MT2A might be more than its role related to the elevated intracellular zinc level in cancer cells, considering the recent finding that MT2A expression is associated with cancer cell proliferation and invasion (Liu et al., 2022). The fact that it is located close to the plasma membrane (**Figure 4.7A**) suggests MT2A plays a role in cell proliferation and migration. This notion is supported by the previous studies where MT2A was found in extracellular space and involved in cancer cell migration and invasion (Lynes et al., 1993; Youn et al., 1995; Lynes et al., 2006; Subramanian Vignesh and Deepe, 2017). Furthermore, the expression of MT2A varies with cancer types, such as its down-regulation in gastric cancer (Pan et al., 2016) and up-regulation in breast cancer cells, as demonstrated by the current study (**Table 4.1**).

Protein kinase CK2 is overexpressed in multiple cancers such as breast and prostate cancers (Borgo et al., 2021). The immunofluorescence results demonstrate that the catalytic CK2α/α' subunits were overexpressed in both breast cancer cells (MCF-7, MDA-MB-231) and prostate cancer cells (PC3, DU145) compared to their normal counterparts MCF10A and RWPE-1 cells (**Table 4.1**). Similar findings were also observed in breast and prostate cancerous tissues relative to the normal tissues (Chua et al., 2017). In contrast, CK2β showed overexpression in prostate cancer cells but reduced in breast cancer cells compared to their normal counterparts (**Table 4.1**). However, the significant findings are in their localisations. Both CK2α/α' and CK2β are localised in the proximity of the plasma membrane of breast cancer cells while no such localisation in normal breast epithelial cells (**Figure 4.9A**, **Figure 4.11A**). Neither prostate cancer cells nor normal prostate epithelial cells showed CK2 localisation close to plasma membrane (**Figure 4.9B**, **Figure 4.11B**). The data indicate protein kinase CK2 is likely more involved in breast cancers. CK2 was found to bind to the plasma membrane tightly by a specific domain of its regulatory subunit CK2β (Sarrouilhe et al., 1998) and further investigation reported that 'Pleckstrin homology domain' of CK2 plays a crucial role in its interaction with the plasma membrane (Olsten et al., 2004). Its localisation close to the plasma membrane confirms the likely role of protein kinase CK2 as an ecto-kinase (Montenarh and Götz, 2018). Its function on the plasma membrane of the breast cancer cells could be related to the regulation of ZIP12, because ZIP12 is uniquely localised in plasma membrane of breast cancer cells (**Figure 4.3A**) as shown in this study, and there are multiple phosphorylation motifs in the extracellular loop of ZIP12 (**Table 4.2**). However, there is thus far no experimental evidence for the phosphorylation of those postulated phosphorylation sites in ZIP12 transporter protein by CK2 kinase in breast cancer cells.

4.4 Conclusion

The immunofluorescence confocal microscopy of this study revealed two lines of data for ZIP12, ZnT1, MT2A, CK2 α/α' and CK2β in their overall expression and plasma membrane localisation in breast and prostate cancer cells (MCF-7, MDA-MB-231, PC3, DU145) as well as their normal counterparts (MCF10A, RWPE-1). The pronounced membrane localisation of ZIP12 in breast cancer cells with and without zinc exposure highlights its prominence in zinc homeostasis. Furthermore, the localisation of CK2 α/α' and CK2β in the proximity to the plasma membrane of breast cancer cells points to a likelihood of its interaction with ZIP12 in regulating zinc homeostasis of breast cancer cells. In contrast, the absence of ZIP12, CK2 α/α' and CK2β in or close to the plasma membrane of prostate cancer cells indicates their minimal involvement in zinc homeostasis of prostate cancer cells. The novel findings provide molecular details for our understanding of zinc homeostasis of breast and prostate cancer cells and should form a basis for further research in breast and prostate cancers.

Chapter 5 Proteomic insights into the zinc homeostasis of breast and prostate cancer cells

5.1 Introduction

Breast cancer is the most common malignancy in females worldwide (Sung et al., 2021; Siegel et al., 2022). In males, prostate cancer is the second and fifth highest in incidence and mortality, respectively (Sung et al., 2021). As described in **Sections 1.5.1** and **1.5.2**, **Chapter 1**, breast cancer cells and prostate cancer cells exhibit opposite intracellular zinc profiles compared to their respective normal cells. By using both breast and prostate cancer cells, the molecular details and insights were obtained in the zinc homeostasis of the cancer cells, as described in **Chapters 3** and **4**. In this chapter, the proteomic analysis of breast and prostate cancer cells was carried out, and the resultant datasets were described and discussed.

Proteomic analysis on breast and prostate cancer tissues or cell lines was employed in previous studies for the discovery of breast cancer biomarkers and differentially expressed proteins (Sardana et al., 2008; Morrison et al., 2012; Nie et al., 2015; Ziegler et al., 2018; Katsogiannou et al., 2019; Yoneten et al., 2019; Zhou et al., 2019). However, the proteomic research on both breast and prostate cancer cells has not been carried out simultaneously. In this study, the top-down proteomic analysis was systematically carried out on MCF-7 breast cancer cells and MCF10A normal breast epithelial cells, PC3 prostate cancer cells and RWPE-1 normal prostatic epithelial cells, with and without exogenous zinc exposure. The differentially expressed proteoforms have been identified and compared in both cancerous and normal breast cells (MCF-7, MCF10A), and cancerous and normal prostate cells (PC3, RWPE-1). The following comparisons were performed in the data analysis: (1) the cancer cells versus the corresponding normal cells without zinc treatment (T_0) including MCF-7 cells versus MCF10A cells, PC3 cells versus RWPE-1 cells, (2) again the cancer cells versus the respective normal cells with exogenous zinc treatment for 120 min (T_{120}) including MCF-7 cells versus MCF10A cells, PC3 cells versus RWPE-1 cells, (3) comparison between cancer cells at T_0 and T_{120} including MCF-7 cells T_{120} versus MCF-7 cells T_0, PC3 cells T_{120} versus PC3 cells T_0, (4) normal cells treated with zinc at T_0 and T_{120} including MCF10A cells T_{120} versus MCF10A cells T_0, RWPE-1 cells T_{120} versus RWPE-1 cells T_0. Such detailed comparative analyses provide the complete protein expression profiles of breast and prostate cells in the context of

with or without extracellular zinc treatment, which reveals significant insights and enhance our understanding of the zinc homeostasis in breast and prostate cancer cells.

5.2 Results

5.2.1 Differentially expressed proteoforms in breast cancer cells (MCF-7) without zinc treatment

By comparing the protein profiles of MCF-7 breast cancer cells against the normal breast epithelial cells (MCF10A), the differentially expressed proteins in breast cancer cells (MCF-7) were identified. Quantitative analysis of the two-dimensional electrophoresis (2-DE) gels by DECODON Delta 2-D software revealed 23 up-regulated (red circles) and 18 down-regulated (green circles) protein spots in MCF-7 breast cancer cells compared to MCF10A normal breast epithelial cells without exogenous zinc exposure (T_0) (**Figure 5.1A**). After LC-MS/MS analysis, the identified proteoforms were enlisted in **Table 5.1**. The proteoforms such as 14-3-3 protein σ (*SFN*), 14-3-3 protein θ (*YWHAQ*), protein S100A2 were down-regulated in MCF-7 cells and were shown to have tumour suppression activity by the previous studies (Li et al., 2009; Young et al., 2015). In addition, calcium-binding annexin protein notably annexin A1 (*ANXA1*) is found to be down-regulated. Those overexpressed proteins (**Table 5.1)** are associated with breast cancer cell progression and invasion, including α-smooth muscle actin α2 (*ACTA2*), cytochrome b5 type B (*CYB5B*), D-3-phosphoglycerate dehydrogenase (*PHGDH*), dihydrolipoamide S-succinyltransferase (*DLST*), elongation factor Tu (*TUFM*), F-actin-capping protein subunit β (*CAPZB*), FUBP1 (*FUBP1*), glutathione S-transferase Mu 3 (*GSTM3*), glutathione synthetase (*GSS*), heterogeneous nuclear ribonucleoproteins C1/C2 (*HNRNPC*), high mobility group protein B1 (*HMGB1*), histone H4 (*HIST1H4J*), nucleoside diphosphate kinase (*NME*), proliferating cell nuclear antigen (*PCNA*), peroxiredoxin 6 (*PRDX6*), protein S100A13 (*S100A13*), radixin (*RDX*), triosephosphate isomerase (*TPI1*) and tumour protein D53 (*TPD52L1*).

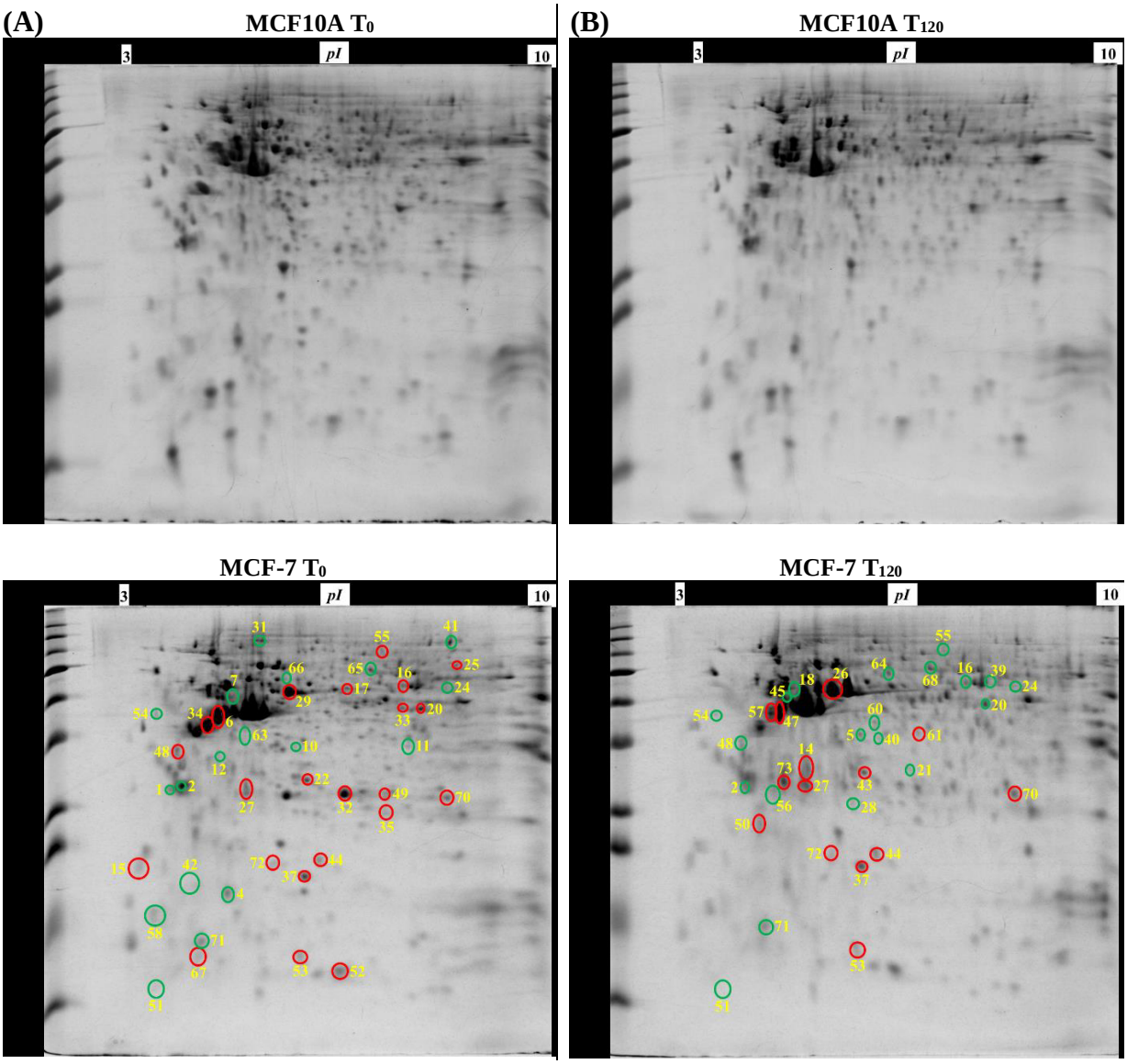

Figure 5.1 Differentially expressed protein spots in 2-DE gels by comparisons of MCF-7 T_0 vs MCF10A T_0 and MCF-7 T_{120} vs MCF10A T_{120}. (A) Representative 2-DE gel images (in the left panel) of breast normal MCF10A cells (MCF10A T_0) and breast cancer MCF-7 cells (MCF-7 T_0) without zinc exposure (T_0). (B) Representative 2-DE gel images (in the right panel) of breast normal MCF10A cells (MCF10A T_{120}) and breast cancer MCF-7 cells (MCF-7 T_{120}) with exogenous zinc exposure for 120 min (T_{120}). Each protein extract (100 µg) was resolved based on isoelectric point (*pI*) and molecular weight (MW). The differentially expressed protein spots are shown with red circles denoting up-regulation and green circles down-regulation.

Table 5.1 Identified proteoforms in breast cancer cells (MCF-7) and normal breast epithelial cells (MCF10A) with or without exogenous zinc exposure

Spot ID	Identified proteoforms	Gene ID	Protein accession	Theoretical MW (kDa)/*pI*	Observed MW (kDa)/*pI*	PLGS score	Matched peptides	Sequence coverage (%)	(Fold change/ *p* value)				Molecular functions
									MCF-7 T_0/ MCF10A T_0	MCF-7 T_{120}/ MCF10A T_{120}	MCF-7 T_{120}/ MCF-7 T_0	MCF10A T_{120}/ MFC10A T_0	
1	14-3-3 protein σ	*SFN*	P31947	27.8/4.5	27.9/4.5	2586	24	44	(0.54/ 0.02) ↓				I
2	14-3-3 protein θ	*YWHAQ*	P27348	27.8/4.5	29.0/4.7	10806	14	43	(0.43/ 0.003) ↓	(0.34/ 0.0001) ↓			II
3	26S proteasome non-ATPase regulatory subunit 4	*PSMD4*	Q5VWC4	41.1/4.5	62.0/4.6	1085	22	23			(0.19/ 0.003) ↓		III
4	39S ribosomal protein L12 mitochondrial	*MRPL12*	P52815	21.3/9.2	17.7/5.3	4066	8	30	(0.72/ 0.03) ↓				IV
5	60S acidic ribosomal protein P0	*RPLP0*	A0A024RBS2	34.3/5.6	42.0/5.6	588	6	16		(0.26/ 0.002) ↓			V
6	α-smooth muscle actin 2	*ACTA2*	D2JYH4	42.0/5.1	44.4/5.2	6831	22	28	(6.79/ 0.0003) ↑		(0.33/ 0.003) ↓		VI
7	Actin cytoplasmic 1	*ACTB*	P60709	41.7/5.1	59.6/5.3	17835	27	60	(0.34/ 0.0004) ↓				VII
8	Actinin α 1 isoform CRA a	*ACTN1*	A0A024R694	103.0/5.1	156.6/5.5	35257	64	45			(1.92/ 0.02) ↑		VIII
9	Adenosylhomocysteinase	*AHCY*	A0A384MTQ3	47.7/5.9	50.1/6.0	911	24	19			(0.47/ 0.04) ↓		III
10	Annexin	*ANXA8L1*	A0A075B752	40.7/5.6	35.2/5.6	623	8	17	(0.14/ 0.04) ↓				VIII
11	Annexin A1	*ANXA1*	P04083	38.7/6.6	36.0/6.6	21563	27	62	(0.18/ 0.03) ↓				VIII
12	Annexin A5	*ANXA5*	P08758	35.9/4.7	29.0/5.0	3292	8	20	(0.54/ 0.03) ↓		(4.39/ 0.02) ↑		VIII
13	Calmodulin-1	*CALM1*	P0DP23	17.0/3.9	13.9/3.3	1613	6	41			(0.22/ 0.006) ↓		VIII, III
14	Cathepsin D	*CTSD*	A0A1B0GW44	43.7/6.1	30.2/5.4	1908	11	19		(8.37/ 0.0001) ↑	(3.32/ 0.007) ↑		III

Table 5.1 (continued)

Spot ID	Identified proteoforms	Gene ID	Protein accession	Theoretical MW (kDa)/*pI*	Observed MW (kDa)/*pI*	PLGS score	Matched peptides	Sequence coverage (%)	(Fold change/ *p* value)				Molecular functions
									MCF-7 T_0/ MCF10A T_0	MCF-7 T_{120}/ MCF10A T_{120}	MCF-7 T_{120}/ MCF-7 T_0	MCF10A T_{120}/ MFC10A T_0	
15	Cytochrome b5 type B	*CYB5B*	O43169	16.3/4.7	18.2/3.7	867	3	17	(4.16/ 0.0003) ↑				VIII
16	D-3-phosphoglycerate dehydrogenase	*PHGDH*	A0A286YF22	55.9/6.3	69.2/6.7	4302	8	16	(1.98/ 0.02) ↑	(0.88/ 0.04) ↓		(1.40/ 0.02) ↑	III
17	Dihydrolipoamide S-succinyltransferase (E2 component of 2-oxo-glutarate complex) isoform CRA a	*DLST*	A0A024R6C9	48.7/9.3	62.0/6.0	1601	4	10	(2.63/ 0.01) ↑				III
18	Dynactin 2 (P50) isoform CRA c	*DCTN2*	A0A384MDU9	44.2/4.9	59.2/5.2	6320	21	52		(0.42/ 0.03) ↓	(0.75/ 0.04) ↓		VII
19	Elongation factor 1 δ	*EEF1D*	A0A087X1X7	69.2/6.8	42.0/4.3	52531	21	25			(0.72/ 0.001) ↓		V
20	Elongation factor Tu	*TUFM*	A0A384ME17	49.8/7.4	50.1/7.0	2644	49	36	(5.24/ 0.01) ↑	(0.49/ 0.003) ↓	(0.52/ 0.01) ↓	(1.35/ 0.02) ↑	V
21	Exosome complex component MTR3	*EXOSC6*	Q5RKV6	28.2/6.0	32.4/5.9	350	4	17		(0.53/ 0.04) ↓			IV
22	F-actin-capping protein subunit β	*CAPZB*	A0A384MR50	30.6/5.6	28.5/5.7	1812	10	26	(2.97/ 0.0003) ↑		(2.35/ 0.03) ↑		VI
23	ATP-dependent RNA helicase DDX1	*DDX1*	A0A087X2G1	73.9/7.6	136.2/8.1	298	19	12				(1.35/ 0.04) ↑	III
24	Adenylosuccinate lyase	*ADSL*	A0A1B0GTJ7	54.4/6.7	67.2/7.6	584	4	8	(0.25/ 0.002) ↓	(0.36/ 0.005) ↓			III
25	FUBP1	*FUBP1*	A0A1Z1G4M2	67.6/7.9	89.5/8.2	372	5	9	(2.08/ 0.02) ↑				II
26	Peptidyl-prolyl cis-trans isomerase FKBP4	*FKBP4*	Q02790	51.8/5.2	62.0/5.6	32827	47	65		(1.87/ 0.01) ↑	(2.46/ 0.003) ↑		IX
27	Glutathione S-transferase Mu 3	*GSTM3*	P21266	26.5/5.2	26.9/5.4	8436	20	54	(3.03/ 0.04) ↑	(5.00/ 0.005) ↑			III

Table 5.1 (continued)

Spot ID	Identified proteoforms	Gene ID	Protein accession	Theoretical MW (kDa)/*pI*	Observed MW (kDa)/*pI*	PLGS score	Matched peptides	Sequence coverage (%)	(Fold change/ *p* value)				Molecular functions
									MCF-7 T_0/ MCF10A T_0	MCF-7 T_{120}/ MCF10A T_{120}	MCF-7 T_{120}/ MCF-7 T_0	MCF10A T_{120}/ MFC10A T_0	
28	Glutathione S-transferase P	*GSTP1*	P09211	23.3/5.3	24.6/5.6	12769	31	66		(0.21/ 0.002) ↓			III
29	Glutathione synthetase	*GSS*	P48637	52.4/5.6	62.0/5.6	11269	26	57	(1.48/ 0.04) ↑				III
30	Inorganic pyrophosphatase	*PPA1*	Q15181	32.6/5.4	37.8/5.5	957	4	11			(2.50/ 0.03) ↑		III
31	Heat shock protein 90kDa alpha (Cytosolic) class B member 1 isoform CRA a	*HSP90AB1*	A0A024RD80	83.2/4.8	143.0/5.4	5834	28	33	(0.51/ 0.0006) ↓				IX
32	Heat shock protein β 1	*HSPB1*	P04792	22.8/6.0	26.0/5.9	46679	22	78	(3.48/ 0.002) ↑		(0.21/ 0.002) ↓		IX
33	Pyruvate dehydrogenase E1 component subunit α	*PDHA1*	A0A024RBX9	43.3/8.0	50.1/6.5	373	3	6	(1.67 /0.04) ↑				III
34	Heterogeneous nuclear ribonucleoproteins C1/C2	*HNRNPC*	B2R5W2	31.9/4.9	40.8/5.0	7292	24	43	(8.03/ 0.0002) ↑		(0.45/ 0.009) ↓		X, IV
35	High mobility group protein B1	*HMGB1*	A0A024RDR0	24.9/5.5	23.5/6.3	3179	8	26	(1.91/ 0.03) ↑				X
36	Histidine-tRNA ligase cytoplasmic	*HARS1*	P12081	57.4/5.6	62.0/5.8	3224	15	25			(1.50/ 0.04) ↑		III
37	Histone H4	*HIST1H4J*	B2R4R0	11.4/11.8	18.2/5.7	897	4	36	(2.46/ 0.007) ↑	(1.95/ 0.001) ↑			VII, X
38	Heat shock 70 kDa protein 1A	*HSPA1A*	A0A1U9X7W4	70.0/5.3	89.5/5.5	29565	38	49			(1.66/ 0.02) ↑		IX
39	Inosine-5'-monophosphate dehydrogenase	*IMPDH*	A0A384N6C2	55.8/6.5	69.2/7.0	3921	8	14		(0.65/ 0.04) ↓		(1.51/ 0.005) ↑	III
40	L-lactate dehydrogenase B chain	*LDHB*	P07195	36.6/5.6	38.9/5.7	6282	11	28		(0.62/ 0.004) ↓			III

Table 5.1 (continued)

Spot ID	Identified proteoforms	Gene ID	Protein accession	Theoretical MW (kDa)/*pI*	Observed MW (kDa)/*pI*	PLGS score	Matched peptides	Sequence coverage (%)	(Fold change/ *p* value)				Molecular functions
									MCF-7 T_0/ MCF10A T_0	MCF-7 T_{120}/ MCF10A T_{120}	MCF-7 T_{120}/ MCF-7 T_0	MCF10A T_{120}/ MFC10A T_0	
41	C-1-tetrahydrofolate synthase, cytoplasmic	*MTHFD1*	A0A024R652	101.5/6.8	156.6/7.8	342	18	18	(0.50/ 0.04) ↓				XI, V
42	Myosin regulatory light chain 12A	*MYL12A*	J3QRS3	20.4/4.4	17.3/4.8	1142	5	29	(0.35/ 0.0003) ↓				VIII
43	NADH dehydrogenase (ubiquinone) iron-sulfur protein 3 mitochondrial	*NDUFS3*	O75489	30.2/7.4	29.0/5.7	1561	5	20		(2.45/ 0.0004) ↑			III
44	Nucleoside diphosphate kinase	*NME*	A0A384MTW7	17.1/5.8	19.1/5.8	3957	6	30	(2.75/ 0.01) ↑	(1.67/ 0.03) ↑			III
45	Perilipin	*PLIN*	A0A140VJN8	46.9/5.1	55.1/5.1	3760	11	32		(0.14/ 0.005) ↓			XII
46	Plastin 3	*PLS3*	P13797	70.8/5.3	92.2/5.6	4429	20	31				(1.82/ 0.04) ↑	VIII
47	Actin γ	*ACTG2*	P63267	41.9/5.2	47.1/5.1	11163	11	30		(5.23/ 0.001) ↑			VII
48	Proliferating cell nuclear antigen	*PCNA*	P12004	28.8/4.4	36.0/4.7	3412	13	44	(1.50/ 0.004) ↑	(0.65/ 0.02) ↓			X
49	Peroxiredoxin 6	*PRDX6*	A0A024R938	25.0/6.0	26.0/6.3	2521	26	34	(1.68/ 0.04) ↑				III
50	Proteasome subunit β type 6	*PSMB6*	P28072	25.3/4.6	21.4/4.9	1361	5	21		(1.40/ 0.04) ↑	(0.34/ 0.03) ↓		III
51	Protein S100A2	*S100A2*	P29034	11.0/4.5	12.0/4.5	2026	3	18	(0.039/ 0.004) ↓	(0.075/ 0.01) ↓	(0.34/ 0.02) ↓		VIII
52	Cytochrome c oxidase subunit 6B1	*COX6B1*	P14854	10.2/6.9	12.4/5.9	833	8	28	(1.86/ 0.02) ↑		(0.74/ 0.04) ↓		XII
53	Protein S100A13	*S100A13*	Q99584	11.5/5.8	13.1/5.7	9088	17	60	(4.06/ 0.001) ↑	(3.98/ 0.0002) ↑			VIII
54	Protein SET	*SET*	Q01105	33.5/4.0	50.1/4.4	8811	16	34	(0.17/ 0.0009) ↓	(0.18/ 0.0001) ↓			IX, X

Table 5.1 (continued)

Spot ID	Identified proteoforms	Gene ID	Protein accession	Theoretical MW (kDa)/*pI*	Observed MW (kDa)/*pI*	PLGS score	Matched peptides	Sequence coverage (%)	(Fold change/ *p* value)				Molecular functions
									MCF-7 T_0/ MCF10A T_0	MCF-7 T_{120}/ MCF10A T_{120}	MCF-7 T_{120}/ MCF-7 T_0	MCF10A T_{120}/ MFC10A T_0	
55	Radixin	*RDX*	B0YJ88	68.5/6.0	110.1/6.3	5828	28	36	(1.30/ 0.02) ↑	(0.30/ 0.0004) ↓		(1.55/ 0.004) ↑	VI
56	ρ GDP-dissociation inhibitor 1	*ARHGDIA*	P52565	23.2/4.8	26.8/5.1	1996	8	28		(0.63/ 0.04) ↓			III
57	40S ribosomal protein SA	*RPSA*	A0A024R2L6	32.8/4.6	47.1/5.1	2510	8	16		(4.35/ 0.0005) ↑			VII
58	60S acidic ribosomal protein P2	*RPLP2*	A0A024RCA7	11.7/4.2	15.9/4.3	8497	11	77	(0.75/ 0.004) ↓				V
59	Serine/threonine-protein kinase PAK 2	*PAK2*	Q13177	58.0/5.6	73.4/5.8	2239	17	28			(0.48/ 0.03) ↓		III
60	Serpin B5	*SERPINB5*	A0A024R2B6	42.1/5.6	45.7/5.8	2466	15	38		(0.17/ 0.0007) ↓			III
61	START domain containing 10 isoform CRA a	*STARD10*	A0A024R5L8	33.0/6.7	39.8/6.0	1134	5	20		(3.05/ 0.002) ↑			XIII
62	Stathmin	*STMN1*	P16949	17.3/5.7	16.5/5.7	8524	12	53			(0.43/ 0.002) ↓		VII
63	SUMO-1 activating enzyme subunit 1 isoform CRA b	*SAE1*	A0A024R0R4	38.4/5.0	42.0/5.4	3930	11	28	(0.13/ 0.03) ↓				III
64	T-complex protein 1 subunit α	*TCP1*	P17987	60.3/5.7	75.5/5.8	4508	17	30		(0.42/ 0.008) ↓			IX
65	T-complex protein 1 subunit γ	*CCT3*	B3KX11	57.9/6.5	89.5/6.1	1050	17	23	(0.85/ 0.02) ↓				IX
66	T-complex protein 1 subunit θ	*CCT8*	P50990	59.6/5.3	73.4/5.6	1289	15	28	(0.24/ 0.03) ↓				IX
67	Thioredoxin	*TXN*	H9ZYJ2	11.7/4.6	14.5/5.1	1389	15	34	(1.35/ 0.0004) ↑				III

Table 5.1 (continued)

Spot ID	Identified proteoforms	Gene ID	Protein accession	Theoretical MW (kDa)/*pI*	Observed MW (kDa)/*pI*	PLGS score	Matched peptides	Sequence coverage (%)	(Fold change/ *p* value)				Molecular functions
									MCF-7 T_0/ MCF10A T_0	MCF-7 T_{120}/ MCF10A T_{120}	MCF-7 T_{120}/ MCF-7 T_0	MCF10A T_{120}/ MFC10A T_0	
68	Torsin-1A-interacting protein 1	*TOR1AIP1*	A0A0A0MSK5	52.4/6.6	75.5/6.1	1086	9	21		(0.16/ 0.001) ↓		(2.33/ 0.0005) ↑	III
69	Transitional endoplasmic reticulum ATPase	*VCP*	P55072	89.3/5.0	132.3/5.4	2552	27	28			(0.61/ 0.01) ↓		V, III
70	Triosephosphate isomerase	*TPI1*	P60174	30.8/5.6	25.5/7.7	4224	8	32	(3.00/ 0.002) ↑	(3.75/ 0.03) ↑			III
71	Tubulin alpha-1C chain	*TUBA1C*	Q9BQE3	50.1/4.8	14.8/5.3	1665	4	12	(0.18/ 0.0001) ↓	(0.22/ 00) ↓	(3.13/ 0.03) ↑		VII
72	Tumor protein D53	*TPD52L1*	E9PNK6	18.7/5.5	19.1/5.6	1601	3	9	(4.76/ 0.0005) ↑	(13.59/ 0.001) ↑			II
73	Tumor protein D54	*TPD52L2*	A0A087WYR3	23.8/6.1	27.9/5.2	3042	11	38		(2.47/ 0.04) ↑			II
74	Vesicle amine transport protein 1	*VAT1*	A0A024R1Z6	41.9/5.9	57.5/6.0	5485	12	21			(0.70/ 0.04) ↓		III

MW stands for molecular weight, kDa for kilo Dalton, *pI* for isoelectric point, PLGS for ProteinLynx Global Server, T_0 for 0 min or without zinc exposure (control), T_{120} for 120 min, symbol ↑ for up-regulation and ↓ for down-regulation, MCF-7 (breast cancer cells), MCF10A (breast normal epithelial cells). The PLGS score, protein accession, theoretical MW/*pI*, matched peptides and sequence coverage (%) were obtained using ProteinLynx Global Server (PLGS) software (version 3.0 Waters Corporation, USA) and the UniProt (*Homo sapiens*, human) database. Gene ID was derived from Uniprot database. The observed MW and *pI* were calculated according to the protein standards. The fold changes and *p* values were acquired from the quantitative analysis of the gel images (each group n = 3) by Delta2D software (version 4.0.8, DECODON Gmbh, Germany). MCF-7 T_0/MCF10A T_0 is the expression fold change of the proteins in MCF-7 cells compared to MCF10A cells without zinc exposure (T_0), MCF-7 T_{120}/MCF10A T_{120} is the expression fold change of the proteins in MCF-7 cells compared to MCF10A cells following the zinc exposure for 120 min (T_{120}), MCF-7 T_{120}/MCF-7 T_0 is the expression fold change of the proteins in MCF-7 cells following zinc exposure for T_{120} compared to T_0, MCF10A T_{120}/MFC10A T_0 is the fold change of the proteins in MCF10A cells following zinc exposure for T_{120} compared to T_0. Molecular functions: I-Apoptosis; II-Signalling; III-Catalytic activity; IV-RNA binding; V-Protein synthesis; VI-Protein binding; VII-Structural; VIII-Metal ion binding; IX-Molecular chaperone; X-DNA binding, XI-DNA synthesis; XII-Metabolism; XIII-Lipid binding.

Those 41 differentially expressed proteoforms were classified based on their molecular functions as per literature survey and Uniprot database, revealing three prominent groups including catalytic (26%), metal ion binding (16%) and molecular chaperone (11%) (**Figure 5.2A**). PANTHER database-based protein classification agrees with the molecular function-based classification as catalytic enzyme (33%) and calcium binding-protein classes (13%) are the prominent (**Figure 5.2B**). The subcellular localisation classification showed those proteoforms in cytoplasm (39%), nucleus (22%) and mitochondrion (11%) (**Figure 5.2C**).

(A) Molecular function

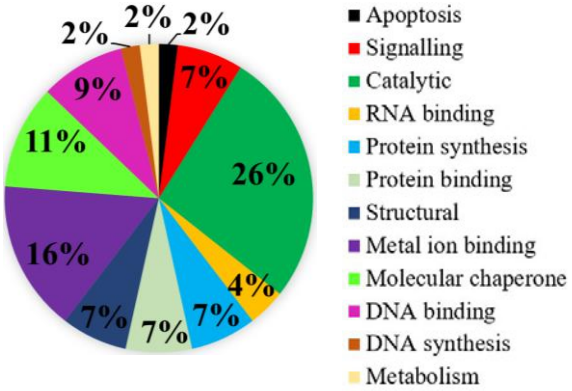

(B) Protein class

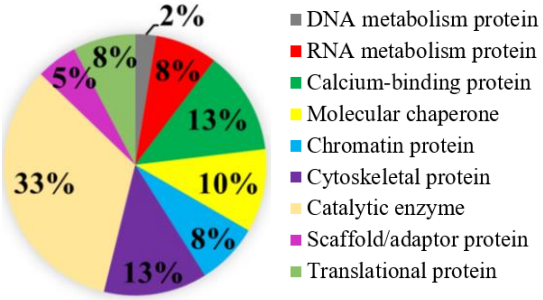

(C) Subcellular localisation

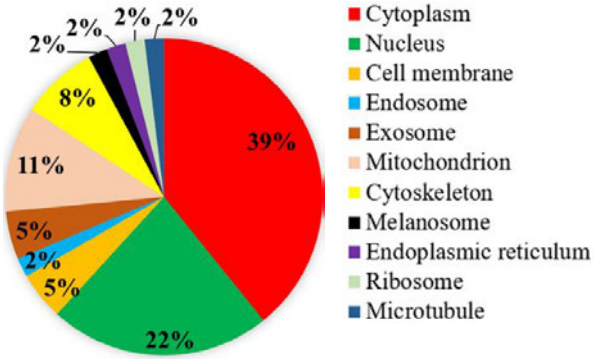

Figure 5.2 Functional classifications of the identified proteoforms in MCF-7 breast cancer cells compared to MCF10A breast normal epithelial cells without zinc exposure (T_0). The pie charts demonstrate the distributions of the identified proteoforms in MCF-7 cells compared to MCF10A cells at T_0 based on (A) Molecular functions (obtained from literature survey and UniProt database) (B) Protein classes (categorized using PANTHER database) and (C) Sub-cellular localisations (derived from literature review and UniProt database).

5.2.2 Differentially expressed proteoforms in MCF-7 breast cancer cells compared to MCF10A normal breast epithelial cells following exogeneous zinc exposure

The extracellular zinc exposure at T_{120} resulted 20 down-regulated (green circle) and 14 up-regulated (red circle) protein spots (**Figure 5.1B**) in MCF-7 breast cancer cells compared to MCF10A normal breast epithelial cells. Tumour suppressor 14-3-3 protein θ (*YWHAQ*) and serpin B5 (*SERPINB5*) were down-regulated. The suppressed proteoforms, including D-3-phosphoglycerate dehydrogenase (*PHGDH*), elongation factor Tu (*TUFM*), adenylosuccinate lyase (*ADSL*), inosine-5'-monophosphate dehydrogenase (*IMPDH*), L-lactate dehydrogenase B chain (*LDHB*), perilipin (*PLIN*), were shown to have catalytic activity (**Table 5.1**). The overexpressed proteoforms, such as cathepsin D (*CTSD*), glutathione S-transferase Mu 3 (*GSTM3*), NADH dehydrogenase (ubiquinone) iron-sulfur protein 3 (*NDUFS3*), actin γ (*ACTG2*), protein S100A13 (*S100A13*), 40S ribosomal protein SA (*RPSA*), triosephosphate isomerase (*TPI1*), tumour protein D53 (*TPD52L1*), tumour protein D54 (*TPD52L2*), are associated with cellular structure, proliferation and metastasis. The differentially expressed 34 proteoforms showed 38% catalytic, 14% structural and 8% signalling based on molecular function according to literature survey and UniProt database (**Figure 5.3A**). PANTHER database-based classification demonstrated three prominent groups including catalytic enzyme (34%), cytoskeletal (11%) and translational (11%) (**Figure 5.3B**). The proteoforms showed their subcellular localisation in cytoplasm (48%), nucleus (18%) and mitochondrion (12%) (**Figure 5.3C**).

(A) Molecular function

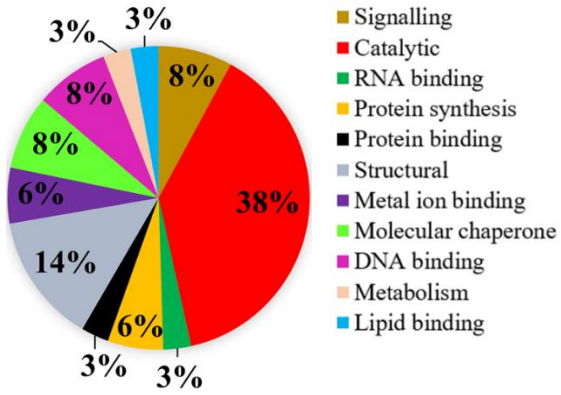

(B) Protein class

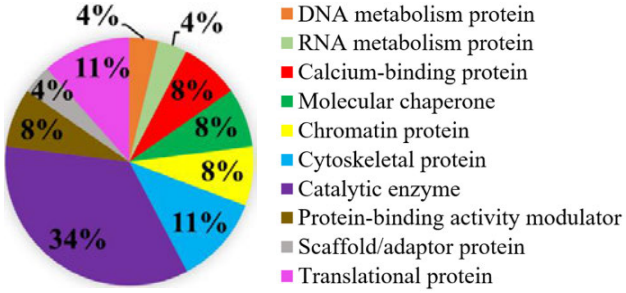

(C) Subcellular localisation

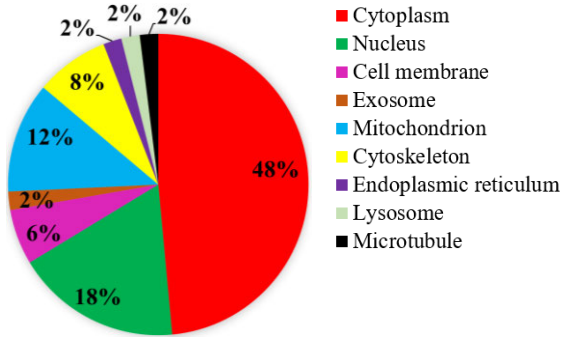

Figure 5.3 Functional classifications of the identified proteoforms in MCF-7 breast cancer cells compared to MCF10A breast normal epithelial cells under zinc exposure at T_{120}. The pie charts demonstrate the distributions of the identified proteoforms in MCF-7 cells compared to MCF10A cells with zinc exposure based on (A) Molecular functions (obtained from literature survey and UniPro database) (B) Protein classes (categorized using PANTHER database) and (C) Subcellular localisations (derived from literature review and UniProt database).

5.2.3 Differentially expressed proteoforms in MCF-7 breast cancer cells with exogenous zinc exposure compared to MCF-7 cells without zinc exposure

MCF-7 breast cancer cells demonstrated 16 down-regulated (green circle) and 9 up-regulated (red circle) protein spots (**Figure 5.4A**) following exogenous zinc exposure at T_{120} compared to MCF-7 cells at T_0. The down-regulated proteoforms, including α-smooth muscle actin 2 (*ACTA2*), adenosylhomocysteinase (*AHCY*), calmodulin 1 (*CALM1*), heterogeneous nuclear ribonucleoproteins C1/C2 (*HNRNPC*), stathmin (*STMN1*), cytochrome c oxidase subunit 6B1 (*COX6B1*), vesicle amine transport protein 1 (*VAT1*), were shown in regulating cancer cell proliferation and migration (**Table 5.1**). Tumour suppressor protein S100A2 (*S100A2*) is down-regulated under zinc exposure. The overexpressed proteoforms, including actinin α1 isoform (*ACTN1*), annexin A5 (*ANXA5*), cathepsin D (*CTSD*), F-actin-capping protein subunit β (*CAPZB*), inorganic pyrophosphatase (*PPA1*), tubulin α1c chain (*TUBA1C*), show their roles in cellular structure, growth or cancer cell invasion. Stress protein, heat shock 70 kDa protein 1A (*HSPA1A*) is overexpressed under zinc exposure. The classification of those 25 proteoforms (**Table 5.1**) based on molecular function revealed 35% catalytic, 13% metal ion binding and

11% molecular chaperone obtained from literature review and Uniprot (**Figure 5.5A**). PANTHER-based classification showed remarkably 29% catalytic enzyme and 21% cytoskeletal (**Figure 5.5B**). The identified proteoforms are found to be localised in cytoplasm (48%), nucleus (22%) and cytoskeletal (13%) (**Figure 5.5C**).

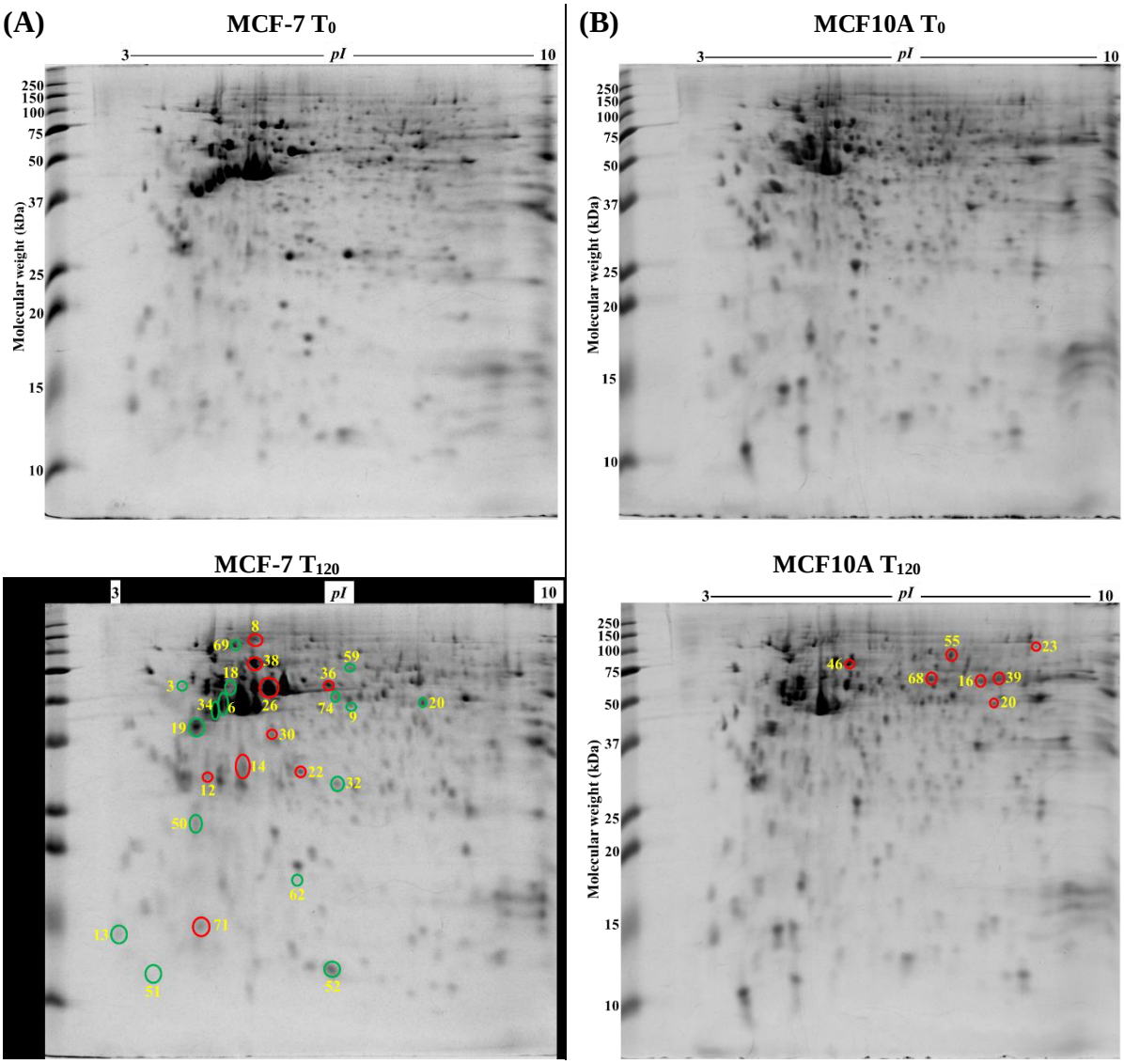

Figure 5.4 Differentially expressed protein spots in 2-DE gels by comparisons of MCF-7 T_{120} vs MCF-7 T_0 and MCF10A T_{120} vs MCF10A T_0. (A) Representative 2-DE gel images (in the left panel) of breast cancer MCF-7 cells without zinc (MCF-7 T_0) and with exogenous zinc exposure for 120 min (MCF-7 T_{120}). (B) Representative 2-DE gel images (in the right panel) of breast normal MCF10A cells without zinc (MCF10A T_0) and with exogenous zinc exposure for 120 min (MCF10A T_{120}). Each protein extract (100 µg) extract was resolved based on isoelectric point (*pI*) and molecular weight (MW). The differentially expressed protein spots are shown, with red circles denoting up-regulation and green circles down-regulation.

(A) Molecular function

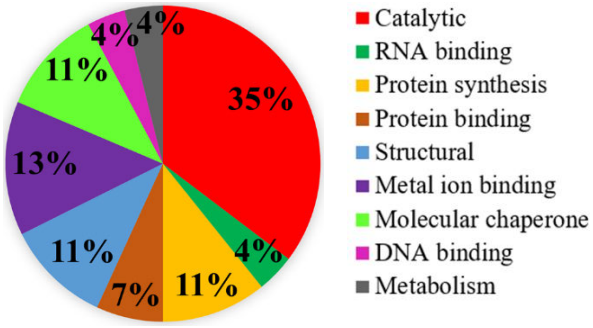

(B) Protein class

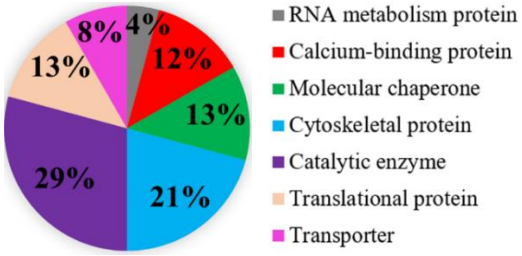

(C) Subcellular localisation

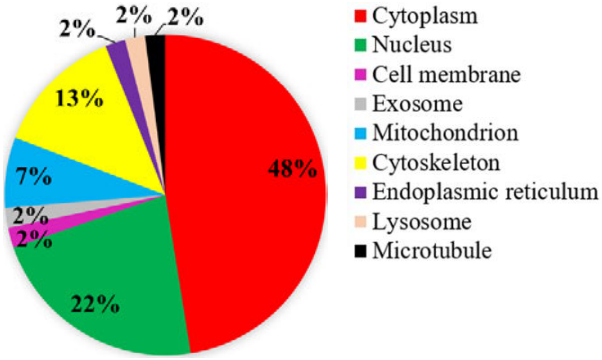

Figure 5.5 Functional classifications of the identified proteoforms in MCF-7 breast cancer cells with exogenous zinc exposure for 120 min (T_{120}) compared to without zinc exposure (T_0). The pie charts demonstrate the distributions of the identified proteoforms in MCF-7 cells based on (A) Molecular functions (based on literature survey and UniProt database) (B) Protein classes (categorized using PANTHER database) and (C) Subcellular localisations (based on literature review and UniProt database).

5.2.4 Differentially expressed proteoforms in MCF10A breast normal epithelial cells with exogenous zinc exposure compared to MCF10A cells without zinc exposure

MCF10A normal breast epithelial cells showed overexpression of 7 protein spot, red circle in **Figure 5.4B** under exogenous zinc exposure for 120 min (T_{120}) compared to without zinc exposure (T_0). D-3-phosphoglycerate dehydrogenase (*PHGDH*), elongation factor Tu (*TUFM*), ATP-dependent RNA helicase DDX1 (*DDX1*), inosine-5'-monophosphate dehydrogenase (*IMPDH*), plastin-3 (*PLS3*), radixin (*RDX*) and torsin-1A-interacting protein 1 (*TOR1AIP1*) were reported to show catalytic activity for cell metabolism and cell proliferation (**Table 5.1**). The classification all of these proteoforms were grouped according to molecular function (**Figure 5.6A**), protein class (**Figure 5.6B**) and subcellular localisation (**Figure 5.6C**) as follows.

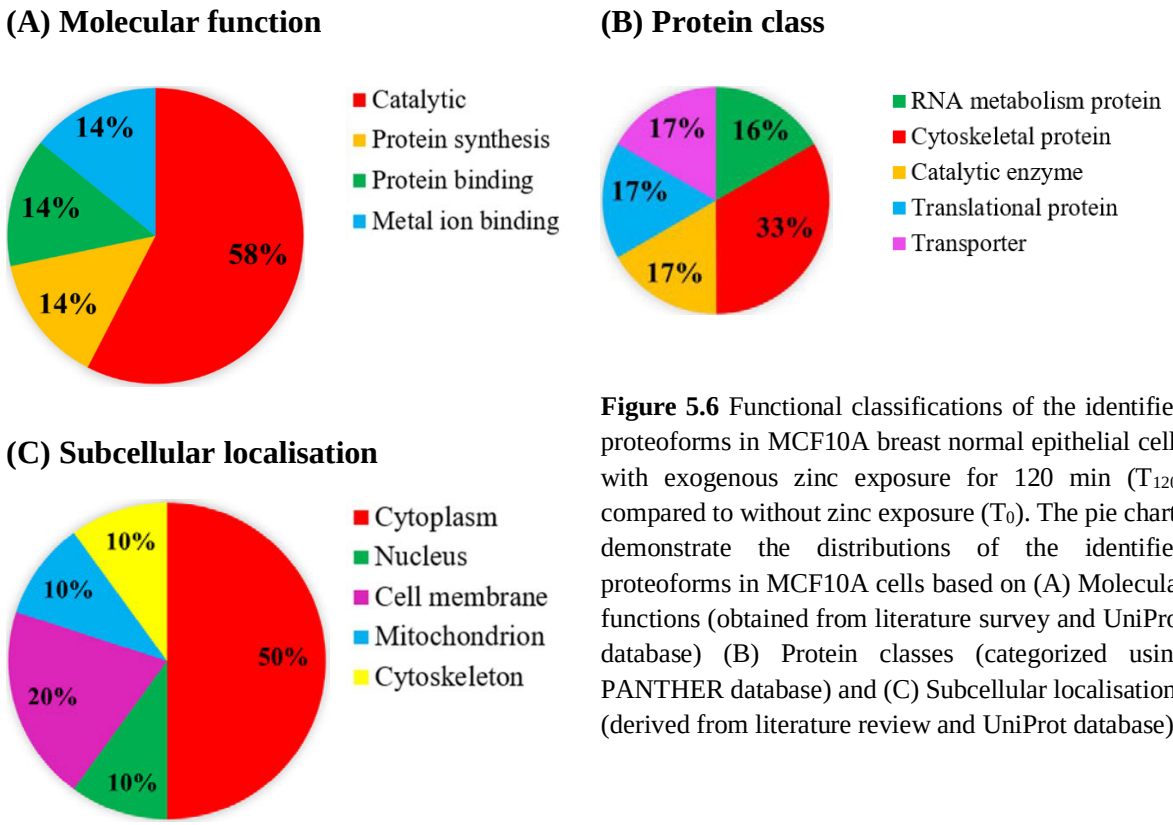

Figure 5.6 Functional classifications of the identified proteoforms in MCF10A breast normal epithelial cells with exogenous zinc exposure for 120 min (T_{120}) compared to without zinc exposure (T_0). The pie charts demonstrate the distributions of the identified proteoforms in MCF10A cells based on (A) Molecular functions (obtained from literature survey and UniProt database) (B) Protein classes (categorized using PANTHER database) and (C) Subcellular localisations (derived from literature review and UniProt database).

5.2.5 Differentially expressed proteoforms in PC3 prostate cancer cells against RWPE-1 normal prostate epithelial cells without exogeneous zinc exposure

PC3 prostate cancer cells showed 30 down-regulated (green circle) and 14 up-regulated (red circle) (**Figure 5.7A**) protein spots compared to RWPE-1 prostate normal epithelial cells without zinc exposure (T_0). Tumour suppressor proteins, such as 14-3-3 protein σ (*SFN*), latexin (*LXN*), glutathione S-transferase P (*GSTP1*), ρ GDP-dissociation inhibitor 1 (*ARHGDIA*), serpin B5 (*SERPINB5*), glycine tRNA ligase (*GARS1*), were reduced in PC3 cells compared to RWPE-1 at T_0 (**Table 5.2**). Calcium-binding proteins annexin A1 (*ANXA1*) and annexin A5 (*ANXA5*) were reduced at T_0. The identified proteoforms, including ATP synthase subunit α mitochondrial (*ATP5F1A*), ATP-dependent RNA helicase DDX39A (*DDX39A*), RNA helicase (*DDX48*), dihydrolipoamide S-succinyltransferase (*DLST*), exosome complex component MTR3 (*EXOSC6*), T-complex protein 1 subunit α (*TCP1*), ubiquitin carboxyl-terminal hydrolase (*USP14*), were also down-regulated in PC3 cell compared to RWPE-1 cell at T_0. The up-regulated proteoforms, such as protein S100A6 (*S100A6*), aldehyde dehydrogenase 1 family member A3 isoform (*ALDH1A3*), 26S proteasome non-ATPase regulatory subunit 11 (*PSMD11*), elongation factor 1 δ (*EEF1D*), 60 kDa heat shock protein mitochondrial (*HSPD1*), heat shock protein 90 kDa α (cytosolic) class B member 1 isoform

(*HSP90AB1*), heat shock protein β 1 (*HSPB1*), L-lactate dehydrogenase B chain (*LDHB*), peroxiredoxin 6 (*PRDX6*), proteasome subunit α type 1 (*PSMA1*), superoxide dismutase (Cu-Zn) (*SOD1*), acetyltransferase component of pyruvate dehydrogenase complex (*DLAT*), were reported to be involved in cancer cell proliferation, growth and invasions (**Table 5.2**).

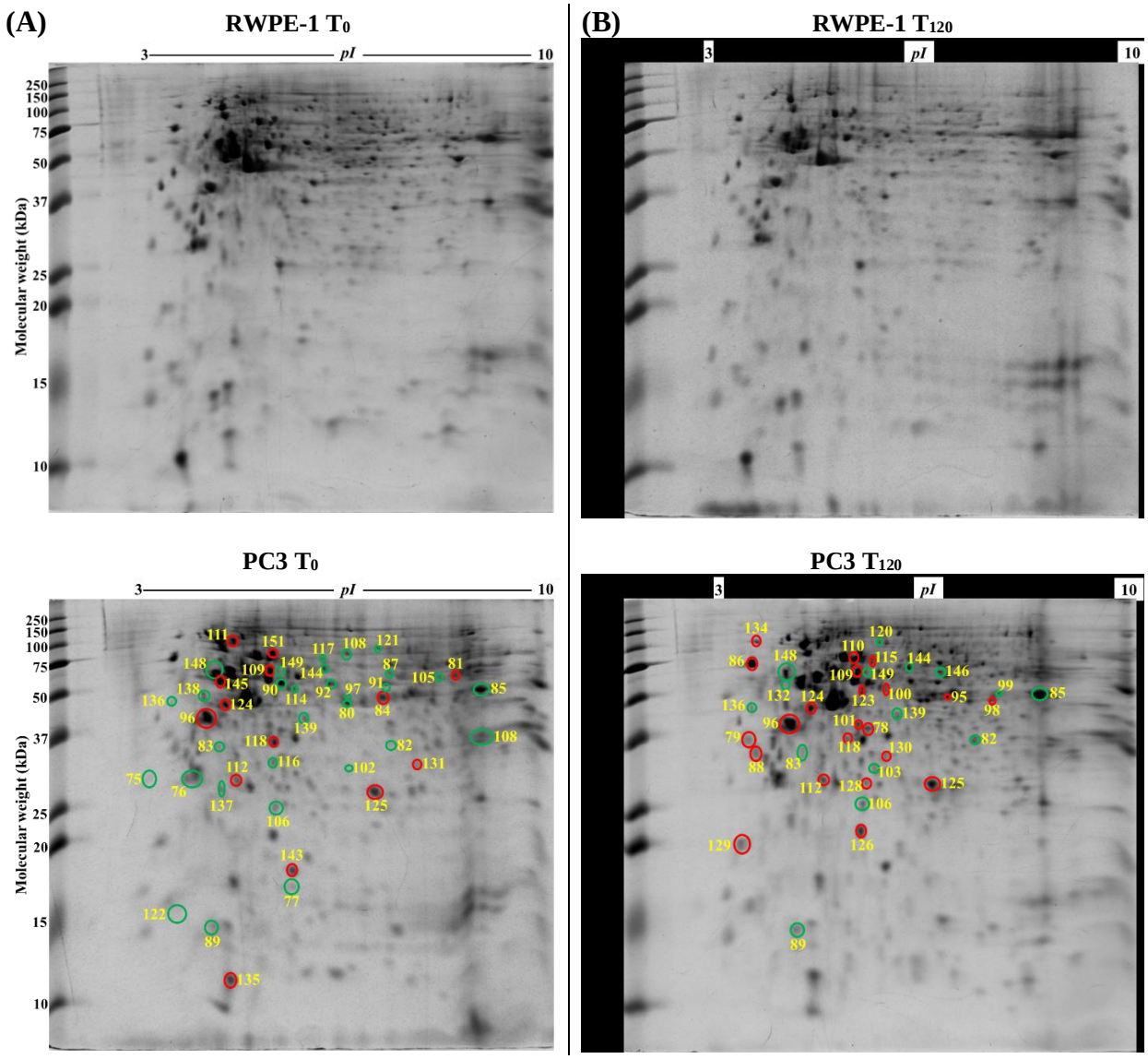

Figure 5.7 Differentially expressed protein spots in 2-DE gels by comparisons of PC3 T_0 vs RWPE-1 T_0 and PC3 T_{120} vs RWPE-1 T_{120}. (A) Representative 2-DE gel images (in the left panel) of prostate normal RWPE-1 cells without zinc exposure (RWPE-1 T_0) and prostate cancer PC3 cells without zinc exposure (PC3 T_0). (B) Representative 2-DE gel images (in the right panel) of prostate normal RWPE-1 cells with exogenous zinc exposure for 120 min (RWPE-1 T_{120}) and prostate cancer PC3 cells with exogenous zinc exposure for 120 min (PC3 T_{120}). Each protein extract (100 μg) was resolved based on isoelectric point (*pI*) and molecular weight (MW). The differentially expressed protein spots are shown, with red circles denoting up-regulation and green circles down-regulation.

Table 5.2 Identified proteoforms in prostate cancer cells (PC3) and normal prostate epithelial cells (RWPE-1) with or without exogenous zinc exposure

Spot ID	Identified proteoforms	Gene ID	Protein accession	Theoretical MW (kDa)/*pI*	Observed MW (kDa)/*pI*	PLGS score	Matched peptides	Sequence coverage (%)	(Fold change/ *p* value)				Molecular functions
									PC3 T_0/ RWPE-1 T_0	PC3 T_{120}/ RWPE-1 T_{120}	PC3 T_{120}/ PC3 T_0	RWPE-1 T_{120}/ RWPE-1 T_0	
75	14-3-3 protein σ	*SFN*	P31947	27.8/4.5	27.3/3.8	932	3	6	(0.36/ 0.001) ↓				I
76	14-3-3 protein θ	*YWHAQ*	P27348	27.8/4.5	27.3/4.7	15878	15	40	(0.44/ 0.003) ↓		(1.49/ 0.0009) ↑		II
77	40S ribosomal protein S18	*RPS18*	P62269	17.7/11.4	17.5/5.7	2004	6	38	(0.49/ 0.03) ↓			(0.32/ 0.02) ↓	III, IV
78	Transaldolase	*TALDO1*	A0A140VK56	37.5/6.4	39.1/5.6	423	11	18		(1.67/ 0.01) ↑			V
79	60S acidic ribosomal protein P0	*RPLP1*	A0A024RBS2	34.3/5.6	42.3/4.1	208	3	7		(1.39/ 0.01) ↑	(1.45/ 0.006) ↑		VI
80	Adenosylhomocysteinase	*AHCY*	A0A384MTQ3	47.7/5.9	50.9/5.9	657	20	22	(0.51/ 0.005) ↓				V
81	Aldehyde dehydrogenase 1 family member A3 isoform CRA a	*ALDH1A3*	A0A024RC95	56.1/7	74.4/7.7	3883	39	30	(1.35/ 0.02) ↑				V
82	Annexin A1	*ANXA1*	P04083	38.7/6.6	42.6/6.6	24829	27	55	(0.17/ 0.02) ↓	(0.26/ 0.04) ↓			VII
83	Annexin A5	*ANXA5*	P08758	35.9/4.7	33.4/5.1	12361	20	50	(0.15/ 0.0008) ↓	(0.34/ 0.004) ↓			VII
84	26S proteasome non-ATPase regulatory subunit 11	*PSMD11*	O00231	47.4/6.1	53.9/6.7	1037	18	34	(3.97/ 0.0009) ↑		(0.29/ 0.004) ↓		V
85	ATP synthase subunit α mitochondrial	*ATP5F1A*	P25705	59.7/9.4	56.3/7.8	26896	25	45	(0.35/ 0.008) ↓	(0.65/ 0.04) ↓			III, V
86	Calreticulin	*CALR*	P27797	48.1/4.1	81.3/4.4	9707	32	70		(1.70/ 0.007) ↑			VIII
87	Chaperonin containing TCP1 subunit 6A (ζ 1) isoform CRA a	*CCT6A*	A0A024RDL1	58/6.2	78.0/6.2	1700	21	33	(0.70/ 0.02) ↓			(0.56/ 0.003) ↓	VIII

Table 5.2 (continued)

Spot ID	Identified proteoforms	Gene ID	Protein accession	Theoretical MW (kDa)/*pI*	Observed MW (kDa)/*pI*	PLGS score	Matched peptides	Sequence coverage (%)	(Fold change/ *p* value)				Molecular functions
									PC3 T_0/ RWPE-1 T_0	PC3 T_{120}/ RWPE-1 T_{120}	PC3 T_{120}/ PC3 T_0	RWPE-1 T_{120}/ RWPE-1 T_0	
88	Clathrin light chain A	*CLTA*	P09496	27/4.2	35.4/4.2	1196	8	14		(1.82/ 0.02) ↑			IV
89	Cytochrome c oxidase subunit 5A mitochondrial	*COX5A*	H3BRM5	7.8/5.7	14.2/5.0	1969	4	35	(0.60/ 0.01) ↓	(0.54/ 0.03) ↓			VII
90	ATP-dependent RNA helicase DDX39A	*DDX39A*	O00148	49.1/5.3	62.9/5.6	3285	8	14	(0.61/ 0.004) ↓				V
91	RNA helicase	*DDX48*	A0A024R8W0	46.8/6.3	58.3/6.2	4579	49	38	(0.52/ 0.02) ↓			(2.88/ 0.006) ↑	V
92	Dihydrolipoamide S-succinyltransferase (E2 component of 2-oxo-glutarate complex) isoform CRA a	*DLST*	A0A024R6C9	48.7/9.3	62.9/5.8	2675	12	18	(0.20/ 0.0003) ↓			(0.64/ 0.03) ↓	V
93	Dihydropyrimidinase-related protein 2	*DPYSL2*	A0A1C7CYX9	73.5/5.9	81.9/6.0	3385	19	29				(0.28/ 0.001) ↓	V
94	Dopamine receptor interacting protein 4	*DRIP4*	Q4W4Y1	96.0/6.1	158.9/6.1	5782	44	38				(0.27/ 0.004) ↓	II
95	S-adenosylmethionine synthase	*MAT2A*	B4DEX8	39.7/5.6	52.2/6.1	1183	16	27		(1.28/ 0.03) ↑			V
96	Elongation factor 1 δ	*EEF1D*	A0A087X1X7	69.2/6.8	40.1/5.0	26412	18	23	(1.61/ 0.03) ↑	(1.37/ 0.04) ↑	(1.22/ 0.03) ↑		VI
97	Elongation factor 1 γ	*EEF1G*	P26641	50.1/6.2	54.3/6.0	2159	10	18	(0.41/ 0.004) ↓				VI
98	Elongation factor Tu	*TUFM*	A0A384ME17	49.8/7.4	50.5/6.7	2726	51	33		(5.06/ 0.0004) ↑			VI
99	Ethanolamine-phosphate cytidylyltransferase	*PCYT2*	I3L1R7	41.4/7.0	54.3/7.2	803	9	23		(0.11/ 0.008) ↓			IX
100	Eukaryotic translation initiation factor 3 subunit E	*EIF3E*	B2R806	52.2/5.6	57.9/5.7	1850	11	21		(1.59/ 0.002) ↑			VI

Table 5.2 (continued)

Spot ID	Identified proteoforms	Gene ID	Protein accession	Theoretical MW (kDa)/*pI*	Observed MW (kDa)/*pI*	PLGS score	Matched peptides	Sequence coverage (%)	(Fold change/ *p* value)				Molecular functions
									PC3 T_0/ RWPE-1 T_0	PC3 T_{120}/ RWPE-1 T_{120}	PC3 T_{120}/ PC3 T_0	RWPE-1 T_{120}/ RWPE-1 T_0	
101	Eukaryotic translation initiation factor 3 subunit I	*EIF3I*	Q13347	36.5/5.3	40.1/5.6	1091	6	17		(3.41/ 0.0003) ↑			VI
102	Exosome complex component MTR3	*EXOSC6*	Q5RKV6	28.2/6.0	29.5/5.9	795	13	19	(0.30/ 0.001) ↓			(0.59/ 0.01) ↓	III
103	F-actin-capping protein subunit β	*CAPZB*	A0A384MR50	30.6/5.6	30.1/5.7	3939	12	27		(0.62/ 0.006) ↓			X
104	Glucose-6-phosphate 1-dehydrogenase	*G6PD*	A0A384NL00	59.2/6.4	71.2/7.1	8928	24	38				(5.47/ 0.01) ↑	IX
105	Glutamate dehydrogenase	*GLUD1*	B4DMF5	56.6/6.8	65.4/7.5	4823	19	37	(0.59/ 0.009) ↓				IX
106	Glutathione S-transferase P	*GSTP1*	P09211	23.3/5.3	24.6/5.6	21246	47	67	(0.25/ 0.006) ↓	(0.39/ 0.0002) ↓			V
107	Histone H4	*HIST1H4J*	B2R4R0	11.4/11.8	34.9/9.2	3206	8	62	(0.33/ 0.02) ↓			(1.49/ 0.03) ↑	IV
108	Glycine tRNA ligase	*GARS1*	A0A090N8G0	77.5/5.8	116.0/5.9	5889	112	41	(0.29/ 0.00001) ↓				V
109	60 kDa heat shock protein, mitochondrial	*HSPD1*	A0A024R3W0	61.0/5.6	70.7/5.6	16269	32	48	(1.53/ 0.02) ↑	(1.94/ 0.0005) ↑		(2.88/ 0.01) ↑	VIII
110	Heat shock 70 kDa protein 1B	*HSPA1B*	A0A0G2JIW1	70.1/5.3	90.2/5.6	10234	35	40		(1.52/ 0.02) ↑		(0.54/ 0.004) ↓	VIII
111	Heat shock protein 90kDa alpha (Cytosolic) class B member 1 isoform CRA a	*HSP90AB1*	A0A024RD80	83.2/4.8	123.6/5.3	10935	37	41	(1.77/ 0.002) ↑				VIII
112	Heat shock protein β 1	*HSPB1*	P04792	22.8/6.0	27.1/5.4	5134	9	42	(2.10/ 0.02) ↑	(2.15/ 0.02) ↑			VIII
113	Aspartate aminotransferase	*GOT1*	A0A140VK69	46.2/6.6	46.4/7.5	682	20	24				(0.40/ 0.004) ↓	V

Table 5.2 (continued)

Spot ID	Identified proteoforms	Gene ID	Protein accession	Theoretical MW (kDa)/*pI*	Observed MW (kDa)/*pI*	PLGS score	Matched peptides	Sequence coverage (%)	(Fold change/ *p* value)				Molecular functions
									PC3 T_0/ RWPE-1 T_0	PC3 T_{120}/ RWPE-1 T_{120}	PC3 T_{120}/ PC3 T_0	RWPE-1 T_{120}/ RWPE-1 T_0	
114	Histidine tRNA ligase, cytoplasmic	*HARS1*	B4DDD8	48.5/5.0	58.3/5.6	548	5	11	(0.57/ 0.03) ↓				V
115	Copine 1	*CPNE1*	B0QZ18	59.7/5.6	90.2/5.6	11670	27	26		(1.82/ 0.004) ↑			V
116	Latexin	*LXN*	Q9BS40	25.7/5.4	29.8/5.6	1946	19	23	(0.78/ 0.02) ↓				II
117	Leukotriene A (4) hydrolase	*LTA4H*	A0A140VK27	69.2/5.7	90.9/5.8	2315	27	24	(0.22/ 0.01) ↓				VII
118	L-lactate dehydrogenase B chain	*LDHB*	A0A5F9ZHM4	37.4/5.8	34.6/5.6	2746	8	23	(1.97/ 0.01) ↑	(2.23/ 0.0003) ↑		(0.71/ 0.03) ↓	V
119	L-lactate dehydrogenase	*LDHA*	A0A3B3IS95	30.7/6.1	45.0/5.7	3821	14	25				(1.89/ 0.02) ↑	V
120	MAD1 mitotic arrest deficient-like 1	*MAD1L1*	A4D218	91.7/8.1	134.2/4.8	738	23	26		(0.52/ 0.04) ↓			II
121	Moesin	*MSN*	P26038	67.8/6.0	102.0/6.1	3846	26	32	(0.66/ 0.004) ↓			(1.57/ 0.002) ↑	VIII
122	Myosin light polypeptide 6	*MYL6*	B7Z6Z4	26.7/4.8	14.1/4.7	5045	6	24	(0.30/ 0.006) ↓				VII
123	Protein NDRG1	*NDRG1*	A0A024R9I3	39.5/6.1	53.9/5.6	8387	11	27		(1.81/ 0.03) ↑			II
124	NSFL1 cofactor p47	*NSFL1C*	Q9UNZ2	40.6/4.8	47.4/5.2	11230	29	65	(4.96/ 0.0003) ↑	(2.41/ 0.004) ↑			VIII
125	Peroxiredoxin 6	*PRDX6*	A0A024R938	25.0/6.0	25.3/6.2	4671	45	52	(8.38/ 0.0007) ↑	(2.84/ 0.02) ↑	(0.22/ 0.03) ↓		V
126	Peroxiredoxin 2	*PRDX2*	P32119	21.9/5.6	20.9/5.6	4964	13	40		(2.44/ 0.0003) ↑			V
127	Plastin 3	*PLS3*	P13797	69.3/5.5	86.1/5.6	1149	12	17				(0.58/ 0.01) ↓	VII

Table 5.2 (continued)

Spot ID	Identified proteoforms	Gene ID	Protein accession	Theoretical MW (kDa)/*pI*	Observed MW (kDa)/*pI*	PLGS score	Matched peptides	Sequence coverage (%)	(Fold change/ *p* value)				Molecular functions
									PC3 T_0/ RWPE-1 T_0	PC3 T_{120}/ RWPE-1 T_{120}	PC3 T_{120}/ PC3 T_0	RWPE-1 T_{120}/ RWPE-1 T_0	
128	Prohibitin	*PHB*	A8K401	29.8/5.4	26.6/5.6	3671	17	55		(2.50/ 0.0001) ↑			XI
129	Prostaglandin E synthase 3	*PTGES3*	A0A087WYT3	19.1/4.2	19.8/4.1	339	11	14		(2.14/ 0.03) ↑			VIII
130	Proteasome (Prosome macropain) activator subunit 3 (PA28 γ Ki) isoform CRA a	*PSME3*	A0A024R203	30.9/6.3	31.7/5.7	3923	12	36		(1.66/ 0.04) ↑			I
131	Proteasome subunit α type 1	*PSMA1*	P25786	29.5/6.2	29.8/6.8	3657	10	35	(9.46/ 0.0005) ↑				III
132	Protein DDI1 homolog 2	*DDI2*	Q5TDH0	44.5/4.8	56.3/5.1	320	4	12		(0.22/ 0.007) ↓			V
133	Protein disulfide-isomerase	*P4HB*	A0A024R8S5	57.1/4.6	67.7/4.9	21868	53	66			(1.37/ 0.03) ↑		V
134	Protein kinase C substrate 80K-H isoform CRA a (Glucosidase 2 subunit beta)	*PRKCSH*	A0A024R7F1	59.3/4.1	133.2/4.5	2052	10	18		(2.13/ 0.01) ↑			V, VII
135	Protein S100A6	*S100A6*	P06703	10.2/5.2	12.1/5.3	3080	6	33	(1.57/ 0.039) ↑				VII
136	Protein SET	*SET*	Q01105	33.5/4.0	50.9/4.4	4249	14	33	(0.16/ 0.0002) ↓	(0.40/ 0.0001) ↓	(1.74/ 0.02) ↑	(0.68/ 0.004) ↑	VIII, XII
137	ρ GDP-dissociation inhibitor 1	*ARHGDIA*	P52565	23.2/4.8	25.5/5.1	4058	13	43	(0.59/ 0.006) ↓				V
138	40S ribosomal protein SA	*RPSA*	A0A024R2L6	32.8/4.6	52.2/5.0	8860	69	27	(0.54/ 0.0003) ↓		(1.54/ 0.006) ↑		IV
139	Serpin B5	*SERPINB5*	A0A024R2B6	42.1/4.9	42.6/5.7	14963	33	63	(0.30/ 0.002) ↓	(0.43/ 0.006) ↓			V

Table 5.2 (continued)

Spot ID	Identified proteoforms	Gene ID	Protein accession	Theoretical MW (kDa)/*pI*	Observed MW (kDa)/*pI*	PLGS score	Matched peptides	Sequence coverage (%)	(Fold change/ *p* value)				Molecular functions
									PC3 T_0/ RWPE-1 T_0	PC3 T_{120}/ RWPE-1 T_{120}	PC3 T_{120}/ PC3 T_0	RWPE-1 T_{120}/ RWPE-1 T_0	
140	Staphylococcal nuclease domain-containing protein	*SND1*	A0A140VK49	101.9/6.8	158.9/7.6	4962	70	48				(0.28/ 0.00009) ↓	V
141	Stathmin	*STMN1*	P16949	17.3/5.7	18.0/5.4	2472	9	45				(5.08/ 0.03) ↑	IV
142	Succinate dehydrogenase (ubiquinone) flavoprotein subunit mitochondrial	*SDHA*	A0A024QZ30	72.7/7.0	90.9/6.2	2908	15	20				(0.58/ 0.03) ↓	V
143	Superoxide dismutase (Cu-Zn)	*SOD1*	P00441	15.9/6.7	17.4/5.7	6360	3	18	(2.31/ 0.004) ↑				VIII
144	T-complex protein 1 subunit α	*TCP1*	P17987	60.3/5.7	74.4/5.8	4205	14	22	(0.59/ 0.025) ↓	(0.39/ 0.05) ↓		(4.57/ 0.02) ↑	VIII
145	Eukaryotic translation initiation factor 3 subunit F	*EIF3F*	B3KSH1	39.1/5.1	54.3/5.1	10070	7	25	(1.42/ 0.005) ↑				II
146	Torsin-1A-interacting protein 1	*TOR1AIP1*	A0A0A0MSK5	52.4/6.6	71.2/6.1	1483	14	33		(0.23/ 0.003) ↓			V
147	Tropomyosin 3 isoform 2	*TPM3*	A0A0S2Z4G8	28.7/4.5	32.4/4.9	12626	25	63			(1.48/ 0.002) ↑		X
148	Tubulin α 1A chain	*TUBA1A*	Q71U36	50.1/4.8	68.2/5.1	74078	20	49	(0.50/ 0.002) ↓	(0.59/ 0.007) ↓		(1.26/ 0.02) ↑	IV
149	Ubiquitin carboxyl-terminal hydrolase	*USP14*	A6NJA2	51.1/5.6	78.0/5.6	2543	4	8	(0.47/ 0.03) ↓	(0.45/ 0.003) ↓		(2.99/ 0.004) ↑	V
150	Zyxin	*ZYX*	Q15942	61.2/6.2	116.0/6.2	768	7	16				(0.55/ 0.02) ↓	VII

Table 5.2 (continued)

Spot ID	Identified proteoforms	Gene ID	Protein accession	Theoretical MW (kDa)/*pI*	Observed MW (kDa)/*pI*	PLGS score	Matched peptides	Sequence coverage (%)	(Fold change/ *p* value)				Molecular functions
									PC3 T_0/ RWPE-1 T_0	PC3 T_{120}/ RWPE-1 T_{120}	PC3 T_{120}/ PC3 T_0	RWPE-1 T_{120}/ RWPE-1 T_0	
151	Acetyltransferase component of pyruvate dehydrogenase complex	*DLAT*	B4DJX1	62.7/5.4	101.2/5.6	1844	24	17	(1.61/ 0.01) ↑				V

MW stands for molecular weight, kDa for kilo Dalton, *pI* for isoelectric point, PLGS for ProteinLynx Global Server, T_0 for 0 min or without zinc exposure (control), T_{120} for 120 min, symbol ↑ for up-regulation and ↓ for down-regulation, PC3 (prostate cancer cells), RWPE-1 (prostate normal epithelial cells). The PLGS score, protein accession, theoretical MW/*pI*, matched peptides and sequence coverage (%) were obtained using ProteinLynx Global Server (PLGS) software (version 3.0 Waters Corporation, USA) and the UniProt (*Homo sapiens*, human) database. Gene ID was derived from Uniprot database. The observed MW and *pI* were calculated according to the protein standards. The fold changes and *p* values were acquired from the quantitative analysis of the gel images (each group n = 3) by Delta2D software (version 4.0.8, DECODON Gmbh, Germany). PC3 T_0/RWPE-1 T_0 is the expression fold change of the proteins in PC3 cells compared to RWPE-1 cells without zinc exposure (T_0), PC3 T_{120}/RWPE-1 T_{120} is the expression fold change of the proteins in PC3 cells compared to RWPE-1 cells following the zinc exposure for 120 min (T_{120}), PC3 T_{120}/PC3 T_0 is the expression fold change of the proteins in PC3 cells following zinc exposure for T_{120} compared to T_0, RWPE-1 T_{120}/RWPE-1 T_0 is the expression fold change of the proteins in RWPE-1 cells following zinc exposure for T_{120} compared to T_0. Molecular functions: I-Apoptosis; II-Signalling; III-RNA binding; IV-Structural; V-Catalytic activity; VI-Protein synthesis; VII-Metal ion binding; VIII-Molecular chaperone; IX-Metabolism; X-Protein binding; XI-Transcription; XII-DNA Binding.

The classification based on molecular functions of 44 proteoforms showed three prominent groups catalytic (34%), molecular chaperone (19%) and metal ion binding (13%) (**Figure 5.8A**). Application of PANTHER database also categorised 44 proteoforms into different groups including 29% catalytic enzyme and 14% translational proteins (**Figure 5.8B**). The proteoforms apparently localise in cytoplasm (44%), nucleus (23%) and mitochondrion (12%) (**Figure 5.8C**).

(A) Molecular function

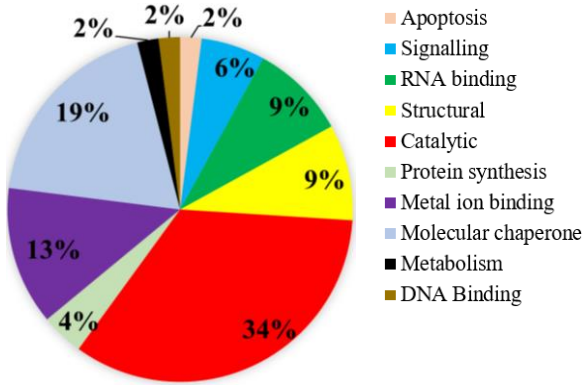

(B) Protein class

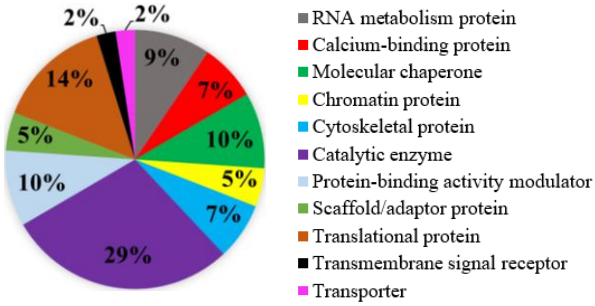

(C) Subcellular localisation

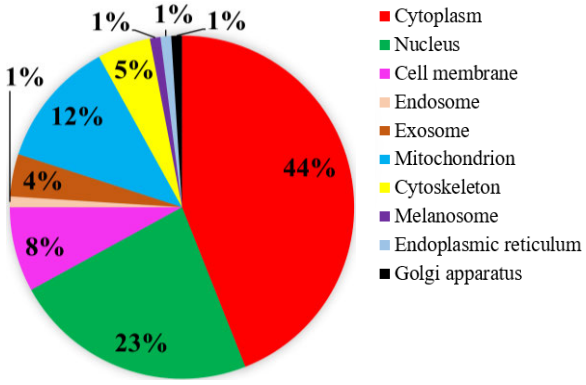

Figure 5.8 Functional classifications of the identified proteoforms in PC3 prostate cancer cells compared to RWPE-1 prostate normal epithelial cells without zinc exposure (T_0). The pie charts demonstrate the distributions of the identified proteoforms in PC3 cells compared to RWPE-1 cells without zinc exposure based on (A) Molecular functions (obtained from literature survey and UniProt database) (B) Protein classes (categorized using PANTHER database) and (C) Subcellular localisations (derived from literature review and UniProt database).

5.2.6 Differentially expressed proteoforms in PC3 prostate cancer cells compared to RWPE-1 normal prostate epithelial cells with exogeneous zinc exposure

Zinc exposure for 120 min (T_{120}) showed 15 down-regulated (green circle) and 22 up-regulated (red circle) protein spots in PC3 cells compared to RWPE-1 cells (**Figure 5.7B**). Calcium binding proteoforms annexin A1 (*ANXA1*) and annexin A5 (*ANXA5*) were suppressed and reported to be involved in tumorigenesis (**Table 5.2**). The suppressed proteoforms, including ATP synthase subunit α mitochondrial (*ATP5F1A*), cytochrome c oxidase subunit 5A mitochondrial (*COX5A*), ethanolamine-phosphate cytidylyltransferase (*PCYT2*), F-actin-capping protein subunit beta (*CAPZB*), glutathione S-transferase P (*GSTP1*), MAD1 mitotic arrest deficient-like 1 (*MAD1L1*), serpin B5 (*SERPINB5*), ubiquitin carboxyl-terminal hydrolase (*USP14*), and overexpressed proteoforms such as L-lactate dehydrogenase B chain (*LDHB*), prostaglandin E synthase 3 (*PTGES3*), protein kinase C substrate 80K-H isoform (*PRKCSH*), were reported to be involved in cell proliferation and apoptosis (**Table 5.2**). Tumour suppressor protein NDRG1 (*NDRG1*) and prohibitin (*PHB*) was increased in PC3 cells under zinc exposure. The overexpressed proteoforms, such as 60S acidic ribosomal protein P0 (*RPLP1*), calreticulin (*CALR*), elongation factor 1δ (*EEF1D*), elongation factor Tu (*TUFM*), eukaryotic translation initiation factor 3 subunit E (*EIF3E*), eukaryotic translation initiation factor 3 subunit I (*EIF3I*), were involved in translation (**Table 5.2**). Molecular chaperones including 60 kDa heat shock protein mitochondrial (*HSPD1*), heat shock 70 kDa protein 1B (*HSPA1B*), heat shock protein β1 (*HSPB1*) were overexpressed. Antioxidant proteins peroxiredoxin 6 (*PRDX6*) and peroxiredoxin 2 (*PRDX2*) were also up-regulated. The 37 proteoforms showed three key groups catalytic (32%), molecular chaperone (19%) and protein synthesis (12%) based on literature and Uniprot database (**Figure 5.9A**). PANTHER database-based protein classes agreed to molecular function categories since catalytic enzyme (34%), molecular chaperone (16%) and translation protein (16%) (**Figure 5.9B**). The identified proteoforms localise mainly in the cytoplasm (44%), nucleus (20%) and mitochondrion (11%) (**Figure 5.9C**).

(A) Molecular function

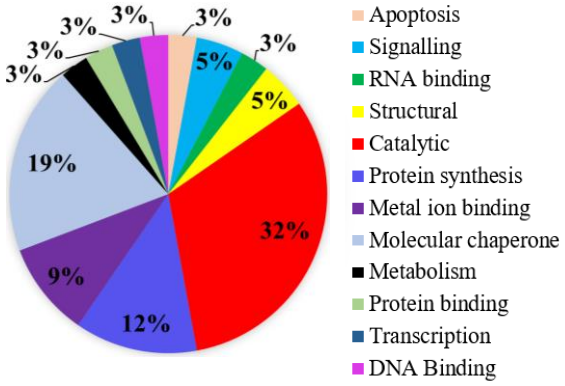

(B) Protein class

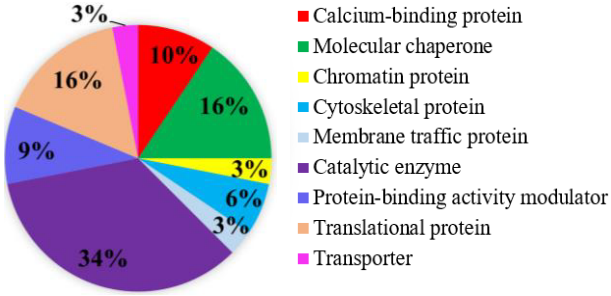

(C) Subcellular localisation

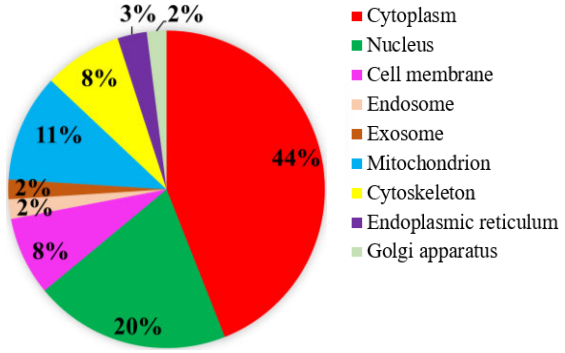

Figure 5.9 Functional classifications of the identified proteoforms in PC3 prostate cancer cells compared to RWPE-1 prostate normal epithelial cells under zinc exposure for 120 min (T_{120}). The pie charts demonstrate the distributions of the identified proteoforms in PC3 cells compared to RWPE-1 cells with zinc exposure based on (A) Molecular functions (obtained from literature survey and UniProt database) (B) Protein classes (categorized using PANTHER database) and (C) Subcellular localisations (derived from literature review and UniProt database).

5.2.7 Differentially expressed proteoforms in PC3 prostate cancer cells with exogenous zinc exposure compared to PC3 cells without zinc exposure

PC3 cells demonstrated 2 suppressed and 7 overexpressed protein spots under exogenous zinc exposure for 120 min (T_{120}) compared to PC3 cells without zinc exposure (T_0) (**Figure 5.10A**). Tumour suppressor 14-3-3 protein θ (*YWHAQ*) and translational proteins such as 60S acidic ribosomal protein P0 (*RPLP1*), elongation factor 1δ (*EEF1D*), 40S ribosomal protein SA (*RPSA*) were overexpressed (**Table 5.2**). Overexpressed tropomyosin 3 isoform 2 (*TPM3*) was involved in cancer progression and migration (**Table 5.2**). Protein disulfide-isomerase (*P4HB*) was also up-regulated which serves as molecular chaperone. Peroxiredoxin 6 (*PRDX6*) and 26S proteasome non-ATPase regulatory subunit 11 (*PSMD11*) were down-regulated under zinc exposure in PC3 cells. The 9 identified proteoforms showed two prominent molecular functional groups, catalytic (30%) and protein synthesis (20%) (**Figure 5.11A**). PANTHER database analysis showed 38% translational protein class (**Figure 5.11B**). The identified proteoforms localise predominantly in cytoplasm (50%), nucleus (25%) and endoplasmic reticulum (13%) (**Figure 5.11C**).

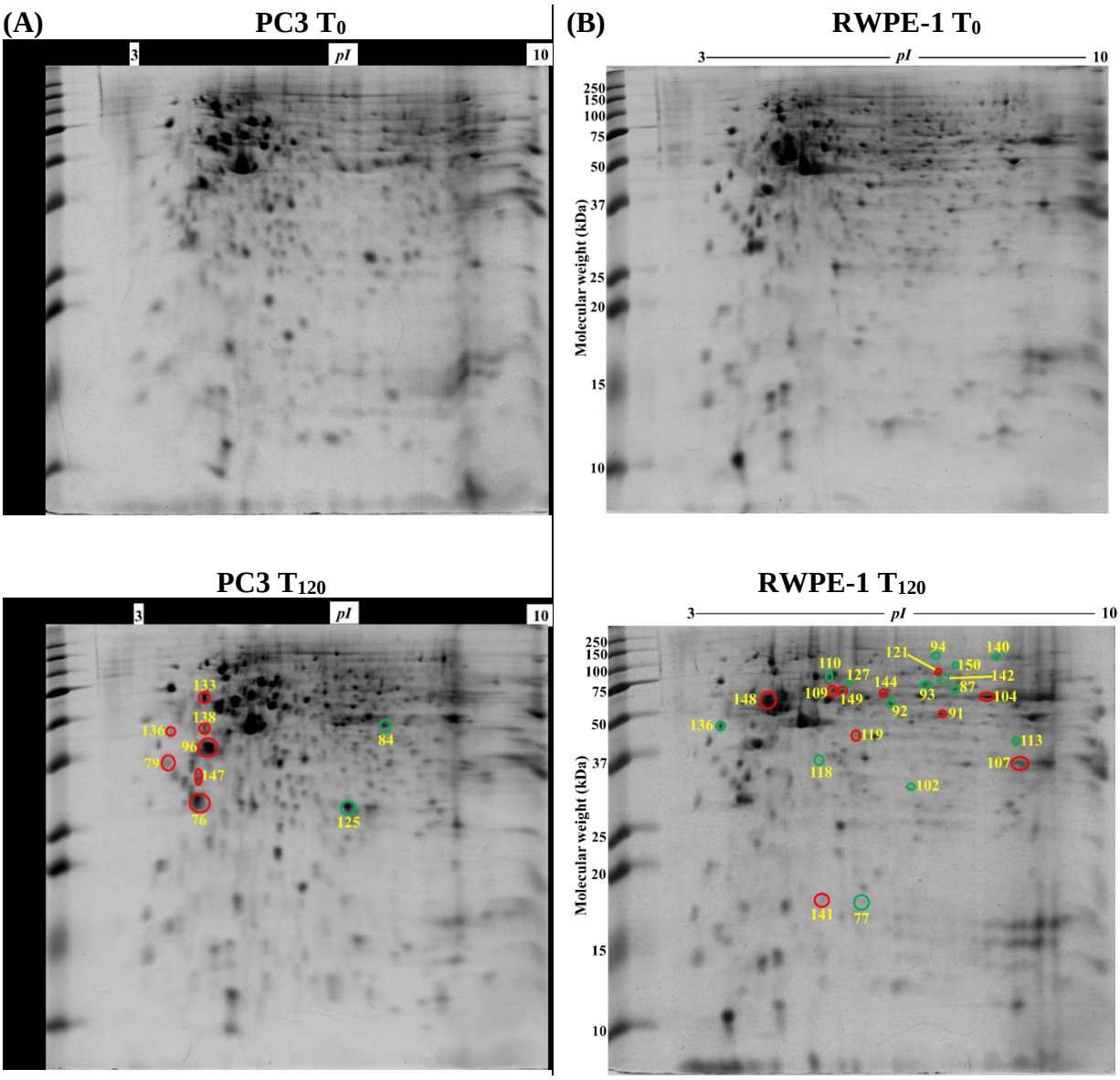

Figure 5.10 Differentially expressed protein spots in 2-DE gels by comparisons of PC3 T_{120} vs PC3 T_0 and RWPE-1 T_{120} vs RWPE-1 T_0. (A) Representative 2-DE gel images (in the left panel) of prostate cancer PC3 cells without zinc exposure (PC3 T_0) and with exogenous zinc exposure for 120 min (PC3 T_{120}). (B) Representative 2-DE gel images (in the right panel) of prostate normal RWPE-1 cells without zinc exposure (RWPE-1 T_0) and with exogenous zinc exposure for 120 min (RWPE-1 T_{120}). Each protein extract (100 µg) was resolved based on isoelectric point (*pI*) and molecular weight (MW). The differentially expressed protein spots are shown, with red circles denoting up-regulation and green circles down-regulation.

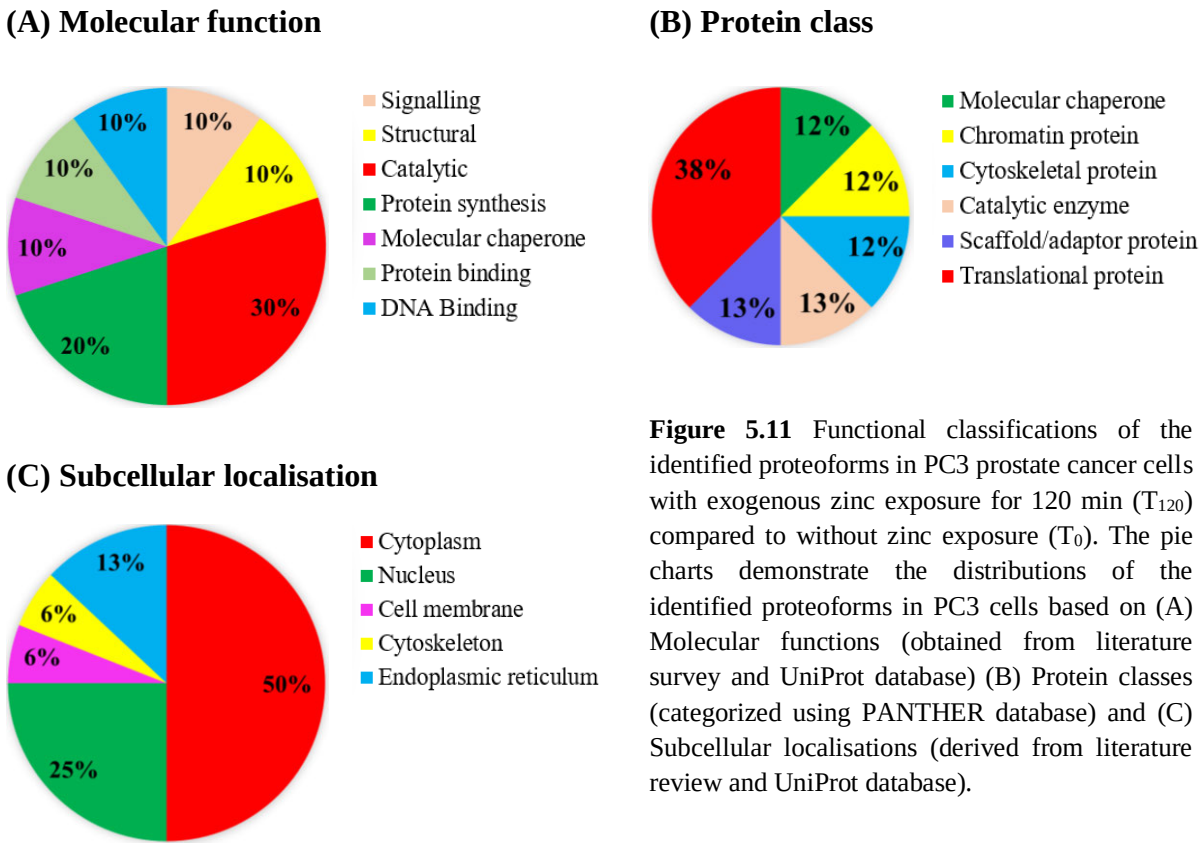

Figure 5.11 Functional classifications of the identified proteoforms in PC3 prostate cancer cells with exogenous zinc exposure for 120 min (T_{120}) compared to without zinc exposure (T_0). The pie charts demonstrate the distributions of the identified proteoforms in PC3 cells based on (A) Molecular functions (obtained from literature survey and UniProt database) (B) Protein classes (categorized using PANTHER database) and (C) Subcellular localisations (derived from literature review and UniProt database).

5.2.8 Differentially expressed proteoforms in RWPE-1 prostate normal epithelial cells with exogenous zinc exposure compared to RWPE-1 cells without zinc exposure

In RWPE-1 cell, 14 suppressed (green circle) and 10 overexpressed (red circle) protein spots were identified following exogenous zinc exposure for 120 min (T_{120}) compared to RWPE-1 cells without zinc exposure (T_0) (**Figure 5.10B**). The reduced proteoforms, such as chaperonin containing TCP1 subunit 6A (*CCT6A*), dihydropyrimidinase-related protein 2 (*DPYSL2*), dihydrolipoamide S-succinyltransferase (*DLST*), succinate dehydrogenase (ubiquinone) flavoprotein subunit mitochondrial (*SDHA*), aspartate aminotransferase (*GOT1*), L-lactate dehydrogenase B chain (*LDHB*), are involved in cellular metabolism and proliferation (**Table 5.2**). Up-regulated proteoforms, such as glucose-6-phosphate 1-dehydrogenase (*G6PD*), histone H4 (*HIST1H4J*), tubulin α1A chain (*TUBA1A*), L-lactate dehydrogenase (*LDHA*), stathmin (*STMN1*), ubiquitin carboxyl-terminal hydrolase (*USP14*), were also reported in metabolism as well as cell growth. The proteoforms involved in protein folding such as 60 kDa heat shock protein mitochondrial (*HSPD1*), T-complex protein 1 subunit α (*TCP1*) were overexpressed under zinc exposure. Based on molecular functions, 24 proteoforms were categorised into different groups including catalytic (34%) and molecular chaperone (23%)

(**Figure 5.12A**). Catalytic enzyme (38%) was the prominent protein class according to PANTHER database analysis (**Figure 5.12B**). The majority proteoforms localise in the cytoplasm (48%) and nucleus (22%) (**Figure 5.12C**).

(A) Molecular function

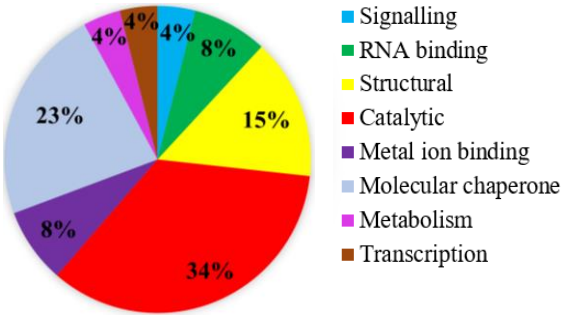

(B) Protein class

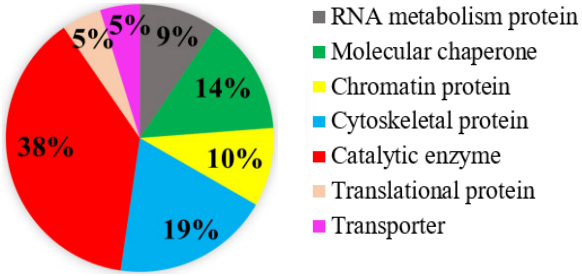

(C) Subcellular localisation

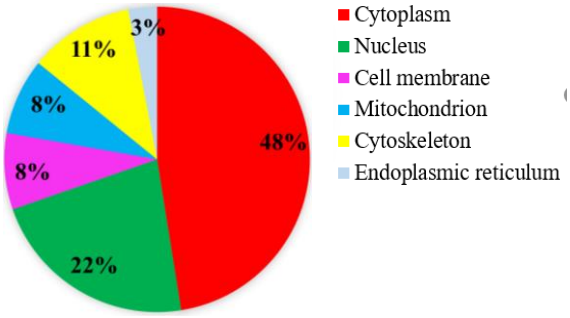

Figure 5.12 Functional classifications of the identified proteoforms in RWPE-1 prostate normal epithelial cells with exogenous zinc exposure for 120 min (T_{120}) compared to without zinc exposure (T_0). The pie charts demonstrate the distributions of the identified proteoforms in RWPE-1 cells based on (A) Molecular functions (obtained from literature survey and UniProt database) (B) Protein classes (categorized using PANTHER database) and (C) Subcellular localisations (derived from literature review and UniProt database).

5.3 Discussion

Zinc dyshomeostasis is the hallmark of breast and prostate cancer cells. Numerous studies have focused on the zinc homeostasis of breast cancer cells or prostate cancer cells, although the current work in this PhD project is the first to investigate these two kinds of cancer cells together in tandem. Furthermore, I examined the total proteomic profiles of breast cancer cells *versus* normal breast epithelial cells, prostate cancer cells *versus* normal prostate epithelial cells, in the presence or absence of extracellular zinc treatment. The differentially expressed proteoforms with or without zinc exposure in breast cells (MCF-7, MCF10A) (**Table 5.1**) and prostate cells (PC3, RWPE-1) (**Table 5.2**) in this study are the key datasets, which enriches our knowledge and enhances the understanding of the zinc homeostasis in both breast and prostate cancer cells.

5.3.1 The intrinsic differences between the cancer cells and their normal counterparts (without extracellular zinc exposure)

This study firstly obtained the dataset without extracellular zinc treatment which demonstrates the intrinsic differences between breast cancer cells MCF-7 and the normal breast epithelial cells MCF10A, as well as between prostate cancer cells PC3 and the normal counterpart RWPE-1 cells. The proteomic results demonstrate a key feature of breast and prostate cancer cells, namely, the down-regulation of tumour suppressors or anti-tumour proteins.

Firstly, the results showed the reduction of tumour suppressor 14-3-3 protein σ and θ in MCF-7 and PC3 cancer cells compared to the normal counterparts (**Tables 5.1** and **5.2**), which is in agreement with the previous findings (Li et al., 2009; Young et al., 2015). The 14-3-3 proteins include seven isoforms such as σ and θ are associated with cell cycle, signalling and apoptosis, they are usually down-regulated for cancer progression. The tumour suppressor protein S100A2 was decreased in MCF-7 cells (**Table 5.1**) as previously reported (Koch et al., 2007; Buckley et al., 2014). However, the expression of S100A2 was unchanged in PC3 cells (**Table 5.2**), which is consistent with the previous study (Kwon et al., 2010). Anti-tumour proteins such as latexin, glutathione S-transferase P, ρ GDP-dissociation inhibitor 1, serpin B5 were reduced in their expression in PC3 prostate cancer cells (**Table 5.2**), in agreement with the previous studies (Zhu et al., 2012; Chang et al., 2018; Gurioli et al., 2018; Seed et al., 2019). Annexin A1 was found to be down-regulated in MCF-7 and PC3 cancer cells (**Tables 5.1** and **5.2)**, which is related to breast and prostate cancer development (Shen et al., 2006; Deng et al., 2013; Bizzarro et al., 2017; Ganesan et al., 2020). A novel anti-tumour protein, glycine tRNA ligase (Khaghanzadeh et al., 2016), was found to be down-regulated in PC3 prostate cancer cells, but its role in cancer development is unknown.

The proteomic results demonstrate another feature of breast and prostate cancer cells, that is, the up-regulation of proteins related to cancer growth and metastasis. α-smooth muscle actin (α-SMA) and tumour protein D53 (hD53) were overexpressed in MCF-7 cells (**Table 5.1**). α-SMA serves as the marker of epithelial-to-mesenchymal transition (EMT) for cancer metastasis (Kim et al., 2019; Muchlińska et al., 2022) and hD53 promotes breast cancer cell proliferation and their expressions are correlated (Kim et al., 2019). High expression of F-actin-capping protein subunit β (*CAPZB*) in the breast cancer cells (**Table 5.1**) is linked with α-SMA in regulating breast cancer cell growth and motility (Mukaihara et al., 2016; Mukherjee et al.,

2016). Over-expression of antioxidants in cancer cells should enhance the cancer cell proliferation, hence cancer growth in cancer patients. Peroxiredoxin 6, an antioxidant protein, promotes cancer cell proliferation in an oxidative stress environment (Basu et al., 2007; Chang et al., 2007). Thus, markedly overexpressed peroxiredoxin 6 in MCF-7 cancer cells (1.68-fold, **Table 5.1**) and PC3 cancer cells (8.38-fold, **Table 5.2**) indicates its role in breast and prostate cancer development. This finding also suggests that peroxiredoxin 6 (*PRDX6*) is a potential target for anti-cancer drug development. Glutathione S-transferase Mu 3 (*GSTM3*) is another antioxidant overexpressed in MCF-7 breast cancer cells (**Table 5.1**), while superoxide dismutase (*SOD1*) was overexpressed in PC3 prostate cancer cells (**Table 5.2**). D-3-phosphoglycerate dehydrogenase, a metabolic enzyme, is involved in redox homeostasis (Zhao et al., 2020). Its overexpression in MCF-7 breast cancer cells (**Table 5.1**) indicates that this enzyme is associated with breast cancer development.

In addition, the results in **Tables 5.1** and **5.2** demonstrate the overexpression of the proteins related to cancer cell growth, invasion and metastasis, including heat shock protein β1 (Zoubeidi and Gleave, 2012; Cyran and Zhitkovich, 2022), 60 kDa heat shock protein (Guyon et al., 2009), heterogeneous nuclear ribonucleoproteins C1/C2 (Park et al., 2012), histone H4 (Fraga et al., 2005), nucleoside diphosphate kinase, protein S100A13, (Miao et al., 2018), radixin (Yuan et al., 2020), and triosephosphate isomerase (Jin et al., 2022). Metabolic proteoforms including aldehyde dehydrogenase 1 family member A3, L-lactate dehydrogenase B chain, cytochrome b5 type B and elongation factor Tu, elongation factor 1δ were overexpressed in the breast cancer cells (**Table 5.1**) and prostate cancer cells (**Table 5.2**). Their overexpression is related to proliferation of the cancer cells. Intriguingly, dihydrolipoamide S-succinyltransferase (E2 component of 2-oxo-glutarate complex) (*DLST*), a metabolic enzyme of Kerbs cycle (Anderson et al., 2021), was up-regulated in MCF-7 breast cancer cells (**Table 5.1**), but down-regulated in PC3 prostate cancer cells (**Table 5.2**). The underlying reason for such opposite expression profiles of this enzyme is unknown.

5.3.2 The dynamic expression of proteins in breast and prostate cancer cells in response to extracellular zinc exposure

The proteomic datasets were obtained by the comparison between breast cancer cells MCF-7 and the normal breast epithelial cells MCF10A in response to extracellular zinc exposure, as well as the comparison between prostate cancer cells PC3 and the normal counterpart RWPE-1 cells in response to extracellular zinc exposure. The datasets demonstrate that the cancer cells up-regulated the proteins which are related to lysosomal activity, antioxidant activity, stress response, cancer growth, cellular structure and metabolism.

MCF-7 breast cancer cells showed overexpression of cathepsin D in response to zinc exposure (**Table 5.1**). Cathepsin D is an aspartic endoproteinase in lysosome, and is well-known for its roles in angiogenesis, proliferation, invasion in breast cancer (Kang et al., 2020; Seo et al., 2022). The extracellular zinc exposure should lead to the elevation of cytoplasmic zinc in MCF-7 cells, which might in turn result in higher zinc level in lysosome and hence cathepsin D up-regulation, because zinc enhances cathepsin D activity in lysosome (Kim et al., 2022).

The extracellular zinc exposure resulted in overexpression of the antioxidant protein, peroxiredoxin 6, in both breast and prostate cancer cells (**Tables 5.1** and **5.2**), demonstrating that this protein is not only related to cancer development, but also associated with the stress response incurred by the zinc exposure. The overexpression of peroxiredoxin 2 in PC3 prostate cancer cells upon zinc exposure (**Table 5.2**) is likely due to the same reason. Antioxidant proteins, including glutathione S-transferase Mu 3 and mitochondrial NADH dehydrogenase (ubiquinone) iron-sulfur protein 3, were overexpressed in breast cancer cells (**Table 5.1**). A previous study showed that glutathione S-transferase Mu 3 expression has a positive relationship with zinc (Kudo et al., 2000). The molecular chaperones such as mitochondrial 60 kDa heat shock protein, heat shock 70 kDa protein 1B and heat shock protein β1 were overexpressed in PC3 cancer cells upon zinc exposure (**Table 5.2**), which is likely a part of stress response for the prostate cancer cells.

Zinc enhances breast cancer growth. This is evidently supported by the increased intracellular zinc level in breast cancer cells compared to the normal breast epithelial cells (Taylor et al., 2012; Franz et al., 2013; Nimmanon et al., 2017). The proteomic dataset showed the elevated expression of tumour protein D53 (hD53 encoded by *TPD52L1*) and tumour protein D54 (hD54 encoded by *TPD52L2*) of MCF-7 breast cancer cells in response to extracellular zinc exposure (**Table 5.1**), which explains to some extent why zinc promotes breast cancer growth. This finding also suggests hD53 and hD54 are potential targets for anti-cancer drug development against breast cancers.

Intriguingly, extracellular zinc exposure resulted in overexpression of prohibitin (*PHB*) in prostate cancer cells (PC3) (**Table 5.2**). Prohibitin can act as a tumour suppressor in prostate cancers (Najm et al., 2021). As is known, the intracellular zinc level in prostate cancer cells is lower than the normal counterparts (Franz et al., 2013; Sauer et al., 2020). The extracellular zinc exposure should lead to the increased level of zinc inside the PC3 cancer cells, which is detrimental to the prostate cancer cells. The overexpression of prohibitin might partly explain the cytotoxicity of excess of zinc for the prostate cancer cells. The reduction of metabolic enzymes including D-3-phosphoglycerate dehydrogenase, adenylosuccinate lyase, inosine-5'-monophosphate dehydrogenase, L-lactate dehydrogenase B chain and translational elongation factor Tu under zinc exposure at T_{120} is relevant to decrease cell viability in MCF-7 breast cancer cells as described previously (**Chapter 3**, **Figure 3.1A**) (Barman et al., 2022).

Further proteomic analysis was also done by comparing breast cancer cells MCF-7 with and without zinc treatment, as well as comparing the prostate cancer cells PC3 with and without zinc treatment. Firstly, MCF-7 breast cancer cells exhibited 25 differentially expressed proteins (**Table 5.1**) under zinc exposure at T_{120} compared to without zinc exposure (T_0), whilst PC3 prostate cancer cells showed 9 differentially expressed proteins (**Table 5.2**). This very fact demonstrates that breast cancer cells are more capable responsers to the variation of zinc levels. Their molecular network of zinc homeostasis might be more sophisticated than the one in prostate cancer cells.

The findings demonstrate that zinc up-regulates the proteins related to breast cancer growth and metastasis. Zinc exposure up-regulated actinin α1 and annexin A5 in MCF-7 cells (**Table 5.1**). The cytokinetic protein actinin α1 is shown to promote tumorigenesis and epithelial-to-mesenchymal transition (EMT) in cancer via AKT/GSK3β/β catenin signalling pathways

(Zhang et al., 2021). Among 12 annexin A isoforms (annexin A1-11 and annexin A13), annexin A5 in particular has unphosphorylated short N-terminus which enables this protein to exhibit a wide range of functions such as signalling, cancer cell growth and invasion (Tang et al., 2017). The overexpression of both inorganic pyrophosphatase (*PPA1*) and tubulin α1c (*TUBA1C*) in response to exogenous zinc exposure in MCF-7 cells (**Table 5.1**) suggests that high intracellular zinc promotes the metabolic activity of breast cancer cells, because tubulin α1c promotes glycolysis as well as cell growth in breast cancer (Wu et al., 2022), and inorganic pyrophosphatase is involved in cell metabolism and is overexpressed in cancer tissues (Mishra et al., 2015; Wang et al., 2022). In addition, the dataset demonstrates that heat shock 70 kDa protein was overexpressed in MCF-7 cells (**Table 5.1**), correlating well with its overexpression at the gene level (Zaman et al., 2021).

5.3.3 Differences between theoretical and observed molecular weight/isoelectric point

Some proteins in **Tables 5.1** and **5.2** showed discrepancy in their theoretical and observed molecular weight/isoelectric point, likely due to post-translational modifications and dimerization. The dimerization might occur for ATP-dependent RNA helicase DDX1 (theoretical 73.9 kDa/7.6 vs experimentally observed 136.2 kDa/8.1) and radixin (68.5 kDa/6.0 vs 110.1 kDa/6.3) (**Table 5.1**). Dimerization for example protein kinase C substrate 80K-H isoform (59.3 kDa/4.1 vs 133.2 kDa/4.5) and trimerization for example histone H4 (11.4 kDa/11.8 vs 34.9 kDa/9.2) might be the result of down-regulation of chaperone proteoforms such as chaperonin containing TCP1 subunit 6A (ζ1) isoform, heat shock 70 kDa protein 1B, protein SET and T-complex protein 1 subunit α in prostate cells (**Table 5.2**). The discrepancies of MW/pI of the other identified proteoforms for example cathepsin D (43.7 kDa/6.1 vs 30.2 kDa/5.4), cytochrome b5 type B (16.3 kDa/4.7 vs 18.2 kDa/3.7), D-3-phosphoglycerate dehydrogenase (55.9 kDa/6.3 vs 69.2 kDa/6.7) (**Table 5.1**) were probably due to post-translational modifications or gel shifting (Sen et al., 2021; Almuslehi et al., 2022). The post-translational modifications might explain the discrepancy for annexin A1 (38.7 kDa/6.6 vs 42.6kDa/6.6), annexin A5 (35.9kDa/4.7 vs 33.4 kDa/5.1), L-lactate dehydrogenase (30.7 kDa/6.1 vs 45.0 kDa/5.7), and NSFL1 cofactor p47 (40.6 kDa/4.8 vs 47.4 kDa/5.2) (**Table 5.2**).

5.4 Conclusion

The systematic approach of high-resolution top-down proteomics was carried out simultaneously, for the first time, on the cancerous breast and prostate cells (MCF-7, PC3) and the normal breast and prostate cells (MCF10A, RWPE-1). The datasets revealed the intrinsic differences in the proteomes of cancer cells (MCF-7 and PC3) and their normal counterparts without zinc treatment, such as the down-regulation of anti-tumour proteins (14-3-3 protein σ, protein S100A2, latexin, annexin A1), and the up-regulation of tumour protein (hD53), anti-oxidants (peroxiredoxin 6, superoxide dismutase) and metabolic enzymes (dihydrolipoamide S-succinyltransferase, aldehyde dehydrogenase 1) in both breast and prostate cancer cells. The zinc-responsive proteomes were then unravelled by their dynamic expressions prodded by the extracellular zinc exposure. The increased expression of tumour proteins (hD53, hD54) in breast cancer cells under zinc treatment may explain the role of high intracellular zinc level in breast cancer development, while the overexpression of the tumour suppressor prohibitin (*PHB*) in prostate cancer cells (PC3) by the extracellular zinc exposure provides an explanation for the inhibitory effect of zinc in prostate cancer development. The up-regulation of antioxidants in both kinds of cancer cells by zinc exposure, such as peroxiredoxin 6, would benefit cancer cell growth in response to the change of environmental conditions, therefore, they could be potential targets for anti-cancer drug development. Overall, the findings here enhance our knowledge and understanding of the role of zinc in breast and prostate cancer cells.

Chapter 6 General discussion

Breast and prostate cancers are two disparate malignancies. However, the dysregulation of Zn^{2+} homeostasis is prominent in both kinds of cancer cells (Sauer et al., 2020; Wang et al., 2020; Rusch et al., 2021). They exhibit contrasting intracellular zinc profiles, i.e., the intracellular zinc level in breast cancer cells is markedly higher than the normal breast epithelial cells, whilst the intracellular zinc level in prostate cancer cells is much lower than the normal prostate epithelial cells (Sauer et al., 2020; Wang et al., 2020; Rusch et al., 2021). The molecular details related to the machinery of Zn^{2+} homeostasis in breast and prostate cancer cells are not fully known. The contrasting zinc profiles of breast and prostate cancer cells provide a convenient avenue for this PhD project to investigate the Zn^{2+} homeostasis of breast and prostate cancer cells. A systematic approach of gene profiling, immunofluorescence confocal microscopy and proteomic analysis was carried out here, as described in **Chapters 3**, **4** and **5**, using a panel of cell lines which include two breast cancer cell lines (MCF-7, MDA-MB-231), two prostate cancer cell lines (PC3 and DU145), along with normal breast epithelial and prostate epithelial cell lines (MCF10A, RWPE-1). The transcriptomic insights of zinc homeostasis-associated genes including 14 *SLC39A* (ZIP), 10 *SLC30A* (ZnT) and 4 *MT* (MT) genes were obtained in **Chapter 3**. The differentially expressed *SLC39A12*, *SLC30A1* and *MT2A* genes were further studied at the protein level, together with the subunits of protein kinase CK2 (CK2α/α' and CK2β), by immunofluorescence confocal microscopy. Their expression and localisation data were described in **Chapter 4**. Finally, the top-down proteomic approach was applied to the cancerous and normal breast cells (MCF-7, MCF10A), and the cancerous and normal prostate cells (PC3, RWPE-1). The proteomic datasets were described in **Chapter 5**. The findings of these three experimental chapters were discussed below in order to highlight and connect the key findings and provide insights into the Zn^{2+} homeostasis of breast and prostate cancers.

6.1 Molecular explanation for the intrinsic differences of intracellular Zn^{2+} levels in breast and prostate cancer cells

The findings of this study provide molecular details for understanding the contrasting intracellular zinc profiles observed in breast and prostate cancer cells, that is, breast cancer cells exhibit higher intracellular zinc level than normal breast epithelial cells (Chandler et al., 2016; Rusch et al., 2021), but prostate cancer cells show markedly reduced cellular zinc level compared to prostate normal epithelial cells (Dowarha et al., 2020; Sauer et al., 2020). Such

differential intracellular zinc levels in these two kinds of cancer cells can be explained by the differential expression of the genes and proteins associated with zinc homeostasis as described in **Chapters 3**, **4** and **5** (Barman et al., 2022). The up-regulation of zinc importer genes such as *SLC39A4*, *SLC39A6*, *SLC39A8* and *SLC39A11* in both breast and prostate cancer cells (**Chapter 3**, **Table 3.1**) suggests their common role in these two kinds of cancers. *SLC39A2* (ZIP2) was found to be intrinsically over-expressed in breast cancer cells only and was dynamically responsive to extracellular zinc level (**Chapter 3**, **Table 3.2**), suggesting that ZIP2 plays a role in the zinc homeostasis of breast cancer cells. The down-regulation of the zinc exporter genes such as *SLC30A1* (ZnT1), *SLC30A4* (ZnT4) and *SLC30A10* (ZnT10) may contribute to the elevated intracellular Zn^{2+} level in breast cancer cells. In particular, ZnT1 is the only zinc exporter predominantly located in plasma membrane (Nishito and Kambe, 2019) and is prominently involved in zinc efflux (Fong et al., 2018; Lehvy et al., 2019; Zaman et al., 2021). Its down-regulation of expression in breast cancer cells may render itself as a therapeutic target for anticancer drug development by aiming to up-regulate its expression in breast cancer cells.

The significant down-regulation of the zinc importer *SLC39A1* (ZIP1) gene expression in prostate cancer cells, and the up-regulation of the zinc exporter *SLC30A1* (ZnT1) gene expression provide explanation to the decreased intracellular zinc level of prostate cancer cells compared to the normal counterparts. The gene expression of *SLC39A2* (ZIP2) was also markedly reduced in PC3 prostate cancer cells (**Chapter 3**, **Table 3.1**), which indicates that ZIP2 plays a role as well in the zinc homeostasis of prostate cancer cells. As mentioned earlier, ZnT1 is a prominent zinc exporter, its up-regulation in prostate cancer cells may result in the leaking of zinc via ZnT1, hence leading to the reduction of cytoplasmic zinc level in prostate cancers. Therefore, *SLC30A1* (ZnT1) could also be a therapeutic target for prostate cancers.

ZIP12 was found to be localised in the plasma membrane of the breast cancer cells but not in normal breast epithelial cells (**Chapter 4**, **Figure 4.3A**), neither in cancerous nor in normal prostate cells (**Chapter 4**, **Figure 4.3B**,). Such findings suggest ZIP12 is part of the machinery regulating the zinc homeostasis in breast cancer cells. ZIP12 localisation in the cell membrane might enable the breast cancer cells to uptake extracellular Zn^{2+} in order to maintain consistently elevated Zn^{2+} concentration (**Chapter 4**, **Figure 4.3A**). In contrast, ZIP12 is not involved in regulating intracellular Zn^{2+} in normal breast cells, or normal and cancerous prostate cells (**Chapter 4**, **Figure 4.3**). Protein kinase CK2 is involved in zinc homeostasis of

breast cancer and prostate cancer cells (Taylor et al., 2012; Zaman et al., 2019). The localisation in close proximity to the plasma membrane of catalytic subunits CK2α/α' and regulatory subunit CK2β in breast cancer cells demonstrates that CK2 kinase could function as an ecto-kinase (**Chapter 4**, **Figures 9A** and **11A**). Therefore, CK2 may regulate the plasma membrane-bound ZIP12 for Zn^{2+} uptake (**Chapter 4**, **Figure 4.3A**). Intriguingly, the overexpression of catalytic CK2α/α' subunits (Gray et al., 2014; Chua et al., 2017) but down-regulation of regulatory CK2β subunits in breast cancer cells compared to the normal counterparts might be a reason behind CK2 hyperactivity for regulating high Zn^{2+} as well as cancer promotion (Dubois et al., 2016). Metallothioneins are small Zn^{2+} buffering proteins as previously described, found to be up-regulated in breast and prostate cancer cells (**Chapter 4**, **Table 4.1**). MT2A localisation close to the plasma membrane in breast cancer cells (**Chapter 4**, **Figure 4.7A**) indicates its likely participation in cell growth and invasion, as extracellularly localised metallothionein contribute cancer cell proliferation and metastasis (Lynes et al., 1993; Youn et al., 1995; Lynes et al., 2006; Subramanian Vignesh and Deepe, 2017). Metallothionein serves as a double-edged dagger as it is involved in cellular Zn^{2+} regulation as well as cancer progression. Thereby metallothionein could be targeted for cancer treatment.

Additionally, the expression profiles of *SLC39A*, *SLC30A* and *MT* genes between two cancer cell lines of breast (i.e., MCF-7 vs MDA-MB-231), and between two prostate cancer cell lines (PC3 vs DU145) in **Table 3.1** showed the differential gene expression in the cell lines of two varying breast or prostate cancerous subtypes. For example, the higher expression of *SLC30A2* (ZnT2) gene in luminal breast cancer cells (MCF-7) than basal breast cancer cells (MDA-MB-231) highlights the potentially distinctive role of ZnT2 in luminal breast cancers. This notion is supported by the study of Chandler et al. (2016). Similarly, the up-regulation of *SLC30A2* gene in the highly metastatic prostate cancer cells (PC3) compared to the moderately metastatic prostate cancer cells (DU145) indicates a potential positive relationship between ZnT2 and cancer invasiveness. The down-regulation of ZIP12 at gene (**Table 3.1**) and protein levels (**Table 4.1**) in PC3 cells suggests that ZIP12 plays a role in prostate cancer cell migration. The higher expression of *MT* genes (*MT1F*, *MT1X*, *MT2A*) in MDA-MB-231 cells compared to MCF-7 breast cancer cells suggests their prominent participation in cancer aggressiveness of basal breast cancer subtype, which is supported by the previous findings (Tai et al., 2003; Si and Lang, 2018; Barman et al., 2022).

The cancer cell lines are the model systems in medical research (Mirabelli et al., 2019; Sajjad et al., 2021; Yee et al., 2022), they are widely employed for basic molecular understanding of cancers and drug discoveries. The differential expression of the genes such as *SLC39A4* (ZIP4), *SLC39A6* (ZIP6), *SLC39A8* (ZIP8), *SLC39A11* (ZIP11) in breast and prostate cancer cells (**Table 3.1**) here correlates with the breast and prostate cancer tissues. However, many findings of this study should be verified in the clinical cancer tissues such as the role of ZIP12 and ZIP4 in breast cancers, because of the inherent limitations of the adapted cancer cell lines as they lack tumour microenvironment interactions (Ben-David et al., 2018; Hynds et al., 2018; Jarnuczak et al., 2021).

Further top-down proteomic analysis on the total proteins of MCF-7 breast cancer cells and PC3 prostate cancer cells compared to their normal counterparts also showed differential protein expressions (**Chapter 5**, **Tables 5.1** and **5.2**). For example, MCF-7 breast cancer cells showed greater number of differentially expressed metal ion binding protein (16%) than PC3 prostate cancer cell (13%) based on UniProt and literature survey (**Chapter 5**, **Figures 5.2A** and **5.8A**). PANTHER database also demonstrated higher number of differentially expressed divalent ion Ca^{2+} binding proteins in MCF-7 cells (13%) than PC3 cells (7%) (**Chapter 5**, **Figures 5.2B** and **5.8B**). In breast cancer cells, metal ion and Ca^{2+} binding protein S100A13 showed significant up-regulation (**Chapter 5**, **Table 5.1**) for zinc homeostasis as the study revealed the positive relationship between Ca^{2+} and Zn^{2+} ions in cancer cells (Zaman et al., 2016). The prevalence of higher Ca^{2+} binding proteins in breast cancer cells also reflects their elevated intrinsic zinc profiles, in contrast low zinc in prostate cancer cells. Based on these findings one would understand that breast cancer cell has more molecular workhorses than prostate cancer cells for regulating elevated level of intracellular Zn^{2+}. The down-regulation of tumour suppressor proteins such as 14-3-3 protein σ, 14-3-3 protein θ in both breast and prostate cancer cells compared to their normal cells (**Chapter 5**, **Tables 5.1** and **5.2**) promotes tumorigenesis (Li et al., 2009; Young et al., 2015). The up-regulation of the antioxidant protein peroxiredoxin 6 in the breast and prostate cancer cells reflects the adaptive response of the cancer cells against the stress incurred by the extracellular zinc exposure (**Chapter 5**, **Tables 5.1** and **5.2**) (Basu et al., 2007; Chang et al., 2007). Thereby peroxiredoxin 6, 14-3-3 protein σ and θ could be targeted for developing common therapeutics for both breast and prostate cancers.

6.2 Dynamic changes at gene and protein levels in breast and prostate cancer cells upon extracellular zinc exposure

The molecular machinery is prodded into action by the extracellular zinc exposure. As intracellular zinc levels are fluctuating in the cells of living human beings, the findings of dynamic changes in genes and proteins of the breast and prostate cancer cells are indeed relevant to our understanding of the zinc homeostasis in cancer cells. This study uncovered the dynamic changes at gene and protein levels in breast and prostate cancer cells in response to the extracellular zinc exposure. The exogenous zinc exposure increased the gene expression of *SLC39A4* (ZIP4), *SLC39A12* (ZIP12), *SLC30A1* (ZnT1), *SLC30A2* (ZnT2), *MT1B* (MT1B), *MT1F* (MTIF), *MT1X* (MT1X) and *MT2A* (MT2A) in breast cells (**Chapter 3**, **Tables 3.2** and **3.3**) and prostate cells (**Chapter 3**, **Table 3.2**) (Barman et al., 2022). In addition, the greater expression of *SLC39A12*, *SLC30A1*, *MT1B*, *MT1F*, *MT1X* and *MT2A* was observed in MDA-MB-231 basal breast cancer cells than MCF-7 luminal breast cancer cells. Such differential expression following exogenous zinc exposure supports the distinctive behaviours of these two subtypes of breast cancer cells. For example, MDA-MB-231 has a higher tolerance of zinc (**Chapter 3**, **Figure 3.1A**), which might relate to the higher tumorigenicity of basal breast cancer than luminal breast cancer (Chandler et al., 2016). *MT2A* exhibited higher expression in normal prostate epithelial cells (RWPE-1) than cancerous prostate cells (PC3, DU145) following zinc treatment (**Chapter 3, Table 3.2**), suggesting that *MT2A* plays a role in regulating the high zinc level in normal prostate epithelial cells by sequestering excess Zn^{2+}.

ZnT1 showed overexpression in RWPE-1 normal prostate epithelial cell at protein level whereas it remained unchanged in prostate cancer cells under zinc exposure (**Chapter 4**, **Figure 4.4B**), suggesting that ZnT1 is likely required to compartmentalise excess Zn^{2+} in order to tolerate high zinc level in normal prostate epithelial cells. The mild cytotoxic zinc dosage (186.88 µM $ZnSO_4$) and the viability (85%) of RWPE-1 normal prostate cells under zinc exposure at T_{120} were greater than cancerous counterpart PC3 or DU145 cells (**Chapter 4**, **Figure 4.1C**). In contrast, ZnT1 was found to be localised in the plasma membrane in only breast cancer cells (**Chapter 4**, **Figure 4.5A**), likely due to the high intracellular Zn^{2+} in breast cancer cells since ZnT1 is associated with Zn^{2+} efflux.

Top-down proteomic approach identified 25 differentially expressed protein spots (16 suppressed, 9 overexpressed) in MCF-7 breast cancer cells (**Chapter 5**, **Figure 5.4A**) while 9 (2 suppressed, 7 overexpressed) in PC3 prostate cancer cells (**Chapter 5**, **Figure 5.10A**) following zinc exposure at T_{120} compared to T_0. This suggests that breast cancer cell is highly equipped compared to prostate cancer cell in regulating elevated cellular Zn^{2+} and responding to extracellular zinc. In contrast, MCF10A normal breast epithelial cells showed 7 differentially expressed protein spots (**Chapter 5**, **Figure 5.4B**) whereas 24 (14 suppressed, 10 overexpressed) in RWPE-1 normal prostate epithelial cells (**Chapter 5**, **Figure 5.10B**) under zinc exposure at T_{120} compared to T_0, suggesting that normal prostate cell is molecularly enriched for maintaining high cellular Zn^{2+}. Such observations provide further explanation for the elevated cellular Zn^{2+} in breast cancer cells but reduced in prostate cancer cells compared to their respective normal cells under zinc exposure.

The dysregulations of the proteins in response to zinc revealed by proteomic datasets are associated with metabolism, cell growth, stress response, lysosomal and antioxidant activity. The overexpression of an endoproteinase cathepsin D in the lysosome in breast cancer cells increases its activity, which depends on the high cellular Zn^{2+} (Kim et al., 2022). The overexpressed antioxidant proteins (peroxiredoxin 6 and 2) and stress response proteins (60 kDa and 70 kDa heat shock proteins) indicate the respective roles to protect the cancerous cells in high zinc detrimental environment (**Chapter 5**, **Tables 5.1** and **5.2**). Tumour protein D53 (hD53) and tumour protein D54 (hD54) overexpression under exogenous zinc exposure (**Chapter 5**, **Table 5.1**) may be associated directly or indirectly with the breast cancer development and progression in the context of elevated intracellular zinc level. On contrary, zinc exposure reduced the tumour suppressor prohibitin (*PHB*) in prostate cancer cells (**Chapter 5**, **Table 5.2**) under zinc exposure, might partly explain that the reduced intracellular zinc is the precondition of prostate cancer development (Sauer et al., 2020).

6.3 Potential roles of ZIP4 and ZIP12 in regulating zinc uptake

SLC39A4 (encoding ZIP4) showed overexpression at gene level in response to the exogenous zinc exposure in breast and prostate cancer cells (**Chapter 3**, **Tables 3.2** and **3.3**), and it was also intrinsically overexpressed in both cancer cells without any treatment (**Chapter 3**, **Table 3.1**) (Barman et al., 2022). The gene expression of *SLC39A12* (encoding ZIP12) was up-regulated in breast cancer cells following mild cytotoxic $ZnSO_4$ treatment (**Chapter 3**, **Table**

3.2, **Figure 3.4**). Furthermore, the immunofluorescence confocal microscope revealed that ZIP12 protein was only localised in the cell membrane of breast cancer cells (**Chapter 4**, **Figure 4.3A**). The structural and functional studies on ZIP4 proposed that its long extracellular N-terminal domain could be responsible sensing or regulating zinc uptake (Zhang et al., 2017; Chun et al., 2019; Hu, 2021). As ZIP4 and ZIP12 are close homologues (Chun et al., 2019), ZIP12 might also function as an extracellular zinc sensor. Therefore, the findings of this project provoke a novel thought on the zinc homeostasis in breast cancer cells, that is, two routes of zinc sensing and regulation of zinc level in the cell, namely the extracellular zinc sensor by ZIP4 and ZIP12 encoded by *SLC39A4* and *SLC39A12*, respectively, and the intracellular zinc sensor by MTF-1 (metal-response element binding transcription factor 1 encoded by *MTF1* gene). The extracellular zinc sensor (ZIP4 and ZIP12) is likely responsible for the up-regulation of ZIP genes such as *SLC39A2* and *SLC39A12*, while the intracellular zinc sensor (MTF-1) is responsible for the up-regulation of ZnT and metallothionein genes such as *SLC30A1* (ZnT1) and *MT2A* when the intracellular zinc level is high. It is well documented that MTF-1 regulated ZnT genes (e.g., *SLC30A1*) (Langmade et al., 2000; Giedroc et al., 2001). The concept for the intracellular zinc sensor (MTF-1) is established in the literature (Andrews, 2001; Hardyman et al., 2016; Zaman et al., 2021), however, the proposed extracellular zinc sensor (ZIP4 and ZIP12) in this study is novel. Further experimental evidence is required from future research.

6.4 Potential role of CK2 in regulating ZIP transporters for zinc uptake in breast cancer cells

Protein kinase CK2 is a tetrameric enzyme consisting of two catalytic subunits (CK2α and CK2α') and two regulatory subunits (CK2β), as previously described in **Figures 1.7** and **1.8** of **Chapter 1**. Two regulatory β subunits form the homodimer at which catalytic subunit α or α' attach to form functional tetrameric configurations such as ααββ, αα'ββ and α'α'ββ. The crystal structural analysis provides detailed insights into how the zinc finger in CK2β mediates the dimerization of the regulatory CK2β subunits (Chantalat et al., 1999; Bibby and Litchfield, 2005; Filhol et al., 2005). It reveals the specific arrangement of amino acid residues (Cys109, Cys114, Cys137 and Cys140) for the coordination of Zn^{2+} within the zinc finger domain (Chantalat et al., 1999; Filhol et al., 2005). Clearly, being a structural component of CK2, Zn^{2+} is critical for the enzymatic function of the kinase. CK2 is indeed a pleiotropic protein kinase, involving in cellular processes such as proliferation, survival and apoptosis (Nimmanon et al.,

2017; Chen et al., 2023; Trembley et al., 2023). But its role in Zn^{2+} homeostasis is just emerging.

CK2 can phosphorylate Ser^{275} and Ser^{276} amino acid residues for the activation of ZIP7 in MCF-7 breast cancer cells (Taylor et al., 2012). Since ZIP7 is localised in the membrane of endoplasmic reticulum (ER), Zn^{2+} is released from ER into cytoplasm following phosphorylation in order to activate numerous cellular signalling networks for breast cancer progression (Nimmanon et al., 2017). This study demonstrated the localisation of ZIP12 in the plasma membrane of MCF-7 luminal and MDA-MB-231 basal subtype breast cancer cells (**Chapter 4**, **Figure 4.3A**). Importantly catalytic subunits CK2α/α' and regulatory subunit CK2β of CK2 were also found in close proximity to the plasma membrane (**Chapter 4**, **Figures 4.9A** and **4.11A**), indicating that CK2 might serve as an ecto-kinase (Montenarh and Götz, 2018) in breast cancer cells. Based on such localisation of ZIP12 in breast cancer cells and numerous possible phosphorylation sites in ZIP12 for CK2 (**Chapter 4**, **Table 4.2**), it is possible that CK2 kinase can regulate ZIP12 by phosphorylation.

In summary, **Figure 6.1** shows the molecular illustration of zinc homeostasis in breast and prostate cancer cells. Cytosolic Zn^{2+} in breast cancer cells can be imported from extracellular space via ZIP such as ZIP12 and can be released from intracellular organelles such as endoplasmic reticulum (ER) via ZIP7 (**Figure 6.1A**). To import extracellular Zn^{2+} into cytosol via ZIP12, the sensing of extracellular Zn^{2+} by ZIP4 or ZIP12 might be required as discussed earlier. Also, Zn^{2+} uptake via ZIP12 might be initiated following its phosphorylation by protein kinase CK2. The increased intracellular Zn^{2+} level might mediate numerous signalling pathways such as MAPK, mTOR, PI3K, GSK3 and AKT signalling networks (Taylor et al., 2012; Nimmanon et al., 2017; Fukada and Kambe, 2018; Wang et al., 2020).

In contrast, the extracellular Zn^{2+} sensing by ZIP12 and the collective roles of ZIP12 and CK2 for regulating Zn^{2+} homeostasis might be absent in prostate cancer cells (**Figure 6.1B**) as neither ZIP12 nor CK2 kinase was localised in the plasma membrane (**Chapter 4**, **Figure 4.3B**, **4.9B** and **11B**). Additionally, MTF-1 based intracellular Zn^{2+} sensing might not be very active in prostate cancer cells due to low Zn^{2+} level in prostate cancer cells (**Figure 6.1B**). These findings collectively shed light on the underlying reasons for the reduced zinc level in prostate cancer cells.

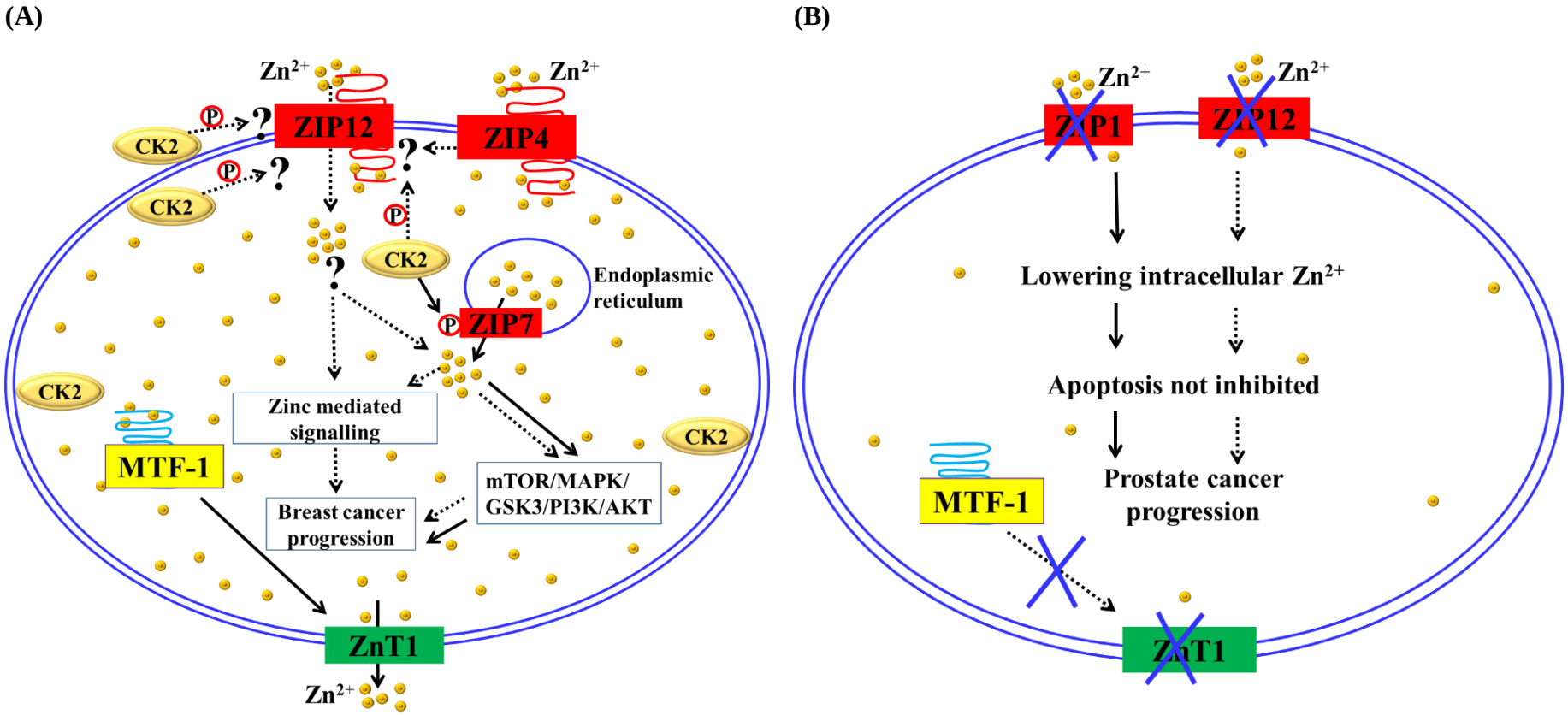

Figure 6.1 Schematic diagrams for the molecular networks of Zn^{2+} homeostasis in breast and prostate cancer cells. (A) Cytosolic Zn^{2+} level in breast cancer cells is increased by importing Zn^{2+} from extracellular space via ZIP such as ZIP12, and by releasing Zn^{2+} from intracellular organelles. Both ZIP4 and ZIP12 could function as extracellular Zn^{2+} sensor. ZIP12 could be regulated by CK2 kinase in response to the hormonal cues or other stimuli. Such elevated cytosolic Zn^{2+} might lead to signalling pathways and cancer progression. MTF-1 is an intracellular Zn^{2+} sensor and is found to regulate the expression of ZnT1 and metallothionein. (B) In prostate cancer cells, ZIP12 and ZnT1 are not localised in the plasma membrane. Neither was CK2 localised close to the plasma membrane in prostate cancer cells. So ZIP12, ZnT1 and CK2 might not be involved in Zn^{2+} homeostasis of prostate cancer cells. MTF-1 might not be in action, due to the low intracellular Zn^{2+} level in prostate cancer cells. Broken line arrow denotes for the proposed consequences, solid line arrow for the established consequences.

6.5 Zinc dysregulation and development of breast and prostate cancers

Zn^{2+} dyshomeostasis is a striking feature in human breast and prostate cancers. However, the answer is elusive to the question whether this phenomenon is a cause of the cancers or an effect of the cancers. Because it is a fact that zinc dysregulation occurs in breast and prostate cancer cells (Sauer et al., 2020; Rusch et al., 2021), the findings of this study provide the molecular details for our understanding of the role of zinc in breast and prostate cancer development.

As mentioned in the previous chapters, there are mainly four classes of proteins, ZIP, ZnT, MT and transcription factors, which are involved in Zn^{2+} import, efflux, sequestration and regulation in the cell (Giedroc et al., 2001; Kambe et al., 2015). Zn^{2+} importers ZIP1-14 increase cytoplasmic Zn^{2+} by transporting Zn^{2+} into cytoplasm from extracellular space or intracellular organelles (Bin et al., 2018; Kambe et al., 2021). In contrast, cytoplasmic Zn^{2+} level is decreased via ZnT proteins which efflux Zn^{2+} out of the cell or transport Zn^{2+} into the intracellular organelles (Bin et al., 2018; Kambe et al., 2021). Metallothioneins are essential in sequestration of Zn^{2+} when there is excess amount of Zn^{2+} in the cytoplasm (Kambe et al., 2015). Zn^{2+}-dependent metal-responsive transcription factor 1 (MTF-1) is the key regulator for the expression of ZnT genes (e.g., *SLC30A1*) and metallothionein genes (e.g., *MT1B*, *MT1X*, *MT1F*, *MT2A*, *MT4*) in response to the fluctuation of intracellular Zn^{2+} levels (Langmade et al., 2000; Giedroc et al., 2001; Grzywacz et al., 2015).

This study demonstrated the intrinsic up-regulation of the ZIP genes such as *SLC39A4*, *SLC39A6*, *SLC39A8* and *SLC39A11* in breast and prostate cancer cells compared to their respective normal cells (**Figure 3.3**), which correlates well with the expression profiles of those genes in cancer tissues (**Table 3.1**). The findings indicate that ZIP4, ZIP6, ZIP8 and ZIP11 might be involved in the zinc dysregulation of breast and prostate cancers in clinical settings, and therefore highlights the significance of this study by employing the cancer cell lines. The finding of ZIP4 (*SLC39A4*) here in breast cancer cells is intriguing, because the previous studies demonstrated that it can be an extracellular Zn^{2+} sensor for intracellular Zn^{2+} regulation (Zhang et al., 2017; Chun et al., 2019; Hu, 2021) and its high expression is corelated with epithelial-to-mesenchymal transition, metastasis and invasion for cancer development (Zeng et al., 2019). Furthermore, ZIP6 (*SLC39A6*) is associated with Zn^{2+} hyperaccumulation for the development of breast cancers (Kasper et al., 2005; Chandler et al., 2016). Hence, the results

of this study support the notion that Zn^{2+} dysregulation is involved in breast cancer development.

Significant down-regulation of Zn^{2+} importer gene *SLC39A1* (ZIP1) in prostate cancer cells (**Figure 3.3**, **Table 3.1**) is supported by the previous findings in malignant prostatic tissues (Franz et al., 2013; Sauer et al., 2020). Thereby, the down-regulation of ZIP1 is likely associated with the low intracellular Zn^{2+} level in prostate cancer tissues. The cytoplasmic localisation of ZIP12, not in the plasma membrane of prostate cancer cells (**Figure 4.3B**), suggests that ZIP12 is not required for either extracellular Zn^{2+} sensing or uptake in prostate cancer cells. Furthermore, the up-regulation of *SLC30A1* (ZnT1) at gene level (**Table 3.1**) and protein level (**Table 4.1**) in prostate cancer cells indicates that ZnT1 is involved in prostate cancer progression, and this notion is supported by Lehvy et al. (2019).

Metallothioneins are the key players for Zn^{2+} homeostasis, its dynamic change in expression has ramifications in Zn^{2+} dysregulation and cancer development. The overexpression of *MT2A* gene and its encoded protein in breast and prostate cancer cells (**Tables 3.1** and **4.1**) suggests that it is involved in both cancers. Importantly, the close localisation of MT2A to the plasma membrane in the breast cancer cells indicates that MT2A might play a role in cell proliferation, migration and invasion, which is in agreement with the previous studies in clinical cancers (Lynes et al., 1993; Youn et al., 1995; Liu et al., 2022). Hence, the findings of this study on metallothioneins provide evidence for the role of Zn^{2+} dysregulation in cancer development.

Protein kinase CK2 was up-regulated in breast cancer cells (**Table 4.1**), which is supported by the previous study on malignant breast tissues (Chua et al., 2017). Importantly, the close localisation of CK2 (CK2α/α' and CK2β subunits) to the plasma membrane of breast cancer cells (**Figures 4.9** and **4.10**) indicates that it might be involved in the phosphorylation of ZIP12, as ZIP12 is localised in the plasma membrane of breast cancer cells (**Figure 4.3A**) and has multiple postulated phosphorylation motifs for CK2 (**Table 4.2**). Further studies need to be carried out on this front to delineate the role of CK2 in regulating the membrane-bound zinc transporters such as ZIP12. The previous studies demonstrated that CK2 phosphorylated ZIP7, triggering the gated release of Zn^{2+} into the cytoplasm from the lumen of endoplasmic reticulum, thereby elevated cytoplasmic Zn^{2+} concentration and in turn activated the signalling pathways for breast cancer progression (Taylor et al., 2012; Nimmanon et al., 2017).

The final piece of data for the role of Zn^{2+} dysregulation in breast and prostate cancer development is described in **Chapter 5**. The zinc-responsive proteins to the exposure of extracellular zinc were uncovered by the proteomic profiling, such as antioxidants (peroxiredoxin 2, peroxiredoxin 6) and stress responders (heat shock 60 kDa, heat shock 70 kDa) (**Tables 5.1** and **5.2**). The up-regulation of both antioxidants and heat shock proteins indicates that these proteins play a role in breast and prostate cancer cells. Previous studies demonstrated that peroxiredoxins 2 and 6 enhance breast and prostate cancer progression (Chang et al., 2007; Basu et al., 2011). Tumour proteins hD53 and hD54 were overexpressed under exogenous zinc treatment in breast cancer cells, suggesting that the elevated intracellular Zn^{2+} level might accelerate cancer development via hD53 and hD54 tumour proteins. This notion is supported by the study carried out by Kim et al. (2019). Also, the overexpressed cathepsin D (**Table 5.1**), an endoproteinase, in response to extracellular zinc exposure, might increase its activity in the lysosome in breast cancer cells for proliferation and invasion according to the previous studies (Kang et al., 2020; Kim et al., 2022; Seo et al., 2022). Therefore, the proteomic findings of this study provide further insights into the role of Zn^{2+} dysregulation in breast and prostate cancer development.

Additionally, as Zn^{2+} is involved in multitudes of biological functions, its dysregulation can trigger transcription factors into action, and interestingly many transcription factors are zinc finger proteins which can bind Zn^{2+}. Previous studies demonstrated that zinc finger proteins such as metal-responsive transcription factor 1 (MTF-1) is involved in managing Zn^{2+} regulation for the cell and is involved in cancer progression (Langmade et al., 2000; Giedroc et al., 2001; Zhang et al., 2012; Grzywacz et al., 2015). Although *MTF-1* expression did not change in breast cancer cells under extracellular zinc exposure, as described in our previous RNA sequencing study (Zaman et al., 2021), its activation by the increased cytoplasmic Zn^{2+} level is unequivocally proven by numerous studies (Andrews, 2001; Giedroc et al., 2001; Lichten et al., 2011; Grzywacz et al., 2015; Hardyman et al., 2016). MTF-1 senses intracellular Zn^{2+} level, and regulates the expression of *SLC30A1* (ZnT1), *MT1B*, *MT1X*, *MT1F*, *MT2A* and *MT4* genes in response to intracellular Zn^{2+} levels (Langmade et al., 2000; Giedroc et al., 2001; Grzywacz et al., 2015). Furthermore, the down-regulation of *SLC39A10* (ZIP10) gene is observed in adequate intracellular Zn^{2+} environment, which is also mediated by MTF-1 (Lichten et al., 2011). Another zinc finger transcription factor ZKSCAN3 was up-regulated in prostate cancer tissues and cells (Zhang et al., 2012), but whether it is activated by the change of intracellular Zn^{2+} levels is not yet certain. In fact, there are hundreds of zinc finger proteins

in the cell (Bu et al., 2021; Rakhra and Rakhra, 2021; Li et al., 2022), and there are scant data on the role of intracellular Zn^{2+} level in their regulations. More research is needed on this front.

6.6 Future work

The molecular details of zinc homeostasis are not only vital to understanding the role of zinc in cancer development but may also uncover new targets for anticancer drug development. By the means of gene profiling, immunofluorescence and proteomic analysis, this study revealed a number of molecules such as ZIP1, ZIP4, ZIP12 and ZnT1 transporters as well as CK2 kinase subunits as promising candidates for the targeted cancer therapy. It should be exciting to follow up this study by investigating the potential role of ZIP12 in extracellular Zn^{2+} sensing and uptake in breast cancer cells, and the role of protein kinase CK2 in regulating ZIP12 through phosphorylation and signal transduction pathways. It should be worthwhile as well to see if the dysregulation of intracellular Zn^{2+} levels in breast and prostate cancer cells can be corrected by molecular manipulation of gene expression of ZIP12 and ZIP1, that is, by down-regulation of ZIP12 expression, the intracellular Zn^{2+} level in breast cancer cells might be reduced whilst by up-regulation of ZIP1, the intracellular Zn^{2+} level in prostate cancer cells might be increased. In this way, a new cancer treatment strategy could be developed for breast and prostate cancers. Because the discoveries are based on the cultured breast and prostate cancer cells, it is essential for future studies to extend to clinical cancer tissues. Therefore, the experimental approach, such as the gene profiling, immunofluorescence and proteomics applied successfully on the cultured cells here, should be applied to clinical cancer tissues.

The proteomic datasets did not uncover the expression details of zinc transporters. The limited representation of membrane-bound proteins such as ZIP and ZnT is likely due to the limitation of the protein extraction buffer used in this project, which is more effective for water-soluble proteins. Therefore, it should be valuable to carry out another proteomic study by employing an effective extraction buffer for membrane-bound proteins.

Due to the financial constraint, the immunofluorescent confocal experiments did not cover ZIP4 transporter. It should be a top priority in follow-up studies to investigate the expression details of ZIP4 in breast and prostate cancer cells, as well as in the cancer tissues if possible. ZIP12 is localised in the plasma membrane of MCF-7 and MDA-MB-231 breast cancer cells but not in MCF10A breast normal cells and prostate cells (RWPE-1, PC3, DU145). ZIP12

might uptake exogenous Zn^{2+} for intracellular Zn^{2+} accumulation in both luminal and basal type breast cancer cells. The measurement of intracellular Zn^{2+} in ZIP12 knockdown or knockout breast cancer cells with and without exogenous zinc exposure will demonstrate whether ZIP12 imports exogeneous Zn^{2+} or not. The localisation of protein kinase CK2 in close proximity to the cell membrane and its potential phosphorylation sites in ZIP12 should set the basis for carrying out a further study to investigate ZIP12 phosphorylation by CK2 in breast cancer cells.

The differentially expressed proteins including tumour protein (hD53, hD54), endoproteinase (cathepsin D), metal ion binding (S100A13), metabolic enzyme (triosephosphate isomerase), antioxidant (peroxiredoxin 6), molecular chaperone (heat shock protein 70 kDa) in MCF-7 breast cancer cell under zinc exposure (**Chapter 5**, **Table 5.1**) might provide molecular clues for the role of zinc in cancer development. Similarly, PC3 prostate cancer cell showed numerous differentially expressed proteoforms such as metal ion binding (annexin A1), translational factor (elongation factor Tu), stress protein (heat shock protein β1), antioxidant (peroxiredoxin 6, peroxiredoxin 2) or other protein (NSFL1 cofactor p47) (**Chapter 5**, **Table 5.2**). The future studies on cancer tissues may validate the significance of those differentially expressed proteins discovered in this project.

As zinc dyshomeostasis is increasingly linked to the development and progression of cancers such as breast and prostate cancers, and zinc is emerging as an important signalling molecule in normal and cancerous cells, the future research focus on the molecular network of zinc homeostasis in breast and prostate cancer cells should lead to further understanding of the role of zinc in cancers and some meaningful molecular targets for anti-cancer drug development.

7 References

Abdo AI, Tran HB, Hodge S, Beltrame JF, Zalewski PD (2021) Zinc homeostasis alters zinc transporter protein expression in vascular endothelial and smooth muscle cells. Biol Trace Elem Res **199:** 2158-2171

Ackermann K, Neidhart T, Gerber J, Waxmann A, Pyerin W (2005) The catalytic subunit alpha' gene of human protein kinase CK2 (CSNK2A2): genomic organization, promoter identification and determination of Ets1 as a key regulator. Mol Cell Biochem **274:** 91-101

Adams TK, Saydam N, Steiner F, Schaffner W, Freedman JH (2002) Activation of gene expression by metal-responsive signal transduction pathways. Environ Health Perspect **110:** 813

Al-Humaidi RB, Fayed B, Shakartalla SB, Jagal J, Jayakumar MN, Al Shareef ZM, Sharif SI, Noreddin A, Semreen MH, Omar HA, Haider M, Soliman SSM (2022) Optimum inhibition of MCF-7 breast cancer cells by efficient targeting of the macropinocytosis using optimized paclitaxel-loaded nanoparticles. Life Sci **305:** 120778

Alam S, Kelleher SL (2012) Cellular mechanisms of zinc dysregulation: a perspective on zinc homeostasis as an etiological factor in the development and progression of breast cancer. Nutrients **4:** 875-903

Albrecht AL, Somji S, Sens MA, Sens DA, Garrett SH (2008) Zinc transporter mRNA expression in the RWPE-1 human prostate epithelial cell line. Biometals **21:** 405-416

Allende JE, Allende CC (1995) Protein kinases. 4. Protein kinase CK2: an enzyme with multiple substrates and a puzzling regulation. FASEB J **9:** 313-323

Almuslehi MSM, Sen MK, Shortland PJ, Mahns DA, Coorssen JR (2022) Histological and Top-Down Proteomic Analyses of the Visual Pathway in the Cuprizone Demyelination Model. J Mol Neurosci **72:** 1374-1401

Amos A, Razzaque MS (2022) Zinc and its role in vitamin D function. Curr Res Physiol **5:** 203-207

Anderson NM, Qin X, Finan JM, Lam A, Athoe J, Missiaen R, Skuli N, Kennedy A, Saini AS, Tao T, Zhu S, Nissim I, Look AT, Qing G, Simon MC, Feng H (2021) Metabolic Enzyme DLST Promotes Tumor Aggression and Reveals a Vulnerability to OXPHOS Inhibition in High-Risk Neuroblastoma. Cancer Res **81:** 4417-4430

Andreini C, Banci L, Bertini I, Rosato A (2006) Counting the zinc-proteins encoded in the human genome. J Proteome Res **5:** 196-201.

Andreini C, Banci L, Bertini I, Rosato A (2006) Zinc through the three domains of life. J Proteome Res **5:** 3173-3178

Andreini C, Bertini I (2012) A bioinformatics view of zinc enzymes. J Inorg Biochem **111:** 150-156

Andreini C, Bertini I, Cavallaro G, Holliday GL, Thornton JM (2008) Metal ions in biological catalysis: from enzyme databases to general principles. J Biol Inorg Chem **13:** 1205-1218

Andreini C, Bertini I, Rosato A (2009) Metalloproteomes: a bioinformatic approach. Acc Chem Res **42:** 1471-1479

Andrews GK (2001) Cellular zinc sensors: MTF-1 regulation of gene expression. Biometals **14:** 223-237

Andrews GK, Wang H, Dey S, Palmiter RD (2004) Mouse zinc transporter 1 gene provides an essential function during early embryonic development. Genesis **40:** 74-81

Asano N, Kondoh M, Ebihara C, Fujii M, Nakanishi T, Soares MJ, Nakashima E, Tanaka K, Sato M, Watanabe Y (2004) Expression profiles of zinc transporters in rodent placental models. Toxicol Lett **154:** 45-53

Asgarov R, Sen MK, Mikhael M, Karl T, Gyengesi E, Mahns DA, Malladi CS, Münch GW (2021) Characterisation of the Mouse Cerebellar Proteome in the GFAP-IL6 Model of Chronic Neuroinflammation. Cerebellum**:** 1-21

Attner B, Landin-Olsson M, Lithman T, Noreen D, Olsson H (2012) Cancer among patients with diabetes, obesity and abnormal blood lipids: a population-based register study in Sweden. Cancer Causes Control **23:** 769-777

Aydemir TB, Chang S-M, Guthrie GJ, Maki AB, Ryu M-S, Karabiyik A, Cousins RJ (2012) Zinc transporter ZIP14 functions in hepatic zinc, iron and glucose homeostasis during the innate immune response (endotoxemia). PloS One **7:** e48679

Aydemir TB, Sitren HS, Cousins RJ (2012) The zinc transporter Zip14 influences c-Met phosphorylation and hepatocyte proliferation during liver regeneration in mice. Gastroenterology **142:** 1536-1546. e1535

Aydemir TB, Troche C, Kim M-H, Cousins RJ (2016) Hepatic ZIP14-mediated zinc transport contributes to endosomal insulin receptor trafficking and glucose metabolism. J Biol Chem **291:** 23939-23951

Bafaro E, Liu Y, Xu Y, Dempski RE (2017) The emerging role of zinc transporters in cellular homeostasis and cancer. Signal Transduct Target Ther **2:** 17029

Barman SK, Zaman MS, Veljanoski F, Malladi CS, Mahns DA, Wu MJ (2022) Expression profiles of the genes associated with zinc homeostasis in normal and cancerous breast and prostate cells. Metallomics **14:** mfac038

Barresi V, Valenti G, Spampinato G, Musso N, Castorina S, Rizzarelli E, Condorelli DF (2018) Transcriptome analysis reveals an altered expression profile of zinc transporters in colorectal cancer. J Cell Biochem **119:** 9707-9719

Basu A, Banerjee H, Rojas H, Martinez SR, Roy S, Jia Z, Lilly MB, De León M, Casiano CA (2011) Differential expression of peroxiredoxins in prostate cancer: consistent upregulation of PRDX3 and PRDX4. Prostate **71:** 755-765

Basu A, Martinez S, Melendez L, Mediavilla-Varela M, Casiano C (2007) High expression of peroxiredoxins in prostate cancer cells. Cancer Res **67:** 2911-2911

Bay BH, Jin R, Huang J, Tan PH (2006) Metallothionein as a prognostic biomarker in breast cancer. Exp Biol Med (Maywood) **231:** 1516-1521

Becaria, Campbell A, Bondy SC (2002) Aluminum as a toxicant. Toxicol Ind Health **18:** 309-320

Beck FW, Prasad AS, Butler CE, Sakr WA, Kucuk O, Sarkar FH (2004) Differential expression of hZnT-4 in human prostate tissues. Prostate **58:** 374-381

Begum NA, Kobayashi M, Moriwaki Y, Matsumoto M, Toyoshima K, Seya T (2002) Mycobacterium bovis BCG cell wall and lipopolysaccharide induce a novel gene, BIGM103, encoding a 7-TM protein: identification of a new protein family having Zn-transporter and Zn-metalloprotease signatures. Genomics **80:** 630-645

Beharier O, Dror S, Levy S, Kahn J, Mor M, Etzion S, Gitler D, Katz A, Muslin AJ, Moran A (2012) ZnT-1 protects HL-1 cells from simulated ischemia–reperfusion through activation of Ras–ERK signaling. J Mol Med (Berl) **90:** 127-138

Bellomo EA, Meur G, Rutter GA (2011) Glucose regulates free cytosolic Zn(2)(+) concentration, Slc39 (ZiP), and metallothionein gene expression in primary pancreatic islet beta-cells. J Biol Chem **286:** 25778-25789

Ben-David U, Siranosian B, Ha G, Tang H, Oren Y, Hinohara K, Strathdee CA, Dempster J, Lyons NJ, Burns R, Nag A, Kugener G, Cimini B, Tsvetkov P, Maruvka YE, O'Rourke R, Garrity A, Tubelli AA, Bandopadhayay P, Tsherniak A, Vazquez F,

Wong B, Birger C, Ghandi M, Thorner AR, Bittker JA, Meyerson M, Getz G, Beroukhim R, Golub TR (2018) Genetic and transcriptional evolution alters cancer cell line drug response. Nature **560:** 325-330

Benhalevy D, Gupta SK, Danan CH, Ghosal S, Sun HW, Kazemier HG, Paeschke K, Hafner M, Juranek SA (2017) The Human CCHC-type Zinc Finger Nucleic Acid-Binding Protein Binds G-Rich Elements in Target mRNA Coding Sequences and Promotes Translation. Cell Rep **18:** 2979-2990

Bennett JL, Jackson BN, Miller RJ, Tsui H, Martin-Caraballo M (2023) IL-6 evoked biochemical changes in prostate cancer cells. Cytokine **161:** 156079

Besecker B, Bao S, Bohacova B, Papp A, Sadee W, Knoell DL (2008) The human zinc transporter SLC39A8 (Zip8) is critical in zinc-mediated cytoprotection in lung epithelia. Am J Physiol Lung Cell Mol Physiol **294:** L1127-L1136

Beyer N, Coulson DT, Heggarty S, Ravid R, Hellemans J, Irvine GB, Johnston JA (2012) Zinc transporter mRNA levels in Alzheimer's disease postmortem brain. J Alzheimers Dis **29:** 863-873

Beyer N, Coulson DT, Heggarty S, Ravid R, Irvine GB, Hellemans J, Johnston JA (2009) ZnT3 mRNA levels are reduced in Alzheimer's disease post-mortem brain. Mol Neurodegener **4:** 53

Bibby AC, Litchfield DW (2005) The multiple personalities of the regulatory subunit of protein kinase CK2: CK2 dependent and CK2 independent roles reveal a secret identity for CK2beta. Int J Biol Sci **1:** 67-79

Bin B-H, Bhin J, Kim N-H, Lee S-H, Jung H-S, Seo J, Kim D-K, Hwang D, Fukada T, Lee A-Y (2017) An acrodermatitis enteropathica-associated Zn transporter, ZIP4, regulates human epidermal homeostasis. J Invest Dermatol **137:** 874-883

Bin B-H, Bhin J, Takaishi M, Toyoshima K-e, Kawamata S, Ito K, Hara T, Watanabe T, Irié T, Takagishi T (2017) Requirement of zinc transporter ZIP10 for epidermal development: Implication of the ZIP10–p63 axis in epithelial homeostasis. Proc Natl Acad Sci U S A **114:** 12243-12248

Bin B-H, Hojyo S, Ryong Lee T, Fukada T (2014) Spondylocheirodysplastic Ehlers-Danlos syndrome (SCD-EDS) and the mutant zinc transporter ZIP13. Rare Dis **2:** e974982

Bin BH, Fukada T, Hosaka T, Yamasaki S, Ohashi W, Hojyo S, Miyai T, Nishida K, Yokoyama S, Hirano T (2011) Biochemical characterization of human ZIP13 protein: a homo-dimerized zinc transporter involved in the spondylocheiro dysplastic Ehlers-Danlos syndrome. J Biol Chem **286:** 40255-40265

Bin BH, Hojyo S, Hosaka T, Bhin J, Kano H, Miyai T, Ikeda M, Kimura-Someya T, Shirouzu M, Cho EG (2014) Molecular pathogenesis of Spondylocheirodysplastic Ehlers-Danlos syndrome caused by mutant ZIP13 proteins. EMBO Mol Med **6:** 1028-1042

Bin BH, Seo J, Kim ST (2018) Function, Structure, and Transport Aspects of ZIP and ZnT Zinc Transporters in Immune Cells. J Immunol Res **2018:** 9365747

Bischoff N, Olsen B, Raaf J, Bretner M, Issinger OG, Niefind K (2011) Structure of the human protein kinase CK2 catalytic subunit CK2alpha' and interaction thermodynamics with the regulatory subunit CK2beta. J Mol Biol **407:** 1-12

Bizzarro V, Belvedere R, Migliaro V, Romano E, Parente L, Petrella A (2017) Hypoxia regulates ANXA1 expression to support prostate cancer cell invasion and aggressiveness. Cell Adh Migr **11:** 247-260

Bjellqvist B, Ek K, Righetti PG, Gianazza E, Görg A, Westermeier R, Postel W (1982) Isoelectric focusing in immobilized pH gradients: principle, methodology and some applications. J Biochem Biophys Methods **6:** 317-339

Bochkareva E, Korolev S, Bochkarev A (2000) The Role for Zinc in Replication Protein A. J Biol Chem **275:** 27332-27338

Bonovas S, Filioussi K, Tsantes A (2004) Diabetes mellitus and risk of prostate cancer: a meta-analysis. Diabetologia **47:** 1071-1078

Borgo C, D'Amore C, Sarno S, Salvi M, Ruzzene M (2021) Protein kinase CK2: a potential therapeutic target for diverse human diseases. Signal Transduct Target Ther **6:** 183

Bosomworth HJ, Adlard PA, Ford D, Valentine RA (2013) Altered expression of ZnT10 in Alzheimer's disease brain. PLoS One **8**

Bosomworth HJ, Thornton JK, Coneyworth LJ, Ford D, Valentine RA (2012) Efflux function, tissue-specific expression and intracellular trafficking of the Zn transporter ZnT10 indicate roles in adult Zn homeostasis. Metallomics **4:** 771-779

Brethour D, Mehrabian M, Williams D, Wang X, Ghodrati F, Ehsani S, Rubie EA, Woodgett JR, Sevalle J, Xi Z, Rogaeva E, Schmitt-Ulms G (2017) A ZIP6-ZIP10 heteromer controls NCAM1 phosphorylation and integration into focal adhesion complexes during epithelial-to-mesenchymal transition. Sci Rep **7:** 40313

Bruinsma JJ, Jirakulaporn T, Muslin AJ, Kornfeld K (2002) Zinc ions and cation diffusion facilitator proteins regulate Ras-mediated signaling. Dev Cell **2:** 567-578

Bu S, Lv Y, Liu Y, Qiao S, Wang H (2021) Zinc Finger Proteins in Neuro-Related Diseases Progression. Front Neurosci **15:** 760567

Buckley NE, D'Costa Z, Kaminska M, Mullan PB (2014) S100A2 is a BRCA1/p63 coregulated tumour suppressor gene with roles in the regulation of mutant p53 stability. Cell Death Dis **5:** e1070-e1070

Burnett G, Kennedy EP (1954) The enzymatic phosphorylation of proteins. J Biol Chem **211:** 969-980

Bustin S (2002) Quantification of mRNA using real-time reverse transcription PCR (RT-PCR): trends and problems. J Mol Endocrinol **29:** 23-39

Bustin S, Nolan T (2017) Talking the talk, but not walking the walk: RT-qPCR as a paradigm for the lack of reproducibility in molecular research. Eur J Clin Invest **47:** 756-774

Calton BA, Chang SC, Wright ME, Kipnis V, Lawson K, Thompson FE, Subar AF, Mouw T, Campbell DS, Hurwitz P (2007) History of diabetes mellitus and subsequent prostate cancer risk in the NIH-AARP Diet and Health Study. J Cancer Causes **18:** 493-503

Cao J, Bobo JA, Liuzzi JP, Cousins RJ (2001) Effects of intracellular zinc depletion on metallothionein and ZIP2 transporter expression and apoptosis. J Leukoc Biol **70:** 559-566

Cassandri M, Smirnov A, Novelli F, Pitolli C, Agostini M, Malewicz M, Melino G, Raschellà G (2017) Zinc-finger proteins in health and disease. Cell Death Discov **3:** 17071

Chandler P, Kochupurakkal BS, Alam S, Richardson AL, Soybel DI, Kelleher SL (2016) Subtype-specific accumulation of intracellular zinc pools is associated with the malignant phenotype in breast cancer. Mol Cancer **15:** 2

Chandrashekar DS, Bashel B, Balasubramanya SAH, Creighton CJ, Ponce-Rodriguez I, Chakravarthi B, Varambally S (2017) UALCAN: A Portal for Facilitating Tumor Subgroup Gene Expression and Survival Analyses. Neoplasia **19:** 649-658

Chang IW, Liu K-W, Ragunanan M, He H-L, Shiue Y-L, Yu S-C (2018) SERPINB5 expression: Association with CCRT response and prognostic value in rectal cancer. Int J Med Sci **15:** 376

Chang X-Z, Li D-Q, Hou Y-F, Wu J, Lu J-S, Di G-H, Jin W, Ou Z-L, Shen Z-Z, Shao Z-M (2007) Identification of the functional role of peroxiredoxin 6 in the progression of breast cancer. Breast Cancer Res **9:** R76

Chantalat L, Leroy D, Filhol O, Nueda A, Benitez MJ, Chambaz EM, Cochet C, Dideberg O (1999) Crystal structure of the human protein kinase CK2 regulatory subunit reveals its zinc finger-mediated dimerization. EMBO J **18:** 2930-2940

Chen H-T, Hahn S (2003) Binding of TFIIB to RNA polymerase II: mapping the binding site for the TFIIB zinc ribbon domain within the preinitiation complex. Molecular cell **12:** 437-447

Chen QG, Zhang Z, Yang Q, Shan GY, Yu XY, Kong CZ (2012) The role of zinc transporter ZIP4 in prostate carcinoma. Urol Oncol **30:** 906-911

Chen Y, Wang Y, Wang J, Zhou Z, Cao S, Zhang J (2023) Strategies of Targeting CK2 in Drug Discovery: Challenges, Opportunities, and Emerging Prospects. J Med Chem **66:** 2257-2281

Cheng X, Wang J, Liu C, Jiang T, Yang N, Liu D, Zhao H, Xu Z (2021) Zinc transporter SLC39A13/ZIP13 facilitates the metastasis of human ovarian cancer cells via activating Src/FAK signaling pathway. J Exp Clin Cancer Res **40:** 199

Chimienti F, Devergnas S, Favier A, Seve M (2004) Identification and cloning of a beta-cell-specific zinc transporter, ZnT-8, localized into insulin secretory granules. Diabetes **53:** 2330-2337

Chimienti F, Devergnas S, Pattou F, Schuit F, Garcia-Cuenca R, Vandewalle B, Kerr-Conte J, Van Lommel L, Grunwald D, Favier A, Seve M (2006) In vivo expression and functional characterization of the zinc transporter ZnT8 in glucose-induced insulin secretion. J Cell Sci **119:** 4199-4206

Chimienti F, Favier A, Seve M (2005) ZnT-8, a pancreatic beta-cell-specific zinc transporter. Biometals **18:** 313-317

Chowanadisai W, Graham DM, Keen CL, Rucker RB, Messerli MA (2013) Neurulation and neurite extension require the zinc transporter ZIP12 (slc39a12). Proc Natl Acad Sci U S A **110:** 9903-9908

Chowanadisai W, Lonnerdal B, Kelleher SL (2006) Identification of a mutation in SLC30A2 (ZnT-2) in women with low milk zinc concentration that results in transient neonatal zinc deficiency. J Biol Chem **281:** 39699-39707

Christudoss P, Selvakumar R, Fleming JJ, Mathew G (2010) Zinc levels in paired normal and malignant human stomach and colon tissue. Biomedical Res **21:** 445-450

Chua MMJ, Ortega CE, Sheikh A, Lee M, Abdul-Rassoul H, Hartshorn KL, Dominguez I (2017) CK2 in Cancer: Cellular and Biochemical Mechanisms and Potential Therapeutic Target. Pharmaceuticals (Basel, Switzerland) **10:** 18

Chumsuwan N, Khongkow P, Kaewsuwan S, Kanokwiroon K (2022) Interruptin C, a Radioprotective Agent, Derived from Cyclosorus terminans Protect Normal Breast MCF-10A and Human Keratinocyte HaCaT Cells against Radiation-Induced Damage. Molecules **27:** 3298

Chun H, Korolnek T, Lee CJ, Coyne HJ, 3rd, Winge DR, Kim BE, Petris MJ (2019) An extracellular histidine-containing motif in the zinc transporter ZIP4 plays a role in zinc sensing and zinc-induced endocytosis in mammalian cells. J Biol Chem **294:** 2815-2826

Churchward MA, Butt RH, Lang JC, Hsu KK, Coorssen JR (2005) Enhanced detergent extraction for analysis of membrane proteomes by two-dimensional gel electrophoresis. Proteome Sci **3:** 5

Cole TB, Wenzel HJ, Kafer KE, Schwartzkroin PA, Palmiter RD (1999) Elimination of zinc from synaptic vesicles in the intact mouse brain by disruption of the ZnT3 gene. Proc Natl Acad Sci U S A **96:** 1716-1721

Costello L, Franklin R, Stacey R (1976) Mitochondrial isocitrate dehydrogenase and isocitrate oxidation of rat ventral prostate. Enzyme **21:** 495-506

Costello LC, Fenselau CC, Franklin RB (2011) Evidence for operation of the direct zinc ligand exchange mechanism for trafficking, transport, and reactivity of zinc in mammalian cells. J Inorg Biochem **105:** 589-599

Costello LC, Franklin RB (2006) The clinical relevance of the metabolism of prostate cancer; zinc and tumor suppression: connecting the dots. Mol Cancer **5:** 17

Costello LC, Franklin RB (2014) The status of zinc in the development of hepatocellular cancer: an important, but neglected, clinically established relationship. Cancer Biol Ther **15:** 353-360

Costello LC, Franklin RB (2016) A comprehensive review of the role of zinc in normal prostate function and metabolism; and its implications in prostate cancer. Arch Biochem Biophys **611:** 100-112

Costello LC, Franklin RB, Feng P (2005) Mitochondrial function, zinc, and intermediary metabolism relationships in normal prostate and prostate cancer. Mitochondrion **5:** 143-153

Costello LC, Franklin RB, Zou J, Feng P, Bok R, Swanson MG, Kurhanewicz J (2011) Human prostate cancer ZIP1/zinc/citrate genetic/metabolic relationship in the TRAMP prostate cancer animal model. Cancer Biol Ther **12:** 1078-1084

Costello LC, Levy BA, Desouki MM, Zou J, Bagasra O, Johnson LA, Hanna N, Franklin RB (2011) Decreased zinc and downregulation of ZIP3 zinc uptake transporter in the development of pancreatic adenocarcinoma. Cancer Biol Ther **12:** 297-303

Costello LC, Liu Y, Zou J, Franklin RB (1999) Evidence for a zinc uptake transporter in human prostate cancer cells which is regulated by prolactin and testosterone. J Biol Chem **274:** 17499-17504

Costello LC, Zou J, Desouki MM, Franklin RB (2012) Evidence for changes in RREB-1, ZIP3, and Zinc in the early development of pancreatic adenocarcinoma. J Gastrointest Cancer **43:** 570-578

Coudray N, Valvo S, Hu M, Lasala R, Kim C, Vink M, Zhou M, Provasi D, Filizola M, Tao J, Fang J, Penczek PA, Ubarretxena-Belandia I, Stokes DL (2013) Inward-facing conformation of the zinc transporter YiiP revealed by cryoelectron microscopy. Proc Natl Acad Sci U S A **110:** 2140-2145

Cousins RJ, Blanchard RK, Popp MP, Liu L, Cao J, Moore JB, Green CL (2003) A global view of the selectivity of zinc deprivation and excess on genes expressed in human THP-1 mononuclear cells. Proc Natl Acad Sci U S A **100:** 6952-6957

Cousins RJ, Liuzzi JP, Lichten LA (2006) Mammalian zinc transport, trafficking, and signals. J Biol Chem **281:** 24085-24089

Coyle P, Philcox JC, Carey LC, Rofe AM (2002) Metallothionein: the multipurpose protein. Cell Mol Life Sci **59:** 627-647

Croxford TP, McCormick NH, Kelleher SL (2011) Moderate zinc deficiency reduces testicular Zip6 and Zip10 abundance and impairs spermatogenesis in mice. J Nutr **141:** 359-365

Cyran AM, Zhitkovich A (2022) Heat Shock Proteins and HSF1 in Cancer. Front Oncol **12**

Dai H, Wang L, Li L, Huang Z, Ye L (2021) Metallothionein 1: A New Spotlight on Inflammatory Diseases. Front immunol **12**

Daniels MJ, Jagielnicki M, Yeager M (2020) Structure/Function Analysis of human ZnT8 (SLC30A8): A Diabetes Risk Factor and Zinc Transporter. Curr Res Struct Biol **2:** 144-155

Darbinian JA, Ferrara AM, Van Den Eeden SK, Quesenberry CP, Fireman B, Habel LA (2008) Glycemic status and risk of prostate cancer. Cancer Epidemiol Biomarkers Prev **17:** 628-635

Dasgupta S, Kar K, Barua A, Ghosh D, Kabi B, Dewan K, Chandra A (2022) A significantly non-toxic novel Cobalt(III) Schiff base complex induces apoptosis via G2-M cell cycle arrest in human breast cancer cell line MCF-7. Life Sci **308:** 120963

De A, Ng JC, Seawright AA (1988) Assessment of copper and zinc status of farm horses and training thoroughbreds in south-east Queensland. Aust Vet J **65:** 317-320

Deng S, Wang J, Hou L, Li J, Chen G, Jing B, Zhang X, Yang Z (2013) Annexin A1, A2, A4 and A5 play important roles in breast cancer, pancreatic cancer and laryngeal carcinoma, alone and/or synergistically. Oncol Lett **5:** 107-112

Desouki MM, Geradts J, Milon B, Franklin RB, Costello LC (2007) hZip2 and hZip3 zinc transporters are down regulated in human prostate adenocarcinomatous glands. Mol Cancer **6:** 37

Diez M, Arroyo M, Cerdan F, Munoz M, Martin M, Balibrea J (1989) Serum and tissue trace metal levels in lung cancer. Oncology **46:** 230-234

Dong X, Kong C, Zhang Z, Liu X, Zhan B, Chen Z, Shi D (2014) hZIP1 that is down-regulated in clear cell renal cell carcinoma is negatively associated with the malignant potential of the tumor. Urol Oncol **32:** 885-892

Dowarha D, Chou RH, Yu C (2020) S100A1 blocks the interaction between p53 and mdm2 and decreases cell proliferation activity. PLoS One **15:** e0234152

Dubois N, Willems M, Nguyen-Khac MT, Kroonen J, Goffart N, Deprez M, Bours V, Robe PA (2016) Constitutive activation of casein kinase 2 in glioblastomas: Absence of class restriction and broad therapeutic potential. Int J Oncol **48:** 2445-2452

Dufner-Beattie J, Huang ZL, Geiser J, Xu W, Andrews GK (2005) Generation and characterization of mice lacking the zinc uptake transporter ZIP3. Mol Cell Biol **25:** 5607-5615

Dufner-Beattie J, Kuo YM, Gitschier J, Andrews GK (2004) The adaptive response to dietary zinc in mice involves the differential cellular localization and zinc regulation of the zinc transporters ZIP4 and ZIP5. J Biol Chem **279:** 49082-49090

Dufner-Beattie J, Langmade SJ, Wang F, Eide D, Andrews GK (2003) Structure, function, and regulation of a subfamily of mouse zinc transporter genes. J Biol Chem **278:** 50142-50150

Dufner-Beattie J, Wang F, Kuo YM, Gitschier J, Eide D, Andrews GK (2003) The acrodermatitis enteropathica gene ZIP4 encodes a tissue-specific, zinc-regulated zinc transporter in mice. J Biol Chem **278:** 33474-33481

Dutta A, Sankavaram K, Chong L, Palermo A, Michel RG, Freake HC (2011) Rapid homeostatic response of H4IIE cells to diethylenetriaminepentaacetic acid is not due to changes in the amount or localization of ZnT-1 protein. Nutr Res **31:** 404-411

Ehsani S, Huo H, Salehzadeh A, Pocanschi CL, Watts JC, Wille H, Westaway D, Rogaeva E, George-Hyslop PHS, Schmitt-Ulms G (2011) Family reunion–the ZIP/prion gene family. Prog Neurobiol **93:** 405-420

Ehsani S, Tao R, Pocanschi CL, Ren H, Harrison PM, Schmitt-Ulms G (2011) Evidence for retrogene origins of the prion gene family. PLoS One **6**

Ejaz I, Javed MA, Jan MS, Ikram M, Sadiq A, Ahmad S, Rashid U (2022) Rational design, synthesis, antiproliferative activity against MCF-7, MDA-MB-231 cells, estrogen receptors binding affinity, and computational study of indenopyrimidine-2,5-dione analogs for the treatment of breast cancer. Bioorg Med Chem Lett **64:** 128668

El-Tanani MK, Green CD (1997) Interaction between estradiol and growth factors in the regulation of specific gene expression in MCF-7 human breast cancer cells. J Steroid Biochem Mol Biol **60:** 269-276

Énée É, Kratzer R, Arnoux J-B, Barilleau E, Hamel Y, Marchi C, Beltrand J, Michaud B, Chatenoud L, Robert J-J (2012) ZnT8 is a major CD8+ T cell–recognized autoantigen in pediatric type 1 diabetes. Diabetes **61:** 1779-1784

ErgÜN S, Ferda ARI, Benli E, Altay DU, Noyan T, Erdem H, Arici YK (2022) YY1 and NFYA: Potential tr-KIT Specific Transcription Factors in Prostate Cancer. Mid Blac Sea J Health Sci **8:** 16-21

Estirado S, Fernández-Delgado E, Viñuelas-Zahínos E, Luna-Giles F, Rodríguez AB, Pariente JA, Espino J (2022) Pro-Apoptotic and Anti-Migration Properties of a Thiazoline-Containing Platinum(II) Complex in MDA-MB-231 Breast Cancer Cells: The Role of Melatonin as a Synergistic Agent. Antioxidants **11:** 1971

Falcon-Perez JM, Dell'Angelica EC (2007) Zinc transporter 2 (SLC30A2) can suppress the vesicular zinc defect of adaptor protein 3-depleted fibroblasts by promoting zinc accumulation in lysosomes. Exp Cell Res **313:** 1473-1483

Fan Q, Cai Q, Li P, Wang W, Wang J, Gerry E, Wang TL, Shih IM, Nephew KP, Xu Y (2017) The novel ZIP4 regulation and its role in ovarian cancer. Oncotarget **8:** 90090-90107

Feng P, Li TL, Guan ZX, Franklin RB, Costello LC (2002) Direct effect of zinc on mitochondrial apoptogenesis in prostate cells. Prostate **52:** 311-318

Filhol O, Benitez MJ, Cochet C (2005) A zinc ribbon motif is essential for the formation of functional tetrameric protein kinase CK2. *In* Zinc Finger Proteins. Springer, pp 121-127

Fleige S, Pfaffl MW (2006) RNA integrity and the effect on the real-time qRT-PCR performance. Mol Aspects Med **27:** 126-139

Flores-Morales A, Iglesias-Gato D (2017) Quantitative Mass Spectrometry-Based Proteomic Profiling for Precision Medicine in Prostate Cancer. Front Oncol **7:** 267

Fong LY, Jing R, Smalley KJ, Wang Z-X, Taccioli C, Fan S, Chen H, Alder H, Huebner K, Farber JL, Fiehn O, Croce CM (2018) Human-like hyperplastic prostate with low ZIP1 induced solely by Zn deficiency in rats. Proc Natl Acad Sci U S A **115:** E11091-E11100

Forgrave LM, Wang M, Yang D, DeMarco ML (2022) Proteoforms and their expanding role in laboratory medicine. Pract Lab Med **28:** e00260

Fraga MF, Ballestar E, Villar-Garea A, Boix-Chornet M, Espada J, Schotta G, Bonaldi T, Haydon C, Ropero S, Petrie K, Iyer NG, Pérez-Rosado A, Calvo E, Lopez JA, Cano A, Calasanz MJ, Colomer D, Piris MÁ, Ahn N, Imhof A, Caldas C, Jenuwein T, Esteller M (2005) Loss of acetylation at Lys16 and trimethylation at Lys20 of histone H4 is a common hallmark of human cancer. Nat Genet **37:** 391-400

Franklin RB, Costello LC (2009) The important role of the apoptotic effects of zinc in the development of cancers. J Cell Biochem **106:** 750-757

Franklin RB, Feng P, Milon B, Desouki MM, Singh KK, Kajdacsy-Balla A, Bagasra O, Costello LC (2005) hZIP1 zinc uptake transporter down regulation and zinc depletion in prostate cancer. Mol Cancer **4:** 32

Franklin RB, Levy BA, Zou J, Hanna N, Desouki MM, Bagasra O, Johnson LA, Costello LC (2012) ZIP14 zinc transporter downregulation and zinc depletion in the development and progression of hepatocellular cancer. J Gastrointest Cancer **43:** 249-257

Franklin RB, Ma J, Zou J, Guan Z, Kukoyi BI, Feng P, Costello LC (2003) Human ZIP1 is a major zinc uptake transporter for the accumulation of zinc in prostate cells. J Inorg Biochem **96:** 435-442

Franklin RB, Zou J, Costello LC (2014) The cytotoxic role of RREB1, ZIP3 zinc transporter, and zinc in human pancreatic adenocarcinoma. Cancer Biol Ther **15:** 1431-1437

Franz MC, Anderle P, Burzle M, Suzuki Y, Freeman MR, Hediger MA, Kovacs G (2013) Zinc transporters in prostate cancer. Mol Aspects Med **34:** 735-741

Franz MC, Simonin A, Graeter S, Hediger MA, Kovacs G (2014) Development of the First Fluorescence Screening Assay for the SLC39A2 Zinc Transporter. J Biomol Screen **19:** 909-916

Freeman WM, Walker SJ, Vrana KE (1999) Quantitative RT-PCR: pitfalls and potential. BioTechniques **26:** 112-125

Fujishiro H, Kambe T (2022) Manganese transport in mammals by zinc transporter family proteins, ZNT and ZIP. J Pharmacol Sci **148:** 125-133

Fukada T, Civic N, Furuichi T, Shimoda S, Mishima K, Higashiyama H, Idaira Y, Asada Y, Kitamura H, Yamasaki S, Hojyo S, Nakayama M, Ohara O, Koseki H, Dos Santos HG, Bonafe L, Ha-Vinh R, Zankl A, Unger S, Kraenzlin ME, Beckmann JS, Saito I, Rivolta C, Ikegawa S, Superti-Furga A, Hirano T (2008) The zinc transporter SLC39A13/ZIP13 is required for connective tissue development; its involvement in BMP/TGF-beta signaling pathways. PLoS One **3:** e3642

Fukada T, Kambe T (2018) Welcome to the World of Zinc Signaling. Int J Mol Sci **19**

Fukunaka A, Suzuki T, Kurokawa Y, Yamazaki T, Fujiwara N, Ishihara K, Migaki H, Okumura K, Masuda S, Yamaguchi-Iwai Y, Nagao M, Kambe T (2009) Demonstration and characterization of the heterodimerization of ZnT5 and ZnT6 in the early secretory pathway. J Biol Chem **284:** 30798-30806

Gaetke L, McClain C, Talwalkar R, Shedlofsky SJAJoP-E, Metabolism (1997) Effects of endotoxin on zinc metabolism in human volunteers. Am J Physiol **272:** E952-E956

Gaither LA, Eide DJ (2000) Functional expression of the human hZIP2 zinc transporter. J Biol Chem **275:** 5560-5564

Gaither LA, Eide DJ (2001) Eukaryotic zinc transporters and their regulation. Biometals **14:** 251-270

Gaither LA, Eide DJ (2001) The human ZIP1 transporter mediates zinc uptake in human K562 erythroleukemia cells. J Biol Chem **276:** 22258-22264

Ganesan T, Sinniah A, Ibrahim ZA, Chik Z, Alshawsh MA (2020) Annexin A1: a bane or a boon in cancer? a systematic review. Molecules **25**

Garbis S, Lubec G, Fountoulakis M (2005) Limitations of current proteomics technologies. J Chromatogr A **1077:** 1-18

Garrett SH, Sens MA, Shukla D, Flores L, Somji S, Todd JH, Sens DA (2000) Metallothionein isoform 1 and 2 gene expression in the human prostate: Downregulation of MT-1X in advanced prostate cancer. Prostate **43:** 125-135

Gartmann L, Wex T, Grüngreiff K, Reinhold D, Kalinski T, Malfertheiner P, Schütte K (2018) Expression of zinc transporters ZIP4, ZIP14 and ZnT9 in hepatic carcinogenesis—an immunohistochemical study. J Trace Elem Med Biol **49:** 35-42

Gauci VJ, Padula MP, Coorssen JR (2013) Coomassie blue staining for high sensitivity gel-based proteomics. J Proteomics **90:** 96-106

Geiser J, Venken KJ, De Lisle RC, Andrews GK (2012) A mouse model of acrodermatitis enteropathica: loss of intestine zinc transporter ZIP4 (Slc39a4) disrupts the stem cell niche and intestine integrity. PLoS Genet **8:** e1002766

Giacconi R, Malavolta M, Costarelli L, Busco F, Galeazzi R, Bernardini G, Gasparini N, Mocchegiani E (2012) Comparison of intracellular zinc signals in nonadherent lymphocytes from young-adult and elderly donors: role of zinc transporters (Zip family) and proinflammatory cytokines. J Nutr Biochem **23:** 1256-1263

Giacconi R, Muti E, Malavolta M, Cardelli M, Pierpaoli S, Cipriano C, Costarelli L, Tesei S, Saba V, Mocchegiani E (2008) A novel Zip2 Gln/Arg/Leu codon 2 polymorphism is associated with carotid artery disease in aging. Rejuvenation Res **11:** 297-300

Giedroc DP, Chen X, Apuy JL (2001) Metal response element (MRE)-binding transcription factor-1 (MTF-1): structure, function, and regulation. Antioxid Redox Signal **3:** 577-596

Gillet J-P, Varma S, Gottesman MM (2013) The clinical relevance of cancer cell lines. J Natl Cancer Inst **105:** 452-458

Girijashanker K, He L, Soleimani M, Reed JM, Li H, Liu Z, Wang B, Dalton TP, Nebert DW (2008) Slc39a14 gene encodes ZIP14, a metal/bicarbonate symporter: similarities to the ZIP8 transporter. Mol Pharmacol **73:** 1413-1423

Golan Y, Berman B, Assaraf YG (2015) Heterodimerization, altered subcellular localization, and function of multiple zinc transporters in viable cells using bimolecular fluorescence complementation. J Biol Chem **290:** 9050-9063

Golan Y, Kambe T, Assaraf YG (2017) The role of the zinc transporter SLC30A2/ZnT2 in transient neonatal zinc deficiency. Metallomics **9:** 1352-1366

Gong Z, Neuhouser ML, Goodman PJ, Albanes D, Chi C, Hsing AW, Lippman SM, Platz EA, Pollak MN, Thompson IM (2006) Obesity, diabetes, and risk of prostate cancer: results from the prostate cancer prevention trial. Cancer Epidemiol Biomarkers Prev **15:** 1977-1983

Görg A, Obermaier C, Boguth G, Harder A, Scheibe B, Wildgruber R, Weiss W (2000) The current state of two-dimensional electrophoresis with immobilized pH gradients. Electrophoresis **21:** 1037-1053

Gray GK, McFarland BC, Rowse AL, Gibson SA, Benveniste EN (2014) Therapeutic CK2 inhibition attenuates diverse prosurvival signaling cascades and decreases cell viability in human breast cancer cells. Oncotarget **5:** 6484-6496

Grzywacz A, Gdula-Argasińska J, Muszyńska B, Tyszka-Czochara M, Librowski T, Opoka W (2015) Metal responsive transcription factor 1 (MTF-1) regulates zinc dependent cellular processes at the molecular level. Acta Biochim Pol **62:** 491-498

Guerra B, Boldyreff B, Sarno S, Cesaro L, Issinger OG, Pinna LA (1999) CK2: A protein kinase in need of control. Pharmacol Therapeut **82:** 303-313

Gumulec J, Masarik M, Adam V, Eckschlager T, Provaznik I, Kizek R (2014) Serum and tissue zinc in epithelial malignancies: a meta-analysis. PLoS One **9:** e99790

Gumulec J, Masarik M, Krizkova S, Adam V, Hubalek J, Hrabeta J, Eckschlager T, Stiborova M, Kizek R (2011) Insight to physiology and pathology of zinc(II) ions and their actions in breast and prostate carcinoma. Curr Med Chem **18:** 5041-5051

Guo L, Lichten LA, Ryu MS, Liuzzi JP, Wang F, Cousins RJ (2010) STAT5-glucocorticoid receptor interaction and MTF-1 regulate the expression of ZnT2 (Slc30a2) in pancreatic acinar cells. Proc Natl Acad Sci U S A **107:** 2818-2823

Gupta S, Chai J, Cheng J, D'Mello R, Chance MR, Fu D (2014) Visualizing the kinetic power stroke that drives proton-coupled zinc(ii) transport. Nature **512:** 101-104

Gurioli G, Martignano F, Salvi S, Costantini M, Gunelli R, Casadio V (2018) GSTP1 methylation in cancer: a liquid biopsy biomarker? Clin Chem Lab Med **56:** 702-717

Guthrie GJ, Aydemir TB, Troche C, Martin AB, Chang S-M, Cousins RJ (2015) Influence of ZIP14 (slc39A14) on intestinal zinc processing and barrier function. Am J Physiol Gastrointest Liver Physiol **308:** G171-G178

Guyon I, Fritsche H, Choppa P, Yang L-Y, Barnhill S (2009) A Four-Gene Expression Signature for Prostate Cancer Cells Consisting of UAP1, PDLIM5, IMPDH2, and HSPD1. Urotoday Int J **02**

Gyulkhandanyan AV, Lu H, Lee SC, Bhattacharjee A, Wijesekara N, Fox JE, MacDonald PE, Chimienti F, Dai FF, Wheeler MB (2008) Investigation of transport mechanisms and regulation of intracellular Zn2+ in pancreatic alpha-cells. J Biol Chem **283:** 10184-10197

Hahn S, Roberts S (2000) The zinc ribbon domains of the general transcription factors TFIIB and Brf: conserved functional surfaces but different roles in transcription initiation. Genes Dev **14:** 719-730

Hara T, Yoshigai E, Ohashi T, Fukada T (2022) Zinc transporters as potential therapeutic targets: An updated review. J Pharmacol Sci **148:** 221-228

Hardefeldt PJ, Edirimanne S, Eslick GD (2012) Diabetes increases the risk of breast cancer: a meta-analysis. Endocr Relat Cancer **19:** 793

Hardy AB, Prentice KJ, Froese S, Liu Y, Andrews GK, Wheeler MB (2015) Zip4 mediated zinc influx stimulates insulin secretion in pancreatic beta cells. PLoS One **10:** e0119136

Hardyman J, Tyson J, Jackson K, Aldridge C, Cockell S, Wakeling L, Valentine R, Ford D (2016) Zinc sensing by metal-responsive transcription factor 1 (MTF1) controls metallothionein and ZnT1 expression to buffer the sensitivity of the transcriptome response to zinc. Metallomics **8:** 337-343

Hartiala J, Bennett BJ, Tang WW, Wang Z, Stewart AF, Roberts R, McPherson R, Lusis AJ, Hazen SL, Allayee H (2014) Comparative genome-wide association studies in mice and humans for trimethylamine N-oxide, a proatherogenic metabolite of choline and L-carnitine. Arterioscler Thromb Vasc Biol **34:** 1307-1313

Hasumi M, Suzuki K, Matsui H, Koike H, Ito K, Yamanaka H (2003) Regulation of metallothionein and zinc transporter expression in human prostate cancer cells and tissues. Cancer Lett **200:** 187-195

Hathaway GM, Traugh JA (1979) Cyclic nucleotide-independent protein kinases from rabbit reticulocytes. Purification of casein kinases. J Biol Chem **254:** 762-768

He L, Girijashanker K, Dalton TP, Reed J, Li H, Soleimani M, Nebert DW (2006) ZIP8, member of the solute-carrier-39 (SLC39) metal-transporter family: characterization of transporter properties. Mol Pharmacol **70:** 171-180

Hendrickx G, Borra VM, Steenackers E, Yorgan TA, Hermans C, Boudin E, Waterval JJ, Jansen IDC, Aydemir TB, Kamerling N, Behets GJ, Plumeyer C, D'Haese PC, Busse B, Everts V, Lammens M, Mortier G, Cousins RJ, Schinke T, Stokroos RJ, Manni JJ, Van Hul W (2018) Conditional mouse models support the role of SLC39A14 (ZIP14) in Hyperostosis Cranialis Interna and in bone homeostasis. PLoS Genet **14:** e1007321

Hennigar SR, Kelleher SL (2012) Zinc networks: the cell-specific compartmentalization of zinc for specialized functions. Biol Chem **393:** 565-578.

Hernroth B, Tassidis H (2023) Viability effects on cell cycle synchronization of different prostate cancer cell lines: A brief report. Exp Biomed Res **6:** 1-5

Hershfinkel M, Silverman WF, Sekler I (2007) The zinc sensing receptor, a link between zinc and cell signaling. *In* Molecular Medicine, Vol 13. Springer, pp 331-336

Hessenauer A, Montenarh M, Gotz C (2003) Inhibition of CK2 activity provokes different responses in hormone-sensitive and hormone-refractory prostate cancer cells. Int J Oncol **22:** 1263-1270

Hoch E, Lin W, Chai J, Hershfinkel M, Fu D, Sekler I (2012) Histidine pairing at the metal transport site of mammalian ZnT transporters controls Zn2+ over Cd2+ selectivity. Proc Natl Acad Sci U S A **109:** 7202-7207

Hogstrand C, Kille P, Ackland ML, Hiscox S, Taylor KM (2013) A mechanism for epithelial-mesenchymal transition and anoikis resistance in breast cancer triggered by zinc channel ZIP6 and STAT3 (signal transducer and activator of transcription 3). Biochem J **455:** 229-237

Hogstrand C, Kille P, Nicholson RI, Taylor KM (2009) Zinc transporters and cancer: a potential role for ZIP7 as a hub for tyrosine kinase activation. Trends Mol Med **15:** 101-111

Hojyo S, Fukada T, Shimoda S, Ohashi W, Bin BH, Koseki H, Hirano T (2011) The zinc transporter SLC39A14/ZIP14 controls G-protein coupled receptor-mediated signaling required for systemic growth. PLoS One **6:** e18059

Homma MK, Kiko Y, Hashimoto Y, Nagatsuka M, Katagata N, Masui S, Homma Y, Nomizu T (2021) Intracellular localization of CK2α as a prognostic factor in invasive breast carcinomas. Cancer Sci **112:** 619-628

Hsieh M-C, Lee T-C, Cheng S-M, Tu S-T, Yen M-H, Tseng C-H (2012) The influence of type 2 diabetes and glucose-lowering therapies on cancer risk in the Taiwanese. Exp Diabetes Res **2012**

Hu J (2021) Toward unzipping the ZIP metal transporters: structure, evolution, and implications on drug discovery against cancer. FEBS J **288:** 5805-5825

Huang C, Cui X, Sun X, Yang J, Li M (2016) Zinc transporters are differentially expressed in human non-small cell lung cancer. Oncotarget **7:** 66935

Huang L, Gitschier J (1997) A novel gene involved in zinc transport is deficient in the lethal milk mouse. Nat Genet **17:** 292-297

Huang L, Kirschke CP, Gitschier J (2002) Functional characterization of a novel mammalian zinc transporter, ZnT6. J Biol Chem **277:** 26389-26395

Huang L, Kirschke CP, Zhang Y (2006) Decreased intracellular zinc in human tumorigenic prostate epithelial cells: a possible role in prostate cancer progression. Cancer Cell Int **6:** 10

Huang L, Kirschke CP, Zhang Y, Yu YY (2005) The ZIP7 gene (Slc39a7) encodes a zinc transporter involved in zinc homeostasis of the Golgi apparatus. J Biol Chem **280:** 15456-15463

Huang Q, Du J, Merriman C, Gong Z (2019) Genetic, functional, and immunological study of ZnT8 in diabetes. Int J Endocrinol **2019**

Huggins C (1947) The prostatic secretion. Harvey Lectures **42:** 148-193

Hynds RE, Vladimirou E, Janes SM (2018) The secret lives of cancer cell lines. Dis Model Mech **11**

Iguchi K, Morihara N, Usui S, Hayama M, Sugimura Y, Hirano K (2011) Castration- and aging-induced changes in the expression of zinc transporter and metallothionein in rat prostate. J Androl **32:** 144-150

Iguchi K, Otsuka T, Usui S, Sugimura Y, Hirano K (2006) Correlation between ZIP2 messenger RNA expression and zinc level in rat lateral prostate. Biol Trace Elem Res **112:** 159-167

Inoue K, Matsuda K, Itoh M, Kawaguchi H, Tomoike H, Aoyagi T, Nagai R, Hori M, Nakamura Y, Tanaka T (2002) Osteopenia and male-specific sudden cardiac death in mice lacking a zinc transporter gene, Znt5. Hum Mol Genet **11:** 1775-1784

Inoue Y, Hasegawa S, Ban S, Yamada T, Date Y, Mizutani H, Nakata S, Tanaka M, Hirashima N (2014) ZIP2 protein, a zinc transporter, is associated with keratinocyte differentiation. J Biol Chem **289:** 21451-21462

Irnaten M, Duff A, Clark A, O'Brien C (2021) Intra-Cellular Calcium Signaling Pathways (PKC, RAS/RAF/MAPK, PI3K) in Lamina Cribrosa Cells in Glaucoma. J Clin Med **10:** 62

Jackson KA, Helston RM, McKay JA, O'Neill ED, Mathers JC, Ford D (2007) Splice variants of the human zinc transporter ZnT5 (SLC30A5) are differentially localized and regulated by zinc through transcription and mRNA stability. J Biol Chem **282:** 10423-10431

Jarnuczak AF, Najgebauer H, Barzine M, Kundu DJ, Ghavidel F, Perez-Riverol Y, Papatheodorou I, Brazma A, Vizcaíno JA (2021) An integrated landscape of protein expression in human cancer. Sci Data **8:** 115

Jen J, Wang Y-C (2016) Zinc finger proteins in cancer progression. J Biomed Sci **23:** 53

Jeong J, Eide DJ (2013) The SLC39 family of zinc transporters. Mol Aspects Med **34:** 612-619

Jeong J, Walker JM, Wang F, Park JG, Palmer AE, Giunta C, Rohrbach M, Steinmann B, Eide DJ (2012) Promotion of vesicular zinc efflux by ZIP13 and its implications for spondylocheiro dysplastic Ehlers-Danlos syndrome. Proc Natl Acad Sci U S A **109:** E3530-3538

Jin H, Liu P, Wu Y, Meng X, Wu M, Han J, Tan X (2018) Exosomal zinc transporter ZIP4 promotes cancer growth and is a novel diagnostic biomarker for pancreatic cancer. Cancer Sci **109:** 2946-2956

Jin J, Li Z, Liu J, Wu Y, Gao X, He Y (2015) Knockdown of zinc transporter ZIP5 (SLC39A5) expression significantly inhibits human esophageal cancer progression. Oncol Rep **34:** 1431-1439

Jin R, Bay B, Chow V, Tan P, Lin V (2000) Metallothionein 1E mRNA is highly expressed in oestrogen receptor-negative human invasive ductal breast cancer. Br J Cancer **83:** 319-323

Jin X, Wang D, Lei M, Guo Y, Cui Y, Chen F, Sun W, Chen X (2022) TPI1 activates the PI3K/AKT/mTOR signaling pathway to induce breast cancer progression by stabilizing CDCA5. J Transl Med **20:** 191

Johnson AJ, Veljanoski F, O'Doherty PJ, Zaman MS, Petersingham G, Bailey TD, Münch G, Kersaitis C, Wu MJ (2016) Molecular insight into arsenic toxicity via the genome-wide deletion mutant screening of Saccharomyces cerevisiae. Metallomics **8:** 228-235

Johnson AJ, Wu MJ (2016) The New Role for an Old Kinase: Protein Kinase CK2 Regulates Metal Ion Transport. Pharmaceuticals (Basel) **9**

Johnson AJ, Zaman MS, Veljanoski F, Phrakaysone AA, Li S, O'Doherty PJ, Petersingham G, Perrone GG, Molloy MP, Wu MJ (2017) Unravelling the role of protein kinase CK2 in metal toxicity using gene deletion mutants. Metallomics **9:** 301-308

Johnson FV, Patrick. J. O'Doherty, Mohammad S. Zaman, Gayani Petersingham, Trevor D. Bailey, Gerald Münch, Cindy Kersaitisa and Ming J. Wu (2016) Revelation of molecular basis for chromium toxicity by phenotypes of Saccharomyces cerevisiae gene deletion mutants. Metallomics **8:** 542-550

Johnson LA, Kanak MA, Kajdacsy-Balla A, Pestaner JP, Bagasra O (2010) Differential zinc accumulation and expression of human zinc transporter 1 (hZIP1) in prostate glands. Methods. **52:** 316-321

Johnston SR (2010) New strategies in estrogen receptor-positive breast cancer. Clin Cancer Res **16:** 1979-1987

Jordan VC (2003) Tamoxifen: a most unlikely pioneering medicine. Nat Rev Drug Discov **2:** 205-213

Kagara N, Tanaka N, Noguchi S, Hirano T (2007) Zinc and its transporter ZIP10 are involved in invasive behavior of breast cancer cells. Cancer Sci **98:** 692-697.

Kaler P, Prasad R (2007) Molecular cloning and functional characterization of novel zinc transporter rZip10 (Slc39a10) involved in zinc uptake across rat renal brush-border membrane. Am J Physiol Renal Physiol **292:** F217-229

Kambe T, Narita H, Yamaguchi-Iwai Y, Hirose J, Amano T, Sugiura N, Sasaki R, Mori K, Iwanaga T, Nagao M (2002) Cloning and Characterization of a Novel Mammalian Zinc Transporter, Zinc Transporter 5, Abundantly Expressed in Pancreatic β Cells, Vol 277

Kambe T, Taylor KM, Fu D (2021) Zinc transporters and their functional integration in mammalian cells. J Biol Chem **296:** 100320

Kambe T, Tsuji T, Hashimoto A, Itsumura N (2015) The Physiological, Biochemical, and Molecular Roles of Zinc Transporters in Zinc Homeostasis and Metabolism. Physiol Rev **95:** 749-784.

Kamizono A, Nishizawa M, Teranishi Y, Murata K, Kimura A (1989) Identification of a gene conferring resistance to zinc and cadmium ions in the yeast Saccharomyces cerevisiae. Mol Gen Genet **219:** 161-167

Kang J, Yu Y, Jeong S, Lee H, Heo HJ, Park JJ, Na HS, Ko DS, Kim YH (2020) Prognostic role of high cathepsin D expression in breast cancer: a systematic review and meta-analysis. Ther Adv Med Oncol **12:** 1758835920927838

Kang X, Chen R, Zhang J, Li G, Dai PG, Chen C, Wang HJ (2015) Expression Profile Analysis of Zinc Transporters (ZIP4, ZIP9, ZIP11, ZnT9) in Gliomas and their Correlation with IDH1 Mutation Status. Asian Pac J Cancer Prev **16:** 3355-3360

Kasana S, Din J, Maret W (2015) Genetic causes and gene–nutrient interactions in mammalian zinc deficiencies: acrodermatitis enteropathica and transient neonatal zinc deficiency as examples. J Trace Elem Med Biol **29:** 47-62

Kasper G, Weiser AA, Rump A, Sparbier K, Dahl E, Hartmann A, Wild P, Schwidetzky U, Castanos-Velez E, Lehmann K (2005) Expression levels of the putative zinc transporter LIV-1 are associated with a better outcome of breast cancer patients. Int J Cancer **117:** 961-973

Kasper JS, Liu Y, Giovannucci E (2009) Diabetes mellitus and risk of prostate cancer in the health professionals follow-up study. Int J Cancer **124:** 1398-1403

Katsogiannou M, Boyer J-B, Valdeolivas A, Remy E, Calzone L, Audebert S, Rocchi P, Camoin L, Baudot A (2019) Integrative proteomic and phosphoproteomic profiling of prostate cell lines. PLoS One **14:** e0224148

Kaur G, Subramanian S (2017) Evolutionary analysis of a novel zinc ribbon in the N-terminal region of threonine synthase. Cell Cycle **16:** 1918-1926

Kazi TG, Afridi HI, Jamali MK, Arain MB, Jalbani N, Syed N (2007) Evaluation of zinc status in whole blood and scalp hair of female cancer patients. Clinica Chimica Acta **379:** 66-70

Keilin D, Mann T (1939) Carbonic anhydrase. Nature **144:** 442.

Keilin D, Mann T (1940) Carbonic anhydrase. Purification and nature of the enzyme. Biochem J **34:** 1163-1176

Kelleher SL, Lonnerdal B (2005) Zip3 plays a major role in zinc uptake into mammary epithelial cells and is regulated by prolactin. Am J Physiol Cell Physiol **288:** C1042-1047

Kelleher SL, Lopez V, Lonnerdal B, Dufner-Beattie J, Andrews GK (2009) Zip3 (Slc39a3) functions in zinc reuptake from the alveolar lumen in lactating mammary gland. Am J Physiol Regul Integr Comp Physiol **297:** R194-201

Kelleher SL, McCormick NH, Velasquez V, Lopez V (2011) Zinc in specialized secretory tissues: roles in the pancreas, prostate, and mammary gland. Adv Nutr **2:** 101-111

Kelleher SL, Seo YA, Lopez V (2009) Mammary gland zinc metabolism: regulation and dysregulation. Genes Nutr **4:** 83-94

Kelleher SL, Velasquez V, Croxford TP, McCormick NH, Lopez V, MacDavid J (2012) Mapping the zinc-transporting system in mammary cells: molecular analysis reveals a phenotype-dependent zinc-transporting network during lactation. J Cell Physiol **227:** 1761-1770

Kelliher MA, Seldin DC, Leder P (1996) Tal-1 induces T cell acute lymphoblastic leukemia accelerated by casein kinase IIalpha. EMBO J **15:** 5160-5166

Khaghanzadeh N, Nakamura K, Kuramitsu Y, Ghaderi A, Mojtahedi Z (2016) Immune-associated proteins with potential in vivo anti-tumor activities are upregulated in lung cancer cells treated with umbelliprenin: A proteomic approach. Oncol Lett **12:** 5295-5302

Khan AQ, Kuttikrishnan S, Siveen KS, Prabhu KS, Shanmugakonar M, Al-Naemi HA, Haris M, Dermime S, Uddin S (2019) RAS-mediated oncogenic signaling pathways in human malignancies. *In* Seminars in cancer biology, Vol 54. Elsevier, pp 1-13

Kim BE, Wang F, Dufner-Beattie J, Andrews GK, Eide DJ, Petris MJ (2004) Zn2+-stimulated endocytosis of the mZIP4 zinc transporter regulates its location at the plasma membrane. J Biol Chem **279:** 4523-4530

Kim JH, Jeon J, Shin M, Won Y, Lee M, Kwak JS, Lee G, Rhee J, Ryu JH, Chun CH, Chun JS (2014) Regulation of the catabolic cascade in osteoarthritis by the zinc-ZIP8-MTF1 axis. Cell **156:** 730-743

Kim KR, Park SE, Hong JY, Koh JY, Cho DH, Hwang JJ, Kim YH (2022) Zinc enhances autophagic flux and lysosomal function through transcription factor EB activation and V-ATPase assembly. Front Cell Neurosci **16:** 895750

Kim M-H, Aydemir TB, Kim J, Cousins RJ (2017) Hepatic ZIP14-mediated zinc transport is required for adaptation to endoplasmic reticulum stress. Proc Natl Acad Sci U S A **114:** E5805-E5814

Kim S, Jung Y, Kim D, Koh H, Chung J (2000) Extracellular zinc activates p70 S6 kinase through the phosphatidylinositol 3-kinase signaling pathway. J Biol Chem **275:** 25979-25984

Kim S, You D, Jeong Y, Yu J, Kim SW, Nam SJ, Lee JE (2019) TP53 upregulates α-smooth muscle actin expression in tamoxifen-resistant breast cancer cells. Oncol Rep **41:** 1075-1082

Kimura T, Kambe T (2016) The Functions of Metallothionein and ZIP and ZnT Transporters: An Overview and Perspective. Int J Mol Sci **17:** 336

Kirschke CP, Huang L (2003) ZnT7, a novel mammalian zinc transporter, accumulates zinc in the Golgi apparatus. J Biol Chem **278:** 4096-4102

Kirschke CP, Huang L (2008) Expression of the ZNT (SLC30) family members in the epithelium of the mouse prostate during sexual maturation. J Mol Histol **39:** 359-370

Knoell DL, Smith D, Bao S, Sapkota M, Wyatt TA, Zweier JL, Flury J, Borchers MT, Knutson M (2020) Imbalance in zinc homeostasis enhances lung Tissue Loss following cigarette smoke exposure. J Trace Elem Med Biol**:** 126483

Koch M, Bhattacharya S, Kehl T, Gimona M, Vašák M, Chazin W, Heizmann CW, Kroneck PMH, Fritz G (2007) Implications on zinc binding to S100A2. Biochim Biophys Acta **1773:** 457-470

Koepke L, Winter B, Grenzner A, Regensburger K, Engelhart S, van der Merwe JA, Krebs S, Blum H, Kirchhoff F, Sparrer KMJ (2020) An improved method for high-throughput quantification of autophagy in mammalian cells. Sci Rep **10:** 12241

Kolenko V, Teper E, Kutikov A, Uzzo R (2013) Zinc and zinc transporters in prostate carcinogenesis. Nat Rev Urol **10:** 219

Kong BY, Duncan FE, Que EL, Kim AM, O'Halloran TV, Woodruff TK (2014) Maternally-derived zinc transporters ZIP6 and ZIP10 drive the mammalian oocyte-to-egg transition. Mol Hum Reprod **20:** 1077-1089

Kramerov AA, Ljubimov AV (2012) Focus on molecules: protein kinase CK2. Exp Eye Res **101:** 111-112

Krężel A, Maret W (2017) The Functions of Metamorphic Metallothioneins in Zinc and Copper Metabolism. Int J Mol Sci **18:** 1237

Krishna SS, Majumdar I, Grishin NV (2003) Structural classification of zinc fingers: survey and summary. Nucleic Acids Res **31:** 532-550

Kudo H, Doi Y, Nishino T, Nara S, Hamasaki K, Fujimoto S (2000) Dietary zinc deficiency decreases glutathione S-transferase expression in the rat olfactory epithelium. J Nutr **130:** 38-44

Kumar A, Chatopadhyay T, Raziuddin M, Ralhan R (2007) Discovery of deregulation of zinc homeostasis and its associated genes in esophageal squamous cell carcinoma using cDNA microarray. Int J Cancer **120:** 230-242

Kumar VL, Majumder PK (1995) Prostate gland: structure, functions and regulation. Int Urol Nephrol **27:** 231-243

Kury S, Dreno B, Bezieau S, Giraudet S, Kharfi M, Kamoun R, Moisan JP (2002) Identification of SLC39A4, a gene involved in acrodermatitis enteropathica. Nat Genet **31:** 239-240

Kwon YW, Chang IH, Kim KD, Kim YS, Myung SC, Kim MK, Kim TH (2010) Significance of S100A2 and S100A4 Expression in the Progression of Prostate Adenocarcinoma. Korean J Urol **51:** 456-462

Laity JH, Lee BM, Wright PE (2001) Zinc finger proteins: new insights into structural and functional diversity. Curr Opin Struct Biol **11:** 39-46

Landesman-Bollag E, Romieu-Mourez R, Song DH, Sonenshein GE, Cardiff RD, Seldin DC (2001) Protein kinase CK2 in mammary gland tumorigenesis. Oncogene **20:** 3247-3257

Lang C, Murgia C, Leong M, Tan L-W, Perozzi G, Knight D, Ruffin R, Zalewski P (2007) Anti-inflammatory effects of zinc and alterations in zinc transporter mRNA in mouse models of allergic inflammation. Am J Physiol Lung Cell Mol Physiol **292:** L577-L584

Langmade SJ, Ravindra R, Daniels PJ, Andrews GK (2000) The transcription factor MTF-1 mediates metal regulation of the mouse ZnT1 gene. J Biol Chem **275:** 34803-34809

Laramas M, Pasquier D, Filhol O, Ringeisen F, Descotes JL, Cochet C (2007) Nuclear localization of protein kinase CK2 catalytic subunit (CK2alpha) is associated with poor prognostic factors in human prostate cancer. Eur J Cancer **43:** 928-934

Larner F, Woodley LN, Shousha S, Moyes A, Humphreys-Williams E, Strekopytov S, Halliday AN, Rehkämper M, Coombes RC (2015) Zinc isotopic compositions of breast cancer tissue. Metallomics. **7:** 112-117

Lazarczyk M, Pons C, Mendoza JA, Cassonnet P, Jacob Y, Favre M (2008) Regulation of cellular zinc balance as a potential mechanism of EVER-mediated protection against pathogenesis by cutaneous oncogenic human papillomaviruses. J Exp Med **205:** 35-42

Lee M-G, Choi M-A, Chae S, Kang M-A, Jo H, Baek J-m, In K-R, Park H, Heo H, Jang D (2019) Loss of the dermis zinc transporter ZIP13 promotes the mildness of fibrosarcoma by inhibiting autophagy. Sci Rep **9:** 1-11

Lee S, Hennigar SR, Alam S, Nishida K, Kelleher SL (2015) Essential Role for Zinc Transporter 2 (ZnT2)-mediated Zinc Transport in Mammary Gland Development and Function during Lactation. J Biol Chem **290:** 13064-13078

Lehvy AI, Horev G, Golan Y, Glaser F, Shammai Y, Assaraf YG (2019) Alterations in ZnT1 expression and function lead to impaired intracellular zinc homeostasis in cancer. Cell Death Discov **5:** 144

Lemaire K, Ravier MA, Schraenen A, Creemers JW, Van de Plas R, Granvik M, Van Lommel L, Waelkens E, Chimienti F, Rutter GA (2009) Insulin crystallization depends on zinc transporter ZnT8 expression, but is not required for normal glucose homeostasis in mice. Proc Natl Acad Sci U S A **106:** 14872-14877

Leung KW, Liu M, Xu X, Seiler MJ, Barnstable CJ, Tombran-Tink J (2008) Expression of ZnT and ZIP zinc transporters in the human RPE and their regulation by neurotrophic factors. Invest Ophthalmol Vis Sci **49:** 1221-1231

Li D, Achkar J-P, Haritunians T, Jacobs JP, Hui KY, D'Amato M, Brand S, Radford-Smith G, Halfvarson J, Niess J-H (2016) A pleiotropic missense variant in SLC39A8 is associated with Crohn's disease and human gut microbiome composition. Gastroenterology **151:** 724-732

Li D, Stovall DB, Wang W, Sui G (2020) Advances of zinc signaling studies in prostate cancer. Int J Mol Sci **21:** 667

Li H, Lu Y-F, Chen H, Liu J (2017) Dysregulation of metallothionein and circadian genes in human hepatocellular carcinoma. Chronobiol Int **34:** 192-202

Li M, Zhang Y, Bharadwaj U, Zhai QJ, Ahern CH, Fisher WE, Brunicardi FC, Logsdon CD, Chen C, Yao Q (2009) Down-regulation of ZIP4 by RNA interference inhibits pancreatic cancer growth and increases the survival of nude mice with pancreatic cancer xenografts. Clin Cancer Res **15:** 5993-6001

Li M, Zhang Y, Liu Z, Bharadwaj U, Wang H, Wang X, Zhang S, Liuzzi JP, Chang SM, Cousins RJ, Fisher WE, Brunicardi FC, Logsdon CD, Chen C, Yao Q (2007) Aberrant expression of zinc transporter ZIP4 (SLC39A4) significantly contributes to human pancreatic cancer pathogenesis and progression. Proc Natl Acad Sci U S A **104:** 18636-18641

Li M, Zhang Y, Liu Z, Bharadwaj U, Wang H, Wang X, Zhang S, Liuzzi JP, Chang SM, Cousins RJ, Fisher WE, Brunicardi FC, Logsdon CD, Chen C, Yao Q (2007) Aberrant expression of zinc transporter ZIP4 (SLC39A4) significantly contributes to human pancreatic cancer pathogenesis and progression. Proc Natl Acad Sci U S A **104:** 18636-18641

Li Q, Jin J, Liu J, Wang L, He Y (2016) Knockdown of Zinc Transporter ZIP5 by RNA Interference Inhibits Esophageal Cancer Growth In Vivo. Oncol Res **24:** 205-214

Li T, Jiao R, Ma J, Zang J, Zhao G, Zhang T (2022) Zinc binding strength of proteins dominants zinc uptake in Caco-2 cells. RSC Adv **12:** 21122-21128

Li WM, Ke HL, Kuo YH, Lai HY, Chan TC, Hsing CH, Hsieh KL, Li WS, Chen TJ, Wei YC, Wu WJ, Huang SK, Li CF (2022) High MT2A Expression Predicts Worse Prognosis in Patients with Urothelial Carcinoma. Oncology **100:** 485-497

Li X, Han M, Zhang H, Liu F, Pan Y, Zhu J, Liao Z, Chen X, Zhang B (2022) Structures and biological functions of zinc finger proteins and their roles in hepatocellular carcinoma. Biomark Res **10:** 2

Li Z, Liu JY, Zhang JT (2009) 14-3-3sigma, the double-edged sword of human cancers. Am J Transl Res **1:** 326-340

Lichten LA, Cousins RJ (2009) Mammalian zinc transporters: nutritional and physiologic regulation. Annu Rev Nutr **29:** 153-176

Lichten LA, Ryu MS, Guo L, Embury J, Cousins RJ (2011) MTF-1-mediated repression of the zinc transporter Zip10 is alleviated by zinc restriction. PLoS One **6:** e21526

Lin Y, Chen Y, Wang Y, Yang J, Zhu VF, Liu Y, Cui X, Chen L, Yan W, Jiang T, Hergenroeder GW, Fletcher SA, Levine JM, Kim DH, Tandon N, Zhu JJ, Li M (2013) ZIP4 is a novel molecular marker for glioma. Neuro Oncol **15:** 1008-1016

Lioumi M, Ferguson CA, Sharpe PT, Freeman T, Marenholz I, Mischke D, Heizmann C, Ragoussis J (1999) Isolation and characterization of human and mouse ZIRTL, a member of the IRT1 family of transporters, mapping within the epidermal differentiation complex. Genomics **62:** 272-280

Litchfield DW (2003) Protein kinase CK2: structure, regulation and role in cellular decisions of life and death. Biochem J **369:** 1-15

Liu M-J, Bao S, Gálvez-Peralta M, Pyle CJ, Rudawsky AC, Pavlovicz RE, Killilea DW, Li C, Nebert DW, Wewers MD, Knoell DL (2013) ZIP8 regulates host defense through zinc-mediated inhibition of NF-κB. Cell Rep **3:** 386-400

Liu M, Yang J, Zhang Y, Zhou Z, Cui X, Zhang L, Fung KM, Zheng W, Allard FD, Yee EU, Ding K, Wu H, Liang Z, Zheng L, Fernandez-Zapico ME, Li YP, Bronze MS, Morris KT, Postier RG, Houchen CW, Yang J, Li M (2018) ZIP4 Promotes Pancreatic Cancer Progression by Repressing ZO-1 and Claudin-1 through a ZEB1-Dependent Transcriptional Mechanism. Clin Cancer Res **24:** 3186-3196

Liu X, Quan J, Shen Z, Zhang Z, Chen Z, Li L, Li X, Hu G, Deng X (2022) Metallothionein 2A (MT2A) controls cell proliferation and liver metastasis by controlling the MST1/LATS2/YAP1 signaling pathway in colorectal cancer. Cancer Cell Int **22:** 205

Liu Y, Batchuluun B, Ho L, Zhu D, Prentice KJ, Bhattacharjee A, Zhang M, Pourasgari F, Hardy AB, Taylor KM, Gaisano H, Dai FF, Wheeler MB (2015) Characterization of Zinc Influx Transporters (ZIPs) in Pancreatic beta Cells: ROLES IN REGULATING CYTOSOLIC ZINC HOMEOSTASIS AND INSULIN SECRETION. J Biol Chem **290:** 18757-18769

Liu Y, Franklin RB, Costello LC (1997) Prolactin and testosterone regulation of mitochondrial zinc in prostate epithelial cells. Prostate **30:** 26-32

Liu Y, Liu T, Jin H, Yin L, Yu H, Bi J (2018) MiR-411 suppresses the development of bladder cancer by regulating ZnT1. Onco Targets Ther **11:** 8695

Liuzzi JP, Aydemir F, Nam H, Knutson MD, Cousins RJ (2006) Zip14 (Slc39a14) mediates non-transferrin-bound iron uptake into cells. Proc Natl Acad Sci U S A **103:** 13612-13617

Liuzzi JP, Lichten LA, Rivera S, Blanchard RK, Aydemir TB, Knutson MD, Ganz T, Cousins RJ (2005) Interleukin-6 regulates the zinc transporter Zip14 in liver and contributes to the hypozincemia of the acute-phase response. Proc Natl Acad Sci U S A **102:** 6843-6848

Lopez V, Foolad F, Kelleher SL (2011) ZnT2-overexpression represses the cytotoxic effects of zinc hyper-accumulation in malignant metallothionein-null T47D breast tumor cells. Cancer Lett **304:** 41-51

Lopez V, Kelleher SL (2009) Zinc transporter-2 (ZnT2) variants are localized to distinct subcellular compartments and functionally transport zinc. Biochem J **422:** 43-52

Lopez V, Kelleher SL (2010) Zip6-attenuation promotes epithelial-to-mesenchymal transition in ductal breast tumor (T47D) cells. Exp Cell Res **316:** 366-375

Lovell MA, Smith JL, Xiong S, Markesbery WR (2005) Alterations in zinc transporter protein-1 (ZnT-1) in the brain of subjects with mild cognitive impairment, early, and late-stage Alzheimer's disease. Neurotox Res **7:** 265-271

Lu M, Chai J, Fu D (2009) Structural basis for autoregulation of the zinc transporter YiiP. Nat Struct Mol Biol **16:** 1063-1067

Lu M, Fu D (2007) Structure of the Zinc Transporter YiiP. Science **317:** 1746-1748

Lynes MA, Borghesi LA, Youn J, Olson EA (1993) Immunomodulatory activities of extracellular metallothionein. I. Metallothionein effects on antibody production. Toxicology **85:** 161-177

Lynes MA, Zaffuto K, Unfricht DW, Marusov G, Samson JS, Yin X (2006) The physiological roles of extracellular metallothionein. Exp Biol Med (Maywood) **231:** 1548-1554

Lyubartseva G, Smith JL, Markesbery WR, Lovell MA (2010) Alterations of zinc transporter proteins ZnT-1, ZnT-4 and ZnT-6 in preclinical Alzheimer's disease brain. Brain Pathol **20:** 343-350

Ma X, Duan H, Liu J, Mo Q, Sun C, Ma D, Wang J (2015) Effect of LIV1 on the sensitivity of ovarian cancer cells to trichostatin A. Oncol Rep **33:** 893-898

MacDonald RS (2000) The role of zinc in growth and cell proliferation. J Nutr **130:** 1500s-1508s

Mackay JP, Crossley M (1998) Zinc fingers are sticking together. Trends Biochem Sci **23:** 1-4

Majewska U, Banaś D, Braziewicz J, Góźdź S, Kubala-Kukuś A, Kucharzewski M (2007) Trace element concentration distributions in breast, lung and colon tissues. Phys Med Biol **52:** 3895-3911

Manning DL, Daly RJ, Lord PG, Kelly KF, Green CD (1988) Effects of oestrogen on the expression of a 4.4 kb mRNA in the ZR-75-1 human breast cancer cell line. Mol Cell Endocrinol **59:** 205-212

Mao S, Huang S (2013) Zinc and copper levels in bladder cancer: a systematic review and meta-analysis. Biol Trace Elem Res **153:** 5-10

Maret W (2003) Cellular zinc and redox states converge in the metallothionein/thionein pair. J Nutr **133:** 1460S-1462S

Maret W (2013) Zinc biochemistry: from a single zinc enzyme to a key element of life. Adv Nutr **4:** 82-91

Maret W (2017) Zinc in cellular regulation: The nature and significance of "zinc signals". Int J Mol Sci **18:** 2285

Margalioth EJ, Schenker JG, Chevion M (1983) Copper and zinc levels in normal and malignant tissues. Cancer **52:** 868-872

Martin AB, Aydemir TB, Guthrie GJ, Samuelson DA, Chang SM, Cousins RJ (2013) Gastric and colonic zinc transporter ZIP11 (Slc39a11) in mice responds to dietary zinc and exhibits nuclear localization. J Nutr **143:** 1882-1888

Masiulionytė B, Valiulytė I, Tamašauskas A, Skiriutė D (2019) Metallothionein genes are highly expressed in malignant astrocytomas and associated with patient survival. Sci Rep **9:** 1-7

Matsuura W, Yamazaki T, Yamaguchi-Iwai Y, Masuda S, Nagao M, Andrews GK, Kambe T (2009) SLC39A9 (ZIP9) regulates zinc homeostasis in the secretory pathway: characterization of the ZIP subfamily I protein in vertebrate cells. Biosci Biotechnol Biochem **73:** 1142-1148

Maverakis E, Fung MA, Lynch PJ, Draznin M, Michael DJ, Ruben B, Fazel N (2007) Acrodermatitis enteropathica and an overview of zinc metabolism. J Am Acad Dermatol **56:** 116-124

Maxel T, Smidt K, Petersen CC, Honoré B, Christensen AK, Jeppesen PB, Brock B, Rungby J, Palmfeldt J, Larsen A (2019) The zinc transporter Zip14 (SLC39a14) affects beta-cell function: proteomics, gene expression, and insulin secretion studies in INS-1E cells. Sci Rep **9:** 1-15

McClung JP, Bobilya DJ (1999) The influence of zinc status on the kinetics of zinc uptake into cultured endothelial cells. J Nutr Biochem **10:** 484-489

McCormick NH, Hennigar SR, Kiselyov K, Kelleher SL (2014) The biology of zinc transport in mammary epithelial cells: implications for mammary gland development, lactation, and involution. J Mammary Gland Biol Neoplasia **19:** 59-71

McCormick NH, Kelleher SL (2012) ZnT4 provides zinc to zinc-dependent proteins in the trans-Golgi network critical for cell function and Zn export in mammary epithelial cells. Am J Physiol Cell Physiol **303:** C291-297

McKenna WG, Muschel RJ, Gupta AK, Hahn SM, Bernhard EJ (2003) The RAS signal transduction pathway and its role in radiation sensitivity. Oncogene **22:** 5866-5875

McMahon RJ, Cousins RJ (1998) Mammalian Zinc Transporters. J Nutr **128:** 667-670

McNeal JE (1988) Normal histology of the prostate. Am J Surg Pathol **12:** 619-633
McNulty TJ, Taylor CW (1999) Extracellular heavy-metal ions stimulate Ca2+ mobilization in hepatocytes. Biochem J **339 (Pt 3):** 555-561
Meggio F, Pinna LA (2003) One-thousand-and-one substrates of protein kinase CK2? FASEB J **17:** 349-368
Mercadante CJ, Prajapati M, Conboy HL, Dash ME, Herrera C, Pettiglio MA, Cintron-Rivera L, Salesky MA, Rao DB, Bartnikas TB (2019) Manganese transporter Slc30a10 controls physiological manganese excretion and toxicity. J Clin Invest **129**
Miao S, Qiu T, Zhao Y, Wang H, Sun X, Wang Y, Xuan Y, Qin Y, Jiao W (2018) Overexpression of S100A13 protein is associated with tumor angiogenesis and poor survival in patients with early-stage non-small cell lung cancer. Thorac Cancer **9:** 1136-1144
Michalczyk AA, Allen J, Blomeley RC, Ackland ML (2002) Constitutive expression of hZnT4 zinc transporter in human breast epithelial cells. Biochem J **364:** 105-113
Michels KB, Solomon CG, Hu FB, Rosner BA, Hankinson SE, Colditz GA, Manson JE (2003) Type 2 diabetes and subsequent incidence of breast cancer in the Nurses' Health Study. Diabetes Care **26:** 1752-1758
Miller J, McLachlan A, Klug A (1985) Repetitive zinc-binding domains in the protein transcription factor IIIA from Xenopus oocytes. EMBO J **4:** 1609-1614
Millikan RC, Newman B, Tse C-K, Moorman PG, Conway K, Smith LV, Labbok MH, Geradts J, Bensen JT, Jackson S (2008) Epidemiology of basal-like breast cancer. Breast Cancer Res Treat **109:** 123-139
Milon B, Dhermy D, Pountney D, Bourgeois M, Beaumont C (2001) Differential subcellular localization of hZip1 in adherent and non-adherent cells. FEBS Lett **507:** 241-246
Milon BC, Agyapong A, Bautista R, Costello LC, Franklin RB (2010) Ras responsive element binding protein-1 (RREB-1) down-regulates hZIP1 expression in prostate cancer cells. Prostate **70:** 288-296
Mirabelli P, Coppola L, Salvatore M (2019) Cancer Cell Lines Are Useful Model Systems for Medical Research. Cancers (Basel) **11**
Mishra DR, Chaudhary S, Krishna BM, Mishra SK (2015) Identification of Critical Elements for Regulation of Inorganic Pyrophosphatase (PPA1) in MCF7 Breast Cancer Cells. PLoS One **10:** e0124864
Miyai T, Hojyo S, Ikawa T, Kawamura M, Irie T, Ogura H, Hijikata A, Bin BH, Yasuda T, Kitamura H, Nakayama M, Ohara O, Yoshida H, Koseki H, Mishima K, Fukada T (2014) Zinc transporter SLC39A10/ZIP10 facilitates antiapoptotic signaling during early B-cell development. Proc Natl Acad Sci U S A **111:** 11780-11785
Montenarh M, Götz C (2018) Ecto-protein kinase CK2, the neglected form of CK2. Biomed Rep **8:** 307-313
Morrison BJ, Hastie ML, Grewal YS, Bruce ZC, Schmidt C, Reynolds BA, Gorman JJ, Lopez JA (2012) Proteomic comparison of mcf-7 tumoursphere and monolayer cultures. PLoS One **7:** e52692
Muchlińska A, Nagel A, Popęda M, Szade J, Niemira M, Zieliński J, Skokowski J, Bednarz-Knoll N, Żaczek AJ (2022) Alpha-smooth muscle actin-positive cancer-associated fibroblasts secreting osteopontin promote growth of luminal breast cancer. Cell Mol Biol Lett **27:** 45
Mukaihara K, Suehara Y, Kohsaka S, Kubota D, Toda-Ishii M, Akaike K, Fujimura T, Kobayashi E, Yao T, Ladanyi M, Kaneko K, Saito T (2016) Expression of F-actin-capping protein subunit beta, CAPZB, is associated with cell growth and motility in epithelioid sarcoma. BMC Cancer **16:** 206

Mukherjee K, Ishii K, Pillalamarri V, Kammin T, Atkin JF, Hickey SE, Xi QJ, Zepeda CJ, Gusella JF, Talkowski ME, Morton CC, Maas RL, Liao EC (2016) Actin capping protein CAPZB regulates cell morphology, differentiation, and neural crest migration in craniofacial morphogenesis†. Hum Mol Genet **25:** 1255-1270

Mukhopadhyay S (2018) Familial manganese-induced neurotoxicity due to mutations in SLC30A10 or SLC39A14. Neurotoxicology **64:** 278-283

Mulay IL, Roy R, Knox B, Suhr NH, Delaney WE (1971) Trace-metal analysis of cancerous and non-cancerous human tissues. J Natl Cancer Inst **47:** 1-13

Munemasa T, Idaira Y, Fukada T, Shimoda S, Asada Y (2014) Histological Analysis of Dentinogenesis Imperfecta in Slc39a13/Zip13 Knockout Mice. J Hard Tissue Biol **23:** 163-168

Muñoz-Moreno L, Carmena MJ, Prieto JC, Schally AV, Bajo AM (2022) Tumorigenic transformation of human prostatic epithelial cell line RWPE-1 by growth hormone-releasing hormone (GHRH). Prostate **82:** 933-941

Murase H, Sakai S, Kusano K, Hobo S, Nambo Y (2013) Serum zinc levels and their relationship with diseases in racehorses. J Vet Med Sci **75:** 37-41

Murgia C, Devirgiliis C, Mancini E, Donadel G, Zalewski P, Perozzi G (2009) Diabetes-linked zinc transporter ZnT8 is a homodimeric protein expressed by distinct rodent endocrine cell types in the pancreas and other glands. Nutr Metab Cardiovasc Dis **19:** 431-439

Myers SA, Nield A, Chew GS, Myers MA (2013) The zinc transporter, Slc39a7 (Zip7) is implicated in glycaemic control in skeletal muscle cells. PLoS One **8:** e79316

Nagase T, Ishikawa K, Kikuno R, Hirosawa M, Nomura N, Ohara O (1999) Prediction of the coding sequences of unidentified human genes. XV. The complete sequences of 100 new cDNA clones from brain which code for large proteins in vitro. DNA Res **6:** 337-345

Najm MZ, Sadaf, Akhtar N, Kashyap P, Shingatgeri VM, Sharma K, Raghav A, Rout VK, Parveen F (2021) Prohibitin gene regulation in cancer and its possible therapeutic potential. Curr Oncol Rep **4:** 35-40

Napolitano JR, Liu MJ, Bao S, Crawford M, Nana-Sinkam P, Cormet-Boyaka E, Knoell DL (2012) Cadmium-mediated toxicity of lung epithelia is enhanced through NF-kappaB-mediated transcriptional activation of the human zinc transporter ZIP8. Am J Physiol Lung Cell Mol Physiol **302:** L909-918

Nguyen LH, Tran TT, Truong LTN, Mai HH, Nguyen TT (2020) Overcharging of the Zinc Ion in the Structure of the Zinc-Finger Protein Is Needed for DNA Binding Stability. Biochemistry **59:** 1378-1390

Nicolson TJ, Bellomo EA, Wijesekara N, Loder MK, Baldwin JM, Gyulkhandanyan AV, Koshkin V, Tarasov AI, Carzaniga R, Kronenberger KJD (2009) Insulin storage and glucose homeostasis in mice null for the granule zinc transporter ZnT8 and studies of the type 2 diabetes–associated variants. Diabetes **58:** 2070-2083

Nie S, McDermott SP, Deol Y, Tan Z, Wicha MS, Lubman DM (2015) A quantitative proteomics analysis of MCF7 breast cancer stem and progenitor cell populations. Proteomics **15:** 3772-3783

Nimmanon T, Ziliotto S, Morris S, Flanagan L, Taylor KM (2017) Phosphorylation of zinc channel ZIP7 drives MAPK, PI3K and mTOR growth and proliferation signalling. Metallomics **9:** 471-481

Nimmanon T, Ziliotto S, Ogle O, Burt A, Gee JMW, Andrews GK, Kille P, Hogstrand C, Maret W, Taylor KM (2021) The ZIP6/ZIP10 heteromer is essential for the zinc-mediated trigger of mitosis. Cell Mol Life Sci **78:** 1781-1798

Nishida K, Hasegawa A, Nakae S, Oboki K, Saito H, Yamasaki S, Hirano T (2009) Zinc transporter Znt5/Slc30a5 is required for the mast cell–mediated delayed-type allergic reaction but not the immediate-type reaction. J Exp Med **206:** 1351-1364

Nishito Y, Kambe T (2019) Zinc transporter 1 (ZNT1) expression on the cell surface is elaborately controlled by cellular zinc levels. J Biol Chem **294:** 15686-15697

Noaman N, Coorssen JR (2018) Coomassie does it (better): A Robin Hood approach to total protein quantification. Anal Biochem **556:** 53-56

Noh H, Paik HY, Kim J, Chung J (2014) The alteration of zinc transporter gene expression is associated with inflammatory markers in obese women. Biol Trace Elem Res **158:** 1-8

Nomura N, Miyajima N, Sazuka T, Tanaka A, Kawarabayasi Y, Sato S, Nagase T, Seki N, Ishikawa K, Tabata S (1994) Prediction of the coding sequences of unidentified human genes. I. The coding sequences of 40 new genes (KIAA0001-KIAA0040) deduced by analysis of randomly sampled cDNA clones from human immature myeloid cell line KG-1. DNA Res **1:** 27-35

Ohana E, Hoch E, Keasar C, Kambe T, Yifrach O, Hershfinkel M, Sekler IJJoBC (2009) Identification of the Zn2+ binding site and mode of operation of a mammalian Zn2+ transporter. J Biol Chem **284:** 17677-17686

Ohashi W, Kimura S, Iwanaga T, Furusawa Y, Irié T, Izumi H, Watanabe T, Hijikata A, Hara T, Ohara O (2016) Zinc transporter SLC39A7/ZIP7 promotes intestinal epithelial self-renewal by resolving ER stress. PLoS Genet **12:** e1006349

Olsten ME, Canton DA, Zhang C, Walton PA, Litchfield DW (2004) The Pleckstrin homology domain of CK2 interacting protein-1 is required for interactions and recruitment of protein kinase CK2 to the plasma membrane. J Biol Chem **279:** 42114-42127

Ornstein DK, Tyson DR (2006) Proteomics for the identification of new prostate cancer biomarkers. Urol Oncol **24:** 231-236

Ortega CE, Seidner Y, Dominguez I (2014) Mining CK2 in cancer. PLoS One **9:** e115609

Padjasek M, Kocyła A, Kluska K, Kerber O, Tran JB, Krężel A (2020) Structural zinc binding sites shaped for greater works: Structure-function relations in classical zinc finger, hook and clasp domains. J Inorg Biochem **204:** 110955

Pal D, Sharma U, Singh SK, Prasad R (2014) Association between ZIP10 gene expression and tumor aggressiveness in renal cell carcinoma. Gene **552:** 195-198

Palmiter RD, Cole TB, Findley SD (1996) ZnT-2, a mammalian protein that confers resistance to zinc by facilitating vesicular sequestration. EMBO J **15:** 1784-1791

Palmiter RD, Cole TB, Quaife CJ, Findley SD (1996) ZnT-3, a putative transporter of zinc into synaptic vesicles. Proc Natl Acad Sci U S A **93:** 14934-14939

Palmiter RD, Findley SD (1995) Cloning and functional characterization of a mammalian zinc transporter that confers resistance to zinc. EMBO J **14:** 639-649

Palmiter RD, Huang L (2004) Efflux and compartmentalization of zinc by members of the SLC30 family of solute carriers. Pflugers Arch **447:** 744-751

Pan Y, Lin S, Xing R, Zhu M, Lin B, Cui J, Li W, Gao J, Shen L, Zhao Y, Guo M, Wang JM, Huang J, Lu Y (2016) Epigenetic upregulation of metallothionein 2A by diallyl trisulfide enhances chemosensitivity of human gastric cancer cells to docetaxel through attenuating NF-κB activation. Antioxid Redox Signal. **24:** 839-854

Pan Z, Choi S, Ouadid-Ahidouch H, Yang J-M, Beattie JH, Korichneva I (2017) Zinc transporters and dysregulated channels in cancers. Front Biosci **22:** 623

Park S-J, Yoon B-H, Kim S-K, Kim S-Y (2019) GENT2: an updated gene expression database for normal and tumor tissues. BMC Med Genet **12:** 101

Park YM, Hwang SJ, Masuda K, Choi KM, Jeong MR, Nam DH, Gorospe M, Kim HH (2012) Heterogeneous nuclear ribonucleoprotein C1/C2 controls the metastatic potential of glioblastoma by regulating PDCD4. Mol Cell Biol **32:** 4237-4244

Parker JS, Mullins M, Cheang MC, Leung S, Voduc D, Vickery T, Davies S, Fauron C, He X, Hu Z (2009) Supervised risk predictor of breast cancer based on intrinsic subtypes. J Clin Oncol **27:** 1160

Parsons DW, Jones S, Zhang X, Lin JC-H, Leary RJ, Angenendt P, Mankoo P, Carter H, Siu I-M, Gallia GL (2008) An integrated genomic analysis of human glioblastoma multiforme. Science **321:** 1807-1812

Pawan K, Neeraj S, Sandeep K, Kanta Ratho R, Rajendra P (2007) Upregulation of Slc39a10 gene expression in response to thyroid hormones in intestine and kidney. Biochim Biophys Acta **1769:** 117-123

Pechkova E, Zanotti G, Nicolini C (2003) Three-dimensional atomic structure of a catalytic subunit mutant of human protein kinase CK2. Acta Crystallogr D Biol Crystallogr **59(Pt 12):** 2133-2139

Perez Y, Shorer Z, Liani-Leibson K, Chabosseau P, Kadir R, Volodarsky M, Halperin D, Barber-Zucker S, Shalev H, Schreiber R, Gradstein L, Gurevich E, Zarivach R, Rutter GA, Landau D, Birk OS (2017) SLC30A9 mutation affecting intracellular zinc homeostasis causes a novel cerebro-renal syndrome. Brain **140:** 928-939

Peters JL, Dufner-Beattie J, Xu W, Geiser J, Lahner B, Salt DE, Andrews GK (2007) Targeting of the mouse Slc39a2 (Zip2) gene reveals highly cell-specific patterns of expression, and unique functions in zinc, iron, and calcium homeostasis. Genesis **45:** 339-352

Petersen AB, Smidt K, Magnusson NE, Moore F, Egefjord L, Rungby J (2011) siRNA-mediated knock-down of ZnT3 and ZnT8 affects production and secretion of insulin and apoptosis in INS-1E cells. APMIS **119:** 93-102

Pocanschi CL, Ehsani S, Mehrabian M, Wille H, Reginold W, Trimble WS, Wang H, Yee A, Arrowsmith CH, Bozóky Z, Kay LE, Forman-Kay JD, Rini JM, Schmitt-Ulms G (2013) The ZIP5 ectodomain co-localizes with PrP and may acquire a PrP-like fold that assembles into a dimer. PLoS One **8:** e72446

Podany AB, Wright J, Lamendella R, Soybel DI, Kelleher SL (2016) ZnT2-mediated zinc import into Paneth cell granules is necessary for coordinated secretion and Paneth cell function in mice. Cell Mol Gastroenterol Hepatol **2:** 369-383

Pound LD, Sarkar SA, Ustione A, Dadi PK, Shadoan MK, Lee CE, Walters JA, Shiota M, McGuinness OP, Jacobson DA (2012) The physiological effects of deleting the mouse SLC30A8 gene encoding zinc transporter-8 are influenced by gender and genetic background. PloS One **7**

Prasad AS (2012) Discovery of human zinc deficiency: 50 years later. J Trace Elem Med Biol **26:** 66-69

Prasad AS (2013) Discovery of human zinc deficiency: its impact on human health and disease. Adv Nutr **4:** 176-190

Prasad AS, Halsted JA, Nadimi M (1961) Syndrome of iron deficiency anemia, hepatosplenomegaly, hypogonadism, dwarfism and geophagia. Am J Med **31:** 532-546

Prat A, Perou CM (2011) Deconstructing the molecular portraits of breast cancer. Mol Oncol **5:** 5-23

Prueitt RL, Yi M, Hudson RS, Wallace TA, Howe TM, Yfantis HG, Lee DH, Stephens RM, Liu CG, Calin GA (2008) Expression of microRNAs and protein-coding genes associated with perineural invasion in prostate cancer. Prostate **68:** 1152-1164

Quadri M, Federico A, Zhao T, Breedveld GJ, Battisti C, Delnooz C, Severijnen L-A, Mammarella LDT, Mignarri A, Monti L (2012) Mutations in SLC30A10 cause

parkinsonism and dystonia with hypermanganesemia, polycythemia, and chronic liver disease. Am J Hum Genet **90:** 467-477

Rafalo-Ulinska A, Piotrowska J, Kryczyk A, Opoka W, Sowa-Kucma M, Misztak P, Rajkowska G, Stockmeier CA, Datka W, Nowak G (2016) Zinc transporters protein level in postmortem brain of depressed subjects and suicide victims. J Psychiatr Res **83:** 220-229

Raju GN, Sarita P, Kumar MR, Murty GR, Reddy BS, Lakshminarayana S, Vijayan V, Lakshmi PR, Gavarasana S, Reddy SB (2006) Trace elemental correlation study in malignant and normal breast tissue by PIXE technique. Nucl Instrum Methods Phys Res Sect B Beam Interact Mater Atoms **247:** 361-367

Rakhra G, Rakhra G (2021) Zinc finger proteins: insights into the transcriptional and post transcriptional regulation of immune response. Mol Biol Rep **48:** 5735-5743

Ranaldi G, Perozzi G, Truong-Tran A, Zalewski P, Murgia C (2002) Intracellular distribution of labile Zn(II) and zinc transporter expression in kidney and MDCK cells. Am J Physiol Renal Physiol **283:** F1365-1375

Raulin J (1869) Etudes chimique sur la vegetation (Chemical studies on plants). Annales des Sciences Naturelles Botanique et Biologie Vegetale **11:** 293-299

Reddy SB, John Charles M, Naga Raju GJ, Vijayan V, Seetharami Reddy B, Ravi Kumar M, Sundareswar B (2003) Trace elemental analysis of carcinoma kidney and stomach by PIXE method. Nucl Instrum Methods Phys Res Sect B Beam Interact Mater Atoms **207:** 345-355

Rink L, Gabriel P (2000) Zinc and the immune system. Proc Nutr Soc **59:** 541-552.

Rishi I, Baidouri H, Abbasi JA, Bullard-Dillard R, Kajdacsy-Balla A, Pestaner JP, Skacel M, Tubbs R, Bagasra O (2003) Prostate cancer in African American men is associated with downregulation of zinc transporters. Appl Immunohistochem Mol Morphol **11:** 253-260

Ronco AL, Stefani ED, Deneo-Pellegrini H, Quarneti A (2012) Diabetes, overweight and risk of postmenopausal breast cancer: a case-control study in Uruguay. Asian Pac J Cancer Prev **13:** 139-146

Rusch P, Hirner AV, Schmitz O, Kimmig R, Hoffmann O, Diel M (2021) Zinc distribution within breast cancer tissue of different intrinsic subtypes. Arch Gynecol Obstet **303:** 195-205

Ruzzene M, Pinna LA (2010) Addiction to protein kinase CK2: a common denominator of diverse cancer cells? Biochim Biophys Acta **1804:** 499-504

Ryu MS, Lichten LA, Liuzzi JP, Cousins RJ (2008) Zinc transporters ZnT1 (Slc30a1), Zip8 (Slc39a8), and Zip10 (Slc39a10) in mouse red blood cells are differentially regulated during erythroid development and by dietary zinc deficiency. J Nutr **138:** 2076-2083

Sajjad H, Imtiaz S, Noor T, Siddiqui YH, Sajjad A, Zia M (2021) Cancer models in preclinical research: A chronicle review of advancement in effective cancer research. Animal Model Exp Med **4:** 87-103

Salazar G, Falcon-Perez JM, Harrison R, Faundez V (2009) SLC30A3 (ZnT3) oligomerization by dityrosine bonds regulates its subcellular localization and metal transport capacity. PLoS One **4:** e5896

Sánchez-Quesada C, Gutiérrez-Santiago F, Rodríguez-García C, Gaforio JJ (2022) Synergistic Effect of Squalene and Hydroxytyrosol on Highly Invasive MDA-MB-231 Breast Cancer Cells. Nutrients **14:** 255

Sandholt IS, Olsen BB, Guerra B, Issinger OG (2009) Resorufin: a lead for a new protein kinase CK2 inhibitor. Anticancer Drugs **20:** 238-248

Sardana G, Jung K, Stephan C, Diamandis EP (2008) Proteomic analysis of conditioned media from the PC3, LNCaP, and 22Rv1 prostate cancer cell lines: discovery and validation of candidate prostate cancer biomarkers. J Proteome Res **7:** 3329-3338

Sarita P, Naga Raju GJ, Pradeep AS, Rautray TR, Seetharami Reddy B, Bhuloka Reddy S, Vijayan V (2012) Analysis of trace elements in blood sera of breast cancer patients by particle induced X-ray emission. J Radioanal Nucl Chem **294:** 355-361

Sarrouilhe D, Filhol O, Leroy D, Bonello G, Baudry M, Chambaz EM, Cochet C (1998) The tight association of protein kinase CK2 with plasma membranes is mediated by a specific domain of its regulatory beta-subunit. Biochim Biophys Acta **1403:** 199-210

Satarug S, Garrett SH, Somji S, Sens MA, Sens DA (2021) Aberrant Expression of ZIP and ZnT Zinc Transporters in UROtsa Cells Transformed to Malignant Cells by Cadmium. Stresses **1:** 78-89

Sauer AK, Vela H, Vela G, Stark P, Barrera-Juarez E, Grabrucker AM (2020) Zinc Deficiency in Men Over 50 and Its Implications in Prostate Disorders. Front Oncol **10:** 1293

Scarr E, Udawela M, Greenough MA, Neo J, Seo MS, Money TT, Upadhyay A, Bush AI, Everall IP, Thomas EA (2016) Increased cortical expression of the zinc transporter SLC39A12 suggests a breakdown in zinc cellular homeostasis as part of the pathophysiology of schizophrenia. NPJ Schizophr **2:** 1-7

Schilling K, Harris AL, Halliday AN, Schofield CJ, Sheldon H, Haider S, Larner F (2022) Investigations on Zinc Isotope Fractionation in Breast Cancer Tissue Using in vitro Cell Culture Uptake-Efflux Experiments. Front Med **8**

Schmittgen TD, Livak KJ (2008) Analyzing real-time PCR data by the comparative C(T) method. Nat Protoc **3:** 1101-1108

Schneider J, Ruschhaupt M, Buness A, Asslaber M, Regitnig P, Zatloukal K, Schippinger W, Ploner F, Poustka A, Sultmann H (2006) Identification and meta-analysis of a small gene expression signature for the diagnosis of estrogen receptor status in invasive ductal breast cancer. Int J Cancer **119:** 2974-2979

Schnitzler A, Olsen B, Issinger O-G, Niefind K (2014) The protein kinase CK2Andante holoenzyme structure supports proposed models of autoregulation and trans-autophosphorylation. J Mol Biol **426:** 1871-1882

Schroder B, Wrocklage C, Pan C, Jager R, Kosters B, Schafer H, Elsasser HP, Mann M, Hasilik A (2007) Integral and associated lysosomal membrane proteins. Traffic **8:** 1676-1686

Schumann T, König J, Henke C, Willmes DM, Bornstein SR, Jordan J, Fromm MF, Birkenfeld AL (2020) Solute Carrier Transporters as Potential Targets for the Treatment of Metabolic Disease. Pharmacol Rev **72:** 343-379

Seed RI, Taurozzi AJ, Wilcock DJ, Nappo G, Erb HHH, Read ML, Gurney M, Archer LK, Ito S, Rumsby MG, Petrie JL, Clayton A, Maitland NJ, Collins AT (2019) The putative tumour suppressor protein Latexin is secreted by prostate luminal cells and is downregulated in malignancy. Sci Rep **9:** 5120

Sekler I, Moran A, Hershfinkel M, Dori A, Margulis A, Birenzweig N, Nitzan Y, Silverman WF (2002) Distribution of the zinc transporter ZnT-1 in comparison with chelatable zinc in the mouse brain. J Comp Neurol **447:** 201-209

Selli C, Dixon JM, Sims AH (2016) Accurate prediction of response to endocrine therapy in breast cancer patients: current and future biomarkers. Breast Cancer Res **18:** 118

Sen MK, Almuslehi MSM, Shortland PJ, Mahns DA, Coorssen JR (2021) Proteomics of Multiple Sclerosis: Inherent Issues in Defining the Pathoetiology and Identifying (Early) Biomarkers. Int J Mol Sci **22:** 7377

Sens MA, Somji S, Garrett SH, Beall CL, Sens DA (2001) Metallothionein isoform 3 overexpression is associated with breast cancers having a poor prognosis. Am J Pathol **159:** 21-26

Seo SU, Woo SM, Im S-S, Jang Y, Han E, Kim SH, Lee H, Lee H-S, Nam J-O, Gabrielson E, Min K-j, Kwon TK (2022) Cathepsin D as a potential therapeutic target to enhance anticancer drug-induced apoptosis via RNF183-mediated destabilization of Bcl-xL in cancer cells. Cell Death Dis **13:** 115

Seo YA, Lopez V, Kelleher SL (2011) A histidine-rich motif mediates mitochondrial localization of ZnT2 to modulate mitochondrial function. Am J Physiol Cell Physiol **300:** C1479-1489

Seve M, Chimienti F, Devergnas S, Favier A (2004) In silico identification and expression of SLC30 family genes: an expressed sequence tag data mining strategy for the characterization of zinc transporters' tissue expression. BMC Genomics **5:** 32

Sharma SV, Haber DA, Settleman J (2010) Cell line-based platforms to evaluate the therapeutic efficacy of candidate anticancer agents. Nat Rev Cancer **10:** 241-253

Shen D, Nooraie F, Elshimali Y, Lonsberry V, He J, Bose S, Chia D, Seligson D, Chang HR, Goodglick L (2006) Decreased expression of annexin A1 is correlated with breast cancer development and progression as determined by a tissue microarray analysis. Hum Pathol **37:** 1583-1591

Shen H, Qin H, Guo J (2009) Concordant correlation of LIV-1 and E-cadherin expression in human breast cancer cell MCF-7. Mol Biol Rep **36:** 653-659

Shen R, Xie F, Shen H, liu Q, Zheng T, Kou X, Wang D, Yang J (2013) Negative correlation of LIV-1 and E-cadherin expression in hepatocellular carcinoma cells. PLoS One **8:** e56542

Shihan MH, Novo SG, Le Marchand SJ, Wang Y, Duncan MK (2021) A simple method for quantitating confocal fluorescent images. Biochem Biophys Rep **25:** 100916

Shusterman E, Beharier O, Shiri L, Zarivach R, Etzion Y, Campbell CR, Lee I-H, Okabayashi K, Dinudom A, Cook DIJM (2014) ZnT-1 extrudes zinc from mammalian cells functioning as a Zn2+/H+ exchanger. Metallomics **6:** 1656-1663

Si M, Lang J (2018) The roles of metallothioneins in carcinogenesis. J Hematol Oncol **11:** 107

Siegel RL, Miller KD, Fuchs HE, Jemal A (2022) Cancer statistics, 2022. CA Cancer J Clin **72:** 7-33

Sim DL, Chow VT (1999) The novel human HUEL (C4orf1) gene maps to chromosome 4p12-p13 and encodes a nuclear protein containing the nuclear receptor interaction motif. Genomics **59:** 224-233

Simanshu DK, Nissley DV, McCormick F (2017) RAS proteins and their regulators in human disease. Cell **170:** 17-33

Singh CK, Chhabra G, Patel A, Chang H, Ahmad N (2021) Dietary Phytochemicals in Zinc Homeostasis: A Strategy for Prostate Cancer Management. Nutrients **13:** 1867

Singh CK, Malas KM, Tydrick C, Siddiqui IA, Iczkowski KA, Ahmad N (2016) Analysis of zinc-exporters expression in prostate cancer. Sci Rep **6:** 36772

Sladek R, Rocheleau G, Rung J, Dina C, Shen L, Serre D, Boutin P, Vincent D, Belisle A, Hadjadj S (2007) A genome-wide association study identifies novel risk loci for type 2 diabetes. Nature **445:** 881-885

Smith LM, Kelleher NL (2013) Proteoform: a single term describing protein complexity. Nat Methods **10:** 186-187

Soler-Agesta R, Ames TD, Price M, Jimeno J, Yim CY, Moreno-Loshuertos R, Anel A (2022) PT-112 induces potent mitochondrial stress and immunogenic cell death in human prostate cancer cell lines. Cancers (Basel) **82:** 1115-1115

Song Z, Wang Y, Zhang F, Yao F, Sun C (2019) Calcium signaling pathways: key pathways in the regulation of obesity. Int J Mol Sci **20:** 2768

Soule HD, Maloney TM, Wolman SR, Peterson WD, Brenz R, McGrath CM, Russo J, Pauley RJ, Jones RF, Brooks S (1990) Isolation and characterization of a spontaneously immortalized human breast epithelial cell line, MCF-10. Cancer Res **50:** 6075-6086

Su C-Y, Huang G-C, Chen IC, Chen P-Y, Chen Y-J, Fang H-W (2023) Distinct Expression of Surface and Genetic Biomarkers in Prostate Cancer Cell Lines. In Vivo **37:** 242-246

Subramanian Vignesh K, Deepe GS, Jr. (2017) Metallothioneins: emerging modulators in immunity and infection. Int J Mol Sci **18**

Sun D, Zhang L, Wang Y, Wang X, Hu X, Cui FA, Kong F (2007) Regulation of zinc transporters by dietary zinc supplement in breast cancer. Mol Biol Rep **34:** 241-247

Sun Q, Li Q, Zhong W, Zhang J, Sun X, Tan X, Yin X, Sun X, Zhang X, Zhou Z (2014) Dysregulation of hepatic zinc transporters in a mouse model of alcoholic liver disease. Am J Physiol Gastrointest Liver Physiol **307:** G313-G322

Sung H, Ferlay J, Siegel RL, Laversanne M, Soerjomataram I, Jemal A, Bray F (2021) Global Cancer Statistics 2020: GLOBOCAN Estimates of Incidence and Mortality Worldwide for 36 Cancers in 185 Countries. CA Cancer J Clin **71:** 209-249

Tai S-K, Tan OJ-K, Chow VT-K, Jin R, Jones JL, Tan P-H, Jayasurya A, Bay B-H (2003) Differential expression of metallothionein 1 and 2 isoforms in breast cancer lines with different invasive potential: identification of a novel nonsilent metallothionein-1H mutant variant. Am J Clin Pathol **163:** 2009-2019

Tait L, Soule HD, Russo J (1990) Ultrastructural and immunocytochemical characterization of an immortalized human breast epithelial cell line, MCF-10. Cancer Res **50:** 6087-6094

Takatani-Nakase T (2013) Migration behavior of breast cancer cells in the environment of high glucose level and the role of zinc and its transporter. Yakugaku Zasshi **133:** 1195-1199

Takatani-Nakase T, Matsui C, Maeda S, Kawahara S, Takahashi K (2014) High glucose level promotes migration behavior of breast cancer cells through zinc and its transporters. PLoS One **9:** e90136.

Takatani-Nakase T, Matsui C, Takahashi K (2016) Role of the LIV-1 subfamily of zinc transporters in the development and progression of breast cancers: A mini review. Biomed Res Clin Prac **1:** 71-75

Tang J, Qin Z, Han P, Wang W, Yang C, Xu Z, Li R, Liu B, Qin C, Wang Z, Tang M, Zhang W (2017) High Annexin A5 expression promotes tumor progression and poor prognosis in renal cell carcinoma. Int J Oncol **50:** 1839-1847

Tang Z, Kang B, Li C, Chen T, Zhang Z (2019) GEPIA2: an enhanced web server for large-scale expression profiling and interactive analysis. Nucleic Acids Res **47:** W556-W560

Taniguchi M, Fukunaka A, Hagihara M, Watanabe K, Kamino S, Kambe T, Enomoto S, Hiromura M (2013) Essential role of the zinc transporter ZIP9/SLC39A9 in regulating the activations of Akt and Erk in B-cell receptor signaling pathway in DT40 cells. PLoS One **8:** e58022

Tao X, Zheng JM, Xu AM, Chen XF, Zhang SH (2007) Downregulated expression of metallothionein and its clinicopathological significance in hepatocellular carcinoma. Hepatol Res **37:** 820-827

Tasaki M, Hanada K, Hashimoto I (1993) Analyses of serum copper and zinc levels and copper/zinc ratios in skin diseases. J Dermatol **20:** 21-24

Taylor KM (2008) A distinct role in breast cancer for two LIV-1 family zinc transporters. Biochem Soc Trans **36:** 1247-1251

Taylor KM, Hiscox S, Nicholson RI, Hogstrand C, Kille P (2012) Protein kinase CK2 triggers cytosolic zinc signaling pathways by phosphorylation of zinc channel ZIP7. Sci Signal **5:** ra11

Taylor KM, Kille P, Hogstrand C (2012) Protein kinase CK2 opens the gate for zinc signaling. Cell cycle (Georgetown, Tex.) **11:** 1863-1864

Taylor KM, Morgan HE, Johnson A, Hadley LJ, Nicholson RI (2003) Structure-function analysis of LIV-1, the breast cancer-associated protein that belongs to a new subfamily of zinc transporters. Biochem J **375:** 51-59

Taylor KM, Morgan HE, Johnson A, Nicholson RI (2005) Structure-function analysis of a novel member of the LIV-1 subfamily of zinc transporters, ZIP14. FEBS Lett **579:** 427-432

Taylor KM, Morgan HE, Smart K, Zahari NM, Pumford S, Ellis IO, Robertson JFR, Nicholson RI (2007) The emerging role of the LIV-1 subfamily of zinc transporters in breast cancer. Mol Med **13:** 396-406

Taylor KM, Muraina IA, Brethour D, Schmitt-Ulms G, Nimmanon T, Ziliotto S, Kille P, Hogstrand C (2016) Zinc transporter ZIP10 forms a heteromer with ZIP6 which regulates embryonic development and cell migration. Biochem J **473:** 2531-2544

Taylor KM, Vichova P, Jordan N, Hiscox S, Hendley R, Nicholson RI (2008) ZIP7-mediated intracellular zinc transport contributes to aberrant growth factor signaling in antihormone-resistant breast cancer Cells. Endocrinology **149:** 4912-4920

Thomas P, Pang Y, Dong J, Berg AH (2014) Identification and characterization of membrane androgen receptors in the ZIP9 zinc transporter subfamily: II. Role of human ZIP9 in testosterone-induced prostate and breast cancer cell apoptosis. Endocrinology **155:** 4250-4265

To PK, Do MH, Cho J-H, Jung C (2020) Growth modulatory role of zinc in prostate cancer and application to cancer therapeutics. Int J Mol Sci **21:** 2991

Tozlu S, Girault I, Vacher S, Vendrell J, Andrieu C, Spyratos F, Cohen P, Lidereau R, Bieche I (2006) Identification of novel genes that co-cluster with estrogen receptor alpha in breast tumor biopsy specimens, using a large-scale real-time reverse transcription-PCR approach. Endocr Relat Cancer **13:** 1109-1120

Trebak M, Kinet J-P (2019) Calcium signalling in T cells. Nat Rev Immunol **19:** 154-169

Trembley JH, Kren BT, Afzal M, Scaria GA, Klein MA, Ahmed K (2023) Protein kinase CK2 - diverse roles in cancer cell biology and therapeutic promise. Mol Cell Biochem **478:** 899-926

Trembley JH, Wang G, Unger G, Slaton J, Ahmed K (2009) Protein kinase CK2 in health and disease: CK2: a key player in cancer biology. Cell Mol Life Sci **66:** 1858-1867

Uddin MN, Wang X (2022) Identification of key tumor stroma-associated transcriptional signatures correlated with survival prognosis and tumor progression in breast cancer. Breast Cancer **29:** 541-561

Unno J, Satoh K, Hirota M, Kanno A, Hamada S, Ito H, Masamune A, Tsukamoto N, Motoi F, Egawa S, Unno M, Horii A, Shimosegawa T (2009) LIV-1 enhances the aggressive phenotype through the induction of epithelial to mesenchymal transition in human pancreatic carcinoma cells. Int J Oncol **35:** 813-821

Valashedi MR, Roushandeh AM, Tomita K, Kuwahara Y, Pourmohammadi-Bejarpasi Z, Kozani PS, Sato T, Roudkenar MH (2022) CRISPR/Cas9-mediated knockout of Lcn2 in human breast cancer cell line MDA-MB-231 ameliorates erastin-mediated ferroptosis and increases cisplatin vulnerability. Life Sci **304:** 120704

Vallee BL, Neurath H (1954) Carboxypeptidase, a zinc metalloprotein. Am Chem Soc **76:** 5006-5007

van Santen VJB, Zandieh Doulabi B, Semeins CM, Hogervorst JMA, Bratengeier C, Bakker AD (2023) Compressed Prostate Cancer Cells Decrease Osteoclast Activity While Enhancing Osteoblast Activity In Vitro. Int J Mol Sci **24:** 759

Vedoya GM, Galarza TE, Mohamad NA, Cricco GP, Martín GA (2022) Non-tumorigenic epithelial breast cells and ionizing radiation cooperate in the enhancement of mesenchymal traits in tumorigenic breast cancer cells. Life Sci **307:** 120853

Velicer C, Dublin S, White E (2007) Diabetes and the risk of prostate cancer: the role of diabetes treatment and complications. Prostate Cancer Prostatic Dis **10:** 46-51

Venerando A, Ruzzene M, Pinna LA (2014) Casein kinase: the triple meaning of a misnomer. Biochem J **460:** 141-156

Vilas CK, Emery LE, Denchi EL, Miller KM (2018) Caught with One's Zinc Fingers in the Genome Integrity Cookie Jar. Trends Genet **34:** 313-325

Wang C, Xu H, Lin S, Deng W, Zhou J, Zhang Y, Shi Y, Peng D, Xue Y (2020) GPS 5.0: An Update on the Prediction of Kinase-specific Phosphorylation Sites in Proteins. Genomics, Proteomics & Bioinformatics **18:** 72-80

Wang F, Kim BE, Petris MJ, Eide DJ (2004) The mammalian Zip5 protein is a zinc transporter that localizes to the basolateral surface of polarized cells. J Biol Chem **279:** 51433-51441

Wang J, Zhao H, Xu Z, Cheng X (2020) Zinc dysregulation in cancers and its potential as a therapeutic target. Cancer Biol Med **17:** 612

Wang K, Zhou B, Kuo YM, Zemansky J, Gitschier J (2002) A novel member of a zinc transporter family is defective in acrodermatitis enteropathica. Am J Hum Genet **71:** 66-73

Wang L, McDonnell SK, Hebbring SJ, Cunningham JM, St Sauver J, Cerhan JR, Isaya G, Schaid DJ, Thibodeau SN (2008) Polymorphisms in mitochondrial genes and prostate cancer risk. Cancer Epidemiol Biomarkers Prev **17:** 3558-3566

Wang L, Xin F, Lin N, Wang Y, Liu X, Liu J (2018) Metallothioneins may be a potential prognostic biomarker for tumors: A Prisma-compliant meta-analysis. Medicine **97:** e13786

Wang S, Wei J, Li S, Luo Y, Li Y, Wang X, Shen W, Luo D, Liu D (2022) PPA1, an energy metabolism initiator, plays an important role in the progression of malignant tumors. Front Oncol **12**

Wei Y, Dong J, Li F, Wei Z, Tian Y (2017) Knockdown of SLC39A7 suppresses cell proliferation, migration and invasion in cervical cancer. EXCLI J **16:** 1165-1176

Wei Y, Fu D (2005) Selective metal binding to a membrane-embedded aspartate in the Escherichia coli metal transporter YiiP (FieF). J Biol Chem **280:** 33716-33724

Wenzel HJ, Cole TB, Born DE, Schwartzkroin PA, Palmiter RD (1997) Ultrastructural localization of zinc transporter-3 (ZnT-3) to synaptic vesicle membranes within mossy fiber boutons in the hippocampus of mouse and monkey. Proc Natl Acad Sci U S A **94:** 12676-12681

Wenzlau JM, Juhl K, Yu L, Moua O, Sarkar SA, Gottlieb P, Rewers M, Eisenbarth GS, Jensen J, Davidson HW (2007) The cation efflux transporter ZnT8 (Slc30A8) is a major autoantigen in human type 1 diabetes. Proc Natl Acad Sci U S A **104:** 17040-17045

Werynska B, Pula B, Muszczynska-Bernhard B, Gomulkiewicz A, Piotrowska A, Prus R, Podhorska-Okolow M, Jankowska R, Dziegiel P (2013) Metallothionein 1F and 2A overexpression predicts poor outcome of non-small cell lung cancer patients. Exp Mol Pathol **94:** 301-308

Wright E, Dormandy T (1972) Liver zinc in carcinoma. Nature **237:** 166-166

Wu C, Li D, Jia W, Hu Z, Zhou Y, Yu D, Tong T, Wang M, Lin D, Qiao Y, Zhou Y, Chang J, Zhai K, Wang M, Wei L, Tan W, Shen H, Zeng Y, Lin D (2013) Genome-wide association study identifies common variants in SLC39A6 associated with length of survival in esophageal squamous-cell carcinoma. Nat Genet **45:** 632-638

Wu DM, Liu T, Deng SH, Han R, Xu Y (2017) SLC39A4 expression is associated with enhanced cell migration, cisplatin resistance, and poor survival in non-small cell lung cancer. Sci Rep **7:** 7211

Wu L, Chaffee KG, Parker AS, Sicotte H, Petersen GM (2015) Zinc transporter genes and urological cancers: integrated analysis suggests a role for ZIP11 in bladder cancer. Tumour Biol **36:** 7431-7437

Wu Z, Sun S, Fan R, Wang Z (2022) Tubulin alpha 1c promotes aerobic glycolysis and cell growth through upregulation of yes association protein expression in breast cancer. Anticancer Drugs **33:** 132-141

Xie Y, Wang J, Zhao X, Zhou X, Nie X, Li C, Huang F, Yuan H (2018) Higher serum zinc levels may reduce the risk of cervical cancer in Asian women: a meta-analysis. J Int Med Res **46:** 4898-4906

Xu C, Wallace MB, Yang J, Jiang L, Zhai Q, Zhang Y, Hong C, Chen Y, Frank TS, Stauffer JA, Asbun HJ, Raimondo M, Woodward TA, Li Z, Guha S, Zheng L, Li M (2014) ZIP4 is a novel diagnostic and prognostic marker in human pancreatic cancer: a systemic comparison between EUS-FNA and surgical specimens. Curr Mol Med **14:** 309-315

Xu X, Guo HJ, Xie HY, Li J, Zhuang RZ, Ling Q, Zhou L, Wei XY, Liu ZK, Ding SM, Chen KJ, Xu ZY, Zheng SS (2014) ZIP4, a novel determinant of tumor invasion in hepatocellular carcinoma, contributes to tumor recurrence after liver transplantation. Int J Biol Sci **10:** 245-256

Yamashita S, Miyagi C, Fukada T, Kagara N, Che YS, Hirano T (2004) Zinc transporter LIVI controls epithelial-mesenchymal transition in zebrafish gastrula organizer. Nature **429:** 298-302

Yang J, Zhang Y, Cui X, Yao W, Yu X, Cen P, Hodges SE, Fisher WE, Brunicardi FC, Chen C, Yao Q, Li M (2013) Gene profile identifies zinc transporters differentially expressed in normal human organs and human pancreatic cancer. Curr Mol Med **13:** 401-409

Ye C, Lian G, Wang T, Chen A, Chen W, Gong J, Luo L, Wang H, Xie L (2022) The zinc transporter ZIP12 regulates monocrotaline-induced proliferation and migration of pulmonary arterial smooth muscle cells via the AKT/ERK signaling pathways. BMC Pulm Med **22:** 111

Yee C, Dickson KA, Muntasir MN, Ma Y, Marsh DJ (2022) Three-Dimensional Modelling of Ovarian Cancer: From Cell Lines to Organoids for Discovery and Personalized Medicine. Front Bioeng Biotechnol **10:** 836984

Yi B, Huang G, Zhou Z (2016) Different role of zinc transporter 8 between type 1 diabetes mellitus and type 2 diabetes mellitus. J Diabetes Investig **7:** 459-465

Yin S, Duan M, Fang B, Zhao G, Leng X, Zhang T (2022) Zinc homeostasis and regulation: Zinc transmembrane transport through transporters. Crit Rev Food Sci Nutr**:** 1-11

Yoneten KK, Kasap M, Akpinar G, Gunes A, Gurel B, Utkan NZ (2019) Comparative proteome analysis of breast cancer tissues highlights the importance of glycerol-3-phosphate dehydrogenase 1 and monoacylglycerol lipase in breast cancer metabolism. Cancer Genomics Proteomics **16:** 377-397

Youn J, Borghesi LA, Olson EA, Lynes MA (1995) Immunomodulatory activities of extracellular metallothionein. II. Effects on macrophage functions. J Toxicol Environ Health **45:** 397-413

Young GM, Radhakrishnan VM, Centuori SM, Gomes CJ, Martinez JD (2015) Comparative analysis of 14-3-3 isoform expression and epigenetic alterations in colorectal cancer. BMC Cancer **15:** 826

Yu Y, Wu A, Zhang Z, Yan G, Zhang F, Zhang L, Shen X, Hu R, Zhang Y, Zhang K, Wang F (2013) Characterization of the GufA subfamily member SLC39A11/Zip11 as a zinc transporter. J Nutr Biochem **24:** 1697-1708

Yuan J, Xiao C, Lu H, Yu H, Hong H, Guo C, Wu Z (2020) miR-200b regulates breast cancer cell proliferation and invasion by targeting radixin. Exp Ther Med **19:** 2741-2750

Zaman MS, Barman SK, Corley SM, Wilkins MR, Malladi CS, Wu MJ (2021) Transcriptomic insights into the zinc homeostasis of MCF-7 breast cancer cells via next-generation RNA sequencing. Metallomics **13:** mfab026

Zaman MS, Johnson AJ, Bobek G, Kueh S, Kersaitis C, Bailey TD, Buskila Y, Wu MJ (2016) Protein kinase CK2 regulates metal toxicity in neuronal cells. Metallomics **8:** 82-90

Zaman MS, Johnson AJ, Petersingham G, Muench GW, Dong Q, Wu MJ (2019) Protein kinase CK2 is involved in zinc homeostasis in breast and prostate cancer cells. Biometals **32:** 861-873

Zatta P, Drago D, Bolognin S, Sensi SL (2009) Alzheimer's disease, metal ions and metal homeostatic therapy. Trends Pharmacol Sci **30:** 346-355

Zeng Q, Liu YM, Liu J, Han J, Guo JX, Lu S, Huang XM, Yi P, Lang JY, Zhang P, Wang CT (2019) Inhibition of ZIP4 reverses epithelial-to-mesenchymal transition and enhances the radiosensitivity in human nasopharyngeal carcinoma cells. Cell Death Dis **10:** 588

Zhang L-H, Wang X, Zheng Z-H, Ren H, Stoltenberg M, Danscher G, Huang L, Rong M, Wang Z-Y (2010) Altered expression and distribution of zinc transporters in APP/PS1 transgenic mouse brain. Neurobiol Aging **31:** 74-87

Zhang L, Zhang X, Che D, Zeng L, Zhang Y, Nan K, Zhang X, Zhang H, Guo Z (2022) 6-Methoxydihydrosanguinarine induces apoptosis and autophagy in breast cancer MCF-7 cells by accumulating ROS to suppress the PI3K/AKT/mTOR signaling pathway. Phytother Res **37:** 124-139

Zhang S, Wang J, Chen T, Wang J, Wang Y, Yu Z, Zhao K, Zheng K, Chen Y, Wang Z, Li B, Wang C, Huang W, Fu Z, Chen J (2021) α-Actinin1 promotes tumorigenesis and epithelial-mesenchymal transition of gastric cancer via the AKT/GSK3β/β-Catenin pathway. Bioengineered **12:** 5688-5704

Zhang T, Liu J, Fellner M, Zhang C, Sui D, Hu J (2017) Crystal structures of a ZIP zinc transporter reveal a binuclear metal center in the transport pathway. Sci Adv **3:** e1700344

Zhang T, Sui D, Hu J (2016) Structural insights of ZIP4 extracellular domain critical for optimal zinc transport. Nat Commun **7:** 11979

Zhang W, Liu X (2022) Upregulation of metallothionein 1G (MT1G) negatively regulates ferroptosis in clear cell renal cell carcinoma by reducing glutathione consumption. J Oncol **2022:** 4000617

Zhang X, Jing Y, Qin Y, Hunsucker S, Meng H, Sui J, Jiang Y, Gao L, An G, Yang N, Orlowski RZ, Yang L (2012) The zinc finger transcription factor ZKSCAN3 promotes prostate cancer cell migration. Int J Biochem Cell Biol **44:** 1166-1173

Zhang Y, Bharadwaj U, Logsdon CD, Chen C, Yao Q, Li M (2010) ZIP4 regulates pancreatic cancer cell growth by activating IL-6/STAT3 pathway through zinc finger transcription factor CREB. Clin Cancer Res **16:** 1423-1430

Zhao H, Eide D (1996) The yeast ZRT1 gene encodes the zinc transporter protein of a high-affinity uptake system induced by zinc limitation. Proc Natl Acad Sci U S A **93:** 2454-2458

Zhao H, Eide D (1996) The ZRT2 gene encodes the low affinity zinc transporter in Saccharomyces cerevisiae. J Biol Chem **271:** 23203-23210

Zhao L, Chen W, Taylor KM, Cai B, Li X (2007) LIV-1 suppression inhibits HeLa cell invasion by targeting ERK1/2-Snail/Slug pathway. Biochem Biophys Res Commun **363:** 82-88

Zhao L, Oliver E, Maratou K, Atanur SS, Dubois OD, Cotroneo E, Chen C-N, Wang L, Arce C, Chabosseau PL, Ponsa-Cobas J, Frid MG, Moyon B, Webster Z, Aldashev A, Ferrer J, Rutter GA, Stenmark KR, Aitman TJ, Wilkins MR (2015) The zinc transporter ZIP12 regulates the pulmonary vascular response to chronic hypoxia. Nature **524:** 356-360

Zhao N, Gao J, Enns CA, Knutson MD (2010) ZRT/IRT-like protein 14 (ZIP14) promotes the cellular assimilation of iron from transferrin. J Biol Chem **285:** 32141-32150

Zhao X, Fu J, Du J, Xu W (2020) The Role of D-3-Phosphoglycerate Dehydrogenase in Cancer. Int J Biol Sci **16:** 1495-1506

Zhao Y, Feresin RG, Falcon-Perez JM, Salazar G (2016) Differential Targeting of SLC30A10/ZnT10 Heterodimers to Endolysosomal Compartments Modulates EGF-Induced MEK/ERK1/2 Activity. Traffic **17:** 267-288

Zhou B, Yan Y, Wang Y, You S, Freeman MR, Yang W (2019) Quantitative proteomic analysis of prostate tissue specimens identifies deregulated protein complexes in primary prostate cancer. Clin Proteomics **16:** 1-18

Zhu X, Yu C, Wu W, Shi L, Jiang C, Wang L, Ding Z, Liu Y (2022) Zinc transporter ZIP12 maintains zinc homeostasis and protects spermatogonia from oxidative stress during spermatogenesis. Reprod Biol Endocrinol **20:** 17

Zhu Y, Tummala R, Liu C, Nadiminty N, Lou W, Evans CP, Zhou Q, Gao AC (2012) RhoGDIα suppresses growth and survival of prostate cancer cells. Prostate **72:** 392-398

Ziegler YS, Moresco JJ, Tu PG, Yates JR, Nardulli AM (2018) Proteomic analysis identifies highly expressed plasma membrane proteins for detection and therapeutic targeting of specific breast cancer subtypes. Clin Proteomics **15:** 1-9

Ziliotto S, Gee JM, Ellis IO, Green AR, Finlay P, Gobbato A, Taylor KM (2019) Activated zinc transporter ZIP7 as an indicator of anti-hormone resistance in breast cancer. Metallomics **11:** 1579-1592

Zogzas CE, Aschner M, Mukhopadhyay S (2016) Structural Elements in the Transmembrane and Cytoplasmic Domains of the Metal Transporter SLC30A10 Are Required for Its Manganese Efflux Activity. J Biol Chem **291:** 15940-15957

Zou J, Milon BC, Desouki MM, Costello LC, Franklin RB (2011) hZIP1 zinc transporter down-regulation in prostate cancer involves the overexpression of ras responsive element binding protein-1 (RREB-1). Prostate **71:** 1518-1524

Zoubeidi A, Gleave M (2012) Small heat shock proteins in cancer therapy and prognosis. Int J Biochem Cell Biol **44:** 1646-1656

8 Appendices

8.1 Appendix A

8.1.1 List of the CT values of MCF10A cells with and without mild cytotoxic zinc exposure

Gene	CT at T_0	CT at T_{30}	CT at T_{120}	Gene	CT at T_0	CT at T_{30}	CT at T_{120}
GAPDH	21.708	20.967	21.552	*SLC39A1*	24.384	24.183	24.609
GAPDH	21.138	21.134	21.198	*SLC39A1*	24.107	24.147	24.252
GAPDH	21.378	20.75	21.235	*SLC39A1*	24.312	23.947	24.278
GAPDH	21.708	21.33	21.722	*SLC39A2*	36.084	36.763	37.019
GAPDH	21.138	21.192	21.382	*SLC39A2*	35.862	36.074	35.721
GAPDH	21.378	20.951	21.409	*SLC39A2*	35.493	35.399	36.306
GAPDH	21.708	21.665	21.992	*SLC39A3*	30.086	29.692	30.25
GAPDH	21.138	21.54	21.744	*SLC39A3*	29.831	29.664	29.877
GAPDH	21.378	21.445	21.704	*SLC39A3*	29.623	29.521	29.962
GAPDH	21.708	20.963	21.312	*SLC39A4*	35.391	34.553	36.613
GAPDH	21.138	20.848	21.101	*SLC39A4*	36.145	34.534	34.915
GAPDH	21.378	20.665	21.277	*SLC39A4*	35.45	35.159	37.089
GAPDH	21.708	20.918	21.286	*SLC39A5*	34.612	34.608	34.924
GAPDH	21.138	20.886	20.964	*SLC39A5*	33.538	32.606	34.362
GAPDH	21.378	20.781	20.939	*SLC39A5*	34.624	37.071	33.647
GAPDH	21.708	20.967	21.552	*SLC39A6*	26.016	26.763	27.315
GAPDH	21.138	21.134	21.198	*SLC39A6*	25.968	26.551	26.421
GAPDH	21.378	20.75	21.235	*SLC39A6*	26.577	26.478	26.242
GAPDH	21.581	21.33	21.722	*SLC39A7*	27.317	27.105	27.599
GAPDH	21.214	21.192	21.382	*SLC39A7*	27.071	27.018	27.09
GAPDH	21.474	20.951	21.409	*SLC39A7*	27.071	26.963	26.852
GAPDH	21.581	21.665	21.992	*SLC39A8*	28.846	28.875	29.454
GAPDH	21.214	21.54	21.744	*SLC39A8*	28.338	28.894	28.761
GAPDH	21.474	21.445	21.704	*SLC39A8*	28.977	28.524	28.981
GAPDH	21.581	20.963	21.312	*SLC39A9*	26.963	27.089	27.741
GAPDH	21.214	20.848	21.101	*SLC39A9*	26.636	27.101	26.887
GAPDH	21.474	20.665	21.277	*SLC39A9*	27.017	26.928	26.963
GAPDH	21.581	20.918	21.286	*SLC39A10*	29.607	29.559	30.927
GAPDH	21.214	20.886	20.964	*SLC39A10*	29.185	29.629	29.825
GAPDH	21.474	20.781	20.939	*SLC39A10*	29.93	29.539	29.714

GAPDH	21.581	20.967	21.552	*SLC39A11*	29.696	29.969	30.143
GAPDH	21.214	21.134	21.198	*SLC39A11*	29.483	29.998	29.649
GAPDH	21.474	20.75	21.235	*SLC39A11*	29.832	29.723	29.367
GAPDH	21.581	21.33	21.722	*SLC39A12*	27.544	27.014	25.727
GAPDH	21.214	21.192	21.382	*SLC39A12*	27.29	26.93	24.428
GAPDH	21.474	20.951	21.409	*SLC39A12*	27.752	26.955	24.522
GAPDH	21.945	21.665	21.992	*SLC39A13*	29.58	29.625	29.938
GAPDH	21.617	21.54	21.744	*SLC39A13*	29.226	29.581	29.438
GAPDH	21.972	21.445	21.704	*SLC39A13*	29.514	29.637	29.409
GAPDH	21.945	20.963	21.312	*SLC39A14*	26.886	26.974	27.053
GAPDH	21.617	20.848	21.101	*SLC39A14*	26.416	26.948	26.68
GAPDH	21.972	20.665	21.277	*SLC39A14*	26.765	26.77	26.644
GAPDH	21.945	20.918	21.286	*SLC30A1*	28.145	27.751	26.076
GAPDH	21.617	20.886	20.964	*SLC30A1*	27.941	27.896	25.274
GAPDH	21.972	20.781	20.939	*SLC30A1*	28.549	27.548	25.073
GAPDH	21.945	20.967	21.552	*SLC30A2*	36.554	34.606	31.944
GAPDH	21.617	21.134	21.198	*SLC30A2*	35.669	34.157	31.525
GAPDH	21.972	20.75	21.235	*SLC30A2*	35.94	34.524	31.457
GAPDH	21.945	21.33	21.722	*SLC30A3*	32.006	31.966	32.185
GAPDH	21.617	21.192	21.382	*SLC30A3*	31.637	31.868	32.15
GAPDH	21.972	20.951	21.409	*SLC30A3*	32.074	31.615	31.965
GAPDH	21.945	21.665	21.992	*SLC30A4*	31.072	31.281	31.602
GAPDH	21.617	21.54	21.744	*SLC30A4*	30.936	31.088	30.947
GAPDH	21.972	21.445	21.704	*SLC30A4*	31.249	30.915	30.893
GAPDH	21.427	20.963	21.312	*SLC30A5*	28.478	28.263	28.842
GAPDH	21.1	20.848	21.101	*SLC30A5*	27.926	28.347	28.151
GAPDH	21.175	20.665	21.277	*SLC30A5*	28.524	28.189	28.193
GAPDH	21.427	20.918	21.286	*SLC30A6*	28.895	28.782	29.438
GAPDH	21.1	20.886	20.964	*SLC30A6*	28.458	28.87	28.638
GAPDH	21.175	20.781	20.939	*SLC30A6*	28.914	28.462	28.563
GAPDH	21.427	21.33	21.722	*SLC30A7*	27.71	27.712	28.104
GAPDH	21.1	21.192	21.382	*SLC30A7*	27.323	27.929	27.514
GAPDH	21.175	20.951	21.409	*SLC30A7*	27.884	27.495	27.483
GAPDH	21.195	21.665	21.992	*SLC30A8*	21.196	20.857	21.251
GAPDH	20.787	21.54	21.744	*SLC30A8*	20.795	20.815	20.932
GAPDH	21.019	21.445	21.704	*SLC30A8*	21.231	20.761	20.958

GAPDH	21.427	20.963	21.312	*SLC30A9*	27.688	27.462	28.579
GAPDH	21.1	20.848	21.101	*SLC30A9*	27.235	27.658	27.448
GAPDH	21.175	20.665	21.277	*SLC30A9*	27.934	27.275	27.289
GAPDH	21.427	20.918	21.286	*SLC30A10*	26.777	26.907	26.795
GAPDH	21.1	20.886	20.964	*SLC30A10*	26.336	26.959	26.132
GAPDH	21.175	20.781	20.939	*SLC30A10*	26.98	26.618	26.017
GAPDH	21.818	21.339	21.473	*MT1B*	29.508	20.816	20.437
GAPDH	21.494	21.323	21.443	*MT1B*	28.504	20.715	20.373
GAPDH	21.329	21.322	21.438	*MT1B*	26.498	20.636	20.381
GAPDH	21.818	21.339	21.473	*MT1F*	28.093	20.412	19.572
GAPDH	21.494	21.323	21.443	*MT1F*	27.154	20.421	19.665
GAPDH	21.329	21.322	21.438	*MT1F*	26.893	20.528	20.971
GAPDH	21.818	21.339	21.473	*MT1X*	26.542	20.296	20.834
GAPDH	21.494	21.323	21.443	*MT1X*	27.673	20.907	19.832
GAPDH	21.329	21.322	21.438	*MT1X*	29.587	21.418	20.614
GAPDH	21.818	21.339	21.473	*MT2A*	28.526	20.696	20.343
GAPDH	21.494	21.323	21.443	*MT2A*	29.129	19.494	20.123
GAPDH	21.329	21.322	21.438	*MT2A*	28.433	20.133	19.645

8.1.2 List of the CT values of MCF10A cells with and without benign zinc exposure

Gene	CT at T_0	CT at T_{30}	CT at T_{120}	Gene	CT at T_0	CT at T_{30}	CT at T_{120}
GAPDH	22.326	22.297	22.285	*SLC39A1*	24.484	24.594	24.649
GAPDH	22.127	21.966	22.711	*SLC39A1*	24.449	24.304	24.936
GAPDH	22.208	22.292	22.378	*SLC39A1*	24.628	24.523	24.749
GAPDH	22.326	22.297	22.285	*SLC39A2*	35.02	34.996	35.114
GAPDH	22.127	21.966	22.711	*SLC39A2*	34.803	34.575	37.197
GAPDH	22.208	22.292	22.378	*SLC39A2*	35.542	34.958	34.989
GAPDH	22.326	22.297	22.285	*SLC39A3*	30.105	29.956	30.609
GAPDH	22.127	21.966	22.711	*SLC39A3*	29.872	29.89	30.393
GAPDH	22.208	22.292	22.378	*SLC39A3*	29.886	29.957	30.279
GAPDH	22.326	22.297	22.285	*SLC39A4*	36.691	37.095	36.257
GAPDH	22.127	21.966	22.711	*SLC39A4*	35.867	35.764	36.819
GAPDH	22.208	22.292	22.378	*SLC39A4*	36.572	36.353	36.257
GAPDH	22.326	22.297	22.285	*SLC39A5*	34.873	34.882	37.085
GAPDH	22.127	21.966	22.711	*SLC39A5*	35.178	35.631	35.975
GAPDH	22.208	22.292	22.378	*SLC39A5*	35.918	34.693	36.529

GAPDH	22.326	22.297	22.285	*SLC39A6*	25.784	26.335	26.329
GAPDH	22.127	21.966	22.711	*SLC39A6*	25.988	25.961	26.712
GAPDH	22.208	22.292	22.378	*SLC39A6*	25.992	26.115	26.234
GAPDH	22.326	22.297	22.285	*SLC39A8*	27.562	27.719	27.668
GAPDH	22.127	21.966	22.711	*SLC39A8*	27.363	27.444	27.99
GAPDH	22.208	22.292	22.378	*SLC39A8*	27.67	27.658	27.837
GAPDH	22.326	22.297	22.285	*SLC39A10*	28.126	28.085	28.483
GAPDH	22.127	21.966	22.711	*SLC39A10*	28.109	27.757	28.932
GAPDH	22.208	22.292	22.378	*SLC39A10*	28.216	28.264	28.488
GAPDH	22.326	22.297	22.285	*SLC39A12*	28.903	28.926	26.036
GAPDH	22.127	21.966	22.711	*SLC39A12*	29.476	28.655	25.956
GAPDH	22.208	22.292	22.378	*SLC39A12*	29.252	28.793	25.548
GAPDH	22.326	22.297	22.285	*SLC39A14*	26.865	27.083	27.104
GAPDH	22.127	21.966	22.711	*SLC39A14*	26.895	26.916	27.467
GAPDH	22.208	22.292	22.378	*SLC39A14*	26.975	26.954	27.237
GAPDH	21.96	21.984	21.948	*SLC30A1*	28.619	28.494	25.79
GAPDH	21.758	21.951	22.395	*SLC30A1*	28.965	28.36	25.953
GAPDH	21.937	21.962	22.087	*SLC30A1*	29.264	28.426	25.902
GAPDH	21.96	21.984	21.948	*SLC30A2*	36.968	36.388	32.694
GAPDH	21.758	21.951	22.395	*SLC30A2*	36.646	35.821	33.077
GAPDH	21.937	21.962	22.087	*SLC30A2*	35.507	36.836	33.077
GAPDH	21.96	21.984	21.948	*MT1B*	35.631	35.815	34.123
GAPDH	21.758	21.951	22.395	*MT1B*	35.662	35.732	34.172
GAPDH	21.937	21.962	22.087	*MT1B*	34.747	36.955	35.044
GAPDH	21.96	21.984	21.948	*MT1F*	29.191	28.73	26.525
GAPDH	21.758	21.951	22.395	*MT1F*	28.853	28.394	26.926
GAPDH	21.937	21.962	22.087	*MT1F*	28.912	28.733	26.925
GAPDH	21.96	21.984	21.948	*MT1X*	24.727	24.661	23.525
GAPDH	21.758	21.951	22.395	*MT1X*	24.251	24.21	23.953
GAPDH	21.937	21.962	22.087	*MT1X*	24.646	24.538	23.581
GAPDH	21.96	21.984	21.948	*MT2A*	22.48	22.452	21.972
GAPDH	21.758	21.951	22.395	*MT2A*	22.488	22.465	22.167
GAPDH	21.937	21.962	22.087	*MT2A*	22.561	22.543	22.105

8.1.3 List of the CT values of MCF-7 cells with and without mild cytotoxic zinc exposure

Gene	CT at T_0	CT at T_{30}	CT at T_{120}	Gene	CT at T_0	CT at T_{30}	CT at T_{120}
GAPDH	22.87	22.758	22.796	*SLC39A1*	25.492	25.441	25.947
GAPDH	22.885	22.643	22.974	*SLC39A1*	25.494	25.502	25.947
GAPDH	22.905	22.81	22.711	*SLC39A1*	25.559	25.744	25.723
GAPDH	22.87	22.758	22.796	*SLC39A2*	36.221	36.392	35.937
GAPDH	22.885	22.643	22.974	*SLC39A2*	35.111	37.24	34.558
GAPDH	22.905	22.81	22.711	*SLC39A2*	35.548	34.981	34.558
GAPDH	22.87	22.758	22.796	*SLC39A3*	32.057	31.498	32.135
GAPDH	22.885	22.643	22.974	*SLC39A3*	32.139	31.572	31.959
GAPDH	22.905	22.81	22.711	*SLC39A3*	32.012	31.618	31.863
GAPDH	22.87	22.758	22.796	*SLC39A4*	34.886	33.529	35.63
GAPDH	22.885	22.643	22.974	*SLC39A4*	37.183	34.816	34.486
GAPDH	22.905	22.81	22.711	*SLC39A4*	37.707	34.59	34.486
GAPDH	22.87	22.758	22.796	*SLC39A5*	35.125	36.116	34.987
GAPDH	22.885	22.643	22.974	*SLC39A5*	35.217	34.658	35.723
GAPDH	22.905	22.81	22.711	*SLC39A5*	35.217	35.723	35.555
GAPDH	22.382	22.758	22.796	*SLC39A6*	24.753	24.973	25.136
GAPDH	22.438	22.643	22.974	*SLC39A6*	24.796	25.079	24.398
GAPDH	21.951	22.81	22.711	*SLC39A6*	24.67	25.07	25.198
GAPDH	22.382	22.328	22.439	*SLC39A7*	28.561	28.551	28.951
GAPDH	22.438	22.24	21.453	*SLC39A7*	28.622	28.543	27.962
GAPDH	21.951	22.339	22.319	*SLC39A7*	28.553	28.683	28.777
GAPDH	22.382	22.328	22.439	*SLC39A8*	28.958	28.884	28.979
GAPDH	22.438	22.24	21.453	*SLC39A8*	28.956	28.999	28.169
GAPDH	21.951	22.339	22.319	*SLC39A8*	28.809	28.868	28.978
GAPDH	22.382	22.328	22.439	*SLC39A9*	28.061	27.833	28.335
GAPDH	22.438	22.24	21.453	*SLC39A9*	28.043	27.833	27.261
GAPDH	21.951	22.339	22.319	*SLC39A9*	27.933	27.948	28.036
GAPDH	22.382	22.328	22.439	*SLC39A10*	30.771	30.535	30.144
GAPDH	22.438	22.24	21.453	*SLC39A10*	30.813	30.564	30.932
GAPDH	21.951	22.339	22.319	*SLC39A10*	30.669	30.629	30.821
GAPDH	21.992	22.328	22.439	*SLC39A11*	28.829	28.266	29.072
GAPDH	22.245	22.24	21.453	*SLC39A11*	28.898	28.806	29.206
GAPDH	21.959	22.339	22.319	*SLC39A11*	28.907	29.092	28.961

GAPDH	21.992	22.042	22.3	*SLC39A12*	28.454	27.911	28.461
GAPDH	22.245	21.957	22.493	*SLC39A12*	28.6	27.716	28.436
GAPDH	21.959	22.466	22.172	*SLC39A12*	28.896	28.291	28.558
GAPDH	21.992	22.042	22.3	*SLC39A13*	29.717	29.415	30.291
GAPDH	22.245	21.957	22.493	*SLC39A13*	29.953	29.924	30.46
GAPDH	21.959	22.466	22.172	*SLC39A13*	29.956	30.177	30.429
GAPDH	21.992	22.042	22.3	*SLC39A14*	29.757	29.414	29.738
GAPDH	22.245	21.957	22.493	*SLC39A14*	29.953	29.431	29.899
GAPDH	21.959	22.466	22.172	*SLC39A14*	29.835	29.694	29.953
GAPDH	21.992	22.042	22.3	*SLC30A1*	28.841	28.986	26.812
GAPDH	22.245	21.957	22.493	*SLC30A1*	28.141	27.751	26.512
GAPDH	21.959	22.466	22.172	*SLC30A1*	28.818	26.964	25.714
GAPDH	21.992	22.042	22.3	*SLC30A1*	21.233	19.794	19.316
GAPDH	22.245	21.957	22.493	*SLC30A1*	21.569	19.388	19.612
GAPDH	21.959	22.466	22.172	*SLC30A1*	21.705	20.748	20.341
GAPDH	21.992	22.042	22.3	*SLC30A2*	29.013	28.399	28.838
GAPDH	22.245	21.957	22.493	*SLC30A2*	29.106	28.558	28.932
GAPDH	21.959	22.466	22.172	*SLC30A2*	29.297	28.859	29.232
GAPDH	21.992	22.042	22.3	*SLC30A2*	32.517	33.034	33.553
GAPDH	22.245	21.957	22.493	*SLC30A2*	32.951	32.569	33.807
GAPDH	21.959	22.466	22.172	*SLC30A2*	33.702	33.803	33.954
GAPDH	21.992	22.042	22.3	*SLC30A3*	35.537	35.151	36.279
GAPDH	22.245	21.957	22.493	*SLC30A3*	36.341	35.243	32.673
GAPDH	21.959	22.466	22.172	*SLC30A3*	36.984	32.986	32.673
GAPDH	21.992	22.042	22.3	*SLC30A3*	32.274	32.864	31.871
GAPDH	22.245	21.957	22.493	*SLC30A3*	32.964	32.609	32.436
GAPDH	21.959	22.466	22.172	*SLC30A3*	33.509	31.241	30.921
GAPDH	21.992	22.042	22.3	*SLC30A4*	32.941	33.176	33.659
GAPDH	22.245	21.957	22.493	*SLC30A4*	33.079	32.859	32.896
GAPDH	21.959	22.466	22.172	*SLC30A4*	33.221	32.736	33.82
GAPDH	22.87	22.042	22.3	*SLC30A5*	29.191	29.315	30.969
GAPDH	22.885	21.957	22.493	*SLC30A5*	28.944	28.497	27.795
GAPDH	22.905	22.466	22.172	*SLC30A5*	30.187	27.704	31.835
GAPDH	21.992	21.939	22.089	*SLC30A6*	29.387	29.582	28.804
GAPDH	22.245	21.967	22.072	*SLC30A6*	29.447	28.934	31.857
GAPDH	21.959	22.422	22.401	*SLC30A6*	30.249	30.957	31

GAPDH	21.992	21.939	22.089	*SLC30A7*	28.063	27.441	29.412
GAPDH	22.245	21.967	22.072	*SLC30A7*	27.873	29.175	29.257
GAPDH	21.959	22.422	22.401	*SLC30A7*	29.134	26.942	29.124
GAPDH	21.992	21.939	22.089	*SLC30A8*	36.148	35.113	36.999
GAPDH	22.245	21.967	22.072	*SLC30A8*	36.449	35.65	35.981
GAPDH	21.959	22.422	22.401	*SLC30A8*	35.56	35.405	35.13
GAPDH	21.992	21.939	22.089	*SLC30A8*	35.638	35.91	35.973
GAPDH	22.245	21.967	22.072	*SLC30A8*	36.754	35.313	34.909
GAPDH	21.959	22.422	22.401	*SLC30A8*	36.887	34.384	34.474
GAPDH	21.992	21.939	22.089	*SLC30A9*	27.944	27.706	27.604
GAPDH	22.245	21.967	22.072	*SLC30A9*	28.36	27.726	27.591
GAPDH	21.959	22.422	22.401	*SLC30A9*	28.735	26.637	26.84
GAPDH	21.992	21.939	22.089	*SLC30A10*	28.311	27.953	28.602
GAPDH	22.245	21.967	22.072	*SLC30A10*	28.386	27.841	28.458
GAPDH	21.959	22.422	22.401	*SLC30A10*	28.723	28.5	28.694
GAPDH	21.992	21.939	22.089	*SLC30A10*	28.739	29.35	29.484
GAPDH	22.245	21.967	22.072	*SLC30A10*	29.851	29.278	29.951
GAPDH	21.959	22.422	22.401	*SLC30A10*	29.97	28.616	28.463
GAPDH	21.287	21.192	21.428	*MT1B*	21.666	20.514	20.259
GAPDH	21.247	21.152	21.415	*MT1B*	21.655	20.421	19.882
GAPDH	21.239	21.104	21.286	*MT1B*	21.607	20.065	19.683
GAPDH	21.287	21.192	21.428	*MT1F*	21.098	19.529	19.338
GAPDH	21.247	21.152	21.415	*MT1F*	21.194	19.642	19.892
GAPDH	21.239	21.104	21.286	*MT1F*	21.648	20.843	19.693
GAPDH	21.287	21.192	21.428	*MT1X*	21.264	20.628	20.613
GAPDH	21.247	21.152	21.415	*MT1X*	21.745	19.797	19.782
GAPDH	21.239	21.104	21.286	*MT1X*	21.622	20.336	19.537
GAPDH	21.287	21.192	21.428	*MT2A*	21.421	20.536	19.651
GAPDH	21.247	21.152	21.415	*MT2A*	21.762	21.425	19.719
GAPDH	21.239	21.104	21.286	*MT2A*	21.728	21.178	20.904

8.1.4 List of the CT values of MCF-7 cells with and without benign zinc exposure

Gene	CT at T_0	CT at T_{30}	CT at T_{120}	Gene	CT at T_0	CT at T_{30}	CT at T_{120}
GAPDH	21.493	21.507	21.738	*SLC39A1*	24.692	24.84	24.946
GAPDH	21.52	21.518	21.983	*SLC39A1*	24.637	24.698	24.924
GAPDH	21.431	21.608	21.412	*SLC39A1*	24.814	24.945	24.687
GAPDH	21.493	21.507	21.738	*SLC39A2*	36.823	36.283	35.311
GAPDH	21.52	21.518	21.983	*SLC39A2*	35.943	35.174	35.013
GAPDH	21.431	21.608	21.412	*SLC39A2*	36.405	36.283	35.869
GAPDH	21.493	21.507	21.738	*SLC39A3*	30.619	30.741	30.888
GAPDH	21.52	21.518	21.983	*SLC39A3*	30.509	30.721	30.965
GAPDH	21.431	21.608	21.412	*SLC39A3*	30.703	30.897	30.815
GAPDH	21.493	21.507	21.738	*SLC39A4*	35.546	36.636	36.328
GAPDH	21.52	21.518	21.983	*SLC39A4*	36.922	36.901	36.768
GAPDH	21.431	21.608	21.412	*SLC39A4*	36.924	36.595	36.768
GAPDH	21.493	21.507	21.738	*SLC39A5*	35.323	34.655	35.882
GAPDH	21.52	21.518	21.983	*SLC39A5*	35.062	34.931	36.512
GAPDH	21.431	21.608	21.412	*SLC39A5*	34.705	35.6	35.644
GAPDH	21.493	21.507	21.738	*SLC39A6*	24.987	24.74	24.928
GAPDH	21.52	21.518	21.983	*SLC39A6*	24.416	24.678	24.856
GAPDH	21.431	21.608	21.412	*SLC39A6*	24.336	24.884	24.815
GAPDH	21.493	21.507	21.738	*SLC39A8*	27.389	27.295	27.624
GAPDH	21.52	21.518	21.983	*SLC39A8*	27.32	27.528	27.464
GAPDH	21.431	21.608	21.412	*SLC39A8*	27.122	27.554	27.955
GAPDH	21.493	21.507	21.738	*SLC39A10*	28.897	28.912	29.219
GAPDH	21.52	21.518	21.983	*SLC39A10*	29.295	28.868	28.994
GAPDH	21.431	21.608	21.412	*SLC39A10*	28.897	29.096	28.941
GAPDH	21.493	21.507	21.738	*SLC39A12*	26.924	26.816	26.844
GAPDH	21.52	21.518	21.983	*SLC39A12*	26.954	26.53	26.542
GAPDH	21.431	21.608	21.412	*SLC39A12*	27.38	26.819	26.669
GAPDH	21.493	21.507	21.738	*SLC39A14*	28.985	29.097	28.959
GAPDH	21.52	21.518	21.983	*SLC39A14*	29.014	29.173	28.789
GAPDH	21.431	21.608	21.412	*SLC39A14*	29.144	29.059	28.749
GAPDH	21.828	21.843	21.913	*SLC30A1*	27.726	27.406	27.269
GAPDH	21.825	21.825	21.978	*SLC30A1*	27.714	27.545	26.974
GAPDH	21.771	21.929	21.841	*SLC30A1*	27.849	27.75	26.934

GAPDH	21.828	21.843	21.913	*SLC30A2*	32.621	32.843	32.897
GAPDH	21.825	21.825	21.978	*SLC30A2*	32.841	32.824	32.897
GAPDH	21.771	21.929	21.841	*SLC30A2*	33.698	32.879	32.868
GAPDH	21.828	21.843	21.913	*MT1B*	34.266	34.84	35.421
GAPDH	21.825	21.825	21.978	*MT1B*	33.788	33.709	35.42
GAPDH	21.771	21.929	21.841	*MT1B*	34.256	33.708	35.753
GAPDH	21.828	21.843	21.913	*MT1F*	28.36	28.284	28.21
GAPDH	21.825	21.825	21.978	*MT1F*	28.524	28.574	27.92
GAPDH	21.771	21.929	21.841	*MT1F*	28.505	28.518	27.852
GAPDH	21.828	21.843	21.913	*MT1X*	26.952	26.865	26.656
GAPDH	21.825	21.825	21.978	*MT1X*	26.97	26.974	26.409
GAPDH	21.771	21.929	21.841	*MT1X*	26.987	26.923	26.364
GAPDH	21.828	21.843	21.913	*MT2A*	24.708	24.835	24.731
GAPDH	21.825	21.825	21.978	*MT2A*	24.788	24.947	24.569
GAPDH	21.771	21.929	21.841	*MT2A*	25.053	24.913	24.756

8.1.5 List of the CT values of MDA-MB-231 cells with and without mild cytotoxic zinc exposure

Gene	**CT at T_0**	**CT at T_{30}**	**CT at T_{120}**	**Gene**	**CT at T_0**	**CT at T_{30}**	**CT at T_{120}**
GAPDH	22.891	22.649	22.335	*SLC39A1*	25.808	24.38	24.941
GAPDH	22.963	22.425	22.265	*SLC39A1*	25.667	25.552	25.106
GAPDH	22.589	22.374	22.34	*SLC39A1*	25.667	25.207	24.73
GAPDH	22.386	22.649	22.335	*SLC39A2*	28.706	27.657	27.914
GAPDH	22.432	22.425	22.265	*SLC39A2*	28.695	27.949	27.638
GAPDH	21.947	22.374	22.34	*SLC39A2*	28.354	28.018	27.78
GAPDH	22.284	21.67	21.956	*SLC39A3*	32.192	31.638	31.758
GAPDH	22.444	21.948	22.207	*SLC39A3*	32.493	31.567	31.863
GAPDH	21.917	21.943	21.573	*SLC39A3*	31.962	31.9	31.593
GAPDH	22.386	22.649	22.335	*SLC39A4*	28.753	27.954	27.731
GAPDH	22.432	22.425	22.265	*SLC39A4*	28.401	27.887	27.643
GAPDH	21.947	22.374	22.34	*SLC39A4*	28.397	28.037	27.728
GAPDH	22.284	21.67	21.956	*SLC39A5*	37.03	35.199	36.176
GAPDH	22.444	21.948	22.207	*SLC39A5*	36.818	36.065	35.33
GAPDH	21.917	21.943	21.573	*SLC39A5*	35.563	36.136	36.188

GAPDH	22.284	21.67	21.956	*SLC39A6*	24.924	24.971	24.729
GAPDH	22.444	21.948	22.207	*SLC39A6*	25.096	25.084	25.506
GAPDH	21.917	21.943	21.573	*SLC39A6*	24.96	25.373	25.162
GAPDH	22.284	21.67	21.956	*SLC39A7*	28.915	28.562	27.621
GAPDH	22.444	21.948	22.207	*SLC39A7*	28.971	28.675	28.916
GAPDH	21.917	21.943	21.573	*SLC39A7*	28.593	28.685	28.51
GAPDH	22.284	21.67	21.956	*SLC39A8*	28.976	28.651	28.526
GAPDH	22.444	21.948	22.207	*SLC39A8*	29.15	28.717	28.823
GAPDH	21.917	21.943	21.573	*SLC39A8*	28.957	28.803	28.406
GAPDH	21.96	21.684	21.537	*SLC39A9*	27.764	27.375	27.741
GAPDH	21.984	21.754	21.953	*SLC39A9*	27.98	27.513	27.994
GAPDH	22.056	21.742	21.582	*SLC39A9*	28.138	27.946	27.349
GAPDH	21.96	21.684	21.537	*SLC39A10*	30.97	29.613	29.749
GAPDH	21.984	21.754	21.953	*SLC39A10*	30.928	29.716	29.742
GAPDH	22.056	21.742	21.582	*SLC39A10*	30.957	29.929	29.95
GAPDH	21.96	21.684	21.537	*SLC39A11*	28.966	27.942	27.786
GAPDH	21.984	21.754	21.953	*SLC39A11*	28.676	27.547	28.039
GAPDH	22.056	21.742	21.582	*SLC39A11*	28.881	27.68	27.587
GAPDH	22.386	22.649	22.335	*SLC39A12*	28.784	27.97	27.704
GAPDH	22.432	22.425	22.265	*SLC39A12*	28.691	27.842	27.592
GAPDH	21.947	22.374	22.34	*SLC39A12*	28.239	27.836	27.581
GAPDH	21.96	21.684	21.537	*SLC39A13*	29.57	29.561	30.154
GAPDH	21.984	21.754	21.953	*SLC39A13*	29.681	29.612	30.323
GAPDH	22.056	21.742	21.582	*SLC39A13*	29.56	29.722	29.955
GAPDH	21.96	21.684	21.537	*SLC39A14*	29.713	29.431	29.758
GAPDH	21.984	21.754	21.953	*SLC39A14*	29.968	29.575	29.839
GAPDH	22.056	21.742	21.582	*SLC39A14*	30.291	29.742	29.525
GAPDH	22.118	21.967	22.264	*SLC30A1*	29.873	27.806	27.984
GAPDH	22.904	22.1	22.637	*SLC30A1*	29.955	27.566	26.954
GAPDH	22.417	22.289	22.047	*SLC30A1*	29.684	27.708	27.392
GAPDH	22.118	21.967	22.264	*SLC30A1*	21.94	21.957	19.173
GAPDH	22.904	22.1	22.637	*SLC30A1*	22.131	20.113	19.386
GAPDH	22.417	22.289	22.047	*SLC30A1*	22.518	20.517	21.247
GAPDH	22.118	21.967	22.264	*SLC30A2*	36.317	34.804	35.834
GAPDH	22.904	22.1	22.637	*SLC30A2*	37.13	34.67	35.834
GAPDH	22.417	22.289	22.047	*SLC30A2*	35.866	35.564	36.115

GAPDH	22.118	21.967	22.264	*SLC30A3*	33.573	31.966	32.415
GAPDH	22.904	22.1	22.637	*SLC30A3*	33.653	31.758	31.884
GAPDH	22.417	22.289	22.047	*SLC30A3*	33.381	32.224	32.871
GAPDH	22.118	21.967	22.264	*SLC30A4*	34.766	33.097	33.923
GAPDH	22.904	22.1	22.637	*SLC30A4*	34.874	33.021	34.438
GAPDH	22.417	22.289	22.047	*SLC30A4*	34.641	33.234	33.587
GAPDH	22.118	21.967	22.264	*SLC30A5*	28.225	26.26	26.938
GAPDH	22.904	22.1	22.637	*SLC30A5*	28.113	26.752	27.517
GAPDH	22.417	22.289	22.047	*SLC30A5*	28.055	26.888	26.938
GAPDH	22.118	21.967	22.264	*SLC30A6*	30.232	28.243	28.899
GAPDH	22.904	22.1	22.637	*SLC30A6*	30.387	28.537	29.599
GAPDH	22.417	22.289	22.047	*SLC30A6*	30.239	28.928	28.388
GAPDH	22.891	22.271	22.427	*SLC30A7*	28.892	27.389	27.366
GAPDH	22.963	22.441	22.707	*SLC30A7*	28.935	26.967	27.72
GAPDH	22.589	22.673	22.328	*SLC30A7*	28.871	26.73	27.351
GAPDH	22.284	21.67	21.956	*SLC30A8*	36.993	35.344	35.426
GAPDH	22.444	21.948	22.207	*SLC30A8*	37.002	35.238	35.871
GAPDH	21.917	21.943	21.573	*SLC30A8*	36.232	34.889	35.58
GAPDH	22.284	21.67	21.956	*SLC30A9*	28.736	27.531	27.578
GAPDH	22.444	21.948	22.207	*SLC30A9*	28.698	27.619	26.922
GAPDH	21.917	21.943	21.573	*SLC30A9*	28.642	27.679	27.246
GAPDH	22.386	22.649	22.335	*SLC30A10*	28.96	27.829	27.69
GAPDH	22.432	22.425	22.265	*SLC30A10*	28.71	27.786	27.592
GAPDH	21.947	22.374	22.34	*SLC30A10*	28.153	27.539	27.547
GAPDH	21.171	21.765	21.283	*MT1B*	21.524	20.421	19.719
GAPDH	21.048	21.953	21.208	*MT1B*	21.515	20.617	19.581
GAPDH	21.654	21.915	21.196	*MT1B*	21.476	20.631	19.579
GAPDH	21.171	21.765	21.283	*MT1F*	21.784	20.655	19.436
GAPDH	21.048	21.953	21.208	*MT1F*	21.273	20.871	19.691
GAPDH	21.654	21.915	21.196	*MT1F*	21.472	20.537	19.753
GAPDH	21.171	21.765	21.283	*MT1X*	21.464	20.949	19.683
GAPDH	21.048	21.953	21.208	*MT1X*	21.684	20.642	19.732
GAPDH	21.654	21.915	21.196	*MT1X*	21.658	20.586	19.901

GAPDH	21.171	21.765	21.283	*MT2A*	21.339	21.475	19.645
GAPDH	21.048	21.953	21.208	*MT2A*	21.686	20.479	19.626
GAPDH	21.654	21.915	21.196	*MT2A*	21.353	20.142	19.782

8.1.6 List of the CT values of MDA-MB-231 cells with and without benign zinc exposure

Gene	CT at T_0	CT at T_{30}	CT at T_{120}	Gene	CT at T_0	CT at T_{30}	CT at T_{120}
GAPDH	20.775	20.951	20.72	*SLC39A1*	25.539	25.958	25.652
GAPDH	20.681	20.698	20.69	*SLC39A1*	25.506	25.495	25.812
GAPDH	20.645	20.947	20.551	*SLC39A1*	25.484	26.313	25.575
GAPDH	20.775	20.951	20.72	*SLC39A2*	35.988	34.856	36.698
GAPDH	20.681	20.698	20.69	*SLC39A2*	35.964	34.512	36.71
GAPDH	20.645	20.947	20.551	*SLC39A2*	35.67	35.946	36.279
GAPDH	20.775	20.951	20.72	*SLC39A3*	29.677	30.188	29.892
GAPDH	20.681	20.698	20.69	*SLC39A3*	29.633	29.66	29.977
GAPDH	20.645	20.947	20.551	*SLC39A3*	29.922	29.958	29.965
GAPDH	20.775	20.951	20.72	*SLC39A4*	35.74	36.419	35.473
GAPDH	20.681	20.698	20.69	*SLC39A4*	35.234	35.159	35.92
GAPDH	20.645	20.947	20.551	*SLC39A4*	35.654	35.158	34.387
GAPDH	20.775	20.951	20.72	*SLC39A5*	35.658	35.656	35.599
GAPDH	20.681	20.698	20.69	*SLC39A5*	36.079	35.656	35.598
GAPDH	20.645	20.947	20.551	*SLC39A5*	35.407	35.446	35.812
GAPDH	20.775	20.951	20.72	*SLC39A6*	28.448	29.766	28.975
GAPDH	20.681	20.698	20.69	*SLC39A6*	28.215	28.861	28.953
GAPDH	20.645	20.947	20.551	*SLC39A6*	28.24	29.484	28.874
GAPDH	20.775	20.951	20.72	*SLC39A8*	27.912	28.528	27.783
GAPDH	20.681	20.698	20.69	*SLC39A8*	27.718	27.959	27.974
GAPDH	20.645	20.947	20.551	*SLC39A8*	27.537	28.325	27.872
GAPDH	20.775	20.951	20.72	*SLC39A10*	26.539	27.113	26.938
GAPDH	20.681	20.698	20.69	*SLC39A10*	26.233	26.061	26.94
GAPDH	20.645	20.947	20.551	*SLC39A10*	25.974	27.093	26.592
GAPDH	20.775	20.951	20.72	*SLC39A12*	30.256	30.392	25.814
GAPDH	20.681	20.698	20.69	*SLC39A12*	30.656	28.944	25.812
GAPDH	20.645	20.947	20.551	*SLC39A12*	30.598	30.014	25.524

GAPDH	20.775	20.951	20.72	*SLC39A14*	28.393	28.959	28.333
GAPDH	20.681	20.698	20.69	*SLC39A14*	28.009	28.185	28.45
GAPDH	20.645	20.947	20.551	*SLC39A14*	28.129	28.964	28.537
GAPDH	20.786	20.964	20.817	*SLC30A1*	29.966	29.725	25.838
GAPDH	20.964	20.724	20.942	*SLC30A1*	30.128	28.616	25.929
GAPDH	20.748	20.969	20.743	*SLC30A1*	30.16	29.598	25.663
GAPDH	20.786	20.964	20.817	*SLC30A2*	36.317	36.417	37.146
GAPDH	20.964	20.724	20.942	*SLC30A2*	37.13	36.913	37.004
GAPDH	20.748	20.969	20.743	*SLC30A2*	37.007	36.98	37.118
GAPDH	20.786	20.964	20.817	*MT1B*	33.835	31.961	28.895
GAPDH	20.964	20.724	20.942	*MT1B*	32.67	33.517	29.131
GAPDH	20.748	20.969	20.743	*MT1B*	32.921	31.693	28.766
GAPDH	20.786	20.964	20.817	*MT1F*	32.98	32.984	28.791
GAPDH	20.964	20.724	20.942	*MT1F*	32.259	32.132	28.91
GAPDH	20.748	20.969	20.743	*MT1F*	32.304	33.337	28.669
GAPDH	20.786	20.964	20.817	*MT1X*	27.589	27.416	24.944
GAPDH	20.964	20.724	20.942	*MT1X*	27.451	26.371	24.816
GAPDH	20.748	20.969	20.743	*MT1X*	27.842	27.468	24.424
GAPDH	20.786	20.964	20.817	*MT2A*	22.447	22.906	21.948
GAPDH	20.964	20.724	20.942	*MT2A*	22.411	22.447	22.272
GAPDH	20.748	20.969	20.743	*MT2A*	22.911	22.913	21.872

8.1.7 List of the CT values of RWPE-1 cells with and without mild cytotoxic zinc exposure

Gene	**CT at T_0**	**CT at T_{30}**	**CT at T_{120}**	**Gene**	**CT at T_0**	**CT at T_{30}**	**CT at T_{120}**
GAPDH	19.974	20.504	20.49	*SLC39A1*	24.718	25.28	25.252
GAPDH	20.646	20.439	20.957	*SLC39A1*	25.119	25.016	25.655
GAPDH	20.52	20.291	20.836	*SLC39A1*	25.052	24.948	25.473
GAPDH	19.974	20.504	20.49	*SLC39A2*	32.932	33.002	32.664
GAPDH	20.646	20.439	20.957	*SLC39A2*	33.043	33.455	33.255
GAPDH	20.52	20.291	20.836	*SLC39A2*	33.461	32.967	33.046
GAPDH	19.974	20.504	20.49	*SLC39A3*	30.096	30.336	30.871
GAPDH	20.646	20.439	20.957	*SLC39A3*	30.304	30.253	30.911
GAPDH	20.52	20.291	20.836	*SLC39A3*	30.23	30.206	30.956

GAPDH	19.974	20.504	20.49	*SLC39A4*	37.063	36.046	35.761
GAPDH	20.646	20.439	20.957	*SLC39A4*	35.902	35.433	36.002
GAPDH	20.52	20.291	20.836	*SLC39A4*	34.896	36.544	35.884
GAPDH	19.974	20.504	20.49	*SLC39A5*	35.527	37.041	35.861
GAPDH	20.646	20.439	20.957	*SLC39A5*	35.619	36.628	36.149
GAPDH	20.52	20.291	20.836	*SLC39A5*	35.776	35.502	35.898
GAPDH	19.974	20.504	20.49	*SLC39A6*	28.355	29.334	29.199
GAPDH	20.646	20.439	20.957	*SLC39A6*	28.931	29.312	29.628
GAPDH	20.52	20.291	20.836	*SLC39A6*	28.967	28.967	29.568
GAPDH	20.113	20.631	20.684	*SLC39A7*	26.83	26.974	27.018
GAPDH	20.875	20.63	20.975	*SLC39A7*	27.238	27.041	27.96
GAPDH	20.644	20.919	20.946	*SLC39A7*	27.086	26.966	27.49
GAPDH	20.113	20.631	20.684	*SLC39A8*	28.902	29.513	29.392
GAPDH	20.875	20.63	20.975	*SLC39A8*	29.495	29.468	30.206
GAPDH	20.644	20.919	20.946	*SLC39A8*	29.318	29.107	29.945
GAPDH	20.113	20.631	20.684	*SLC39A9*	26.937	27.205	27.358
GAPDH	20.875	20.63	20.975	*SLC39A9*	27.412	27.263	27.841
GAPDH	20.644	20.919	20.946	*SLC39A9*	27.146	27.077	27.713
GAPDH	20.113	20.631	20.684	*SLC39A10*	28.232	28.64	29.224
GAPDH	20.875	20.63	20.975	*SLC39A10*	28.926	28.637	29.847
GAPDH	20.644	20.919	20.946	*SLC39A10*	28.664	28.45	29.843
GAPDH	20.113	20.631	20.684	*SLC39A11*	29.482	29.984	29.772
GAPDH	20.875	20.63	20.975	*SLC39A11*	30.033	29.948	30.481
GAPDH	20.644	20.919	20.946	*SLC39A11*	29.825	29.564	30.051
GAPDH	20.113	20.631	20.684	*SLC39A12*	26.89	25.675	22.398
GAPDH	20.875	20.63	20.975	*SLC39A12*	27.336	25.769	22.909
GAPDH	20.644	20.919	20.946	*SLC39A12*	27.403	25.434	22.88
GAPDH	19.967	20.561	20.538	*SLC39A13*	28.412	28.948	28.93
GAPDH	20.657	20.468	20.75	*SLC39A13*	28.853	28.982	29.144
GAPDH	20.398	20.258	20.86	*SLC39A13*	28.828	28.677	29.382
GAPDH	19.967	20.561	20.538	*SLC39A14*	28.736	29.165	28.849
GAPDH	20.657	20.468	20.75	*SLC39A14*	29.262	29.262	29.177
GAPDH	20.398	20.258	20.86	*SLC39A14*	29.076	28.941	29.27

GAPDH	19.967	20.561	20.538	*SLC30A1*	28.207	26.724	23.614
GAPDH	20.657	20.468	20.75	*SLC30A1*	28.792	27.036	23.913
GAPDH	20.398	20.258	20.86	*SLC30A1*	28.526	26.559	23.943
GAPDH	19.967	20.561	20.538	*SLC30A2*	35.624	35.028	28.173
GAPDH	20.657	20.468	20.75	*SLC30A2*	35.94	35.318	28.621
GAPDH	20.398	20.258	20.86	*SLC30A2*	35.509	35.017	28.766
GAPDH	19.967	20.561	20.538	*SLC30A3*	35.658	34.739	34.253
GAPDH	20.657	20.468	20.75	*SLC30A3*	35.68	36.601	35.187
GAPDH	20.398	20.258	20.86	*SLC30A3*	35.939	36.41	35.278
GAPDH	19.967	20.561	20.538	*SLC30A4*	30.588	31.148	30.894
GAPDH	20.657	20.468	20.75	*SLC30A4*	31.19	31.165	31.282
GAPDH	20.398	20.258	20.86	*SLC30A4*	30.948	30.828	31.288
GAPDH	19.962	20.463	20.374	*SLC30A5*	26.925	27.384	27.494
GAPDH	20.816	20.239	20.748	*SLC30A5*	27.621	27.333	27.881
GAPDH	20.412	20.148	20.682	*SLC30A5*	27.503	27.276	27.842
GAPDH	19.962	20.463	20.374	*SLC30A6*	28.198	28.754	28.442
GAPDH	20.816	20.239	20.748	*SLC30A6*	28.864	28.661	28.921
GAPDH	20.412	20.148	20.682	*SLC30A6*	28.607	28.25	28.843
GAPDH	19.962	20.463	20.374	*SLC30A7*	25.926	26.445	26.292
GAPDH	20.816	20.239	20.748	*SLC30A7*	26.615	26.439	26.791
GAPDH	20.412	20.148	20.682	*SLC30A7*	26.272	26.144	26.701
GAPDH	19.962	20.463	20.374	*SLC30A8*	34.392	35.872	34.083
GAPDH	20.816	20.239	20.748	*SLC30A8*	34.562	34.652	33.844
GAPDH	20.412	20.148	20.682	*SLC30A8*	33.802	33.969	34.134
GAPDH	19.962	20.463	20.374	*SLC30A9*	27.386	27.881	27.923
GAPDH	20.816	20.239	20.748	*SLC30A9*	28.139	27.932	28.455
GAPDH	20.412	20.148	20.682	*SLC30A9*	27.783	27.551	28.258
GAPDH	19.962	20.463	20.374	*SLC30A10*	24.789	24.962	24.362
GAPDH	20.816	20.239	20.748	*SLC30A10*	25.308	25.107	25.068
GAPDH	20.412	20.148	20.682	*SLC30A10*	24.919	24.62	24.842
GAPDH	21.983	21.907	21.188	*MT1B*	25.461	20.194	19.735
GAPDH	21.916	21.841	21.746	*MT1B*	26.444	20.286	18.635
GAPDH	21.907	21.834	21.152	*MT1B*	27.418	19.232	19.113

GAPDH	21.983	21.907	21.188	*MT1F*	26.329	20.429	18.653
GAPDH	21.916	21.841	21.746	*MT1F*	29.364	19.466	18.661
GAPDH	21.907	21.834	21.152	*MT1F*	25.459	20.563	19.672
GAPDH	21.983	21.907	21.188	*MT1X*	25.237	19.556	18.217
GAPDH	21.916	21.841	21.746	*MT1X*	27.642	20.253	19.346
GAPDH	21.907	21.834	21.152	*MT1X*	25.688	19.504	19.298
GAPDH	21.983	21.907	21.188	*MT2A*	27.721	19.381	19.609
GAPDH	21.916	21.841	21.746	*MT2A*	28.278	20.222	19.448
GAPDH	21.907	21.834	21.152	*MT2A*	29.853	20.386	18.452

8.1.8 List of the CT values of PC3 cells with and without mild cytotoxic zinc exposure

Gene	**CT at T_0**	**CT at T_{30}**	**CT at T_{120}**	**Gene**	**CT at T_0**	**CT at T_{30}**	**CT at T_{120}**
GAPDH	22.96	22.279	22.306	*SLC39A1*	25.691	25.484	25.734
GAPDH	22.945	22.381	22.401	*SLC39A1*	25.637	25.522	25.826
GAPDH	22.745	22.439	22.679	*SLC39A1*	25.945	25.828	25.954
GAPDH	22.134	22.26	22.465	*SLC39A2*	35.762	34.814	33.745
GAPDH	22.127	22.297	22.202	*SLC39A2*	36.557	34.468	35.741
GAPDH	22.582	22.516	22.966	*SLC39A2*	37.307	34.603	36.659
GAPDH	22.18	21.958	21.973	*SLC39A2*	37.129	36.105	36.693
GAPDH	22.409	21.946	21.189	*SLC39A2*	36.478	39.957	36.748
GAPDH	22.147	21.946	21.268	*SLC39A2*	35.873	35.263	35.436
GAPDH	22.134	22.26	22.465	*SLC39A3*	32.226	31.826	32.294
GAPDH	22.127	22.297	22.202	*SLC39A3*	32.446	31.839	32.561
GAPDH	22.582	22.516	22.966	*SLC39A3*	32.236	31.892	31.965
GAPDH	22.18	21.958	21.973	*SLC39A3*	31.98	31.831	31.926
GAPDH	22.409	21.946	21.189	*SLC39A3*	32.161	31.671	31.98
GAPDH	22.147	21.946	21.268	*SLC39A3*	32.093	31.697	31.962
GAPDH	22.134	22.26	22.465	*SLC39A4*	28.591	27.791	28.339
GAPDH	22.127	22.297	22.202	*SLC39A4*	28.626	27.916	28.218
GAPDH	22.582	22.516	22.966	*SLC39A4*	28.824	28.283	28.648
GAPDH	22.134	22.26	22.465	*SLC39A5*	35.252	35.118	36.88
GAPDH	22.127	22.297	22.202	*SLC39A5*	35.392	35.048	35.581
GAPDH	22.582	22.516	22.966	*SLC39A5*	36.532	36.995	35.768

GAPDH	22.134	22.26	22.465	*SLC39A6*	24.975	25.815	25.514
GAPDH	22.127	22.297	22.202	*SLC39A6*	24.883	25.739	25.693
GAPDH	22.582	22.516	22.966	*SLC39A6*	25.693	25.884	25.855
GAPDH	22.134	22.26	22.465	*SLC39A7*	28.276	28.48	28.254
GAPDH	22.127	22.297	22.202	*SLC39A7*	28.393	28.579	28.513
GAPDH	22.582	22.516	22.966	*SLC39A7*	28.581	28.406	28.958
GAPDH	22.134	22.26	22.465	*SLC39A8*	28.271	28.834	28.387
GAPDH	22.127	22.297	22.202	*SLC39A8*	28.272	28.863	28.672
GAPDH	22.582	22.516	22.966	*SLC39A8*	29.031	28.957	28.03
GAPDH	22.134	22.26	22.465	*SLC39A9*	27.507	27.94	27.742
GAPDH	22.127	22.297	22.202	*SLC39A9*	27.669	27.956	27.954
GAPDH	22.582	22.516	22.966	*SLC39A9*	28.319	28.319	27.567
GAPDH	22.134	22.26	22.465	*SLC39A10*	29.9	30.528	30.915
GAPDH	22.127	22.297	22.202	*SLC39A10*	29.969	30.468	30.646
GAPDH	22.582	22.516	22.966	*SLC39A10*	30.942	30.939	30.623
GAPDH	22.134	22.26	22.465	*SLC39A11*	28.295	28.136	28.543
GAPDH	22.127	22.297	22.202	*SLC39A11*	28.516	28.335	28.744
GAPDH	22.582	22.516	22.966	*SLC39A11*	28.956	28.732	28.744
GAPDH	22.134	22.26	22.465	*SLC39A12*	37.05	37.147	36.98
GAPDH	22.127	22.297	22.202	*SLC39A12*	37.08	36.44	37.631
GAPDH	22.582	22.516	22.966	*SLC39A12*	37	36.59	37.01
GAPDH	22.134	22.26	22.465	*SLC39A13*	29.267	29.314	29.806
GAPDH	22.127	22.297	22.202	*SLC39A13*	29.526	29.527	29.955
GAPDH	22.582	22.516	22.966	*SLC39A13*	29.584	29.77	29.955
GAPDH	22.134	22.26	22.465	*SLC39A14*	29.184	28.95	29.332
GAPDH	22.127	22.297	22.202	*SLC39A14*	29.321	29.049	29.332
GAPDH	22.582	22.516	22.966	*SLC39A14*	29.765	29.497	29.361
GAPDH	22.353	21.898	22.192	*SLC30A1*	29.039	27.965	27.651
GAPDH	22.413	21.964	21.03	*SLC30A1*	29.061	27.922	26.927
GAPDH	22.389	22.232	22.292	*SLC30A1*	29.145	27.963	28.081
GAPDH	22.18	21.958	21.973	*SLC30A1*	29.93	27.717	26.839
GAPDH	22.409	21.946	21.189	*SLC30A1*	29.999	27.318	27.79
GAPDH	22.147	21.946	21.268	*SLC30A1*	29.916	26.488	29.054

GAPDH	22.134	22.26	22.465	*SLC30A2*	22.404	22.53	22.68
GAPDH	22.127	22.297	22.202	*SLC30A2*	22.572	22.524	22.68
GAPDH	22.582	22.516	22.966	*SLC30A2*	22.974	22.534	22.617
GAPDH	22.353	21.898	22.192	*SLC30A3*	33.49	32.7	32.159
GAPDH	22.413	21.964	21.03	*SLC30A3*	33.497	32.931	33.147
GAPDH	22.389	22.232	22.292	*SLC30A3*	33.53	32.964	33.398
GAPDH	22.18	21.958	21.973	*SLC30A3*	33.98	31.653	32.195
GAPDH	22.409	21.946	21.189	*SLC30A3*	33.968	32.681	32.322
GAPDH	22.147	21.946	21.268	*SLC30A3*	33.811	31.811	33.968
GAPDH	22.353	21.898	22.192	*SLC30A4*	34.523	34.252	33.413
GAPDH	22.413	21.964	21.03	*SLC30A4*	34.741	34.222	34.167
GAPDH	22.389	22.232	22.292	*SLC30A4*	35.052	34.925	35.186
GAPDH	22.353	21.898	22.192	*SLC30A5*	28.113	27.658	26.934
GAPDH	22.413	21.964	21.03	*SLC30A5*	28.236	27.569	27.967
GAPDH	22.389	22.232	22.292	*SLC30A5*	28.291	27.999	28.369
GAPDH	22.584	21.969	22.221	*SLC30A6*	30.252	29.777	29.966
GAPDH	22.643	22.204	22.244	*SLC30A6*	28.914	29.796	29.92
GAPDH	22.772	22.255	22.585	*SLC30A6*	30.265	30.112	30.233
GAPDH	22.584	21.969	22.221	*SLC30A7*	28.938	28.269	28.236
GAPDH	22.643	22.204	22.244	*SLC30A7*	29.063	28.478	28.292
GAPDH	22.772	22.255	22.585	*SLC30A7*	29.213	28.609	28.733
GAPDH	22.584	21.969	22.221	*SLC30A8*	36.782	35.257	35.651
GAPDH	22.643	22.204	22.244	*SLC30A8*	36.854	36.099	37.011
GAPDH	22.772	22.255	22.585	*SLC30A8*	36.598	36.106	36.992
GAPDH	22.584	21.969	22.221	*SLC30A9*	28.842	28.446	28.327
GAPDH	22.643	22.204	22.244	*SLC30A9*	28.938	28.43	28.483
GAPDH	22.772	22.255	22.585	*SLC30A9*	28.972	28.764	28.824
GAPDH	22.134	22.26	22.465	*SLC30A10*	28.042	27.522	27.945
GAPDH	22.127	22.297	22.202	*SLC30A10*	28.133	27.474	28.213
GAPDH	22.582	22.516	22.966	*SLC30A10*	28.382	27.92	28.235
GAPDH	21.877	21.833	21.082	*MT1B*	21.242	21.203	19.358
GAPDH	21.636	21.816	21.075	*MT1B*	21.238	21.116	20.147
GAPDH	21.606	21.767	21.018	*MT1B*	21.226	20.112	19.189

GAPDH	21.877	21.833	21.082	*MT1F*	21.751	21.262	20.258
GAPDH	21.636	21.816	21.075	*MT1F*	21.452	21.188	19.947
GAPDH	21.606	21.767	21.018	*MT1F*	21.692	21.193	21.189
GAPDH	21.877	21.833	21.082	*MT1X*	21.856	20.441	20.232
GAPDH	21.636	21.816	21.075	*MT1X*	21.978	20.621	20.366
GAPDH	21.606	21.767	21.018	*MT1X*	21.743	21.313	19.885
GAPDH	21.877	21.833	21.082	*MT2A*	21.512	21.707	20.457
GAPDH	21.636	21.816	21.075	*MT2A*	21.324	20.795	20.339
GAPDH	21.606	21.767	21.018	*MT2A*	21.567	20.401	20.098

8.1.9 List of the CT values of DU145 cells with and without mild cytotoxic zinc exposure

Gene	**CT at T_0**	**CT at T_{30}**	**CT at T_{120}**	**Gene**	**CT at T_0**	**CT at T_{30}**	**CT at T_{120}**
GAPDH	21.629	22.19	22.984	*SLC39A1*	25.117	25.392	25.958
GAPDH	22.193	22.377	21.973	*SLC39A1*	25.266	25.116	25.549
GAPDH	21.629	22.515	22.426	*SLC39A1*	25.692	25.647	24.404
GAPDH	21.951	22.481	22.385	*SLC39A2*	28.291	27.948	27.855
GAPDH	21.926	22.543	22.441	*SLC39A2*	28.486	27.948	27.774
GAPDH	21.946	22.558	22.379	*SLC39A2*	29.002	27.876	28.712
GAPDH	21.719	22.959	22.631	*SLC39A3*	31.591	32.671	31.962
GAPDH	22.496	23.149	22.874	*SLC39A3*	32.393	31.44	31.829
GAPDH	22.569	22.855	22.123	*SLC39A3*	32.277	31.885	30.971
GAPDH	21.951	22.481	22.385	*SLC39A4*	28.472	27.944	27.946
GAPDH	21.926	22.543	22.441	*SLC39A4*	28.276	27.91	27.961
GAPDH	21.946	22.558	22.379	*SLC39A4*	28.797	27.757	27.81
GAPDH	21.719	22.959	22.631	*SLC39A5*	36.319	35.831	36.569
GAPDH	22.496	23.149	22.874	*SLC39A5*	35.316	37.025	35.719
GAPDH	22.569	22.855	22.123	*SLC39A5*	35.77	35.858	36.225
GAPDH	21.719	22.959	22.631	*SLC39A6*	24.575	25.492	25.39
GAPDH	22.496	23.149	22.874	*SLC39A6*	24.966	24.976	25.536
GAPDH	22.569	22.855	22.123	*SLC39A6*	24.979	24.976	25.402
GAPDH	21.719	22.959	22.631	*SLC39A7*	28.664	28.382	28.668
GAPDH	22.496	23.149	22.874	*SLC39A7*	28.552	29.798	28.724
GAPDH	22.569	22.855	22.123	*SLC39A7*	28.751	28.896	28.978

GAPDH	21.719	22.959	22.631	*SLC39A8*	28.749	28.902	28.36
GAPDH	22.496	23.149	22.874	*SLC39A8*	28.887	28.777	28.712
GAPDH	22.569	22.855	22.123	*SLC39A8*	28.968	29.196	28.298
GAPDH	21.942	22.662	22.203	*SLC39A9*	27.954	27.675	28.064
GAPDH	22.481	22.386	22.322	*SLC39A9*	28.111	27.164	27.801
GAPDH	22.255	22.212	22.265	*SLC39A9*	28.273	27.671	28.547
GAPDH	21.942	22.662	22.203	*SLC39A10*	30.591	30.196	30.922
GAPDH	22.481	22.386	22.322	*SLC39A10*	30.572	30.935	30.567
GAPDH	22.255	22.212	22.265	*SLC39A10*	30.728	30.452	30.883
GAPDH	21.942	22.662	22.203	*SLC39A11*	28.747	29.249	28.962
GAPDH	22.481	22.386	22.322	*SLC39A11*	27.754	28.753	28.742
GAPDH	22.255	22.212	22.265	*SLC39A11*	28.944	28.446	29.822
GAPDH	21.942	22.662	22.203	*SLC39A12*	28.814	28.967	27.474
GAPDH	22.481	22.386	22.322	*SLC39A12*	29.128	27.513	28.641
GAPDH	22.255	22.212	22.265	*SLC39A12*	29.234	27.724	28.62
GAPDH	21.942	22.662	22.203	*SLC39A13*	29.468	29.898	29.981
GAPDH	22.481	22.386	22.322	*SLC39A13*	30.21	29.94	29.981
GAPDH	22.255	22.212	22.265	*SLC39A13*	29.952	29.898	30.758
GAPDH	21.942	22.662	22.203	*SLC39A14*	30.469	29.69	29.247
GAPDH	22.481	22.386	22.322	*SLC39A14*	29.96	29.679	30.184
GAPDH	22.255	22.212	22.265	*SLC39A14*	30.073	29.098	29.847
GAPDH	21.808	22.304	22.239	*SLC30A1*	28.82	27.362	27.53
GAPDH	21.963	22.418	22.44	*SLC30A1*	28.957	27.615	27.866
GAPDH	22.018	23.518	21.94	*SLC30A1*	29.286	26.898	27.641
GAPDH	21.951	22.481	22.385	*SLC30A2*	28.457	26.945	27.61
GAPDH	21.926	22.543	22.441	*SLC30A2*	28.461	26.878	27.305
GAPDH	21.946	22.558	22.379	*SLC30A2*	28.901	27.855	27.479
GAPDH	21.808	22.304	22.239	*SLC30A3*	33.027	32.497	32.603
GAPDH	21.963	22.418	22.44	*SLC30A3*	33.313	32.974	32.732
GAPDH	22.018	23.518	21.94	*SLC30A3*	33.44	33.297	32.41
GAPDH	21.808	22.304	22.239	*SLC30A4*	34.308	34.27	34.099
GAPDH	21.963	22.418	22.44	*SLC30A4*	34.454	34.039	34.064
GAPDH	22.018	23.518	21.94	*SLC30A4*	34.703	34.12	33.938

GAPDH	21.808	22.304	22.239	*SLC30A5*	27.499	26.932	27.341
GAPDH	21.963	22.418	22.44	*SLC30A5*	27.824	27.156	27.321
GAPDH	22.018	23.518	21.94	*SLC30A5*	27.86	27.547	27.42
GAPDH	21.808	22.304	22.239	*SLC30A6*	29.441	29.269	29.41
GAPDH	21.963	22.418	22.44	*SLC30A6*	29.465	28.889	29.343
GAPDH	22.018	23.518	21.94	*SLC30A6*	29.948	29.33	29.582
GAPDH	21.629	22.19	22.984	*SLC30A7*	28.359	28.539	28.164
GAPDH	22.193	22.377	21.973	*SLC30A7*	28.432	27.854	27.754
GAPDH	21.761	22.515	22.426	*SLC30A7*	28.942	27.069	27.271
GAPDH	21.629	22.19	22.984	*SLC30A8*	36.133	35.248	36.103
GAPDH	22.193	22.377	21.973	*SLC30A8*	35.309	35.089	34.75
GAPDH	21.761	22.515	22.426	*SLC30A8*	35.689	37.027	34.311
GAPDH	21.629	22.19	22.984	*SLC30A9*	28.184	28.316	28.406
GAPDH	22.193	22.377	21.973	*SLC30A9*	28.495	27.892	27.911
GAPDH	21.761	22.515	22.426	*SLC30A9*	28.653	28.739	27.935
GAPDH	21.629	22.19	22.984	*SLC30A10*	28.296	27.95	28.17
GAPDH	22.193	22.377	21.973	*SLC30A10*	28.364	27.834	27.707
GAPDH	21.761	22.515	22.426	*SLC30A10*	28.782	27.923	27.744
GAPDH	21.593	21.763	21.983	*MT1B*	21.177	21.012	20.12
GAPDH	21.584	21.724	21.928	*MT1B*	21.066	20.692	21.591
GAPDH	21.578	21.651	21.918	*MT1B*	21.969	20.859	20.922
GAPDH	21.593	21.763	21.983	*MT1F*	21.843	21.576	21.215
GAPDH	21.584	21.724	21.928	*MT1F*	21.986	21.494	20.361
GAPDH	21.578	21.651	21.918	*MT1F*	21.536	21.291	21.604
GAPDH	21.593	21.763	21.983	*MT1X*	21.654	20.749	20.253
GAPDH	21.584	21.724	21.928	*MT1X*	21.465	20.761	20.185
GAPDH	21.578	21.651	21.918	*MT1X*	21.733	20.759	21.184
GAPDH	21.593	21.763	21.983	*MT2A*	21.317	21.457	20.514
GAPDH	21.584	21.724	21.928	*MT2A*	21.975	21.429	20.756
GAPDH	21.578	21.651	21.918	*MT2A*	21.947	20.447	20.254

8.2 Appendix B

8.2.1 Predicted phosphorylation sites of CK2 in ZIP12 isoform 1 (*Homo sapiens*)

Position	Code	Peptide	Score	Localisation
39	S	QDSRSRGSSGQPADL	3.567	Extracellular
51	S	ADLLQVLSAGDHPPH	3.946	Extracellular
160	S	DEDSSFLSQNETEDI	1.748	Extracellular
197	S	KKSGIVSSEGANEST	4.26	Extracellular
250	S	RTNTLRLSELDQLLN	5.175	Cytoplasmic
299	S	SSSMEKESEDGPVSW	4.512	Cytoplasmic
392	S	TALVLFHSCEENYRL	3.169	Extracellular
497	S	LALNSELSDQAGRGK	4.248	Extracellular
513	S	ASTIQLKSPEDSQAA	1.28	Extracellular
565	S	AIGAAFSSSSESGVT	3.924	Cytoplasmic
567	S	GAAFSSSSESGVTTT	2.304	Cytoplasmic
645	S	AGMFLYLSLVEMLPE	3.645	Helical

8.2.2 Predicted phosphorylation sites of CK2 in ZIP12 isoform 2 (*Homo sapiens*)

Position	Code	Peptide	Score	Localisation
39	S	QDSRSRGSSGQPADL	3.567	Extracellular
51	S	ADLLQVLSAGDHPPH	3.946	Extracellular
160	S	DEDSSFLSQNETEDI	1.748	Extracellular
197	S	KKSGIVSSEGANEST	4.26	Extracellular
250	S	RTNTLRLSELDQLLN	5.175	Cytoplasmic
299	S	SSSMEKESEDGPVSW	4.512	Cytoplasmic
392	S	TALVLFHSCEENYRL	3.169	Extracellular
476	S	VSPNDKKSPEDSQAA	3.378	Extracellular
480	S	DKKSPEDSQAAEMPI	4.556	Extracellular
528	S	AIGAAFSSSSESGVT	3.924	Extracellular
530	S	GAAFSSSSESGVTTT	2.304	Extracellular
608	S	AGMFLYLSLVEMLPE	3.645	Helical

8.2.3 Predicted phosphorylation sites of CK2 in ZIP12 isoform 3 (*Homo sapiens*)

Position	Code	Peptide	Score	Localisation
39	S	QDSRSRGSSGQPADL	3.567	Extracellular
51	S	ADLLQVLSAGDHPPH	3.946	Extracellular
160	S	DEDSSFLSQNETEDI	1.748	Extracellular
197	S	KKSGIVSSEGANEST	4.26	Extracellular
250	S	RTNTLRLSELDQLLN	5.175	Cytoplasmic
299	S	SSSMEKESEDGPVSW	4.512	Cytoplasmic
392	S	TALVLFHSCEENYRL	3.169	Extracellular
496	S	LALNSELSDQAGRGK	3.941	Extracellular
512	S	ASTIQLKSPEDSQAA	1.28	Extracellular
564	S	AIGAAFSSSSESGVT	3.924	Cytoplasmic
566	S	GAAFSSSSESGVTTT	2.304	Cytoplasmic
644	S	AGMFLYLSLVEMLPE	3.645	Helical

8.2.4 Predicted phosphorylation sites of CK2 in ZIP12 isoform 4 (*Homo sapiens*)

Position	Code	Peptide	Score	Localisation
26	S	DEDSSFLSQNETEDI	2.45	Extracellular
63	S	KKSGIVSSEGANEST	4.26	Extracellular
116	S	RTNTLRLSELDQLLN	5.175	Extracellular
165	S	SSSMEKESEDGPVSW	4.512	Extracellular
258	S	TALVLFHSCEENYRL	3.169	Cytoplasmic
363	S	LALNSELSDQAGRGK	4.248	Cytoplasmic
379	S	ASTIQLKSPEDSQAA	1.28	Helical
431	S	AIGAAFSSSSESGVT	3.924	Cytoplasmic
433	S	GAAFSSSSESGVTTT	2.304	Cytoplasmic
511	S	AGMFLYLSLVEMLPE	3.645	Extracellular